IMPERIAL

Mechano-regulation of β_2AR signalling pathway of ventricular cardiomyocytes in healthy and failing hearts

Jiarong Fu

National Heart and Lung Institute

Imperial College London

Thesis Submitted for the Degree of Doctor of Philosophy

Statement of Originality

I certify that this thesis, and the research to which it refers, are the product of my own work, conducted during the three years of the PhD in Clinical Medicine Research at Imperial College London. Any ideas or quotations in the work are fully acknowledged in accordance with the standard referencing practices of the discipline.

Copyright Declaration

‘The copyright of this thesis rests with the author. Unless otherwise indicated, its contents are licensed under a Creative Commons Attribution-Non Commercial 4.0 International Licence (CC BY-NC). Under this licence, you may copy and redistribute the material in any medium or format. You may also create and distribute modified versions of the work. This is on the condition that: you credit the author and do not use it, or any derivative works, for a commercial purpose. When reusing or sharing this work, ensure you make the licence terms clear to others by naming the licence and linking to the licence text. Where a work has been adapted, you should indicate that the work has been changed and describe those changes. Please seek permission from the copyright holder for uses of this work that are not included in this licence or permitted under UK Copyright Law.’

Abstract

Myocardial stretch occurs during haemodynamic overload and may be physiological (e.g., exercise) or pathological (e.g., heart failure). Understanding the effects of stretch on signalling pathways associated with mechanosensitive structures, such as caveolae, is therefore essential. Caveolar microdomains regulate the distribution of signalling proteins, including β-adrenoceptors (βARs), and may act as membrane reserves, protecting cells during the mechanical stretch. Phosphodiesterase 4 (PDE4), particularly subtypes PDE4B and PDE4D, have been shown to localise in caveolae-rich membranes, where they tightly regulate βAR-induced cAMP production. Regional differences in membrane structure and βAR signalling also exist across the myocardium. This study investigates the role of caveolae in βAR-signalling in response to membrane deformation, the specific contributions of PDE4B and PDE4D, and regional differences in this regulation. We further assess how this signalling is altered in the context of heart failure. To induce membrane stretch-like stimuli, we used osmotic swelling in left ventricular cardiomyocytes isolated from healthy and failing (16 weeks post-myocardial infarction) rat hearts, as well as from human donor and failing (dilated cardiomyopathy) hearts. The βAR response was measured using a Förster Resonance Energy Transfer (FRET) reporter for the second messenger cyclic adenosine monophosphate (cAMP) and using CytoCypher for the measurement of cell contractility. Our study reveals a stretch-regulation of the β_2AR signalling pathway that is dependent on functional caveolae and PDE4 activity, particularly in the basal region of the myocardium; this regulation is lost in heart failure. These findings indicate that caveolae are mechanosensitive membrane domains that undergo structural and functional changes in response to membrane deformation, thereby mediating the mechanical regulation of caveolae-associated signalling pathways.

Table of Contents

Statement of Originality **2**

Copyright Declaration **3**

Abstract **4**

Posters and Presentations **13**

Publications **13**

Acknowledgements **14**

List of Figures **16**

List of Tables **20**

List of Abbreviations **21**

Chapter 1: General Introduction **24**

1.1 Structure of Cardiomyocytes at the Subcellular Level 24

1.1.1 Caveolae and Caveolins 25

1.1.1.1 Caveolins 25

1.1.1.2 Caveolae in Response to Mechanical Stimuli 28

1.1.1.3 Caveolae, Caveolin and Cardiac Disease 30

1.1.2 Transverse Tubule 32

1.1.2.1 The Role of Transverse Tubule and Its Associated Proteins 33

1.1.2.2 T-Tubule Remodeling and Its Impact on Cardiac Function in Heart Failure 35

1.2 Cardiac Electro-Excitation 36

1.2.1 Ventricular Action Potential 36

1.3 G-Protein Coupled Receptors and Their Role in Signal Transduction 38

1.3.1 The Structure and Function of β-Adrenergic Receptors in the Cardiomyocytes 40

1.2.2 The Compartmentation of β-Adrenergic Receptors 46

1.3.3 β-Adrenergic Receptors in Heart Failure 48

1.4 Phosphodiesterases 49

1.4.1 The Structure and Function of Phosphodiesterases in the Cardiomyocytes 49

1.4.2 The Structure and Function of Phosphodiesterases 4 and its Subtypes in the Cardiomyocytes 51
1.4.3 PDE4 Regulation in Cardiac Disease 53
1.5 Regionality within the Myocardium 54
1.6 Myocardial Stretch: Mechanisms and Implications for Cardiac Function 58
1.7 Models of Stretch 61
1.8 The Effect of Stretch on Contraction-Excitation Feedback 63
1.9 Other Cell Types in the Heart and Their Role in Mechanosensing 67
1.10 The Heart Failure 70
1.11 Summary 75
1.12 Hypothesis 77
1.13 Aims 77
Chapter 2: General Material and Methods 78
2.1 Animal Ethics Approval 79
2.2 Rat Myocardial Infarction 79
2.2.1 Anaesthesia and Pre-operative Care 80
2.2.2 Myocardial Infarction Procedure 81
2.2.3 Post-operative Care 81
2.3 Isolation of Adult Rat Ventricular Cardiomyocytes 82
2.4 Human Ethics Approval 85
2.5 Human Cardiomyocyte Isolation 85
2.6 Hypoosmotic Swelling Model 86
2.7 Transmission Electron Microscopy 88
2.8 Live Cell T-tubule Staining and Measurement 89
2.8.1 Di-8-ANEPPS staining 89
2.8.2 T-tubule Density and Regularity Measurement 89

2.8.3 T-tubule Directionality Measurement 91

2.9 Immunocytochemistry 92

2.9.1 Immunostaining for Cardiomyocyte 92

2.9.2 Colocalisation Measurement 93

2.10 Förster Resonance Energy Transfer (FRET) Microscopy 95

2.10.1 Introduction and Principles of FRET 95

2.10.2 Plasma Membrane Epac2 (pmEPAC2) FRET Sensor for cAMP Measurement 96

2.10.3 Cardiomyocyte FRET Sensor Infection Protocol 98

2.10.4 Multi-cell FRET Microscopy for Measurement of cAMP Activity 98

2.11 CytoCypher 100

2.11.1 Introduction of CytoCypher 100

2.11.2 CytoCypher Protocol 103

2.12 Langendorff-Optical Mapping 104

2.12.1 Introduction and Principle of Langendorff-Optical Mapping Approach 104

2.12.2 Protocol for Langendorff-Optical Mapping Experiments 106

2.12.3 Optical Mapping Set Up 108

2.12.4 Dye Loading 110

2.12.5 Acquisition of Optical Mapping Data 111

2.13. Statistics 112

Chapter 3 The Effect of Membrane Stretch and The Role of Caveolae on β-adrenoceptor Signalling in Cardiomyocytes 115

3.1 Introduction 115

3.2 Hypothesis and Aims 117

3.3 Method 119

3.3.1 Solutions and Drugs 119

3.3.2 CytoCypher 119

3.3.2.1 Investigation of the Contractile Response of Cardiomyocytes to βAR Stimulation Following Hypoosmotic Swelling 120

3.3.2.2 Investigation of the Role of Caveolae in Contractile Response of Cardiomyocytes to Selective βAR Stimulation Following Hypoosmotic Swelling 121
3.3.2.3 Investigation of the Effect of Adenylyl Cyclase Activity Following Hypoosmotic Swelling 121
3.3.2.4 Investigation of the effect of G_i on β_2AR induced Contractile Response Following Hypoosmotic Swelling 121
3.3.3 Multi-cell FRET Microscopy 122
3.3.4 Live Cell T-tubule Staining via Di-8-ANNEPPS 123
3.3.5 Confocal Microscopy of LV Cardiomyocytes Following Caveolin-3 Staining 123
3.3.6 Quantification of Caveolae Number in LV Cardiomyocytes Using Transmission Electron Microscopy 124
3.3.7 Statistics 124
3.4 Results 126
3.4.1 Impact of Hypoosmotic Swelling Model on Isolated Cardiomyocytes 126
3.4.2 Hypoosmotic swelling of isolated cardiomyocytes causes an increase in β_2-adrenoceptor induced cAMP release 131
3.4.3 Hypoosmotic swelling causes an increase in sarcomere shortening following β_2-adrenoceptor stimulation. 133
3.3.4 Dependence of increased β_2AR activity on functional caveolae following hypoosmotic swelling 137
3.4.5 Increased β_2AR Activity Following Hypoosmotic Swelling is Lost in PTX-Treated Cells 141
3.5 Discussion 144
3.5.1 The Effect of Hypoosmotic Swelling on Cardiomyocyte Structure 144
3.5.2 The Effect of Hypoosmotic Swelling on βAR Signalling 145
3.5.3 The Role of Caveolae in β_2AR Signalling Following Hypoosmotic Swelling 147
3.5.4 The Effect of Hypoosmotic Swelling on β_2 mediated G_i-Pathway 148
3.6 Conclusions 150
Chapter 4 The Effect of Phosphodiesterase 4 on β-adrenoceptor Signalling in Cardiomyocytes Following Membrane Stretch 151

4.1 Introduction 151

4.2 Hypothesis and Aims 155

4.3 Methods 157

4.3.1 Solutions and Drugs 157

4.3.2 CytoCypher 157

4.3.2.1 Investigation of the Role of PDE4 on β_2AR Mediated Contractile Response of Cardiomyocytes Following Membrane Stretch 158

4.3.2.2. Investigation of the Role of PDE4B/D on β_2AR Mediated Contractile Response of Cardiomyocytes Following Membrane Stretch 158

4.3.2.3. Investigation of the Effect of β-arrestin-PDE4D5 Complex on β_2AR Mediated Contractile Response During Membrane Stretch 158

4.3.3 Multi-cell FRET Microscopy 159

4.3.4 Confocal Microscopy Double Immunostaining 160

4.3.5 Statistics 160

4.4 Results 161

4.4.1 PDE4 Inhibition Enhances β_2AR Responses and Equilibrates Cell Contractile Responses to β_2AR Stimulation Following Hypoosmotic Swelling 161

4.4.2 Inhibition of PDE4 Further Enhances β_2AR Induced cAMP Production Following Hypoosmotic Swelling 162

4.4.3 PDE4D is Predominately Involved in β_2AR Signalling for Sarcomere Shortening Response and cAMP Production 163

4.4.4 Hypoosmotic Swelling Disrupts Colocalisation of Cav3 and PDE4D in Adult Rat Ventricular Cardiomyocytes 166

4.4.5 PDE4B is Involved in β_2AR Signalling for Sarcomere Shortening Response and cAMP Production 169

4.4.6 Hypoosmotic swelling decreases colocalisation of Cav3 and PDE4B in Adult Rat Ventricular Cardiomyocytes 171

4.4.7 PDE4D5 β-arrestin Disruptive Peptide Removes the Enhanced β_2AR induced Contractility Following Hypoosmotic Swelling 174

4.5 Discussion 176

4.6 Conclusion 181

Chapter 5 The Regional Differences in Cardiomyocytes β_2AR Response Following Hypoosmotic Swelling 182

5.1 Introduction 182

5.2 Hypothesis and Aims 185

5.3 Methods 187

5.3.1 Solutions 187

5.3.2 CytoCypher 187

5.3.3 FRET Microscopy 188

5.3.4 Live Cell T-tubule Staining via Di-8-ANNEPPS 188

5.3.5 Confocal Microscopy of Apical and Basal Cardiomyocytes Following Caveolin-3 Staining 188

5.3.6 Quantification of Caveolae in Apical and Basal Cardiomyocytes Using Transmission Electron Microscopy 189

5.3.7 Balloon Stretched Isolated Rat Heart 189

5.3.8 Isolated Heart Optical Mapping 190

5.3.9 Statistics 191

5.4 Result 192

5.4.1 Effect of Hypoosmotic Swelling Model on Apical and Basial Cardiomyocytes 192

5.4.2 Hypoosmotic Swelling Increases β_2AR-cAMP Activity and Sarcomere Shortening in Basal Cardiomyocytes 196

5.4.3 Differential Responses to Cardiac Stretch following β_2AR stimulation on Action Potential Duration 199

5.5 Discussion 206

5.6 Conclusion 213

Chapter 6 The Effect of Membrane Stretch on β_1 and β_2AR Signalling in Failing Rat and Human Ventricular Cardiomyocytes 214

6.1 Introduction 214

6.2 Hypothesis and Aims 217

6.3 Methods 219

6.3.1 Solutions 219

6.3.2 Animal Ethics Approval 219

6.3.3 Rat Heart Failure Model 219

6.3.4 Human Ethics Approval 220

6.3.5 Human Study Population 220

6.3.6 Human Cardiomyocytes Isolation 221

6.3.7 Confocal Microscopy Following Di-8-ANNEPS and Caveolin-3 Staining 222

6.3.8 Functional Study – CytoCypher & FRET Microscopy 223

6.3.9 Statistics 223

6.4 Results 225

6.4.1 Hypoosmotic Swelling Increases the Width but Not the Length of Rat Left Ventricular Cardiomyocytes in Both Control and Failing Cells 226

6.4.2 Hypoosmotic Swelling Does Not Alter T-Tubule (TT) Structure in Both Control and Failing Cardiomyocytes 227

6.4.3 Caveolin-3 (Cav3) Density is Increased in Failing Cardiomyocytes 229

6.4.4 Hypoosmotic Swelling Enhances cAMP Production and Sarcomere Shortening Following β_2AR Stimulation, but These Effects Are Lost in MI Cells 230

6.4.5 Sarcomere Shortening is Greater Following β_1AR Stimulation, but Hypoosmotic Swelling Does Not Affect β_2AR-Induced Shortening in Human Donor Cardiomyocytes 232

6.4.6 Decreased Sarcomere Shortening Following β_1AR Stimulation in DCM Cardiomyocytes 234

6.4.7 Increased cAMP Response in DCM Cardiomyocytes Following β_2AR Stimulation 236

6.5 Discussion 238

6.6 Conclusion 244

Chapter 7. General Discussion and Conclusions 245

7.1 Summary of Findings and Future Works 246

7.1.1 Caveolae Restructuring Following Membrane Stretch Decompartmented the β_2ARs Signalling and Disrupting the β_2AR-G_i Signalling 246
7.1.2 Future Work 247
7.1.3 Caveolae Restructuring Induced by Membrane Stretch Disrupts PDE4D Regulation, Leading to Increased β_2AR Response 250
7.1.4 Future Work 252
7.1.5 Membrane Stretch Equilibrates the Difference in β_2AR Signalling Between the Apex and the Base 254
7.1.6 Future Work 255
7.1.7 Stretch-sensitivity of β_2-adrenoceptor Signalling was Lost in Falling Cells 256
7.1.8 Future Work 257
7.2 Limitations 258
7.3 Final conclusion 265

Posters and Presentations

Poster Presentation at 2023AKAPcAMP Conference - Stretch regulation of β_2-Adrenoceptor mediated cAMP signalling in cardiomyocytes requires caveolae - 27/09/2023

Publications

Zoe Kwan, Binoy Paulose Nadappuram, Manton M Leung, Sanika Mohagaonkar, Ao Li, Kumuthu S Amaradasa, Ji Chen, Stephen Rothery, Iyobel Kibreab, **Jiarong Fu**, Jose L Sanchez-Alonso, Catherine A Mansfield, Hariharan Subramanian, Alexander Kondrashov, Peter T Wright, Pamela Swiatlowska, Viacheslav O Nikolaev, Beata Wojciak-Stothard, Aleksandar P Ivanov, Joshua B Edel, Julia Gorelik. Microtubule-Mediated Regulation of β_2AR Translation and Function in Failing Hearts. Circulation Research, 2023 November 10

Jiarong Fu, Catherine Mansfield, Ivan Diakonov, Aleksandra Judina, Navneet Bhogal, Jose L. Sanchez-Alonso, Julia Gorelik. Stretch regulation of β_2-Adrenoceptor mediated cAMP signalling in cardiomyocytes requires caveolae. Cardiovascular Research, 2025 February 13

Emilie Marhuenda; loannis Xanthis; Pragati Pandey;Darren Graham Samuel Wilson; Amar Azad; Davor Pavolvic; Megan Richter; Katja Gehmlich; Giuseppe Faggian; Pamela Swiatlowska; **Jiarong Fu**; Julia Gorelik; Elisabeth Ehler; James Levitt; Simon P. Poland; Simon Ameer-Beg; Thomas Iskratsch. Cardiomyocyte mechanical memory is regulated through the talin interactome and DLC1-dependent regulation of RhodA (paper in revision)

Acknowledgements

I would like to express my sincere gratitude to my supervisor Professor Julia Gorelik, for her invaluable guidance, encouragement, and insights throughout my whole PhD journey. I also extend my thanks to my secondary supervisor, Dr Fu Siong Ng, for his guidance in the optical mapping technique.

I would also like to thank the members of Professor Julia Gorelik's research team; their teamwork and commitment were essential to the success of this project. My sincere appreciation goes to Dr Catherine Mansfield, who introduced me to this research topic. I would also like to acknowledge Dr Ivan Diakonov, for doing the electron microscopy. Special thanks to Dr Jose Sanchez, Dr Benedict O'Reilly, Dr Aleksandra Judina, Dr Pamela Swiatlowska, and Dr Peter Wright for their continuous guidance on laboratory equipment usage and troubleshooting and also for their valuable suggestions and support. I am very much thankful to Mr Houcheng Wang for his assistance with immunofluorescent images using confocal microscopy and optical mapping experiments, and to Mr Tony Hua for his help with optical mapping analysis.

I would like to thank my colleagues and also friends - Mr Houcheng Wang, Mr Ao Li, Mr Sibo Lyu, Mr Iyobel Kibreab, Mr Ivan Sherstnev and Miss Veronika Boichenko; thank you for your help and companionship.

A special mention goes to Mr Peter O'Gara for teaching me rat cardiomyocyte isolations and Mr Matthew Delahaye for instructing me in rat myocardial infarction surgery. I am also grateful to Dr Rasheda Chowdhury for providing the opportunity to do the research involving human samples.

Additionally, my sincere thanks go to our collaborator, Professor George Baillie, for generously providing the PDE4B/D antibodies and for his suggestions on the peptides.

Last but not least, I would like to thank my parents and my grandparents for their financial support and encouragement over the years.

To everyone who has contributed to this project in ways both big and small, I extend my heartfelt thanks. Love to you all.

List of Figures

Figure 1.1. Structure of caveolae and caveolin. 27

Figure 1.2. Cells respond to stretch by disassembling and reassembling the caveolae. 30

Figure 1.3. Images of T-tubule Structure. 33

Figure 1.4. Ventricular action potential in (A) human and (B) rat. 37

Figure 1.5 Illustration of the excitation-contraction coupling and calcium cycle in a cardiomyocyte. 38

Figure 1.6. Schematic of G protein-coupled receptor (GPCR) cycle. 40

Figure 1.7. Schematic diagram of the GPCR and the comparison between β_1AR and β_2AR structures. 42

Figure 1.8. Schematic representation of β_1AR and β_2AR signalling in cardiomyocytes. 45

Figure 1.9. Structure and family of PDE. 50

Figure 1.10. Structure of PDE4 isoform. 52

Figure 1.11. Regional differences in response to catecholamine levels 56

Figure 1.12. Classification of heart failure syndromes and underlying causes 71

Figure 2.1. Langendorff perfusion apparatus set up for adult rat cardiomyocytes isolation experiment 84

Figure 2.2. Rat cardiomyocyte isolation protocol (figure created with BioRender). 85

Figure 2.3. Human cardiomyocyte isolation protocol 86

Figure 2.4. Example of CytoCypher sarcomere shortening traces in two different isosmotic solutions 87

Figure 2.5. T-tubule density and regularity measurement protocol. 90

Figure 2.6. T-tubule directionality measurement protocol 91

Figure 2.7. Colocalisation measurement protocol 94

Figure 2.8. Principle of the FRET phenomenon 96

Figure 2.9. Overview of the pmEpac2 Sensor 97

Figure 2.10. Overview of FRET Microscopy system. 99

Figure 2.11. Illustration of FRET experiment calculation 100

Figure 2.12. Overview of CytoCypher setup 101

Figure 2.13. Illustration of the acquisition screen of the CytoCypher system 101

Figure 2.14. Illustration shows a single transient of sarcomere and calcium produced in a cardiomyocyte. 102

Figure 2.15. Overview of the cardiomyocyte morphology analysis using CytoSpectre software ... 103

Figure 2.16. Summary of the cell preparation study protocol for CytoCypher experiment.....104
Figure 2.17. Illustration of the balloon stretched model 108
Figure 2.18. Illustration of Langendorff-optical mapping set up 109
Figure 2.19. Examples of voltage and calcium traces 112
Figure 3.1. Examples of FRET Response and analysis stages demonstrating the role of different pharmacological stimuli in enhancing cellular cAMP responses.....123
Figure 3.2. Hypoosmotic swelling reduces the number of caveolae in cardiomyocytes. 126
Figure 3.3. Hypoosmotic swelling increases the width of rat left ventricular cardiomyocytes rather than cell length. 127
Figure 3.4. The t-tubule of cardiomyocytes does not alter in hypoosmotic swelling.....128
Figure 3.5. The Transverse-Axial Tubule network in MβCD treated did not alter in hypoosmotic swelling 129
Figure 3.6. Caveolin-3 distribution was not altered after hypoosmotic swelling. 130
Figure 3.7. Hypoosmotic swelling causes an increase in β_2-adrenoceptor induced cAMP release. 132
Figure 3.8. No difference of %total cAMP output in two isosmotic solutions (118mM NaCl vs 81mM NaCl + 75mM Mannitol).....133
Figure 3.9. Hypoosmotic swelling increases β_2AR but not β_1AR-induced contractility 135
Figure 3.10. Hypoosmotic swelling did not alter the calcium transient following β_1AR and β_2AR stimulation 136
Figure 3.11. the increased in β_2AR induced cAMP release following hypoosmotic swelling is lost in MβCD treated cells. 137
Figure 3.12. Hypoosmotic swelling did not alter the sarcomere shortening in MβCD treated cells following both β_1AR and β_2AR stimulation 139
Figure 3.13. Hypoosmotic swelling did not alter the calcium transient in MβCD treated cells following β_1AR and β_2AR stimulation.....140
Figure 3.14. Representative traces of sarcomere shortening in isosmotic (black) and hypoosmotic (blue) cells, (A) (B) without and (C) (D) with PTX pretreatment.....142
Figure 3.15. PTX treatment abolishes increased β_2AR activity following hypoosmotic swelling....143
Figure 4.1. Schematic diagram of β_2AR regulation 153
Figure 4.2. Example of FRET response and drug protocol used in the FRET microscopy experiment 159
Figure 4.3. PDE4 Inhibition Enhances β_2AR Responses and Equilibrates Cell Contractile Responses to β_2AR Stimulation Following Hypoosmotic Swelling.....162
Figure 4.4. PDE4 Inhibition enhances β_2AR-cAMP activity in both iso-and hypoosmotic cells.....163

Figure 4.5 PDE4D predominately contributes to β_2AR signalling in sarcomere shortening response in Adult Rat LV cardiomyocyt 164
Figure 4.6 PDE4D inhibition enhances β_2AR-cAMP activity in both iso-and hypoosmotic cells and doesn't have any further elevation after PDE4 inhibition 165
Figure 4.7. Decrease in β_2AR-mediated cAMP production in hypoosmotic cells following PDE4D inhibition 166
Figure 4.8. Cav3 colocalises with PDE4D, but the colocalisation is disrupted following hypoosmotic swelling 168
Figure 4.9. PDE4B contributes to β_2AR signalling in sarcomere shortening response in adult rat LV cardiomyocytes 170
Figure 4.10. PDE4B inhibition enhances β_2AR-cAMP activity in both iso-and hypoosmotic cells and only isosmotic cells have further elevation after PDE4 inhibition 171
Figure 4.11 Hypoosmotic swelling decreases colocalisation of Cav3 and PDE4B in adult rat ventricular cardiomyocytes. 173
Figure 4.12. PDE4D5-β-arrestin disruptive peptide removes the enhanced β_2AR induced contractility following hypoosmotic swelling 175
Figure 5.1 Hypoosmotic swelling reduces the number of caveolae in both apical and basal cardiomyocytes 193
Figure 5.2. Hypoosmotic swelling increases the width, rather than the length, of rat left ventricular cardiomyocytes in both the apical and basal regions 194
Figure 5.3. Basal cardiomyocytes show higher T-tubule organisation than apical cells, while hypoosmotic solution has no effect on T-tubules. 195
Figure 5.4. Basal cardiomyocytes show higher caveolin-3 density than apical cells, while hypoosmotic solution does not affect caveolin-3. 196
Figure 5.5. Hypoosmotic swelling enhances β_2AR-cAMP activity in basal cardiomyocytes 197
Figure 5.6. Hypoosmotic swelling enhances sarcomere shortening following β_2 stimulation in basal, but not apical, cardiomyocytes 198
Figure 5.7 Illustration of optical mapping of transmembrane voltage in sham and stretched rat hearts. 200
Figure 5.8. Optical mapping of transmembrane voltage in sham and stretched rat hearts. 201
Figure 5.9 Illustration of optical mapping of intracellular calcium transient in sham and stretched rat hearts. 203
Figure 5.10 Optical mapping of intracellular calcium transient in sham and stretched rat hearts. 204
Figure 5.11 Time to peak (TTP) of calcium transients in sham and stretched rats. 205

Figure 6.1. Biometric data in rat age-matched control hearts and hearts with myocardial infarction. 225

Figure 6.2 Hypoosmotic swelling increases the width of rat left ventricular cardiomyocytes but not length in both control and MI group..... 226

Figure 6.3. Hypoosmotic stress did not alter the T-tubule (TT) network in control and failing cardiomyocytes..... 228

Figure 6.4. Cav3 Density was increased in the failing cardiomyocytes..... 229

Figure 6.5 Hypoosmotic swelling enhances cAMP production following β_2AR stimulation, but the effect is lost in MI cells..... 231

Figure 6.6 Hypoosmotic swelling enhances sarcomere shortening following β_2AR stimulation, but the effect is lost in MI cells..... 232

Figure 6.7. Sarcomere shortening is greater following β_1AR stimulation, while hypoosmotic swelling does not affect sarcomere shortening following β_2AR stimulation in human donor cardiomyocytes. 234

Figure 6.8. Sarcomere shortening following β_2AR stimulation is equal to that produced by the β_1AR stimulation in human DCM cardiomyocytes 236

Figure 6.9. Enhanced cAMP production in DCM cardiomyocytes following β_2AR stimulation 237

List of Tables

Table 2.1. List of reagents used in this project 79

Table 2.2. List of antibodies used in the immunostaining.....93

Table 3.1. The list of solutions and their compositions used in the experiments for Chapter 3. 119

Table 4.1. The list of solutions and their compositions used in the experiments for Chapter 4. 157

Table 5.1 The list of solutions and their compositions used in the experiments for Chapter 5 187

Table 6.1 The list of solutions and their compositions used in the experiments for Chapter 6. 219

Table 6.2. Clinical characteristics of heart failure patient. 221

List of Abbreviations

AA	Antibiotic-antimycotic
AC	Adenylyl cyclase
APD	Action potential duration
AVN	Atrioventricular node
$CaCl_2$	Calcium chloride
$Ca_v1.2$	L-type calcium channels
cAMP	Cyclic adenosine 3’ 5’-monophosphate
Cav	Caveolin
CFP	Cyan fluorescent protein
cGMP	Cyclic guanosine monophosphate
CICR	Calcium-induced calcium release
CL	Cytoplasmic loop
CMOS	Complementary metal oxide semiconductor
cMyBP-C	Calcium myosin binding protein C
Co-IP	Co-immunoprecipitation
CSD	Caveolin scaffolding domain
DCM	Dilated cardiomyopathy
DMSO	Dimethyl sulfoxide
ECC	Excitation-contraction coupling
ERK	Extracellular signal-regulated kinase
FBS	Fetal Bovine Serum
FRET	Förster resonance energy transfer
GFP	Green fluorescent protein
G_i	Inhibitory G protein
GPCR	G-protein coupled receptor
GRK	G protein-coupled receptor kinase
GRK2	G protein-coupled receptor kinase 2
G_s	Stimulatory G protein

HBSS	Hanks'Balanced Salt Solution
HF	Heart failure
HFpEF	Heart failure with preserved ejection fraction
HFrEF	Heart failure with reduced ejection fraction
IBMX	3-Isobuytl-1-methylxanthine
ICM	Ischaemic cardiomyopathy
I_k	Delayed rectifier K^+ current
I_{KATP}	ATP activated potassium current
I_{to}	Transient outward K^+ current
IR	Ischaemia-reperfusion
JPH2	Junctophilin-2
KCl	Potassium chloride
KH	Krebs-Henseleit
LAD	Left anterior descending
LTCC	L-type calcium channel
LV	Left ventricule
$MgSO_4 7H_2O$	Magnesium sulfate heptahydrate
MI	Myocardial infarction
MOI	Multiplicity of infection
MβCD	Methyl-β-cyclodextrin
NaCl	Sodium chloride
NADH	Nicotinamide adenine dinucleotide
NCX	Sodium-calcium exchanger
NTA	Nitrilotriacetic acid trisodium salt
OCT3	Organic cation transporter 3
PBS	Phosphate buffered saline
PC	Pearson's coefficient
PDE	Phosphodiesterase
PFA	Paraformaldehyde
PKA	Protein kinase A
PLB	Phospholamban

PostC	Post-conditioning
PROTAC	Proteolysis targeting chimera
PreC	Pre-conditioning
PTX	Pertussis toxin
ROI	Region of interest
RyR	Ryanodine receptor
SAN	Sinoatrial node
SEM	Standear error of the mean
SERCA2α	SR calcium-ATPase 2α
SFR	Slow force response
SR	Sarcoplasmic reticulum
TAC	Transverse aortic constriction
T-tubule	Transverse tubule
TM	Transmembrane domain
Tnl	Troponin
TTB	Time to baseline
TTP	Time to peak
UCR	Upstream conserved region
YFP	Yellow fluorescent protein
β_1AR	β_1-adrenergic receptor
β_2AR	β_2-adrenergic receptor
βAR	β-adrenergic receptor

Chapter 1: General Introduction

The heart, a muscular organ essential for body homeostasis, is organised into four chambers that function as two pumps (right and left), supplying blood to the pulmonary and systemic circulations. The right atrium collects deoxygenated blood from the body via the vena cava and coronary sinus, passing it through the tricuspid valve into the right ventricle. The right ventricle then pumps this blood through the pulmonic valve to the lungs for oxygenation. Oxygenated blood returns to the left atrium via the pulmonary veins, flows through the mitral valve into the left ventricle and is pumped through the aortic valve to the systemic circulation (Rehman and Rehman, 2024). The adult mammalian heart consists of various cell types, with cardiomyocytes, fibroblasts, endothelial cells, and perivascular cells being the most predominant (Zhou and Pu, 2016). In this thesis, we focused specifically on the cardiomyocytes.

1.1 Structure of Cardiomyocytes at the Subcellular Level

The myocardium is a well-structured tissue composed of various cell types, including smooth muscle cells, fibroblasts, and cardiomyocytes. Cardiomyocytes are particularly significant, making up about 75% of the total volume of the myocardium, and are the primary cells responsible for contraction in the heart (Moore et al., 1980). These cells are characterised as rod-shaped, bi-nucleated, and striated contractile muscle cells, with sizes ranging from 60 to 140 μm in length and 17 to 25 μm in diameter (Tracy and Sander, 2011). Each cardiomyocyte contains a lipid bilayer membrane known as the sarcolemma, which forms the intercalated disks and the transverse tubular system. The intercalated disks function as strong bonds between myocytes, providing cell-cell junctions and enabling rapid action potential conduction between them. Meanwhile, the transverse tubular system, an invagination of the

sarcolemma, extends the extracellular spaces into the interior of the cell and plays an important role in excitation-contraction coupling (Walker and Spinale, 1999).

1.1.1 Caveolae and Caveolins

Caveolae, first identified by Palade in the 1950s within endothelial cells of rat capillaries using electron microscopy, are described as flask-shaped membrane invaginations measuring 50-100nm in diameter (Palade G, 1953). They are a subset of lipid rafts, enriched in cholesterol and sphingolipids. The distinctive invaginated structure of caveolae is formed through the interaction and oligomerisation of the scaffold protein caveolin with cholesterol, a feature that sets caveolae apart from other lipid rafts (Simons and Ikonen, 1997, Rothberg et al., 1992). Cholesterol is a key component for the formation and maintenance of caveolae, as its depletion leads to the flattening of the invaginations and may result in their reduction or complete removal from the cell (Dreja et al., 2002).

Caveolae are found in the plasma membrane of various cell types. Within the heart, they are found in all cell types that comprise the myocardium, including cardiomyocytes, fibroblasts, vascular smooth muscle cells, and endothelial cells (Norman et al., 2018). As one of the important nanodomains within the cardiomyocytes, caveolae have multiple functions, including acting as signalling platforms, facilitating endocytosis and transcytosis, maintaining membrane lipid homeostasis, and sensing and buffering mechanical membrane stress.

1.1.1.1 Caveolins

Caveolae are largely composed of protein caveolin. Caveolin is synthesised within the endoplasmic reticulum, exported from it as small (~20kDa) oligomeric structures, and subsequently transported to the plasma membrane (Monier et al., 1995). Caveolin has three

isoforms, caveolin-1, -2 and -3 (Cav1, Cav2 and Cav3). Although they are highly homologous, they differ in their distribution across various tissues, and therefore, their specific roles relative to signal transduction. Cav1 and Cav3 are essential for caveolae formation; Cav1 is expressed in most cell types, including endothelial cells, epithelial cells, fibroblasts and smooth muscle cells, whereas Cav3 is mainly expressed in striated muscle cells. Cav2 does not independently form caveolae but associates with Cav1 in hetero-oligomers.

Caveolins consist of four parts: an NH_2-terminal domain, an α-helical caveolin scaffolding domain (CSD), a membrane domain, and a COOH-terminal domain (Figure 1.1). The NH_2-terminal domain of Cav1 includes a phosphorylation site at Tyr^{14}, which recruits signalling molecules in response to shear or osmotic stress in endothelial cells when phosphorylated (Radel and Rizzo, 2005). Cav3 is unique in that, instead of Tyr phosphorylation site, it contains an ubiquitination or SUMOylation site, which takes part in the regulation of the β_2AR desensitisation by Cav3 in response to agonist stimulation (Fuhs and Insel, 2011). The CSD is the most prominent domain of caveolin, playing a crucial role in interactions with other proteins and modulating a large number of signalling molecules (Couet et al., 1997). It is also critical for cholesterol binding and recognition, which is essential for caveolae formation (Hoop et al., 2012). The membrane domain allows interaction with the plasma membrane lipids and positions both the NH2- and COOH-termini of caveolin towards the cytoplasm. The COOH-terminal domain, which shows a high level of similarity across the caveolin protein family, plays a role in maintaining caveolin stability and attaching these proteins to the plasma membrane (Busija et al., 2017).

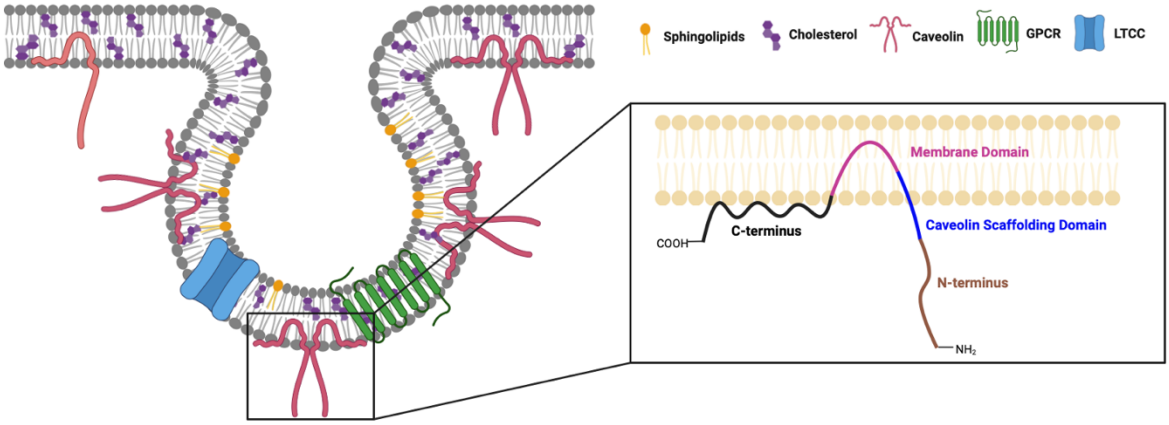


Figure 1.1. Structure of caveolae and caveolin. Caveolae are small invaginations in the plasma membrane, enriched in cholesterol and sphingolipids, which also contain various signalling molecules. Caveolin, the scaffold protein in the caveolae, organises and stabilises their structure and comprises four domains: the N-terminus (brown), the caveolin scaffolding domain (blue), the membrane domain (pink) and the C-terminal (black) (figure created with BioRender).

Caveolae are abundantly present in the heart, particularly in the ventricular cardiomyocytes. Cav3, the cardiac muscle-specific isoform, is predominantly expressed as homo-oligomers and is a crucial component for the development of caveolae in adult cardiomyocytes (Sargiacomo et al., 1995, Balijepalli et al., 2006). While Cav1 and Cav2 are not detected in either ventricular lysate or cardiomyocytes, they are present in other myocardial cells, such as endothelial cells (Yarbrough et al., 2002, Balijepalli and Kamp, 2008, Woodman et al., 2002). In addition, Cav3 expression correlates with the cardiac growth rate; initially low at birth, it increases postnatally, peaking around day 5, and then stabilises in adult cardiomyocytes (Ratajczak et al., 2005). Cav3 is found on the surface plasma membrane and T-tubular membranes of cardiomyocytes, and it has been implicated in the T-tubule formation (Bryant et al., 2018b). It is believed that T-tubules formation starts from specific plasma membrane invaginations that were related to caveolae, a theory dating back to early studies (Forbes et al., 1984).

The role of caveolae in vesicular transport has been well described. Several studies have shown that cells mainly use caveolae to transfer certain molecules across the plasma membrane into the intracellular compartments, in a similar but somewhat different fashion to the traditional uptake machinery via vesicle budding and fusion processes (Fielding and Fielding, 1995). There is also growing evidence showing that the caveolae may act as a signalling platform contributing to the different signalling cascades .

1.1.1.2 Caveolae in Response to Mechanical Stimuli

In various cell types, such as endothelial cells, skeletal muscle cells, cardiomyocytes, and fibroblasts, caveolae exhibit flattening and integrate into the cell membrane as a protective mechanism against cell stretching (Sinha et al., 2011, Kozera et al., 2009, Dulhunty and Franzini-Armstrong, 1975). This process is reversible, allowing caveolae to reassemble at the plasma membrane once the stretch is released (Figure 1.2). Flattened caveolae provide an extra amount of membrane, which buffers membrane tension during mechanical stress and prevents the cell from lysis or rupture. This response is also observed in cells depleted of ATP as well as in vesicles derived from actin-deficient membranes. This suggests that the response is actin- and ATP-independent, indicating that the ability to buffer membrane tension is linked to caveolae themselves (Sinha et al., 2011). Similarly, Kohl et al. observed caveolae unfolding and their incorporation into the sarcolemma during acute ventricular loading in cardiomyocytes (Kohl et al., 2003). Consistent with this, Kozera et al. suggested that caveolae serve as a reserve for the cell membrane, and are involved in the moderation of the membrane tension that occurs during stretch (Kozera et al., 2009). The authors further proposed that this role helps limit the activation of mechanosensitive channels in response to stretch, as disruption of caveolae using methyl-β-cyclodextrin (MβCD) in cardiomyocytes

promoted activation of swelling-activated chloride channels. A study by Pfeiffer et al. also highlighted the role of caveolae in modulating mechanotransduction pathways. They concluded that the stretch slows the ventricular action potential propagation, and it was dependent on the caveolae, as stretch-dependent slowing of conduction was reduced in MβCD treated cells and Cav3KO mice (Pfeiffer et al., 2014). Additionally, Medvedev et al. showed in Langendorff-perfused mouse hearts, pressure/volume overload caused cardiomyocyte stretching and a decrease in caveolae density. In isolated atrial cells, caveolae disruption through hypotonic challenge led to a transient increase in calcium transients, an increase in calcium spark activity, a rise in cAMP levels, and importantly, enhanced PKA-mediated phosphorylated ryanodine receptors (Medvedev et al., 2021). Caveolae deformation following hypoosmotic stress in the smooth muscle cells also induced β_2AR-Gaq mediated calcium release from intracellular stores (Yang and Scarlata, 2017). Taken together, these findings highlighted caveolae as a mechanosensing complex that plays a crucial role in mechanotransduction and cardiac electrophysiology.

In many studies, a hypoosmotic swelling model was used to increase membrane tension. In cardiomyocytes exposed to hypoosmotic condition for 30min, there were no remaining caveolae on the plasma membrane, without changes in sarcomere length (Kohl et al., 2003). Exposure of cardiomyocytes to a hypoosmotic solution for 10 min resulted in a 50% reduction in caveolae number (Kozera et al., 2009). Additionally, swelling caused an increase in cell width, but not in cell length (Gonano et al., 2014). Caveolae integrate into the cell membrane during stretch, thereby exposing the proteins contained within the caveolae to the extracellular environments. This exposure could lead to those proteins becoming spatially activated, subsequently affecting signal transduction. Furthermore, this integration might alter the

activity of proteins within caveolae that interact with caveolin, thereby affecting the associated signalling pathways.

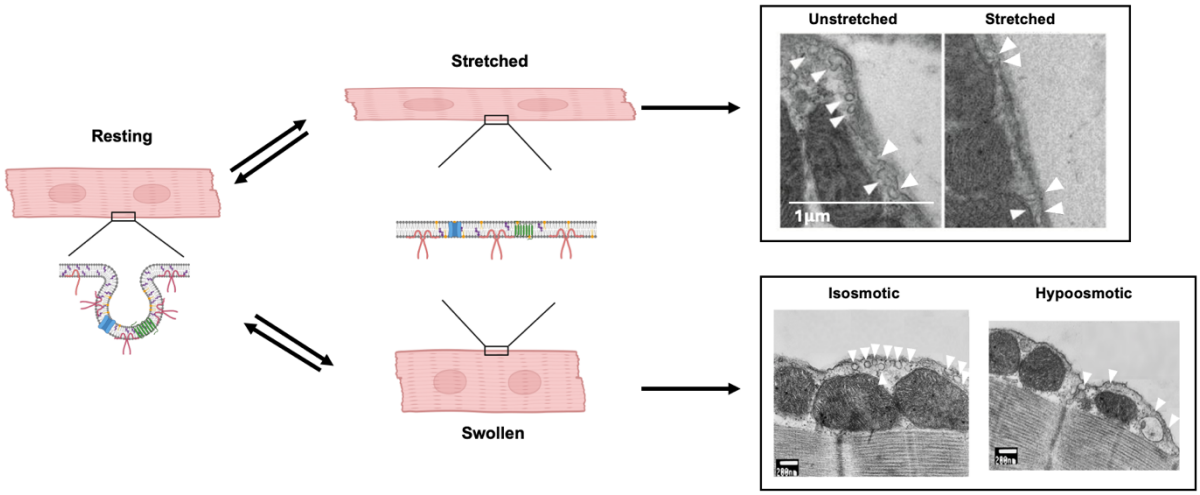


Figure 1.2. Cells respond to stretch by disassembling and reassembling the caveolae. Under resting conditions, caveolae present at the plasma membrane as flask-shaped structures. When subjected to mechanical stretch, such as hypoosmotic swelling, the caveolae integrate into the plasma membrane, thereby buffering the membrane tension. The caveolae reassemble at the plasma membrane upon returning to the resting conditions (Figure adapted from (Sinha et al., 2011, Pfeiffer et al., 2014, Kozera et al., 2009) and created with BioRender).

1.1.1.3 Caveolae, Caveolin and Cardiac Disease

Alterations in caveolae and the expression of caveolar proteins, including Caveolin-3 (Cav3), have been linked to a range of cardiovascular diseases, such as ischaemia-reperfusion (IR) injury, heart failure, cardiac hypertrophy, and myocardial infarction (MI).

During IR injury, cardiomyocytes swell due to the accumulation of metabolites, and caveolae serve as protective structures that prevent membrane rupture during swelling. Besides their structural role, caveolae also play key roles in pre-conditioning (PreC) and post-conditioning

(PostC), which help reduce IR injury. Studies have shown that PreC and PostC stimuli increase the number of caveolae in cardiomyocytes, enhancing their protective function. Cav3 overexpression mimics ischaemic Prec, increasing caveolar formation and activating the phosphorylation of survival kinases, thereby reducing infarct size in the heart (Tsutsumi et al., 2008). Furthermore, cardioprotective ERK1/2 signalling, which is activated during PostC, is transmitted from caveolae to mitochondria to augment mitochondrial antioxidant function. However, when MβCD disrupts caveolae formation, such protective signalling pathway is abolished, suggesting the crucial role of caveolae in protecting against IR injury (García-Niño et al., 2017).

Caveolae dysfunction and Cav3 deficiency have also been implicated in the progression of heart failure. A reduction in Cav3 expression has been associated with left ventricular dysfunction. They found that Cav3 mRNA and protein expression were significantly decreased in mice with A1-adenosine receptor-induced left ventricular dysfunction (Feiner et al., 2011). Similarly, mice with 8-week transverse aortic constriction (TAC)-induced cardiac hypertrophy also showed decreased Cav3 expression and loss of caveolae, suggesting that caveolae-related dysfunction contributes to maladaptive cardiac remodelling. Furthermore, Cav3 Knockout mice develop a progressive cardiomyopathic phenotype with significant dilatation and reduced fractional shortening, leading to contractile dysfunction (Woodman et al., 2002).

Cav3 is also highly enriched in the T-tubule, where it plays a critical role in ion channel localisation and β_2-adrenoceptor (β_2AR) signalling. In rat ventricular cardiomyocytes that underwent 18 weeks of coronary artery ligation, β_2AR and the L-type calcium channel (LTCC) were displaced from T-tubules to the plasma membrane, disrupting compartmentalised signalling. This change was attributed to the loss of Cav3's regulatory function, which is

essential for maintaining T-tubule microdomain integrity (Schobesberger et al., 2017). Additionally, in mice with a dominant-negative Cav3 mutation, β_2AR-cAMP signalling, instead of being localised to T-tubules, which is seen in a normal situation, becomes more generalised and far-reaching, mirroring the patterns seen in heart failure (Wright et al., 2014).

Given these findings, Cav3 has been highlighted as a potential target for heart failure. Multiple studies have shown that Cav3 overexpression attenuates heart failure progression. Overexpression of Cav3 increases caveolae density on the plasma membrane of cardiomyocytes and attenuates the transverse aortic constriction (TAC)-induced cardiac hypertrophy (Markandeya et al., 2015). In rat cardiomyocytes at 16 weeks post-MI, Cav3 overexpression has been shown to partially restore the disrupted β_2AR localisation (Wright et al., 2014). In addition, Cav3 overexpression prevents hypertrophy and the loss of T-tubular calcium current density following TAC in mice (Kong et al., 2019).

1.1.2 Transverse Tubule

The transverse tubule (T-tubule) system is a membranous network extending deep into the cardiomyocytes and is crucial for facilitating excitation-contraction coupling (ECC) (Nakano et al., 2012). Most T-tubules are oriented transversely across the cells along the Z-lines, while some align with the longitudinal axis of the cardiomyocytes, extending into the A-band of the sarcomere (Forbes and Sperelakis, 1976). Thus, the T-tubules are also referred to as the transverse-axial tubule system. T-tubules are responsible for transmitting the action potential generated by the cardiac pacemaker to the sarcoplasmic reticulum (SR) to facilitate electromechanical transduction. T-tubule openings can be visualised in the confocal fluorescent images of control cells stained with Di-8-ANNEPS. Additionally, using the scanning

ion conductance microscopy (SICM), these openings can be seen on the cellular surface, arranged in a Z-groove structure (Figure 1.3) (Lab et al., 2013).

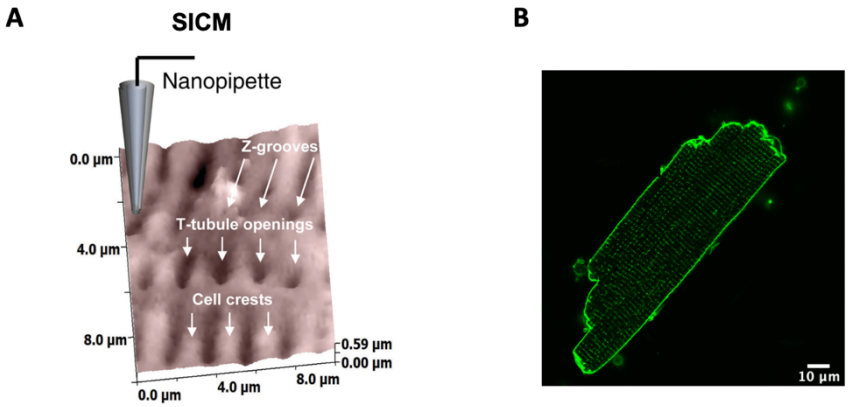


Figure 1.3. Images of T-tubule Structure. A. SICM topographic image of a cardiomyocyte, T-tubule openings and cell crests are arranged in a Z-grooves structure. **B.** Fluorescent image cardiomyocyte with T-tubules labelled with Di-8-ANNEPS (Lab et al., 2013).

1.1.2.1 The Role of Transverse Tubule and Its Associated Proteins

Many of the proteins involved in ECC are localised within the T-tubules. The majority of LTCCs were concentrated in the T-tubules compared to the surface sarcolemma, and they are essential for initiating and regulating ECC (Franzini-Armstrong et al., 1999). Depolarisations generated by action potentials lead to the opening of voltage-gated LTCCs. The entry of calcium from the extracellular space via LTCCs causes a larger amount of calcium release from the SR via the ryanodine receptors (RyRs), this process is called calcium-induced calcium release (CICR). The released calcium then binds to the myofilaments, causing the cells to contract. Following contraction, relaxation takes place as calcium is reabsorbed into the SR by the SR calcium-ATPase 2α (SERCA2α) or is pumped out from the cell by the sodium-calcium exchanger (NCX).

The release of calcium from the SR requires its close alignment with the T-tubule membrane within structures known as "dyads," where LTCCs and RyRs are in close proximity (Sun et al., 1995). Electron microscopy has shown that the dyadic microdomains are approximately 12nm; however, recent data suggest that this space may be narrower, potentially less than 10nm (Takeshima et al., 2000). The spatial distribution between LTCCs and RyRs allows efficient production of CICR, thus generating adequate cardiac contraction (Orchard and Brette, 2008). Moreover, the majority of contractile complexes, including myofilaments, are organised into sarcomeres rather than being close to the surface sarcolemma. In cells lacking T-tubules, calcium propagates to the centre of the cells through diffusion, leading to sub-maximal force production as it activates the sarcomeres on the periphery before reaching those deeper within. The T-tubular system ensures that calcium is in close proximity to all sarcomeres, allowing for simultaneous release of calcium to all sarcomeres, regardless of their depth within the cells, thus generating a larger instantaneous force across the sarcomeres (Hüser et al., 1996).

Besides ion channels, the T-tubular membrane is also enriched in proteins, including Cav3 and junctophilin-2 (JPH2), which critically regulate their structure and function. Research from Bryant et al. demonstrated that Cav3KO mice display cardiac dysfunction in vivo. while isolated ventricular myocytes show cellular hypertrophy, decreased LTCC current density and altered T-tubules organisation (Bryant et al., 2018b). Furthermore, pressure overload induced by 8 weeks of transverse aortic constriction (TAC) in mice leads to a decrease in T-tubular Ca^{2+} current density and impairment of Ca^{2+} release at T-tubules, associated with decreased expression of Cav3 (Bryant et al., 2018a). In addition, mice with Cav3 overexpression showed preserved T-tubular Ca^{2+} current following pressure overload, providing protection against heart failure (Kong et al., 2019).

1.1.2.2 T-Tubule Remodeling and Its Impact on Cardiac Function in Heart Failure

Heart failure (HF) prompts remodelling of the T-tubule network, resulting in reduced T-tubule density, with loss of transversely oriented tubules and increased axially oriented tubules in cardiomyocytes from rats with HF (Schobesberger et al., 2017). Moreover, research on human cardiac samples from various types of HF, including ischaemic, idiopathic dilated, and hypertrophic cardiomyopathy, has also indicated a significant decrease in T-tubule density (Lyon et al., 2009). This reduction is accompanied by increased distances between the T-tubule membrane and the SR, which delays ECC and subsequently diminishes and prolongs contraction (Heinzel et al., 2008).

Studies have shown that chronic mechanical unloading of normal hearts disrupts the T-tubules structure and impairs Ca^{2+} release due to uncoupling of the CICR mechanism, whereas unloading of failing hearts has been shown to reverse the remodelling of the T-tubule structure and improve CICR (Ibrahim et al., 2010a, Ibrahim et al., 2010b). A recent study from Ruud et al. suggested that T-tubule structure varies depending on the degree of load, enabling both compensatory and decompensatory functional remodelling of the heart. The authors demonstrated that T-tubule density in papillary muscles exhibits a bell-shaped relationship with tension. T-tubule growth in response to moderate increases in load is accompanied by enhanced expression of LTCC and increased calcium transients, leading to a compensatory increase in the overall cardiac function. However, when the load becomes excessive, T-tubule density decreases, ultimately resulting in heart failure as the heart continues to experience an increased load (Ruud et al., 2024).

1.2 Cardiac Electro-Excitation

1.2.1 Ventricular Action Potential

Specialised pacemaker cells in the sinoatrial node (SAN) initiate the action potential, which is rapidly conducted across the atria. After a brief delay in the atrioventricular node (AVN), the signal is then transmitted rapidly across the ventricles (Klabunde, 2017). A classic action potential for ventricular cardiomyocytes contains five phases (Figure 1.4). Phase 0 is the fast depolarisation of the cell caused by a rapid increase in sodium conductivity mainly through the opening of $Na_{v1.5}$ Voltage-gated sodium channels in response to an incoming wave of depolarisation from adjacent cells, resulting in the influx of sodium currents (Klabunde, 2017). In phase 1, $Na_{v1.5}$ rapidly inactivates, and there are transient outward potassium currents, I_{to}, through $K_{v4.3}$ voltage-gated potassium channels, resulting in a small degree of repolarisation (Grant, 2009). The continued inward calcium currents through L-type calcium channels ($Ca_v1.2$) lead to phase 2, the prolonged plateau. These calcium channels have much slower kinetics than sodium channels and remain open for longer (Varró et al., 2021). The action potential is then terminated by a phase 3 repolarisation. This returns the membrane to its resting potential, which is driven by the outward currents, including the rapid and slow delayed rectifier potassium currents (I_{Kr} and I_{Ks}, respectively) and adenosine triphosphate (ATP)-activated potassium current (I_{KATP}) (Huang, 2017). Phase 4 represents the resting membrane potential, where the inward rectifying potassium current (I_{k1}) plays a major part in maintaining a stable resting potential (Klabunde, 2017). With repolarisation, $Na_{v1.5}$ channels recover their capacity for re-excitation. Human has a more negative resting potential of -90 mv compared with that of rats -70 mv; this difference may come from the larger density of I_{k1} in human cardiomyocytes (Santana et al., 2010, Joukar, 2021, Huang, 2017). There is a larger density

and high magnitude of I_{to} in rats than in humans, leading to a large initial repolarisation phase and a lack of plateau phase at a lower membrane potential (Wettwer et al., 1993, Varró et al., 1993). In addition, during the contraction cycle, rat ventricular myocytes depend more on calcium release from the sarcoplasmic reticulum rather than calcium influx through the plasma membrane (Terracciano and MacLeod, 1997).

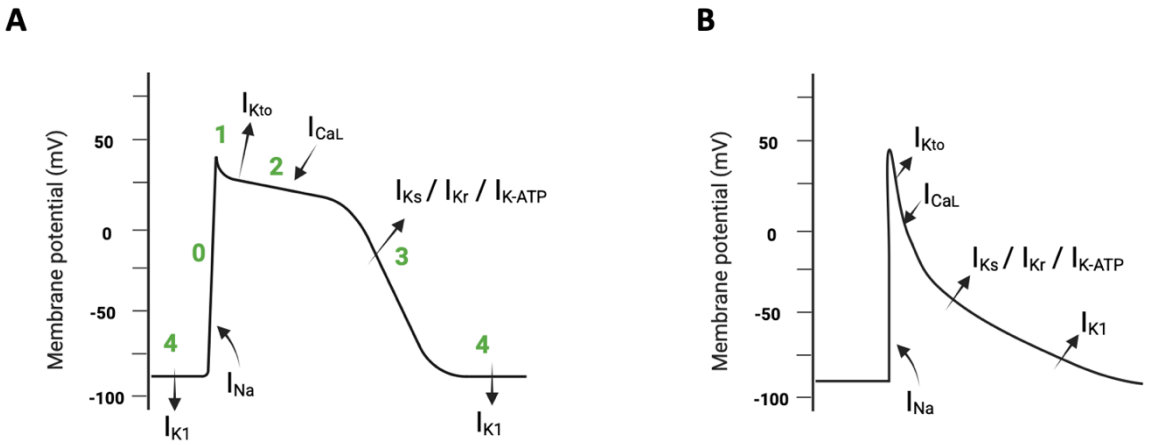


Figure 1.4. Ventricular action potential in (A) human and (B) rat. It contains five phases, phase 0 (depolarisation) is driven by the rapid influx of Na^+ (I_{Na}); Phase 1 (early repolarisation) is mediated by the transient outward K^+ current (I_{Kto}); Phase 2 (plateau phase) is maintained by the continued inward L-type Ca^{2+} current (I_{CaL}); Phase 3 (repolarisation) is dominated by outward K^+ currents (I_{Ks}, I_{Kr}, I_{K-ATP}), restoring the negative membrane potential; and Phase 4 (resting potential) is maintained by the inward rectifier K^+ current (I_{K1}). Figure created with BioRender).

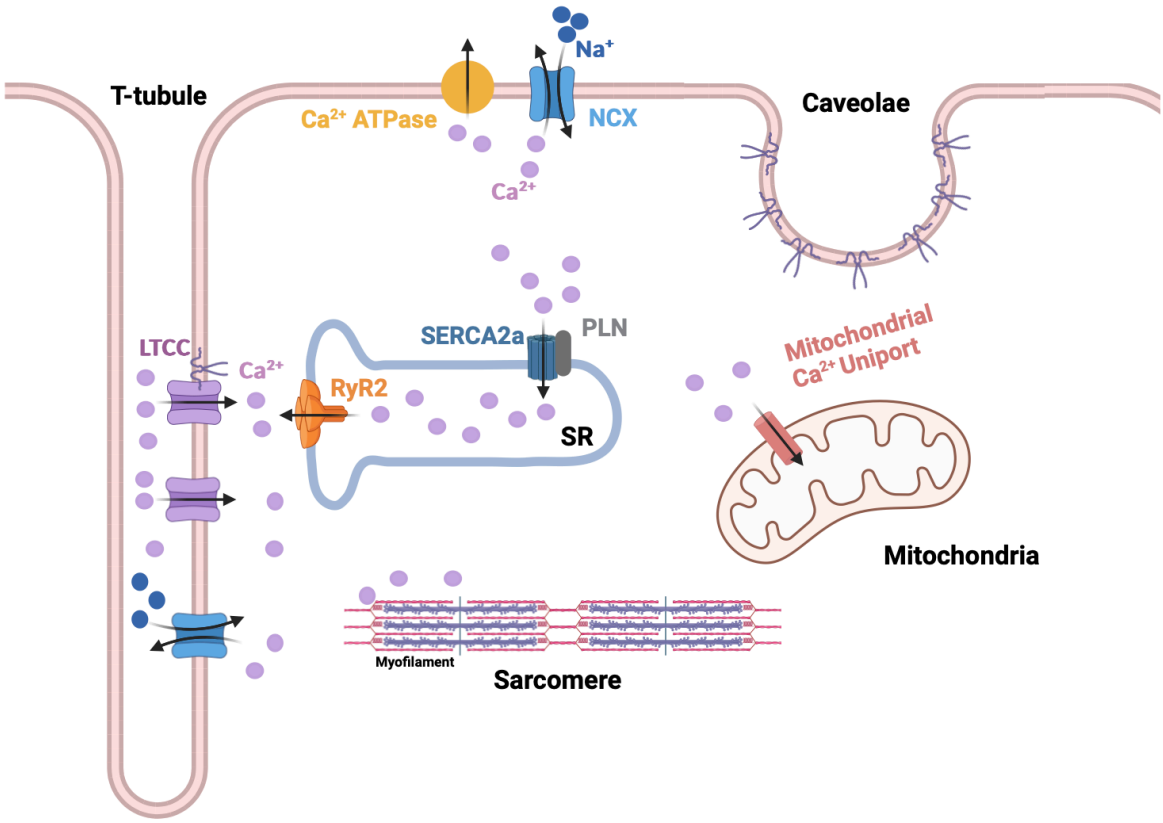


Figure 1.5 Illustration of the excitation-contraction coupling and calcium cycle in a cardiomyocyte. Upon membrane depolarisation, L-type calcium channels (LTCC) located in the T-tubule open, allowing Ca^{2+} influx into the cytoplasm. This triggers calcium-induced calcium release (CICR) from the sarcoplasmic reticulum (SR) through ryanodine receptor 2 (RyR2), leading to a significant increase in intracellular Ca^{2+} concentration. The elevated Ca^{2+} binds to the myofilaments, initiating sarcomere contraction. To facilitate relaxation, cytosolic Ca^{2+} is removed through multiple mechanisms: sarcoplasmic reticulum Ca^{2+}-ATPase (SERCA2a) pumps Ca^{2+} back into the SR; the Na^{+}/Ca^{2+} exchanger (NCX) extrudes Ca^{2+} in exchange for Na^{+}; and sarcolemmal Ca^{2+}-ATPase transports Ca^{2+} out of the cell. In addition, the mitochondrial Ca^{2+} uniporter transfers Ca^{2+} into mitochondria (Figure created with BioRender).

1.3 G-Protein Coupled Receptors and Their Role in Signal Transduction

G-protein-coupled receptors (GPCRs) represent the largest family of membrane proteins and play a key role in transmembrane signal transduction in response to hormones and neurotransmitters. Based on sequence and functional similarities, they are classified into six

classes. A common feature across all these classes is a seven-transmembrane helix structure and the ability to bind and activate G proteins (Smith, 2021).

The heterotrimeric G-protein is composed of three subunits: α, β and γ. In the inactive state, the βγ subunits form a tight complex that is bound to the membrane, while the α subunit is bound to a GDP molecule (Figure 1.6). G-proteins are primarily identified by their Gα monomers, and they can be categorised into four main groups: $G\alpha_s$ (stimulatory), $G\alpha_i$ (inhibitory), $G\alpha_q$, and Gα12/13 (Oldham and Hamm, 2008). When an agonist binds to a GPCR, it facilitates the interaction of the receptor with the GDP-bound Gαβγ heterotrimer. This interaction triggers the replacement of GDP with GTP on the Gα subunit, leading to the dissociation of the G-protein heterotrimer into Gα-GTP and Gβγ subunits (Rasmussen et al., 2011). The activated Gα and Gβγ subunits can now interact with various effective proteins, including channels, kinases, and other enzymes, which may produce diffusible second messengers that may trigger downstream signalling. The interaction between the Gα subunit and the effectors also accelerate the hydrolysis of GTP back into GDP. This enzymatic reaction results in the recombination of Gα-GDP with the Gβγ subunits, effectively ending the signalling process.

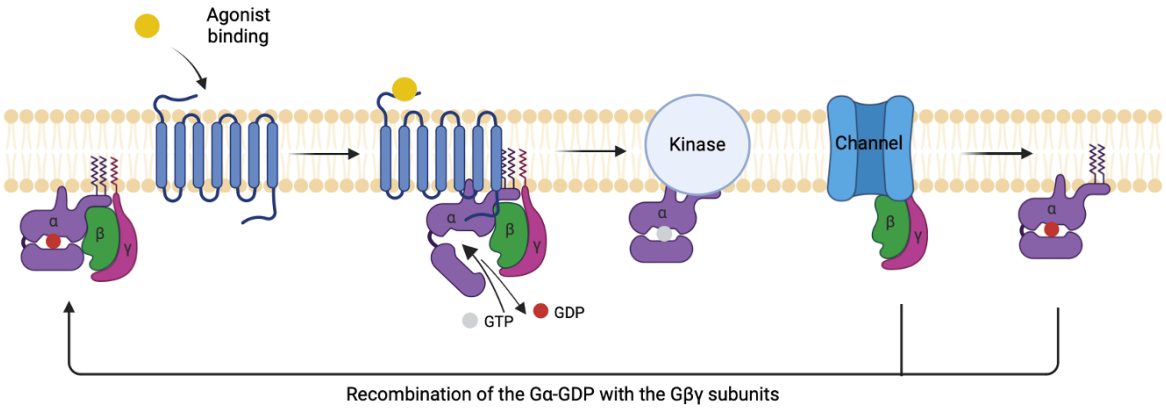


Figure 1.6. Schematic of G protein-coupled receptor (GPCR) cycle. Activation of GPCR via agonist binding changes the structure within receptors, enabling the binding of the Gs heterotrimer, consisting of α, β, and γ subunits, to attach to the receptor. Following the formation of the GPCR-Gs complex, GDP is displaced from the α subunit and exchanged with GTP. This leads to the separation of the α and βγ subunits from the receptor. These subunits then go on to influence their target effector proteins, including channels and kinases. After the GTP on the α subunit is hydrolysed back to GDP, the α and βγ subunits reunite to reform the Gs heterotrimer (figure created with BioRender).

1.3.1 The Structure and Function of β-Adrenergic Receptors in the Cardiomyocytes

Heart tissue responds very dramatically to the stimulation by catecholamines: adrenaline (epinephrine) and noradrenaline (norepinephrine). There are several receptors that can be stimulated by adrenaline, but in the cardiomyocytes, the most important ones are β-Adrenergic Receptors (βARs). These receptors are class A rhodopsin-type GPCRs; they consist of seven transmembrane-spanning α-helices domains, an extracellular N-terminal region, and an intracellular C-terminal region (Figure 1.7). The extracellular region contains the ligand binding site, while the intracellular region is involved in interactions with G proteins and other proteins that provide scaffolding and signalling functions (Ahles and Engelhardt, 2014).

β_1 and β_2ARs are the predominant βAR subtypes expressed in the cardiac tissue; they play important roles in regulating cardiomyocyte contraction and growth. β_1 comprises 75-80% of the βARs found in the heart, while β_2 comprises 20-25% of cardiac βARs (Madamanchi, 2007).

The transmembrane regions of β_1 and β_2ARs share 67% sequence homology (Warne et al., 2008). In the intracellular region, three cytoplasmic loops (CL1, CL2 and CL3) are crucial for the strength of the interaction and the specificity of G proteins. Studies have shown that CL2 in β_1AR forms a short α-helix, whereas in β_2AR, this loop is in an extended conformation (Warne et al., 2008) (Figure 1.7B). Additionally, examination of crystal structures of β_1 and β_2AR has revealed that, while their extracellular catecholamine-binding sites are identical, notable differences exist in the shapes and the charge distribution of their extracellular vestibules, in particular close to the entrance to the ligand binding site (Xu et al., 2021) (Figure 1.7C). These less conserved parts significantly contribute to the selectivity and affinity of the ligands and also to the specificity and the activation of G proteins, thereby giving the two isoforms distinct functions.

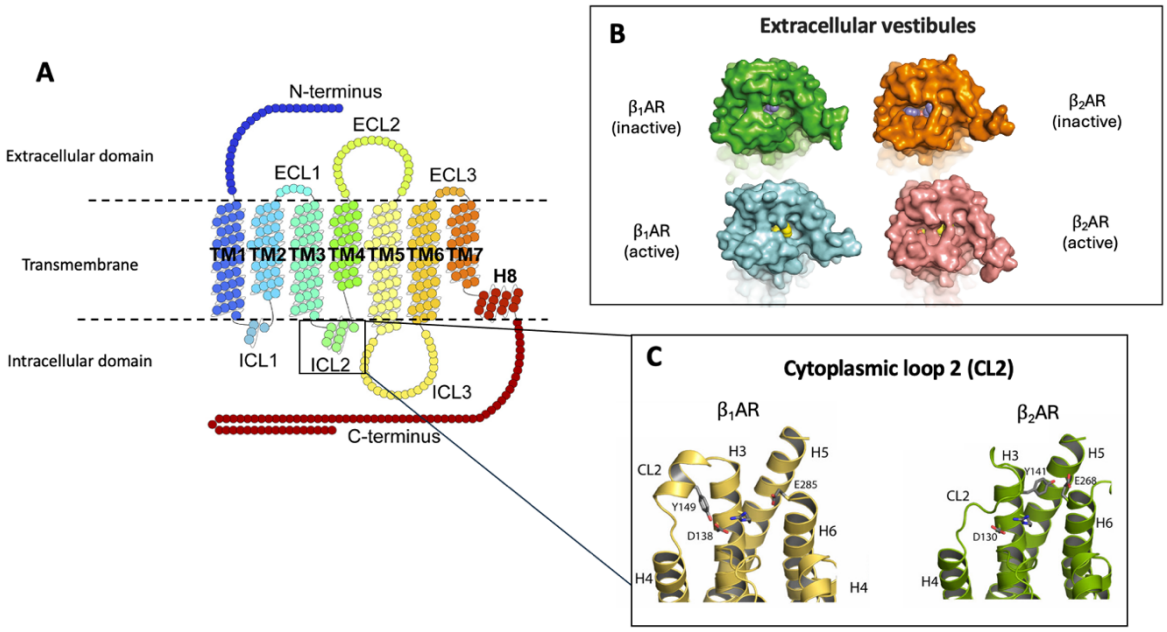


Figure 1.7. Schematic diagram of the GPCR and the comparison between β_1AR and β_2AR structures. A. Schematic view of the overall structure of a G protein-coupled receptor (GPCR). They consist of seven transmembrane domains (TMs), three extracellular loops, and three intracellular loops, with an extracellular N-terminus and intracellular carboxyl terminus. **B.** Comparison of the extracellular vestibules of inactive and active β_1AR with those of inactive and active β_2AR. **C.** Comparison of the CL2 loop regions between β_1AR and β_2AR (Figure adapted from (Xu et al., 2021) and created with BioRender).

In healthy cardiomyocytes, β_1ARs are distributed across the cell crests and T-tubules, while β_2ARs are uniquely localised to the caveolae and T-tubules regions (Nikolaev et al., 2010). Activation of β_1ARs enhances cardiac contractile force, an inotropic effect, and promotes a faster cardiac relaxation, referred to as a lusitropic effect. In addition, adrenaline increases the rate of contraction, referred to as a chronotropic effect. In adult rat ventricular myocytes, β_1AR stimulation results in a higher inotropic effect as compared to β_2AR stimulation, in addition, the lusitropic effect is only seen after β_1AR but not β_2AR-mediated stimulation, which suggests significant variations in the intracellular signalling pathways triggered by β_2AR compared to those initiated by β_1AR (Xiao and Lakatta, 1993). According to studies by Xiao et al., β_2AR stimulation can activate G_i proteins in parallel with the activation of G_s proteins, which have

functionally opposite effects. The concurrent coupling to G_i proteins can completely negate the G_s-mediated contractile response. Indeed, pretreatment with pertussis toxin (PTX), a G_i blocker, potentiated the contractile response to the β_2AR agonist zinterol in rat ventricular cardiomyocytes, making it similar to that of β_1AR stimulation. This reversed the differences observed between β_1AR and β_2AR (Xiao et al., 1995). Furthermore, activation of G_i protein by β_2AR can be blocked by either treating with PTX or using a β_2AR blocker, ICI 118,551. However, stimulating β_1AR under the same conditions does not increase G_i protein activity, indicating that G_i protein activation is specifically linked to β_2AR (Xiao et al., 1999a).

As described above, β_1ARs couple with the stimulatory $G\alpha_s$. Stimulation of β_1ARs through agonist binding activates adenylyl cyclase (AC), leading to the production of cyclic adenosine 3',5'-monophosphate (cAMP). This increase in cAMP levels subsequently activates protein kinase A (PKA), which plays a critical role in phosphorylating various downstream targets. These targets, such as LTCC, RyR, phospholamban (PLB) and troponin I (TnI), are key components in mediating cardiomyocyte contraction and relaxation (Xiao et al., 1999b). Activated LTCCs allow calcium to enter the cardiomyocytes. The increased cytosolic calcium level is further augmented by PKA-mediated phosphorylation of RyR, promoting a significant release of calcium from the SR. Calcium binding to troponin C promotes myosin cross-bridge formation, leading to cardiomyocyte contraction (Layland et al., 2005). PKA also phosphorylates TnI and cardiac myosin binding protein C (cMyBP-C), reducing calcium affinity of the myofilament and thus promoting the dissociation of calcium from the myofilament during diastole. Phosphorylation of cMyBP-C accelerates the cross-bridge detachment rates, leading to cardiomyocyte relaxation. Furthermore, phosphorylation of PLB on the sarcoplasmic reticulum by PKA enhances calcium reuptake into the SR, removing the calcium from the cytosol and facilitating enhanced relaxation (Zhang et al., 2019). β_2AR, as a

pleiotropic receptor, can couple to both $G\alpha_s$ and $G\alpha_i$ in the cardiomyocytes (Rosenbaum et al., 2009, Xiao et al., 1999b). Activation of the β_2AR/ Gαi pathway inhibits cAMP production by inhibiting the activation of AC and the effect is the opposite when coupled with β_1AR/$G\alpha_s$ and β_2AR/$G\alpha_s$. A schematic summary of β_1AR and β_2AR signalling pathways in cardiomyocytes is presented in Figure 1.8.

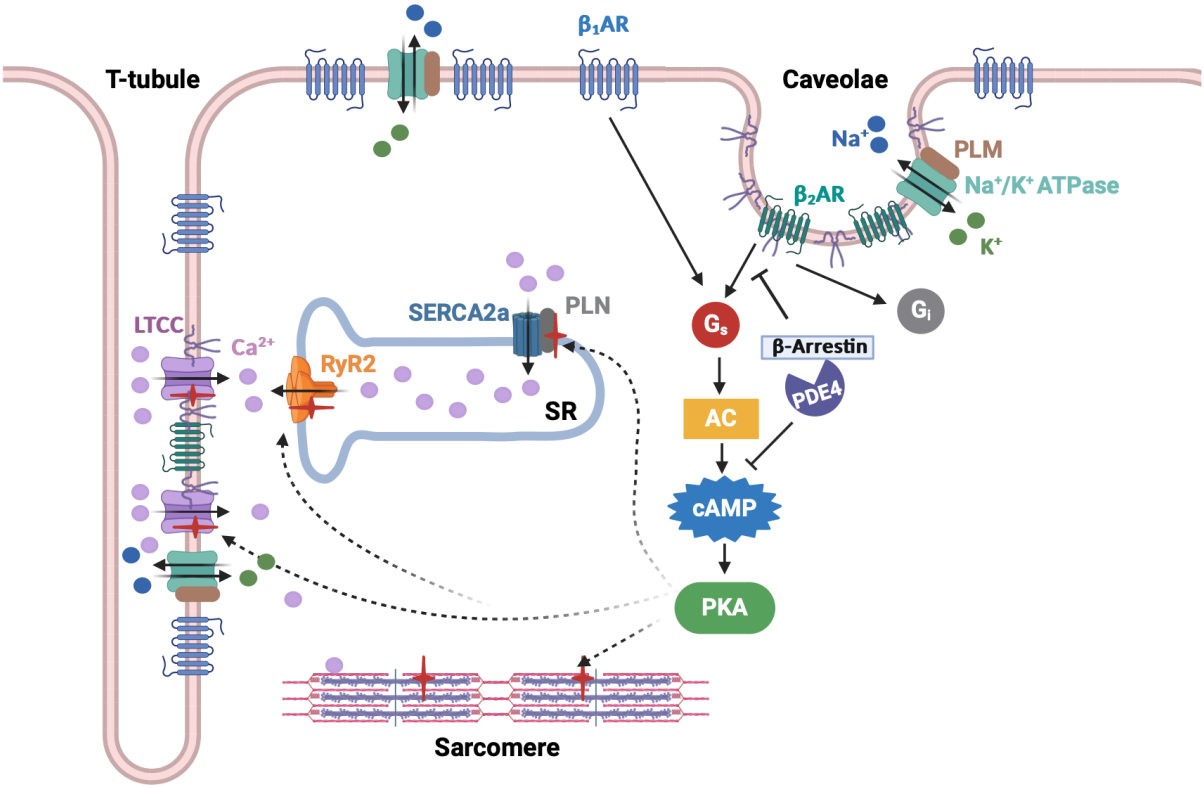


Figure 1.8. Schematic representation of β_1AR and β_2AR signalling in cardiomyocytes. β_1ARs are localised in both caveolae and non-caveolae regions of the cell, while β_2ARs are found exclusively in caveolae and t-tubule regions. Upon activation, β_1ARs initiate the stimulatory G protein (G_s) pathway, activating adenylyl cyclase (AC). This activation results in increased levels of cyclic adenosine monophosphate (cAMP) and protein kinase A (PKA), which subsequently phosphorylates L-type calcium channels (LTCC) and type 2 ryanodine receptors (RyR2). This phosphorylation raises intracellular calcium levels by promoting calcium entry through LTCC and release from the sarcoplasmic reticulum (SR), which stimulates contraction by acting on the sarcomere's myofilaments. Additionally, calcium influx further stimulates RyR2, enhancing calcium release from the SR and augmenting contraction. PKA also targets phospholamban (PLB), which associates with sarcoplasmic reticulum calcium ATPase 2α (SERCA2α), promoting calcium reuptake into the SR and facilitating relaxation. β_2ARs, while activating the same G_s pathway as β_1ARs, can also initiate the inhibitory G protein (G_i) pathway, reducing cAMP production by inhibiting the activation of adenylyl cyclase (AC) and thus decreasing cardiac contractility (figure created with BioRender).

1.2.2 The Compartmentation of β-Adrenergic Receptors

Both β_1AR and β_2AR are coupled to adenylyl cyclase and, when stimulated, lead to an increase in the cellular cAMP level. However, the maximum elevation of the cAMP caused by β_2AR stimulation was only half of what β_1AR stimulation achieved. This suggests that activating different βAR subtypes results in distinct compartmentalisation of cAMP. A study using the patch-clamp method showed that activating either β_1AR and β_2AR within the patch membrane by directly introducing agonists into the patch pipette activates the L-type calcium channels in the patch. However, when the agonist was applied externally to the patch pipette membrane, only β_1AR activation triggered the channel activity. This suggests that β_1AR signalling can diffuse through the cytosol to reach the channels, whereas β_2AR signalling is confined to the membrane area (Chen-Izu et al., 2000). These results are consistent with another study that used a fluorescence resonance energy transfer-based technique to track the spatial and temporal distribution of cAMP. This research revealed that localised activation of β_1AR resulted in a global increase in cAMP across the cardiomyocytes. In addition, a recent study showed that there is a distinct intracellular pool of β_1ARs localised at the SR in the cardiomyocytes, they are functionally coupled to SERCA2 and PLB, enhancing contractility via PKA-mediated PLB phosphorylation (Wang et al., 2021). Unlike plasma membrane β_1ARs, the activation of these intracellular receptors depends on the organic cation transporter 3 (OCT3), as OCT3KO selectively suppresses calcium transients and contraction responses to norepinephrine (Wang et al., 2021). Conversely, when β_2AR was activated using a pipette, it caused a localised increase in cAMP that did not spread through the cell (Nikolaev et al., 2006). In addition, the study found that only β_1AR but not β_2AR stimulation leads to cAMP-dependent phosphorylation of phospholamban in the sarcoplasmic reticulum (Xiao et al., 1994). This might be the reason why β_1AR triggers a strong positive inotropic and lusitropic

effect, whereas β_2AR tends to cause a limited increase in contraction without altering the relaxation rate. Additionally, the localisation of β_2AR signalling relies on the activation of G_i proteins, as study showed β_2AR signalling becomes diffuse and markedly increased PLB phosphorylation that highly comparable with that following β_1AR stimulation in cells treated with pertussis toxin, which inhibits G_i activation. This result suggests that the ability of β_2AR coupled with both G_s- and G_i-proteins creates a localised signalling pathway (Chen-Izu et al., 2000). Furthermore, similar to G_i inhibition, a study found there was enhanced β_2AR-mediated contractile response following treatment with the phosphatase inhibitor, calyculin A, and there was no additive effect following the application of both PTX and calyculin A, suggesting that they act on the same pathway and the spatial restrictive effect of β_2AR signalling pathway might be mediated by modulation of protein phosphatase (Kuschel et al., 1999a).

Another factor that has been attributed to the differences in response between β_1AR and β_2AR might be their localisation - β_2AR exists exclusively in caveolar membrane regions (Head et al., 2005). Caveolae are enriched in various signalling molecules and are thought to serve as a signalling platform, particularly for GPCRs and their downstream signalling components (Patel et al., 2008). All components of β_2AR signalling pathway, including β_2AR, G_s, G_i, AC, PKA and LTCCs have been identified in caveolae-rich membrane (Head et al., 2005, Balijepalli et al., 2006). Several studies highlighted that the caveolae nanodomains play a crucial role in the compartmentation of β_2AR signalling in ventricular cardiomyocytes. A study on isolated rat ventricular cardiomyocytes showed that caveolae depletion using methyl β-cyclodextrin (MβCD) enhances the inotropic response to β_2AR stimulation, but does not alter the response to β_1AR stimulation (Calaghan and White, 2006). Moreover, disrupting caveolae changes the

β_2AR signalling from being confined to the sarcolemma to a global signal affecting the sarcoplasmic reticulum and myofilaments (Calaghan et al., 2008).

1.3.3 β-Adrenergic Receptors in Heart Failure

Heart failure is associated with alterations in βAR populations, with a decreased β_1AR and unchanged β_2AR population (Bristow et al., 1986). In addition, there is uncoupling of the membrane β_1AR and β_2AR from G proteins and an increased myocardial G_i proteins in terminally failing hearts than in controls (Bristow et al., 1982). Surface scans of failing cardiomyocytes using SICM revealed a disrupted surface topography with loss of Z-grooves and T-tubule openings (Lyon et al., 2009). This disruption was linked to the regional repositioning of functional βAR. It was found that the β_2AR-cAMP signal localisation was disturbed, with the cAMP signal propagating along the cardiomyocyte (Nikolaev et al., 2010). This suggests that in heart failure, β_2AR-cAMP signalling shifts from the T-tubules to the cell crest, leading to a more diffusible pattern similar to that of β_1ARs. PKA is considered to be the primary effector of cAMP in cardiomyocytes and is believed to act as a buffer for cAMP. In healthy cells, treatment with the Ht31 peptide, a peptide inhibitor of PKA anchoring, resulted in the propagation of β_2AR-cAMP across the cardiomyocytes (Nikolaev et al., 2010). Immunostaining of the PKA-RII in failing cells showed a loss of the striated PKA localisation pattern. This indicates that the reduced cAMP buffering by PKA and the uncoupling of β_2ARs from the local PKA pools are both responsible for the altered compartmentalisation of β_2ARs signalling, and thus contribute to the altered signalling distribution.

Numerous studies have shown that when subjected to excessive load, the myocardium initially exhibits hypercontractility, and the ventricular cardiomyocytes develop a hypertrophic phenotype with increased contraction and preserved βAR responsiveness.

However, the heart eventually progresses to a more classic failing phenotype, with reduced myocyte contraction, prolonged relaxation, and βAR downregulation. β_2ARs-cAMP signalling in rat left ventricular myocytes was studied at 4-,8-, and 16-week post-MI. β_2ARs induced cAMP production was slightly decreased at 4- and 16-weeks post-MI but increased at 8 weeks. This increase at 8 weeks may be attributed to a hypertrophic compensatory response of the myocardium (Schobesberger et al., 2017). Ruppert et al. investigated ventricular function and structure in relation to sarcomeric function in rats following transverse aortic constriction over 6, 12, and 16 weeks. At 6 weeks post-operation, there was a significant increase in myofilament Ca^{2+} sensitivity and end-systolic pressure-volume relationship, followed by a decrease at 12 and 18 weeks post-operation, indicating an enhanced inotropic rate as a part of a compensatory mechanism and as the condition progresses, these adaptations contribute to the development of heart failure (Ruppert et al., 2019).

1.4 Phosphodiesterases

1.4.1 The Structure and Function of Phosphodiesterases in the Cardiomyocytes

Phosphodiesterases (PDEs) are the only enzymes responsible for degrading cAMP, thus facilitating the compartmentalisation of cAMP, which is crucial for the regulation of cAMP-related cellular functions (Zaccolo, 2006). The PDE superfamily contains 11 different gene families and is the only enzyme family responsible for the hydrolytic degradation of cAMP and cyclic guanosine monophosphate (cGMP) into their inactive forms, 5'-AMP and 5'-GMP, respectively. PDE families are divided into three groups based on their sequence homology and their specific affinity towards cAMP or cGMP. PDE4, PDE7 and PDE8 specifically hydrolyse cAMP; PDE5, PDE6 and PDE9 target cGMP for hydrolysis; PDE1, PDE2, PDE3, PDE10 and PDE11 have dual specificity, meaning they can process both cAMP and cGMP (Azevedo et al., 2014)

(Figure 1.9B). The different PDEs share the following common structural layout: 1) N-terminus which contains targeting domains that are responsible for localisation of the PDE isoform to specific subcellular site, 2) a regulatory region at the N-terminal portion, which contains domains that can be subjected to diverse types of modification, including phosphorylation, and which also serve as a site for effectors binding and protein-protein interaction, 3) a highly conserved catalytic core, and 4) the carboxyl terminus (Barone et al., 2015) (Figure 1.9A).

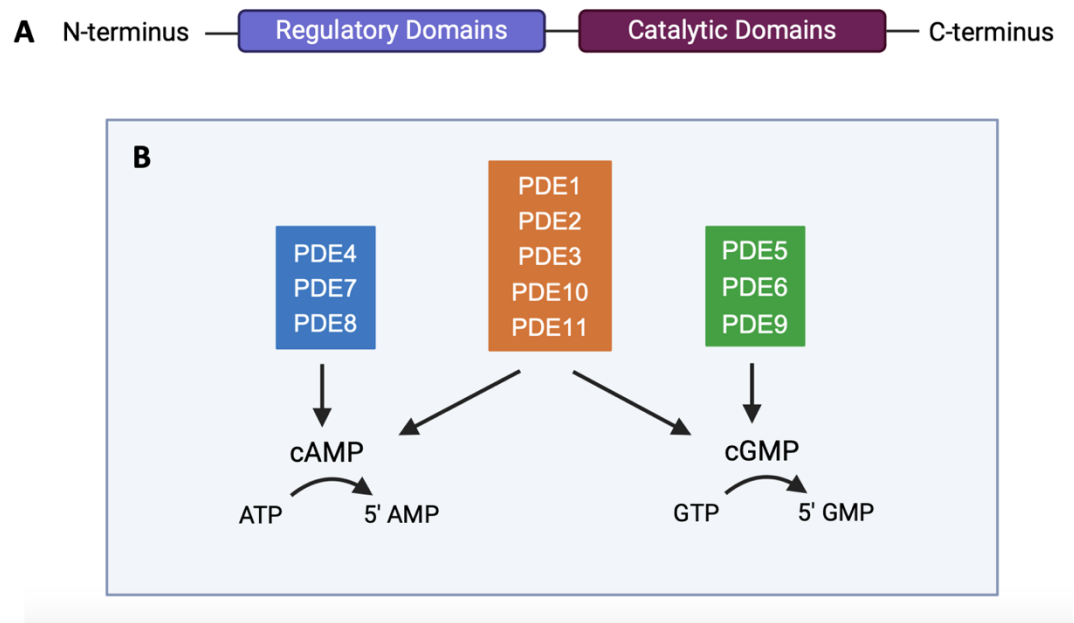


Figure 1.9. Structure and family of PDE. A. General structure of the PDE family. The N-terminal region is crucial for determining their cellular location. Within the regulatory domain, there are sequences unique to each PDE subtype that play a key role in modulating the PDE enzymatic activities. The catalytic domain, located in the C-terminal portion of PDEs, is highly conserved. **B.** The PDE family contains 11 gene families that share structural similarities, some of them specifically target cAMP or cGMP, while others have the ability to act on both (figure created with BioRender).

Among the 11 PDE families, only PDE6, PDE10 and PDE11 are not expressed in the heart (Francis et al., 2011). Of these, PDE3 and PDE4 provide the major PDE activity in the heart. PDE4 accounts for a significant percentage of the total phosphodiesterase (PDE) activity in mice and rats' hearts, contributing 32% and 52%, respectively (Richter et al., 2011) , while PDE3 seems to be a major PDE in human hearts. However, in humans, when PDE3 is inhibited,

PDE4 comes into play and dampens the effect of catecholamines. A study from Leroy et al. suggested that PDE4 is the main PDE subtype modulating βAR cAMP transient, as inhibition of PDE4 increased the amplitude of cAMP, whereas when PDE3 activity was inhibited, there was only a minor effect and only on the subsarcolemmal cAMP pool (Leroy et al., 2008b). Furthermore, application of different PDE inhibitors demonstrated a tight regulation of cAMP after adrenergic stimulation was attributed to PDE4, whereas the cAMP hydrolysing activity via PDE3 was significantly less active (Nikolaev et al., 2006).

1.4.2 The Structure and Function of Phosphodiesterases 4 and its Subtypes in the Cardiomyocytes

The PDE4 is the largest family among all 11 PDEs, containing more than 20 isoforms. These isoforms are encoded by four genes (PDE4A, -B, -C, and -D), and each gene product can be alternatively spliced to generate multiple isoforms. They are divided into long, short, super-short and dead-short forms depending on the presence and length of the upstream conserved region (UCR1) and upstream conserved region 2 (UCR2) domains, which are distinct from the PDE4 hydrolases (Kyurkchieva and Baillie, 2023, Omar et al., 2019) (Figure 1.10). PDE4 isoforms are classified into four groups based on their UCR1/UCR2 composition. The long isoforms contain both UCR1 and UCR2, short isoforms contain only UCR2, and super short isoforms have a truncated UCR2. In contrast, dead-short isoforms lack both UCR1 and UCR2 and have an inactive catalytic domain that is truncated at both the N- and C-termini (Houslay et al., 2007) (Figure 4.1). Studies have shown that among those PDE4 isoforms, in PDE4 long isoforms, UCR1 and UCR2 form a regulatory module for the effects of phosphorylation by PKA and extracellular signal-regulated kinase (ERK) (Baillie et al., 2000, MacKenzie et al., 2002). In the long isoforms of PDE4, the interaction between the UCR1 and UCR2 forms a regulatory

unit. Activation of PDE4 through PKA phosphorylation disrupts the inhibitory effect of UCR1-UCR2, hence increasing cAMP hydrolysis. Unlike the long isoforms, which contain both UCR domains, the short isoforms have UCR2 only and cannot be modulated by PKA. The supershort isoforms are missing UCR1 and contain a truncated UCR2, whereas the dead-short isoforms lack any UCRs and have a truncated catalytic domain (Kyurkchieva and Baillie, 2023).

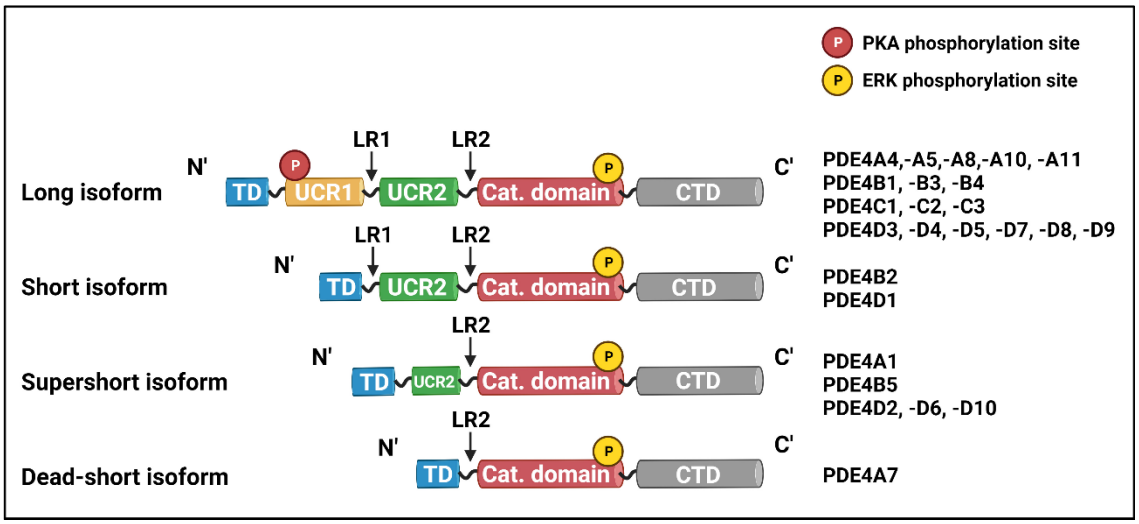


Figure 1.10. Structure of PDE4 isoform. The PDE4 has been classified as long isoform, short isoform, supershort isoform and dead-short isoform depends on the length of their N-terminus. 'TD' represents the targeting domain; 'UCR' means the upstream conserved region; 'LR' refers to the linker region; 'Cat. Domain' is shorthand for the catalytic domain; and 'CTD' is the C-terminal domain (Kyurkchieva and Baillie, 2023).

Richter et al. examined the expression of PDE4 subtypes in rodent and human hearts; they found that in rodents, PDE4A, PDE4B, and PDE4D are expressed at similar levels, while PDE4D is the predominant form found in the human heart (Richter et al., 2011). Earlier research has highlighted the critical role of PDE4D on cardiomyocyte contractility. PDE4D deficient mice have increased baseline cardiomyocyte shortening associated with increased PLN phosphorylation, SR calcium content and calcium transients , without the influence of L-type calcium current or RyR2 phosphorylation (Beca et al., 2011). In addition, PDE4D selectively binds to βARs, which is crucial for regulating βARs induced responses (Xiang, 2011). Deletion of PDE4D, but not PDE4A or PDE4B, not only augments cAMP production in mouse embryonic

fibroblasts, but also slows the desensitisation rate of β_2AR and disrupts its interaction with G_i protein (Bruss et al., 2008). PDE4B and PDE4D are localised in buoyant membrane fractions (lipid rafts/caveolae) (Wright et al., 2018a). Kraft et al. detected the cAMP activity at the caveolin-rich plasma membrane microdomains in transgenic mice expressing the membrane-targeted FRET-based biosensor pmEPAC1. Local cAMP production in response to βAR stimulation by isoprenaline was significantly enhanced in both PDE4B and PDE4D knockout cardiomyocytes, suggesting that both PDE4 subtypes are involved in the regulation of the plasma membrane microdomain, regulating the local cAMP hydrolysis(Kraft et al., 2024). A study carried out by Xiang et al. showed that PDE4D selectively impacts signalling by β_2AR in neonatal cardiac myocytes, while having little or no effect on β_1AR signalling (Xiang et al., 2005). The PDE4D-KO cardiomyocytes exhibited a significant elevation in the maximum contraction rate when compared to the wild-type. The absence of additional response upon inhibition of the remaining PDE4 activity implies that PDE4D plays a significant role in modulating the β-AR pathways. In β_1AR-KO myocytes, β_2AR-mediated maximum response was greatly enhanced by PDE4-specific inhibitors, whereas there was no significant effect in β_2AR-KO myocytes, suggesting that PDE4D plays a major role in shaping the β_2AR signal.

1.4.3 PDE4 Regulation in Cardiac Disease

Inhibiting PDE4 enhances cAMP signalling and can improve cardiomyocyte function, however, prolonged inhibition of PDE4 has been linked to cardiac disease (Lehnart and Marks, 2006). Decreased PDE4 expression has been reported in various models of cardiac hypertrophy or heart failure, including human heart failure (Richter et al., 2011). PDE4D deficient mice exhibit age-related enlargement of the left ventricle along with a corresponding decline in cardiac function, becoming significant by 9 months, indicating a gradually worsening form of dilated

cardiomyopathy. Additionally, exercise triggered persistent ventricular arrhythmias in 66% of these PDE4D-deficient mice, whereas none of the wild-type control mice experienced such arrhythmias (Lehnart et al., 2005b). Inhibition of PDE4 also heightened the spontaneous release of calcium at baseline, increased contractile response, and raised the occurrence of arrhythmias in human atrial strips upon βAR stimulation (Molina et al., 2012). These results suggest that PDE4D deficiency can develop severe arrhythmia. Studies have shown that decreased PDE4B expression is maladaptive in human failing hearts, whereas overexpression of PDE4B in mice blunts the βAR response, relieves the cardiotoxic effects of chronic βAR stimulation, and slow the progression of heart failure (Karam et al., 2020).

1.5 Regionality within the Myocardium

The myocardium exhibits significant regional heterogeneity in βAR signalling, particularly along the baso-apical axis, where βAR expression and downstream signalling are not uniform. An early study in the canine heart revealed a baso-apical gradient of βAR density in the ventricular myocardium, with a greater concentration of βAR observed in the apical myocardium compared to the basal myocardium (Mori et al., 1993). The variation in βAR distribution results in a more pronounced contractile reaction to catecholamine stimulation in the apical myocardium, suggesting that the apex of the myocardium may be more sensitive to circulating catecholamines than the basal myocardium. Despite the lower density of sympathetic innervation in the apical myocardium compared to the basal myocardium, the increased βARs in the apex compensate for the limited sympathetic innervation in that region, ensuring balanced responsiveness throughout the left ventricular myocardium (Figure 1.11). Paur et al. further distinguished between β_1AR and β_2AR, noting that apical cardiomyocytes contain a higher quantity of β_2ARs. They observed that the contractile response of apical

cardiomyocytes to β_2AR stimulation was more pronounced than that of basal cardiomyocytes (Paur et al., 2012). Furthermore, their research revealed that under high levels of epinephrine stimulation, there is a phenomenon known as stimulus trafficking, wherein β_2AR transitions from coupling with G_s protein to coupling with G_i protein. Within the normal physiological range of epinephrine concentrations, the binding of epinephrine to β_2AR initiates the G_s-AC-PKA pathway, leading to a positive inotropic response. Elevated epinephrine concentration intensively activating both the β_1AR-and β_2AR-G_s pathways, triggers the switch in signal trafficking from β_2AR-G_s to β_2AR-G_i and elicits a negative inotropic effect on ventricular cardiomyocytes. Once the epinephrine is back to normal levels, β_2AR either reverts to coupling with G_s protein or undergoes degradation, allowing the cardiomyocytes to regain their inotropic function (Lyon et al., 2008, Paur et al., 2012). The stimulus trafficking effect is observed in Takotsubo cardiomyopathy, an acute yet reversible syndrome of heart failure. Takotsubo cardiomyopathy, also known as stress cardiomyopathy, is characterised by acute dysfunction of the left apical ventricle and presents with a distinctive apical ballooning appearance, typically following sudden emotional or physical stress (Lyon et al., 2008). Moreover, during periods of stress, epinephrine is often the predominant circulating catecholamine. In Takotsubo cardiomyopathy, elevated epinephrine levels activate a negative inotropic effect, which is mediated by the interaction between epinephrine, β_2AR and G_i protein, causing the apical myocardium to lose its contractility.

A recent study by Wright et al. proposed that cardiomyocytes in the basal region of the heart have more structured membranes with a greater number of caveolae and more regular T-tubular elements (Wright et al., 2018a). Additionally, they observed that the contractile response in basal cardiomyocytes following β_2AR stimulation was less pronounced compared to apical cardiomyocytes, and the β_2AR-cAMP signalling in basal cells was more

compartmentalised. Removing caveolae using MβCD or using Cav3KO mice and inhibiting PDE4 using Rolipram equalised the contractile response between apical and basal cells. This suggests that the tighter regulation of β_2AR-cAMP signalling in the basal region is attributed to the increased complexity of the membrane structure and enhanced PDE4-mediated cAMP hydrolysis.

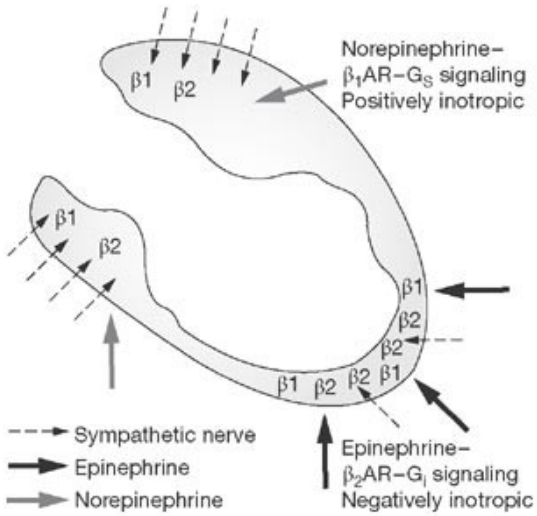


Figure 1.11. Regional differences in response to catecholamine levels. Higher density of βARs and lower sympathetic innervation in the apical myocardium compared to basal myocardium (Lyon et al., 2008).

The myocardium also demonstrates baso-apical differences in action potential duration (APD). Prinzen et al., found that electrical activation is not uniform between the base and apex, with apical regions exhibiting delayed repolarisation compared to the base (Prinzen et al., 1992) . Choi and Salama further demonstrated that APD is shorter at the apex and progressively longer toward the base, forming a gradient of ventricular relaxation. This pattern is mirrored in intracellular calcium transient durations, with shorter calcium transients at the apex and longer ones at the base, suggesting that regional differences in calcium handling contribute to

electrical and mechanical heterogeneity (Choi and Salama, 2000). In parallel with these baso-apical differences, the heart also exhibits transmural heterogeneity in electrophysiology, which plays a crucial role in modulating repolarisation gradients and arrhythmogenesis. In a healthy heart, APD is shortest in the epicardium, longest in midmyocardial cells, and intermediate in the endocardium, forming a transmural repolarisation gradient that ensures synchronised ventricular repolarisation (Antzelevitch and Fish, 2001). This gradient is shaped by regional variations in potassium currents, particularly the transient outward K^+ current (I_{to}), which is more prominent in epicardial than endocardial cells (Clark et al., 1993). The delayed rectifier potassium currents (I_{kr} and I_{ks}) are also differentially expressed across the myocardial wall, contributing to regional differences in repolarisation reserve. In addition, the L-type calcium current ($I_{Ca,L}$) differs across the ventricular wall, with greater $I_{Ca,L}$ density in the endocardial myocytes, which is associated with longer APD in this layer (Wang and Cohen, 2003). In heart failure, this balance is significantly disrupted, with I_{kr} downregulation leading to APD prolongation, steepening repolarisation gradients, and increasing arrhythmic risk (Akar et al., 2002). Prolongation of midmyocardial cell APD exacerbates these repolarisation gradients, leading to conduction block, which promotes polymorphic ventricular tachycardia and increases susceptibility to sudden cardiac death (Akar and Rosenbaum, 2003).

Understanding regional differences within the myocardium is essential, given that βAR stimulatoin influences ion channel activity, it is possible that regional differences in βAR signalling could further modulate these electrophysiological gradients. The interplay between βAR signalling heterogeneity and electrophyhsiological gradients across both the transmural and baso-apical axes has significant implications for cardiac function and disease progression. The apex, with heightened βAR sensitivity and shorter APD, supports rapid contraction but is more vulnerable to stress-induced dysfunction. In contrast, the base, with more

compartmentalised βAR signalling and longer APD, ensures stability but is more prone to arrhythmias. Understanding this concept is crucial for developing regionally targeted therapeutic strategies that restore β AR balance and normalise the electrophysiological gradients, which could help to relieve contractile dysfunction and reduce arrhythmic susceptibility in heart failure and Takosubo cardiomyopathy.

1.6 Myocardial Stretch: Mechanisms and Implications for Cardiac Function

The heart plays a crucial role in maintaining cardiovascular homeostasis, which requires its ability to continually adapt to varying haemodynamic conditions. Acute myocardial stretch due to haemodynamic overload is one of the most common challenges to the myocardium. This acute stretch can occur in both physiological conditions, such as exercise, and pathological conditions, such as myocardial ischaemia and heart failure. During aerobic exercise, skeletal muscle contractions enhance venous return, causing cardiac chamber dilation and acute myocardial stretch. This increase in end-diastolic volume raises end-diastolic pressure, which, if not adequately managed, can result in pulmonary and systemic congestion (Neves et al., 2016). When the myocardium stretches, the heart has a hypertrophic phenotype where the heart size increases without a change in the number of cardiomyocytes, allowing the myocardium to adapt its functional performance to alterations in workload (Wilkins and Molkentin, 2002). Initially, this is beneficial for maintaining normal cardiac function during the early stages of stretch. However, sustained stretch leads to cardiac decompensation, eventually resulting in cardiac dilation, heart failure and sudden death.

There are two well-defined compensatory mechanisms in response to acute myocardial stretch, offsetting the increase in the end-diastolic pressure, and both adaptations increase cardiac output. The first mechanism is the Frank-Starling mechanism, which involves an

immediate rise in contractility due to an increase in calcium sensitivity in the myofilaments and increased overlap between contractile protein myofilaments (Patterson and Starling, 1914, Frank, 1959, Gordon et al., 1966). Allen and Kurihara microinjected calcium-sensitive photoprotein aequorin into cells of rat and cat ventricular muscles, they found that an immediate increase in muscle length enhanced force generation without altering intracellular calcium concentration (Allen and Kurihara, 1982). Hongo et al. further confirmed this using isolated rat ventricular myocytes stretched by carbon fibres and loaded with calcium indicator fura-2. They demonstrated that the immediate increase in contraction following stretch is not due to changes in calcium transient, especially the L-type calcium current (Allen and Kentish, 1985). Concurrently, Hibberd and Jewell used skinned trabeculae and found that increasing sarcomere length from 1.9 to 2.4μm shifted the calcium-force curves leftward, indicating enhanced Ca^{2+} sensitivity (Hibberd and Jewell, 1982). There is a direct proportion between sarcomere length and its sensitivity to calcium. Thus, more force is generated at a given concentration of calcium as sarcomere length is increased (de Tombe, 2003, Konhilas et al., 2002). Several mechanisms have been proposed for this length-dependent activation of myofilaments. Studies have shown that the rise in myofilament calcium sensitivity caused by stretching is partially regulated by the formation of cross-bridges, and this is attributed to the activation of the thin filament cooperative mechanisms. In the absence of calcium, the thin filament protein tropomyosin inhibits the interaction between actin and myosin. Tropomyosin is associated with the troponin complex including troponin T (TnT; binds to tropomyosin), troponin C (TnC; binds to calcium), and troponin I (TnI; inhibits actin-myosin interaction). The troponin complex constrains tropomyosin in a position that covers the myosin binding site on actin. When calcium binds to TnC, tropomyosin moves away from myosin binding sites on actin, allowing myosin heads to form cross-bridges with actin and facilitating the development of

active force (Gordon et al., 2001, Konhilas et al., 2002). This cross-bridge formation increases the binding affinity of troponin for calcium. Additionally, the impact of sarcomere length on myofilament calcium sensitivity is also influenced by changes in the distance between the thick and thin filaments. Elongation of the sarcomere leads to a reduction in the distance between the thick and thin filaments, bringing myosin heads closer to actin. This increases the probability of cross-bridge formation and, therefore, force generation (Irving et al., 2000). Increased passive tension from titin could also enhance the binding between actin and myosin filaments, boosting contraction force (Fukuda and Granzier, 2005).

The second mechanism, known as the slow force response (SFR), was first observed in cat papillary muscle and is a prolonged secondary increase in force accompanied by a gradual rise in the calcium transient. It follows an initial rapid force increase, driven by the Frank-Starling mechanism, which results from enhanced myofilament sensitivity (Parmley and Chuck, 1973). This response ensures that the heart generates sufficient force to counteract the acute haemodynamic overload. The stretch-induced delayed positive inotropic effect has also been observed in the trabecula, isolated cardiomyocyte, and whole-heart preparation (Kockskämper et al., 2008). Neither blocking LTCCs nor inhibiting sarcoplasmic reticular function eliminates the slow response, indicating that the increased calcium does not originate entirely from LTCC channel entry or the sarcoplasmic reticulum (Kentish and Wrzosek, 1998). In addition, such observations have been made in the absence of neural control, suggesting that the response is an intrinsic regulatory mechanism of cardiomyocytes (Todaka et al., 1998). Early studies in both canine hearts and ferret papillary muscles observed a significantly increased cAMP following the slow force response, which was significantly reduced by the cAMP antagonist Rp-8-Br-cAMPs (Todaka et al., 1998, Calaghan et al., 1999b). However, the mechanisms leading to cAMP elevation have not been identified. Furthermore,

the study from Calaghan et al. indicated that although cAMP was increased in muscles that showed the slow response following stretch, there was no increase in phospholamban phosphorylation, suggesting that cAMP increases in a compartment that is inaccessible to the sarcoplasmic reticulum (Calaghan et al., 1999b). Research from Dr Wright has demonstrated that chronic partial mechanical unloading of the heart suppresses the β_2AR-cAMP response compared to the loaded heart but does not reduce the amplitude of βAR-cAMP, indicating the involvement of β_2AR-cAMP signalling under various mechanical load conditions (Wright et al., 2018b).

1.7 Models of Stretch

Physiologically, mechanical stretch in the heart is induced by changes in diastolic volume or peripheral resistance, where the cells are stretched in their x- and y-axes. There are many stretch models in the cardiovascular field, and the effect of stretch can be studied at different levels: from the whole heart to the cardiac tissue and to the isolated cells.

To investigate the physiological effects of stretch at the whole heart level, a common experimental technique involves expanding the chamber lumen in intact, isolated hearts (Franz et al., 1992). In brief, the heart is excised and cannulated on a Langendorff apparatus and a fluid-filled, volume-adjustable latex balloon is then inserted into the left ventricle, where different levels of stretch can be achieved via adjusting the volume inside the balloon. This stretch method has been effectively used in isolated canine (Todaka et al., 1998), rat (White et al., 2020) and guinea pig hearts (Rhodes et al., 2015). Apart from the ventricular stretch, Medvedev et al. developed a model of atrial volume overload in Langendorff-perfused ex vivo mouse hearts, where the atrial pressure and degree of atrial dilation were controlled by adjusting the height of the pulmonary outflow tube. Their findings demonstrated that

stretched atrial myocytes have increased membrane tension and decreased caveolae (Medvedev et al., 2023). Building on these stretch models, they can be combined with optical mapping techniques, which will be further discussed in a later chapter, enabling measurement of cardiac electrophysiology, such as action potential duration, conduction velocity, and calcium transients. This approach enhances the understanding of how mechanical stress influences electrical and calcium signalling in the heart (Jaimes et al., 2019, Choi and Salama, 2000).

With the stretch method described above, the applied stretch is complex, as cells are elongated along both their long and short axes while also being compressed along the z-axis. To minimise the variables involved, bundles of muscle such as papillary muscles and trabeculae can be dissected and stretched longitudinally. The main advantage of this approach is that the stretch is applied in only one direction. Membrane potential, intracellular calcium concentration, and contraction can all be measured (Wakayama et al., 2001, Lyon et al., 2020, Ward et al., 2003).

However, the use of whole tissue requires constant oxygenation of the bathing solutions to avoid hypoxia, which may generate noise during recording. In addition, interpreting data from multicellular preparations is limited by tissue complexity. To address these challenges, techniques for studying isolated cells have been developed. There are two popular cell stretching strategies, and the first involves stretching cells longitudinally by displacing one patch pipette relative to a fixed patch pipette (Sasaki et al., 1992). However, this technique is challenging to operate and presents additional technical difficulties in patch-clamp studies, as cell stretch often disrupts the seal between the membrane and patch pipette (Youm et al., 2005). In addition, this method does not uniformly stretch individual sarcomeres across the

cell, from the surface to the base (Kamkin et al., 2003a). The second method, osmotic cell swelling, is primarily used in this thesis to replicate membrane stretch. This method has been widely used in research studying caveolae function following stretch(Pfeiffer et al., 2014, Medvedev et al., 2021, Sinha et al., 2011). Under hypoosmotic swelling conditions, this model induces the recruitment and flattening of caveolae, which buffer increased membrane tension during cell stretch. Therefore, hypoosmotic swelling-induced stretch is an ideal model for this project, allowing us to investigate the mechanosensory functions of caveolae within cardiomyocytes, particularly their role in βAR signalling and how stretch affects the βAR signalling through caveolae involvement.

1.8 The Effect of Stretch on Contraction-Excitation Feedback

Myocardial stretch plays a critical role in modulating the contraction-excitation feedback, as mechanical deformation of ventricular membranes could alter ionic currents and intracellular calcium homeostasis, therefore changing action potential and contractile function. Early study by Lab et al. demonstrated that mechanical stretch of the myocardium can induce depolarisation of the resting membrane potential, affecting the initiation and propagation of action potentials, which in some cases can lead to spontaneous or early action potentials (Lab, 1978). This is likely due to the activation of stretch-activated ion channels (SACs), particularly non-selective cation channels, which allow Na^+, K^+ and Ca^{2+} influx, increasing the likelihood of ectopic beats (Hansen et al., 1991, Franz et al., 1992). Franz et al. also observed that stretch could enhance excitability and potentially contribute to arrhythmogenesis in stretched myocardium (Franz et al., 1992). However, findings across species and preparations vary. Spear and Neil found that stretching of the rat ventricles did not influence their resting potentials and action potential amplitudes, but did reduce conduction velocity in isolated stretched rat

papillary muscles (Spear and Neil Moore, 1972). They also reported that stretch led to graded and asynchronous electrical activity, possibly due to conduction block resulting from altered Na^+ conductance, changes in depolarisation rate, and disruption of intercellular electrical continuity, and such phenomena were reversible with time (Spear and Neil Moore, 1972). In guinea pig papillary muscle, Nakagawa et al. found that mild stretch caused resting membrane depolarisation. In contrast, larger stretch-induced diastolic hyperpolarisation, leads to a more negative resting membrane potential, suggesting an increase in K^+ conductance, possibly mediated by elevated intracellular Ca^{2+}. Electron microscopy revealed that mild to moderate stretch preserved SR integrity, whereas severe stretch led to SR disarrangement, suggesting that stretch-induced hyperpolarisation may result from Ca^{2+} release from the SR, which in turn enhances K^+ conductance (Nakagawa et al., 1988).

Several reports have shown that stretch can also alter the duration of the APD, though the effects vary across studies, with studies showing prolongation or shortening. This inconsistent effect on APD might be due to different species, or different preparations (single myocytes, tissue and intact hearts), measuring techniques, and stretch magnitude. Zang et al. found that stretch of isolated rat ventricular myocytes led to resting membrane potential depolarisation and an increase in both APD50 and APD90 (Zeng et al., 2000). Similar finding in rat ventricular myocytes were also reported from Wang (Wang et al., 2009) and also in rat ventricular slices (Kiseleva et al., 2000). Stretch induced Na^+ accumulation through SACs inhibits Na^+/K^+-ATPase activity, reducing outward K^+ current and prolonging APD (Kamkin et al., 2000). Stretch also activates Na^+/H^+ exchanger, increasing the Na^+. Such accumulation leads to increased Ca^{2+} influx through NCX via reverse-mode, therefore prolonging APD (Alvarez et al., 1999). At the same time, stretch-induced Ca^{2+} accumulation indirectly reduces $I_{Ca\text{-}L}$ through Ca^{2+}-dependent inactivation, shifting of the plateau of the action potential to more negative potentials (Kamkin

et al., 2000). In guinea pig ventricular cells, White et al. found a significant reduction in APD80 with no other significant changes in action potential parameters. They also found that stretch increased cell shortening and tension development (White et al., 1993). In frog cardiomyocytes, Tung and Zou found that mechanical stretch led to a transient reduction APD, consistent with earlier findings in intact frog ventricle by Lab and also decreased excitation threshold (Tung and Zou, 1995, Lab, 1978). This might be due to activation of the potassium outward current, promoting repolarisation, leading to APD shortening (DiFrancesco and McNaughton, 1979).

Another method of mechanically stimulating cardiomyocytes is osmotic swelling; in contrast to direct mechanical stretch, it will result in the dilution of intracellular contents. An osmotic gradient will also cause a significant increase in circumferential tension, whereas mechanical stretch will cause predominantly an increase in longitudinal tension. A study from Sasaki et.al. recorded the whole cell membrane current in guinea pig cardiomyocytes in both model of mechanical stretch and hypoosmotic stress showed that the hypoosmotic inflation of the cell increased in the amplitude of the delayed rectifier potassium current, while stretching the myocytes by more than 20% of their length did not cause any change in the rectifier potassium current but instead activated non-selective cation channels (Sasaki et al., 1992), suggesting that mechanical stretch induces current changes, which are different from those of the hypoosmotic swelling. In addition, they found an increase in Na^+/K^+ pump current, and the increase was independent of cytosolic Na^+ accumulation, suggesting direct activation by membrane stretch. Unlike I_k, the inward rectifier potassium current (I_{k1}) and LTCC current $I_{Ca,L}$ remained unaffected by swelling (Sasaki et al., 1994). Two subtypes of delayed rectifier potassium currents (I_{kr} and I_{ks}) were further investigated, and they respond differently to cell swelling, where swelling significantly increased I_{ks} and decreased I_{kr} (Rees et al., 1995). Wright

et al. reported that hypoosmotic swelling inhibits Na^+/Ca^{2+} exchanger, and the modulation of the exchanger began immediately on exposure to hypoosmotic solution and was maximal within 5 min (Wright et al., 1995). A study from Whalley et al. showed that in rabbit ventricular muscle, hypoosmotic swelling stimulates the sarcolemmal Na^+/K^+ ATPase pump, which was due to increased affinity of the pump for Na^+ (Whalley et al., 1993). In addition, Lado et al. observed that hypoosmotic swelling decreased the intracellular Ca^{2+} concentration, which was thought to be due to decreased Na^+ leading to a secondary decrease in Ca^{2+}, corresponding with a reduction in the force of contraction in sheep ventricular muscle (Lado et al., 1984). However, Brette et al. suggested that the effects of swelling are time dependent, as they found that short hypoosmotic solution exposure (50-70s) led to a significant increase in contraction amplitude and also calcium transient, despite a reduction in the amplitude of $I_{Ca,L}$ (Brette et al., 2000). This contradictory increase could be due to a reduction in the inactivation of SR Ca^{2+} release. Indeed, they found increased Ca^{2+} release from the SR. In addition, low extracellular sodium concentration inhibits the Ca^{2+} extrusion via the NCX, leading to increased Ca^{2+}, and therefore accounts for an increase in APD (Schouten and ter Keurs, 1985). While long hypoosmotic challenge (7- 10 min) causes a reduction in APD90, contraction amplitude, calcium transient, as well as a further decrease in $I_{Ca,L}$ (Brette et al., 2000). In guinea pig ventricular cells, Vandenberg et al. showed that osmotic swelling initially prolonged APD, followed by a later reduction, both accompanied by resting membrane depolarisation (Vandenberg et al., 1997). Similarly, in canine atrial cells, swelling leads to a diastolic membrane potential depolarisation (Du and Sorota, 1997). With shrinkage, the opposite results were observed – hyperpolarisation of the resting membrane potential and a prolongation of APD (Ehara and Hasegawa, 1983, Ogura et al., 1997). The electrical changes in response to hypoosmotic swelling can be due to the dilution of intracellular potassium

levels, where swelling lowers cytosolic K concentration, enhanced outward K current leading to faster repolarisation and APD shortening. However, the reduction in APD could also be attributed to the activation of the $I_{Cl,swell.}$ Therefore, the reduction in APD observed with hypoosmotic swelling and with axial stretch is likely due to different mechanisms (Vandenberg et al., 1997). Cell swelling during myocardial ischaemia is associated with APD shortening, which may facilitate re-entry and increase the risk of lethal arrhythmias. In addition, some antiarrhythmic drugs, such as dofetilide appear to be less effective in swollen tissue compared to normal cardiac tissue (Rees et al., 1995).

1.9 Other Cell Types in the Heart and Their Role in Mechanosensing

While cardiomyocytes play a central role in cardiac contraction, other cell types such as fibroblasts, endothelial cells, vascular smooth muscle cells and immune cells in the heart also contribute significantly to mechanosensing and mechanotransduction.

One of the most prevalent non-myocyte cell types in the heart is the cardiac fibroblast, accounting for around 30% of total cells in the rat hearts and increases substantially in the pathologically remodelling hearts (Banerjee et al., 2007, Souders et al., 2012). Unlike cardiomyocytes, fibroblasts have potent proliferative capacity and are the main contributors to extracellular matrix (ECM) protein synthesis (Camelliti et al., 2005). Cardiac fibroblasts are not electrically excitable like cardiomyocytes; however, they function as mechanoelectrical transducers. They respond to mechanical stimuli either from the surrounding myocardium or directly external stretch, by activating non-selective cation channels, which therefore leads to membrane potential depolarisation (Kamkin et al., 2003b). Cardiac fibroblasts express multiple mechanosensitive channels across the cell membrane, including cation non-selective channels (such as transient receptor potential channels (TRP) and Piezo1) and potassium

selective channels (such as KATP) (Stewart and Turner, 2021). Upon mechanical stimulation, the increased Piezo1- mediated calcium flow induces actin stress fibre formation and ECM protein synthesis, promoting fibroblast differentiation into activated myofibroblasts (Braidotti et al., 2022). TRP channel, as non-voltage gated Ca^{2+} permeable channels, are responsible for Ca^{2+} influx in cardiac fibroblasts. A study from Adapala et al. showed that mechanical stretch activates TRPV4 dependent calcium influx that is required for cardiac fibroblast differentiation, inhibition of TRPV4 significantly attenuated their differentiation into myofibroblasts (Adapala et al., 2013). Fibroblasts and cardiomyocytes are closely interrelated in their response to mechanical stimulation. Stretching of cardiomyocytes results in the release of growth factors, which activate fibroblasts, causing a mechanical effect that induces myofibroblast differentiation. In addition, fibroblasts co-cultured with myocytes can amplify the hypertrophic response of myocytes to stretch by increasing the release of endothelin and angiotensin II (Kaye et al., 1996, Ruwhof et al., 2001).

Vascular endothelial cells, located at the interface between circulating blood and the vessel wall, play a crucial role in regulating circulatory function. Mechanical stimuli, such as stretch and shear stress generated by circulatory pressure and blood flow, affect endothelial cell activity by activating mechanosensing signalling pathways and modulating gene and protein expression (Chien, 2007). By doing this, they minimise the effect of the external stresses induced by pressure and flow, maintaining vascular homeostasis. As mentioned previously, caveolae are specialised invaginations of the plasma membrane. A study showed that shear stress leads to increased caveolin-1 expression and promotes eNOS accumulation and activation within caveolae in the endothelial cells (Rizzo et al., 1998). Besides, caveolae act as key regulators of endothelial Ca^{2+} signalling and modulate the activity of mechanosensitive proteins such as TRPV4. A study showed that the absence of caveolin-1 induces impairment

of Ca^{2+} entry and also leads to a decrease in activity of Ca^{2+} permeable TRPV4 cation channels that participate in nitric oxide-mediated relaxation in the endothelial cells (Saliez et al., 2008). In addition, a study from Kohler et al. suggests that Ca^{2+} entry through endothelial TRPV4 channels in response to shear stress triggers NO-dependent vasodilation (Köhler et al., 2006).

The communication between endothelial cells and the vascular smooth muscle cells is particularly important under mechanical stretch. Upon shear stress, endothelial cells synthesise and release nitric oxide, which diffuses to neighbouring vascular smooth muscle cells and activates soluble guanylyl cyclase, resulting in cyclic guanosine monophosphate production, which therefore activates protein kinase G, leading to decreased smooth muscle cells' Ca^{2+} concentration and leading to smooth muscle relaxation and eventually vasodilation. In addition, shear stress causes endothelial cell membrane potential hyperpolarisation via K^+ channel activation, and since endothelial cells are coupled electrically to smooth muscle cells, the signal is transmitted to smooth muscle cells, leading to Ca^{2+} channel deactivation, a decrease in Ca^{2+} levels, and ultimately vasodilation. Like the cardiomyocytes, stretch-activated cation channels have been reported in vascular smooth muscle cells. Stretching smooth muscle cells leads to an initial contraction due to the activation of SACs, which allows calcium influx into the cells and this initial influx triggers further calcium release from SR through RyR1, this calcium-induced calcium release mechanism amplifies the intracellular Ca^{2+} levels, promoting smooth muscle contraction. At the same time, the calcium influx activates the large-conductance Ca^{2+}-dependent K^+ channels, which cause membrane hyperpolarisation, increasing the driving force for Ca^{2+} influx, therefore enhancing the contractile response (Gilbert et al., 2014). Where caveolae are also involved in this coupling, forming a complex microenvironment adequate for bringing closer membrane SAC and SR RyR1, and participating

in increased myogenic tone, in caveolae-depleted cells, there was a reduced stretch-induced calcium response (Gilbert et al., 2014).

1.10 The Heart Failure

Chronic heart failure (HF) is a progressive disease due to abnormalities in cardiac structure and function, leading to reduced cardiac output. It is a major cause of morbidity and mortality worldwide, with a significant increase in incidence and prevalence among the elderly (Martin et al., 2024). The causes of HF are diverse, including diseased myocardium (ischaemic heart disease and genetic abnormalities), abnormal loading conditions (hypertension, excessive volume overload) and arrhythmias (tachyarrhythmias and bradyarrhythmia). There are two broad types of heart failure discriminated based on the measurement of the left ventricular ejection fraction, heart failure with reduced ejection fraction (HFrEF: EF <40%) and heart failure with preserved ejection fraction (HFpEF: EF >50%). Around 50% of the HF patients have HFpEF, which is characterised by structural and cellular alterations leading to an inability of the left ventricle to relax properly. Whereas HFrEF is characterised by a substantial cardiomyocyte loss, either acutely or chronically, resulting in systolic dysfunction and the inability of the left ventricle to contract properly. Myocardial ischemia is a common cause of HFrEF, and dilated cardiomyopathy (DCM), often considered a subset of HFrEF, is the most prevalent cardiomyopathy leading to HF syndromes (Figure 1.10) (Tayal et al., 2017).

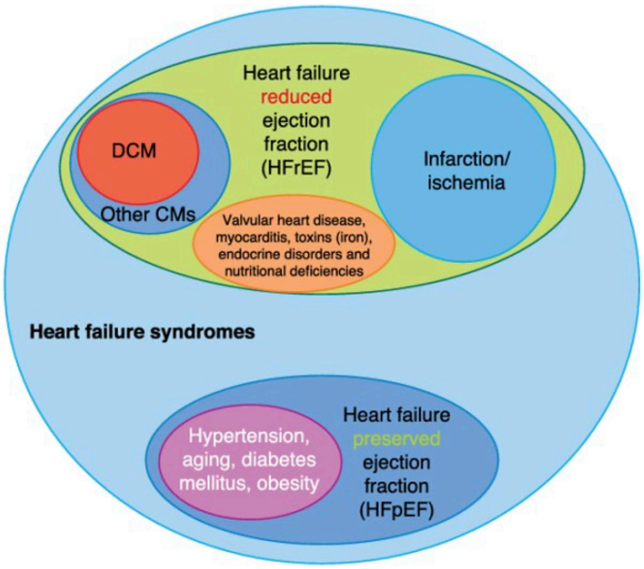


Figure 1.12. Classification of heart failure syndromes and underlying causes. Heart failure can be categorised into two main types: heart failure with reduced ejection fraction (HFrEF) and heart failure with preserved ejection fraction (HFpEF). HFrEF includes conditions such as dilated cardiomyopathy (DCM) and other cardiomyopathies, with common causes including infarction/ischaemia, valvular heart disease, myocarditis, toxins (iron), endocrine disorders, and nutritional deficiencies. HFpEF is commonly associated with hypertension, ageing, diabetes mellitus, and obesity (Tayal et al., 2017).

Myocardial infarction is a leading cause of heart failure, caused by the reduction or interruption of blood supply to a section of the myocardium, and it has been associated with high morbidity and mortality (Bahit et al., 2018, Thygesen et al., 2007). Loss of functional myocardium following MI increases cardiac loading conditions, triggering ventricular remodelling (Swaroop, 2022). This process involves an inflammatory response, leading to fibrosis, scar formation, and myocardial stiffening. To compensate for lost contractile tissue, the left ventricle undergoes dilation and hypertrophy of non-infarcted myocardial regions, initially preserving function (Bogaert et al., 2000). In the short term, LV dilation helps maintain stroke volume through the Frank-Starling mechanism. However, LV dilation progressively increase wall stress and oxygen demand, as described by Laplace's law, which states that wall stress is directly proportional to cavity radius and inversely proportional to wall thickness

(Mitchell et al., 1992). Over time, these compensatory mechanisms become maladaptive, ultimately leading to progressive left ventricular systolic dysfunction and a decline in cardiac output. In patients with acute myocardial infarction, ejection fraction declines in direct relation to infarct size (Pfeffer and Braunwald, 1990, Del Buono et al., 2022)

Cardiomyopathies are disorders of the cardiac muscle that cause mechanical dysfunction, resulting in dilated or hypertrophic pathophysiology. Dilated cardiomyopathy (DCM) usually starts in the left ventricle and is characterised by left ventricular dilation and impaired contraction (Schultheiss et al., 2019). Over time, both ventricles may be affected. The causes of DCM can be genetic or due to other factors such as infection, hypertension, toxins and immune-mediated disease (Heymans et al., 2023). Ischaemic cardiomyopathy (ICM) is another common cardiomyopathy with impaired epicardial blood flow and coronary flow reserve, which results in adverse LV remodelling and contractile dysfunction. This condition typically involves the irreversible loss of viable myocardium following an acute myocardial infarction, combined with dysfunctional but still viable myocardium due to chronically reduced myocardial blood flow and coronary reserve (Del Buono et al., 2022). A study by Dr. Sanchez-Alonso revealed that specific phenotypes of heart failure correlate with distinct functional anomalies. Their findings demonstrated an increase in LTCC activity within the T-tubules of ICM patients, whereas in patients with DCM, the increase was observed at the cell crest (Sanchez-Alonso et al., 2020). This variance in pathophysiology among HF subtypes suggests different prognoses and therapeutic responses. Exploring the signalling dynamics within ventricular cardiomyocytes at the subcellular level across various HF phenotypes in human samples could significantly enhance therapeutic strategies and refine treatment options.

Most of the HF therapies work on improving cardiac remodelling by reducing cardiac hypertrophy. Angiotensin-converting enzyme (ACE) inhibitors, including enalapril, lisinopril, and ramipril, are fundamental treatments for HFrEF (Sapna et al., 2023). They act on the renin-angiotensin-aldosterone system, reduce the production of angiotensin II, a potent vasoconstrictor, and therefore reduce aldosterone levels. This results in vasodilation and decreased sodium and fluid retention. Angiotensin II receptor blockers (ARBs), such as losartan and valsartan, are alternative treatments for patients who cannot tolerate ACE inhibitors, blocking angiotensin II at its receptor level, significantly improving cardiac performance outcomes (Velazquez et al., 2003). Mineralocorticoid receptor antagonists such as spironolactone and eplerenone target aldosterone receptors, preventing water and sodium retention, and helping to reduce the fluid buildup in the body (Sapna et al., 2023). Diuretics such as furosemide and hydrochlorothiazide manage fluid overload in heart failure by promoting diuresis. However, prolonged use can result in electrolyte imbalances and, therefore, renal dysfunction (McDonagh et al., 2021).

β-blockers including bisoprolol, carvedilol and metoprolol inhibit βARs, particularly the β_1AR subtype, thereby reducing excessive sympathetic activity and neuohormonal stimulation (Oliver et al., 2019). These drugs help prevent cardiomyocyte apoptosis and adverse ventricular remodelling, while promoting reverse remodelling. Some β-blockers act as antagonists of the β_1AR, but as partial agonists on β_2AR and also act through β_3AR-mediated nitric oxide signalling, which contributes to vasodilation and negative inotropic effects. Despite their benefits, β-blockers must be used with careful consideration in patients with conduction abnormalities, reactive airway disease, or acute decompensated HF, due to their bradycardic and negative inotropic properties.

Among newer drugs, sodium-glucose cotransporter 2 (SGLT2) inhibitors, initially developed for type 2 diabetes, have become a robust treatment of heart failure with reduced HFrEF. Beyond their role in lowering the glucose level, they exert their cardioprotective effects through different mechanisms. They inhibit the sodium-hydrogen exchanger in cardiomyocytes, reducing the intracellular sodium and calcium overload (Packer et al., 2017). Furthermore, SGLT2 inhibitors improve myocardial energetics by improving mitochondrial energy production and enhancing metabolic flexibility, especially in the failing heart (Murphy et al., 2020).

Beyond pharmacological management, device therapy may be required. For instance, implantable cardioverter defibrillators (ICDs) are recommended for patients with severe left ventricular dysfunction $\leq$ 35%, which has been shown to reduce the rate of sudden death due to electrical disturbances such as ventricular arrhythmias (McDonagh et al., 2021). For patients with HFrEF and a QRS duration $\geq$ 130ms, cardiac resynchronisation therapy (CRT) may be introduced rather than ICD. CRT involves implanting a biventricular pacemaker to restore synchronised ventricular contractions, improving patients with intraventricular conduction delays. Left ventricular assist devices (LVADs) are implantable mechanical pumps that help support the heart's pumping function in patients with severe heart failure as a temporary solution while awaiting heart transplantation or as long-term therapy for those ineligible for transplant (Sapna et al., 2023).

Although medications and device-based therapies have significant improvements for treating HFrEF, their effectiveness in HFpEF remains limited. ACE inhibitors and beta-blockers, though widely used, can lead to side effects such as low blood pressure and kidney dysfunction, which require continuous monitoring. Some patients may experience medication tolerance or

resistance. Device-based therapy, such as ICD and LVADs has potential risks including infection, bleeding, device failure and also financial challenges.

1.11 Summary

Mechanical stretch plays a critical role in regulating heart function. Physiological stretch in the heart influences multiple signalling pathways within cardiac cells, converting the stimuli into intracellular signals that shape cell function. When the stretch is sustained, it can lead to pathological responses, such as pressure overload-induced cardiomyocyte hypertrophy (Ruwhof and van der Laarse, 2000). Despite this, the specific mechanosensors involved and the mechanisms by which they activate intracellular signalling pathways are not yet fully understood. As discussed, caveolae play a significant role in regulating the mechanotransduction pathway, and their deformation can influence signalling pathways. However, the specific role of caveolae in mediating βAR signalling in response to stretch remains incompletely understood.

To address the gaps, this thesis uses two stretch methods: cell-based hypoosmotic swelling and whole-heart mechanical stretch. Through these methods, we aim to investigate how caveolae influence βAR signalling under stretch. In addition, by examining the role of PDE4, the regional distribution of βAR signalling following stretch, this research can give a clearer picture of the molecular mechanisms underlying the stretch regulation of βAR signalling.

To further explore the role of caveolae in cardiac pathology, we use the rat myocardial infarction model to examine how stretch-regulation of βAR signalling is altered under chronic stress conditions. Furthermore, to enhance translational relevance, we also assess caveolae function and βAR compartmentalisation in human donor and failing cells to determine whether findings from rat models are applicable to the human heart. While β-blockers remain

fundamental treatments in heart failure, they act as broad inhibitors, globally suppressing βAR signalling without distinguishing between beneficial and maladaptive downstream effects. Identifying the specific compartments within the signalling pathway that become dysregulated in heart failure could help to develop more precise and targeted therapies. Such strategies could preserve adaptive βAR signalling, which is essential for maintaining cardiac contractility, while selectively inhibiting the pathological components that drive adverse remodelling and disease progression.

1.12 Hypothesis

Membrane stretch, induced by hypoosmotic swelling, leads caveolae integration into the membrane and a reduction in the number of caveolae in cardiomyocytes, thereby enhancing β_2AR-mediated responses. This restructuring of caveolae disrupts the regulation of G_i and PDE4 and its subtypes (PDE4D and PDE4B), leading to increased sarcomere shortening and elevated cAMP production. We further propose that this enhancement is regionally specific, with basal cardiomyocytes showing greater sensitivity to membrane deformation than apical cells. In heart failure, we propose that caveolae disruption attenuates this mechanoregulation, leading to a loss of β_2AR stretch sensitivity and a blunted contractile response.

1.13 Aims

1) Investigate the role of caveolae and the effect of stretch in βAR response in rat ventricular cardiomyocytes.
2) Investigate the role of PDE4 and its subtypes in rat ventricular cardiomyocytes following stretch.
3) Investigate regional differences in caveolae-based stretch-dependent regulation of β_2AR signalling by studying cells from distinct regions of the heart, such as apex and base.
4) Investigate how stretching the left ventricle affects the electrophysiology of the apex and base of the rat heart following β_2AR stimulation.
5) Characterise functional changes resulting from remodelling and βAR redistribution in left ventricular cardiomyocytes affected by heart failure, using both rat and human models.

Chapter 2: General Material and Methods

All reagents used in this project are listed in Table 2.

Reagent	Company	Catalogue #
3-Isobutyl-1-methylxanthine (IBMX)	Tocris, UK	2845/50
A33	Tocris, UK	6313
Antibiotic-antimycotic (AA)	Gibco, UK	11570486
Blebbistatin	Tocris, UK	1760/10
BSA	Sigma-Aldrich, UK	A9418-50G
Calcium chloride solution ($CaCl_2$)	Honeywell	25-055-CVC
Cell culture grade water	Corning, UK	1024/10
CGP 20712	Tocris, UK	C9263
Collagenase (human isolation)	Sigma-Aldrich, UK	LS004176
Collagenase Type 2	Worthington-Biochem	50-99-7
D (+)-Glucose anhydrous	VWR, UK	284504S
D-(+)-Glucose	Sigma-Aldrich, UK	G7021
Di-8-ANEPPS	Biotium	61012
Dimethyl Sulfoxide (DMSO)	Thermo scientific, UK	472301-1L
Fetal Bovine Serum (FBS)	Fisher Scientific, UK	A5209502
Forskolin	Tocris, UK	1099/10
Fura-2 AM	Invitrogen, UK	F1221
GEBR-7b	Sigma	524748
Hanks' Balanced Salt Solution (HBSS)	Gibco, UK	14025092
Heparin	Pfizer, USA	00409-2723-02
HEPES	Sigma-Aldrich, UK	H3375
Hyaluronidase from bovine testes	Sigma-Aldrich, UK	H3506-500MG
ICI 118551	Tocris, UK	0821/10
Isoprenaline hydrochloride	Sigma-Aldrich, UK	I5627
Laminin	Bio-Techne	3400-010-02
L-glutamine	Gibco, UK	25030081
Magnesium Chloride	Biosciences	FJ135-09205
Magnesium sulfate heptahydrate ($MgSO_47H_2O$)	Sigma-Aldrich, UK	63138-250G
Methyl-β-cyclodextrin	Sigma-Aldrich, UK	C4555-1G
Minimum Essential Medium Eagle	Sigma-Aldrich, UK	M2279-100ML
Nitrilotriacetic acid trisodium salt (NTA)	Sigma-Aldrich, UK	N0253-250G
Paraformaldehyde Solution (PFA) 16%	Thermo scientific, UK	28906
Phosphate buffered saline (PBS) tablet	Sigma-Aldrich, UK	6501-200TAB
Pluronic™ F-127 (20% Solution in DMSO)	Invitrogen, UK	P3000MP
Potassium chloride (KCl)	VWR, UK	7447-40-7
Potassium Dihydrogen Orthophosphate	Scientific Laboratory Supplies	CHE2946
Pro-long gold with DAPI	Invitrogen, UK	P36931
Protease (human isolation)	Sigma-Aldrich, UK	P2143
RH237	Invitrogen, UK	S1109

Rhod-2, AM	Invitrogen, UK	R1245MP
Rolipram	Tocris, UK	0905
Sodium bicarbonate	Sigma-Aldrich, UK	S6014
Sodium chloride (NaCl)	VWR, UK	7647-14-5
Sodium hydrogen carbonate	VWR, UK	144-55-8
Sodium hydrogen phosphate anhydrous	Fisher scientific, UK	13206329
Sodium phosphate monobasic monohydrate	Fisher scientific, UK	10657961
Sodium Pyruvate	Fisher Bioreagents	10021513
Taurine	Sigma-Aldrich, UK	T4571
Triton X-100	Sigma-Aldrich, UK	93443
Tween20	Sigma-Aldrich, UK	P9416

Table 2.1. List of reagents used in this project

2.1 Animal Ethics Approval

All animal procedures were carried out in accordance with UK Home Office guidelines (ASPA1986 and EU directive 2010/83) and approved by the Animal Welfare and Ethics Review Board of Imperial College London.

2.2 Rat Myocardial Infarction

The rat myocardial infarction (MI) by left anterior descending (LAD) coronary artery ligation was first established in 1954 and was extensively used in the field of cardiovascular research (Johns and Olson, 1954). This model allows us to study the remodelling of cardiac function in heart failure, including both structural changes and functional changes, which can help us to better understand the pathophysiology and develop a new treatment target for heart failure.

The post-MI rats, induced by 16 weeks of LAD coronary artery ligation, exhibited significant ventricular dilation, reduced ejection fraction, and elevated end-diastolic pressure (Lyon et al., 2009). In addition, dynamic measures of contractile function and ventricular compliance were also significantly impaired in these animals, consistent with the heart failure phenotype.

2.2.1 Anaesthesia and Pre-operative Care

Adult male Sprague-Dawley rats (Charles River, UK) weighing 250-350g were used. The rat was anaesthetised in an induction chamber with a mixture of 5% isoflurane and 95% oxygen. Subsequently, the rat was injected subcutaneously with 0.3mg/ml Buprecare (Animalcare, UK), a potent analgesic agent; 50mg/ml Rimadyl (Zoetis, UK), a non-steroidal anti-inflammatory agent. The hair on the left part of the thorax was removed using clippers. Next, 5mg/ml of Marcaine (AstraZeneca, UK), a local anaesthetic, was injected into the skin where the expected incision would be made. After preparation, the rat was transferred to the operating theatre and suspended on a rigid plastic board. This was done by hanging their superior incisors on a flexible plastic band on the board, thereby aligning the larynx, pharynx and trachea in a straight line. The vocal cords and the tracheal lumen were visualised by placing a light source (Photonic Optics, Vienna, Austria) on the rats 'pharynx. For intubation, a modified blunt ended 16G cannula, sprayed with Xylocaine (Aspen Pharmacare), was passed through the vocal cords. After removing the metal introducer, the rat, with the endotracheal tube in place, was immediately connected to a ventilator (Harvard Apparatus Model 683 Small Animal Ventilator, Massachusetts, USA) set at a tidal volume of 1ml/100g and a rate of 80-90 bpm. Anaesthesia was maintained with isoflurane, the concentration of which was reduced to 2%. The rat was secured onto a heating pad, and a pulse oximeter was connected to the hind leg to monitor its heart rate and oxygen saturation. A temperature probe was inserted into the rectum. The left thoracic wall was cleaned with betadine, and a sterile drape was placed over the rat. A hole of appropriate dimensions was made in the drape using scissors. All surgical steps were performed under strict aseptic conditions; all instruments were autoclaved before the procedure.

2.2.2 Myocardial Infarction Procedure

A 2-3cm incision, approximately 1cm below the armpit, was made using a scalpel. The subcutaneous layer was bluntly dissected, and the chest muscles were dissociated to access the rib cage. Retractors were placed to keep the skin and muscles apart. A blunt probe was gently introduced between the fourth and the fifth interspace, and a transverse thoracotomy was performed with care taken to avoid damaging the heart, lung or intercostal vein. The rib retractor was positioned to expose the pericardial cavity, and the pericardium was gently stripped away. A suture was placed around the proximal part of the left anterior descending (LAD) artery, around 2-3mm below the lower border of the left atrial appendage, using a 7-0 non-resorbable suture (Ethicon, US). A successful infarction could be confirmed by the greyish appearance of the left ventricular anterior wall and apex, supplied by the LAD artery. For the sham procedure, a suture was passed around the LAD and then removed without ligation. The chest wall was then closed using a resorbable 4-0 suture (Ethicon, US), and free air was removed with a blunt-ended cannula connecting to a 1ml syringe, functioning as a chest drain. The muscle and skin layers were closed using a 4-0 non-resorbable suture. Isoflurane was reduced to 1% during the suturing and turned off once the layers were closed.

2.2.3 Post-operative Care

The rat was recovered in a heated recovery cage and given 100% oxygen (5L/min) through a nose cone. Once fully awake, the rat was housed individually in its cage with wet food and water. On the day following surgery, the rat was checked regularly for adverse complications, including wound swelling, infection, missing sutures, and signs of pain or distress. Carprofen was given for two days following surgery, and Buprenorphine was administered for one day after surgery. Thereafter, the rat was reviewed daily until the end of the study protocol. A total

period of 16-20 weeks was required for the development of heart failure in rats using the permanent myocardial infarction model. The hearts were then explanted, weighed, and prepared for cell isolation.

2.3 Isolation of Adult Rat Ventricular Cardiomyocytes

Adult male Sprague-Dawley rats were humanely killed by cervical dislocation with the prior use of 5% isoflurane sedation. An incision was made across the rib cage and on either side to fully expose the chest cavity. The heart was rapidly excised and placed in a heparin-mixed ice-cold Krebs-Henseleit (KH) solution, which contained (mmol/l): NaCl 119.1, KCL 4.7, $MgSO_4$ 0.94, KH_2PO_4 1.2, $NaHCO_3$ 25, Glucose 11.5, and $CaCl_2$ 1; 37℃, 95% O_2, 5% CO_2). In a petri dish with fresh, ice-cold KH solution, excess tissue from the lung and thyroid, pericardial fat, and other vessels connected to the heart were trimmed away, leaving the aorta intact. The heart was then transferred to the Langendorff apparatus, where the aorta was cannulated and secured with nylon thread (Figure 2.1). The heartbeat rhythmically under KH perfusion at 37℃. Upon complete clearance of blood from the coronary circulation, which normally took 5 minutes, the KH solution was switched to a low calcium solution containing (in mmol/l): NaCl 120, KCL 5.4, $MgSO_4$ 5, Pyruvate 5, Glucose 20, Taurine 20, HEPES 10 and Nitrilotriacetic Acid (NTA) 1.286, $CaCl_2$ 0.2; 100% O_2, for an additional 5min. NTA is used as a chelating agent which removes the calcium in the low-calcium solution, disabling the excitation-contraction coupling. An immediate stop of beating was expected, indicating successful calcium removal from the heart. Subsequently, an enzyme solution (NaCl 120, KCL 5.4, $MgSO_4$ 5, Pyruvate 5, Glucose 20, Taurine 20, HEPES 10 and $CaCl_2$ 0.2; 100% O_2) containing 1mg/ml Collagenase II and 0.6 mg/ml Hyaluronidase was perfused into the heart for 10min, allowing break down the extracellular matrix. After this step, the Langendorff portion of the isolation protocol is complete. The heart

was then cut from the cannula and placed in a petri dish with the enzymatic solution for dissection. The atria and the free wall of the right ventricle were removed. For apex and base studies, the midsection of the left ventricle was removed, with the top portion representing the base and the bottom representing the apex. This tissue was sliced and mechanically shaken at 35℃ for 30min in an enzyme solution containing Collagenase and Hyaluronidase, under 100% O_2. After that, the supernatant was filtered through gauze, and the resulting filtrates were centrifuged for 1min at 600rpm. The suspension was discarded, and the cell pellets were resuspended in enzyme solution for further experiments. An illustration of rat isolation is shown in Figure 2.2.



Figure 2.1. Langendorff perfusion apparatus set up for adult rat cardiomyocytes isolation experiment. **A.** A warm hollow glass cylinder in which the heart is placed to help maintain its temperature. **B.** A bubble trap containing an oxygenated Krebs-Henseleit buffer solution, which retrogradely perfuses the heart via the aorta, enabling rhythmic beating. **C.** A bubble trap containing an oxygenated low-calcium solution, which is perfused into the heart once a normal sinus rhythm is established. **D.** A pump that sets the flow rate at approximately 13-15ml/min.

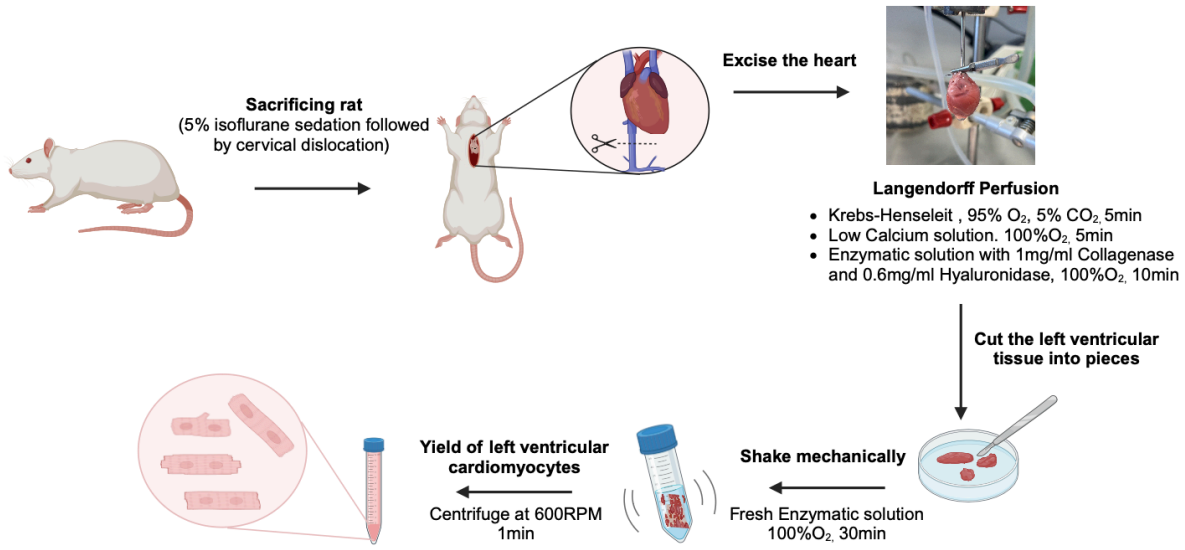


Figure 2.2. Rat cardiomyocyte isolation protocol (figure created with BioRender)**.**

2.4 Human Ethics Approval

Experiments on isolated human cardiomyocytes were approved by Imperial College Institutional Review Board. Samples from failing hearts of patients with end-stage of heart failure were used with the approval of Brompton Harefield & NHLI Ethics Committee under Biobank REC approval reference: 09/H0504/104+5. Samples from donor hearts unsuitable for transplantation were used with approval of NHS BT with REC approval reference: 16/LO/1568.

2.5 Human Cardiomyocyte Isolation

Failing ventricular cardiomyocytes were isolated from hearts of patients with end-stage HF caused by ischemic or dilated cardiomyopathies who were undergoing transplantation. Healthy ventricular cardiomyocytes were prepared from donor hearts unsuitable for transplantation. Regions of LV were excised and diced into small pieces, where the adherent fat and connective tissues were removed. The tissue pieces were washed three times in calcium-free Krebs-Ringer solution at 37℃. The samples were then agitated for 25min at 37℃

in 10ml of Krebs-Ringer solution (in g/L): NaCl 7.012, KCl 0.402, MgSO4 1.332, pyruvate 0.55, Glucose 3.603, Taurine 2.502, HEPES 2.383, pH=7,4 and 0.36mg/ml Protease. The samples were then shaken in Krebs-Ringer solution with 1mg/ml collagenase for 10-15min. Cardiomyocytes were produced after the first digestion in collagenase solution. After each digestion, the filtrate was centrifuged at 600rpm for 3 minutes, and the pellets were re-suspended in Krebs-Ringer solution (Figure 2.3).

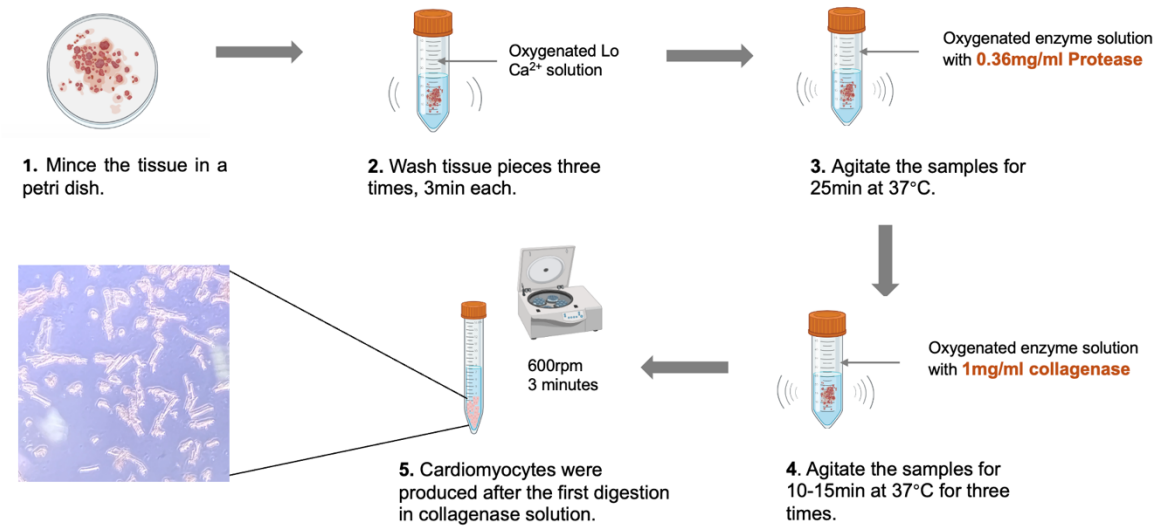


Figure 2.3. Human cardiomyocyte isolation protocol (figure created with BioRender).

2.6 Hypoosmotic Swelling Model

In this project, we used the hypoosmotic swelling model to mimic the membrane stretch. The isosmotic solution consisted of (mM): NaCl, 118; KCl, 5.3; MgCl2, 0.5; CaCl2, 1; Glucose, 10; Na2HPO4, 7.5; NaH2PO4.H2O, 2.5; pH7.4, osmolarity: 290 mOsm/L. Hypoosmotic solution (osmolarity: 214 mOsm/L) had the same composition as the isosmotic solution, except that the NaCl concentration was reduced to 81mM to achieve an osmolarity of 214 mOsm/L.

In contrast to the method used by Gonano et al.,(Gonano et al., 2014) which involved 91mM NaCl for isosmotic and hypoosmotic solutions with osmolarity adjustments made by adding Mannitol to the isosmotic solution, we observed that cardiomyocytes exhibited poor contraction in the presence of Mannitol, likely due to reduced cell viability. Especially for the contraction study, only 30% of the cells remained viable at the end of experiments when using the isosmotic solutions containing Mannitol, compared to 78% viability in our isosmotic solution with high NaCl (Figure 2.4).

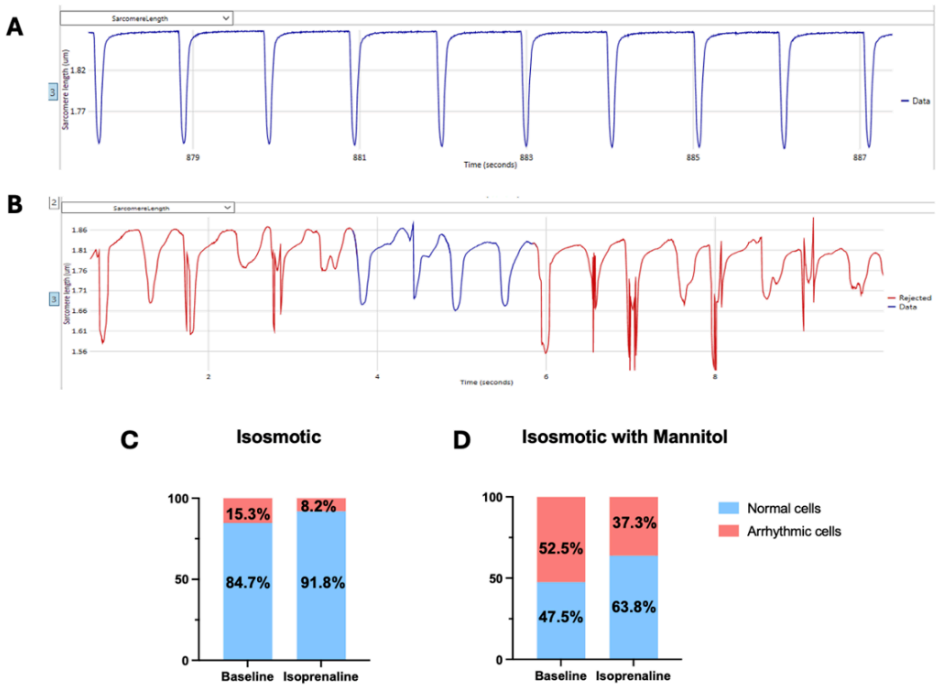


Figure 2.4. Example of CytoCypher sarcomere shortening traces in two different isosmotic solutions. CytoCypher sarcomere shortening traces using **(A)** our isosmotic solution and **(B)** the isosmotic solution from Gonano et al. Stacked bar charts **(C** and **D)** show the percentage of normal cells (blue) and arrhythmic cells (red) at baseline and after the application of isoprenaline under two different isosmotic solutions.

2.7 Transmission Electron Microscopy

Isolated cardiomyocytes were washed using PBS and then fixed in a cacodylate buffer with 2.5% glutaraldehyde for 2-4h. Further preparation was performed by Dr Ivan Diakonov from NHLI. These cells were centrifuged at 500g for 5min, forming a cell pellet and left in 2.5% glutaraldehyde overnight. Subsequently, the pellet was subjected to triple rinsing using cacodylate buffer, followed by fixation in 1% osmium-tetroxide. Post-fixation, it was washed for 5-10min with distilled water. Prior to dehydration, 25-50µL of 2% agarose (heated to 45℃) was added to the sample. This mixture was then portioned onto polythene to solidify, resulting in small agar blocks containing evenly distributed cells. The solidified agar blocks were then dehydrated using graded alcohols and propylene oxide and embedded in Araldite. Sections of 0.1µM thickness were prepared for transmission electron microscopy and were stained using uranyl acetate and lead citrate. Images of the longitudinal cardiomyocyte membrane sections were taken. A group of 10 cells were selected from each isolation, and for each of these cells, 10 different fields of view were captured.

Caveolae were identified as flask-shaped invaginations of the plasma membrane, or vesicles located along the plasma membrane, in close proximity to it. In contrast, clathrin-coated pits were distinguished by their larger, round invaginations of exactly 100nm and the presence of a distinctive dark coat lining the cytoplasmic face of the membrane. Only caveolae fitting the morphological criteria were counted. Fiji was used to trace and measure the length of the plasma membrane, which was calculated using the scale bar in the image (500nm), which was provided by the software of the electron microscope. On average, the cardiomyocyte membrane length for each frame was approximately 5µm; depending on the shape of the cell, the length of the membrane was corrected. The density of caveolae was then calculated by

dividing the number of caveolae by the membrane length, giving us a final unit of caveolae per 1μm of membrane (Wright et al., 2014).

2.8 Live Cell T-tubule Staining and Measurement

2.8.1 Di-8-ANEPPS staining

T-tubule staining was performed using Di-8-ANNEPS, a lipophilic membrane marker. To prepare a 10mM stock solution of Di-8-ANEPPS, 1.5ml of DMSO was mixed with 0.5g Pluronic acid, which helps in membrane binding, and the mixture was heated until the Pluronic acid dissolved. Then, 630μl of this mixture was combined with 5mg of the Di-8-ANEPPS to make a 10mM stock. A 10 μM Di-8-ANNEPS working solution was prepared in 1ml FRET buffer (composed of 144 mM NaCl, 5.4 mM KCl, 1 mM $MgCl_2 \times 6H_2O$, 1 mM $CaCl_2$, and 10 mM HEPES; pH 7.4) and sonicated for 20min under sweeping mode at 50℃. Isolated cardiomyocytes were washed once with FRET buffer, stained with Di-8-ANNEPS for 3 min in the dark, and then washed twice with FRET buffer. Cells were then stabilised in 2ml iso/hypoosmotic solution prior to imaging. Images were taken using a Zeiss LSM-780 inverted confocal microscope with an oil 65x objective. 10 cells were selected per dish for imaging. Di-8-ANEPPS was excited at a wavelength of 488nm, and emission was detected at 520nm (Lyon et al., 2009).

2.8.2 T-tubule Density and Regularity Measurement

The resulting images of the T-tubule network were analysed using Fiji. Initially, the images were adjusted to a resolution of 1024x1024 pixels, converted to 8-bit, and rotated to align the long axis of the cells horizontally. Five regions, each 170.5 pixels in width and 21.5 pixels in height, of the best T-tubule areas were selected for analysis. These regions were then duplicated, and the threshold was auto-adjusted to convert the images into black-and-white

binarised formats. The T-tubule density was quantified by calculating the percentage of the area covered by black pixels (Schobesberger et al., 2017). Simultaneously, the regularity of the T-tubule was assessed. Waveforms were generated from the binarised images. The regularity of T-tubules was quantified by transforming these waveforms through a power peak transformation using a custom-written macro in MATLAB (version R2021b). This transformation calculates "cycles per micron", equivalent to the inverse of the distance between T-tubules, and a power value on the y-axis indicating the cumulative frequency of each distance. The peak power of the periodogram from the MATALB analysis represents the regularity of the T-tubule striation. The amplitude of this peak increases as the regularity of the T-tubule increases (Ibrahim et al., 2012). The values obtained were then averaged for each cell to provide a quantified measure of T-tubule density and regularity. A detailed protocol for T-tubule density and regularity measurement is shown in Figure 2.5

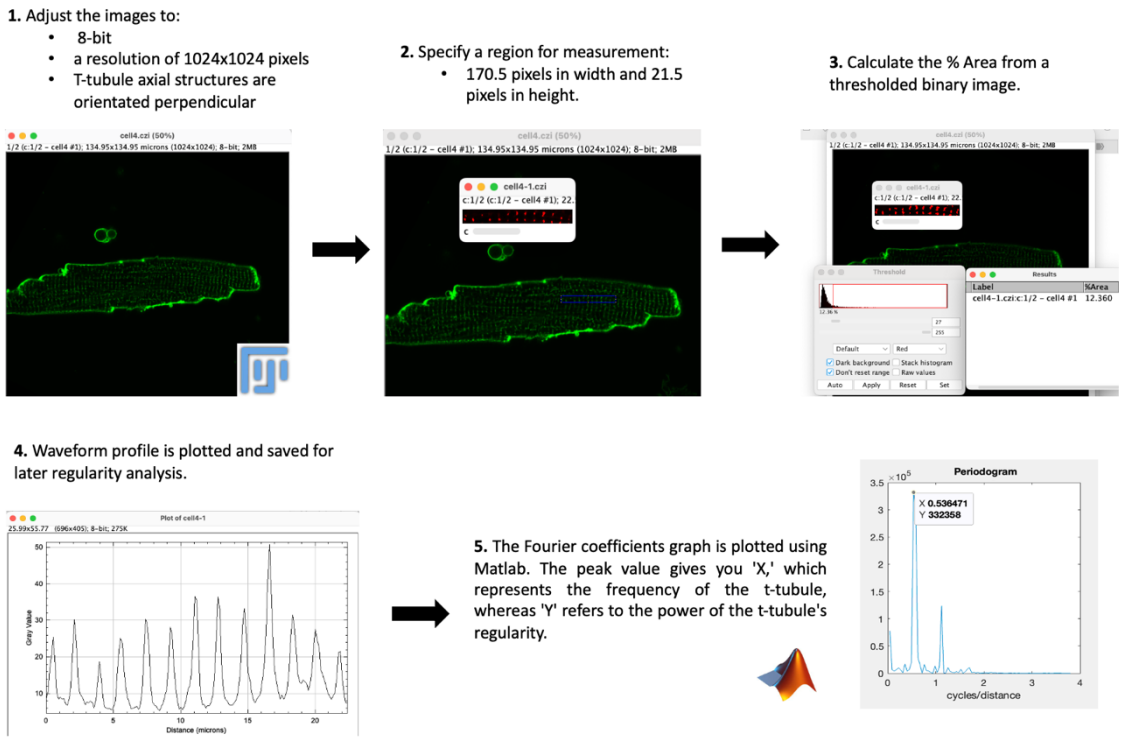


Figure 2.5. T-tubule density and regularity measurement protocol.

2.8.3 T-tubule Directionality Measurement

T-tubules are the invagination of the sarcolemma membrane, consisting of both transverse and axial elements, and those structures were analysed using Fiji software with a custom-written macro. Images were first rotated to ensure that the cells were horizontal, allowing the transverse elements to be perpendicular. The outer surface membrane area was removed, leaving only the intracellular membrane area selected. The threshold was adjusted to allow most of the T-tubule structures to be detected without any background noise. The skeletonised images were then generated, and the frequency of the T-tubule orientated axially (0° ± 5°) or transversely (90°± 5°) was quantified (Wagner et al., 2014). A detailed protocol of T-tubule directionality measurement is shown in Figure 2.6.

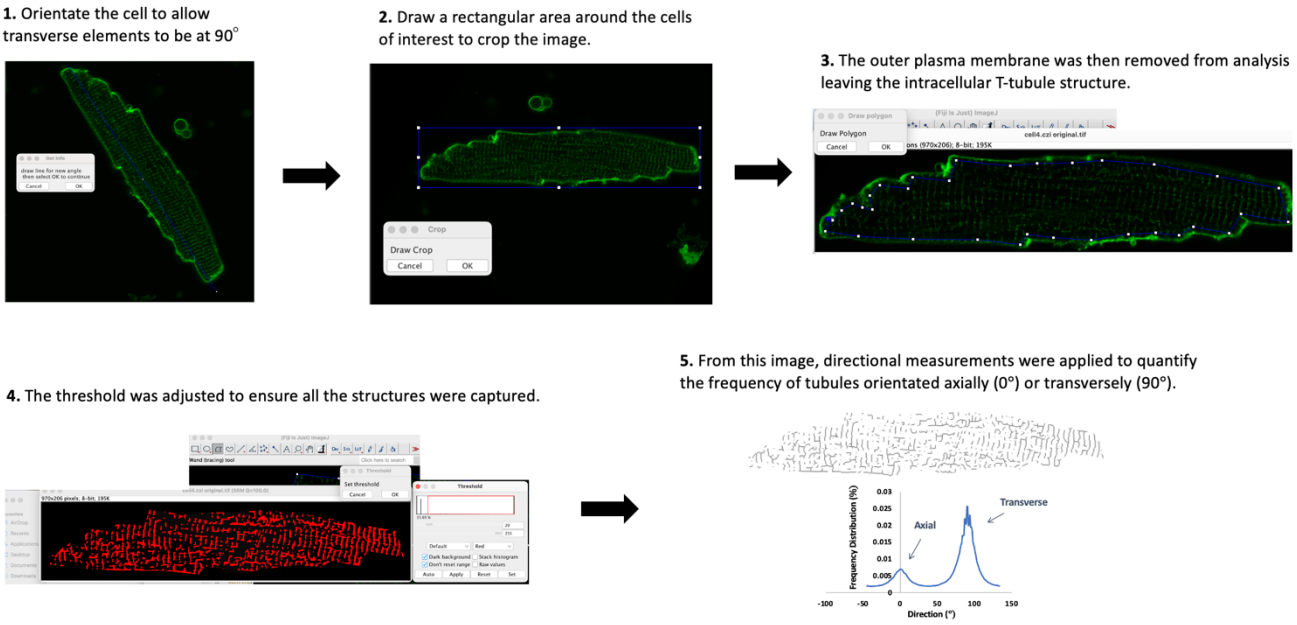


Figure 2.6. T-tubule directionality measurement protocol.

2.9 Immunocytochemistry

2.9.1 Immunostaining for Cardiomyocyte

Isolated cardiomyocytes were exposed to 2ml isosmotic/hypoosmotic solution for 15 minutes. Subsequently, the solution was removed, and the cells were fixed in 4% paraformaldehyde (PFA) for 10 minutes. The cells were then washed three times in phosphate-buffered saline (PBS) and permeabilised with 0.1% Triton-X in PBS for 20 minutes at room temperature. After permeabilisation, the cells were washed three times with PBS and blocked in a solution containing PBS, 5% bovine serum albumin (BSA), 20% Tween 20 and 10% goat serum for 30 minutes at room temperature. The cells were incubated with the primary antibodies (Table 2.2) in the blocking solution for 24 hours at 4 ℃. The next day, the cells were washed three times in PBS and incubated with the secondary antibodies (Table 2.2) in the blocking solution in the dark for 2 hours at room temperature. Finally, the cells were washed three times in PBS, and mounted onto glass coverslips using Prolong Gold mounting medium with DAPI for nuclear staining. The edges of the coverslips were sealed with nail varnish and left to dry for 1 hour.

	Host	Dilution	Source
Primary antibodies			
Purified mouse anti-caveolin-3	Mouse	1:100	BD Bioscience
Non-commercial Sheep anti-PDE4B	Sheep	1:200	Baillie, Glasgow
Non-commercial Sheep anti-PDE4D	Sheep	1:200	Baillie, Glasgow
Secondary antibodies			
Alexa Fluor 488 conjugated donkey anti-mouse IgG	Donkey	1:500	ThermoScientific
Alexa Fluor 546 conjugated donkey anti-sheep IgG	Donkey	1:500	ThermoScientific

Table 2.2. List of antibodies used in the immunostaining.

2.9.2 Colocalisation Measurement

The images were taken using the Leica Stellaris 8 Inverted confocal microscopy (FILM, Imperial College London) with an x65 oil immersion objective lens. Alexa Fluor 488 was excited at a wavelength of 499nm, with emission detected at 520nm. Similarly, Alexa Flour 546 was excited at 556nm, and emission was detected at 573nm. The settings remained the same throughout the imaging: smart gain at 11.5%, smart intensity at 15.51%, a pinhole of 1.00 AU, zoom at 1.28, a Z-step size of 0.115μm, and a total Z-stack distance of 6.98 μm.

Cardiomyocyte and tissue colocalisation were assessed by measuring the overlap of pixel intensity between two proteins, and it was processed using Fiji software. Initially, the Cav3 and PDE4D channels were separated using the "Split Channels". A circle was then drawn around the cells to minimise the background noise and exclude unrelated cells. Subsequently, the JACoP plugin was applied to quantify colocalisation (Oliver et al., 2019). Two colocalisation coefficients were used in this thesis. The first one is Pearson's correlation coefficient, which is

the most common measure of linear correlation between two variables, ranging from -1 to 1. A value close to 1 indicates perfect colocalisation. The other one is Mander's coefficient (M1 & M2), which indicates the percentage of the total signal from one channel that overlaps with the signal from the other channel. Instead of using the automatic thresholds, we used the threshold that was acquired from the negative control of two proteins. A detailed protocol of colocalisation measurement is shown in Figure 2.7.

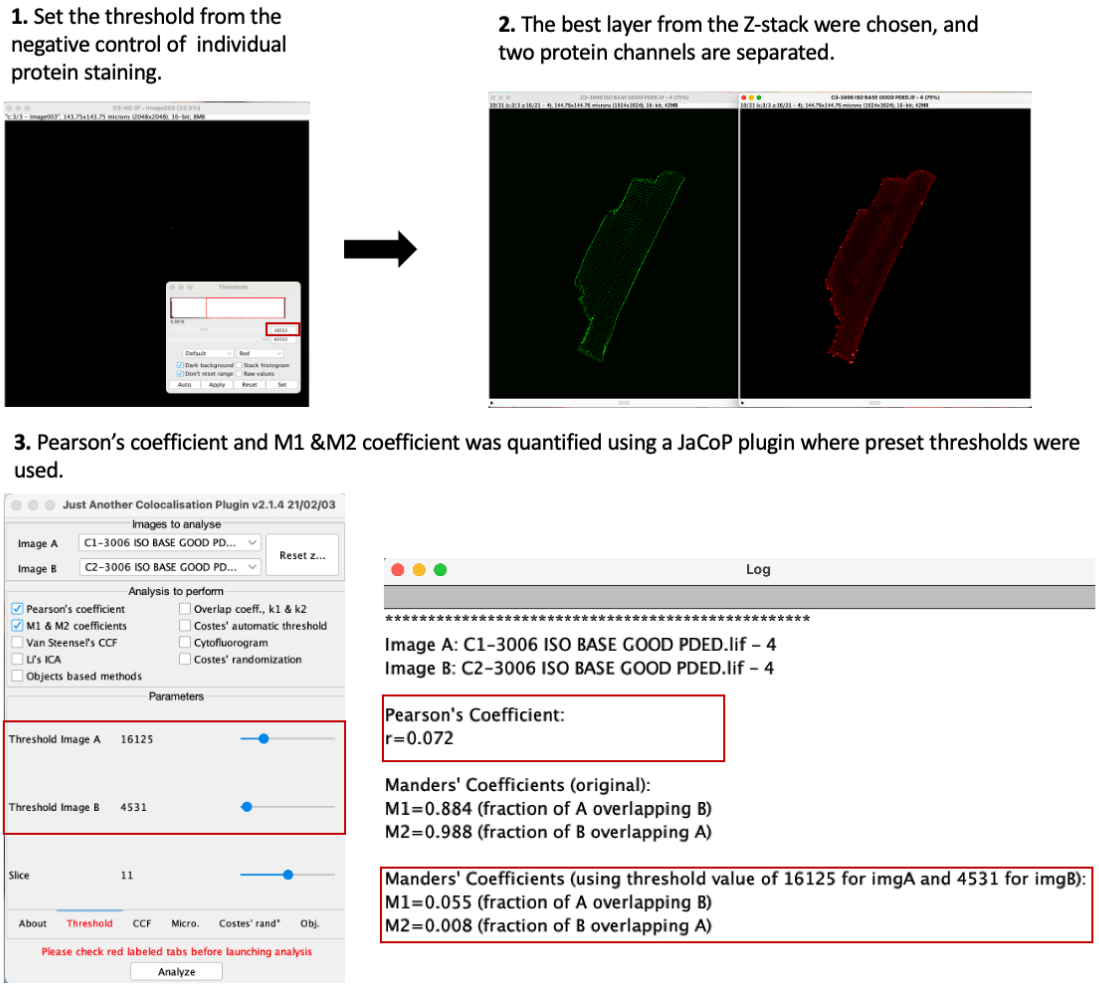


Figure 2.7. Colocalisation measurement protocol.

2.10 Förster Resonance Energy Transfer (FRET) Microscopy

2.10.1 Introduction and Principles of FRET

Förster resonance energy transfer (FRET) microscopy is a highly effective functional imaging technique that enables the observation of changes in protein conformation and protein-protein interaction within living cells with nanometer resolution (Padilla-Parra and Tramier, 2012) (Sekar and Periasamy, 2003). FRET is a distance-dependent physical process in which energy is transferred radiationlessly from an excited donor fluorophore to an acceptor fluorophore (Főrster, 1959). For this process to occur, the two fluorophores must be in close proximity, typically within a range of 1-10nM. The efficiency of FRET not only depends on this proximity but also requires spectral overlap between the emission spectrum of the donor fluorophore and the absorption spectrum of the acceptor fluorophore, as well as the appropriate orientation of their dipoles (Padilla-Parra and Tramier, 2012) (Figure 2.8). Green fluorescent protein (GFP) and its derivatives have been widely used as donor and acceptor fluorophores in FRET experiments. The cyan fluorescent protein (CFP) – yellow fluorescent protein (YFP) pair is the most commonly used, known for its good photostability and brightness, which permits accurate ratiometric measurement (Pollok and Heim, 1999).

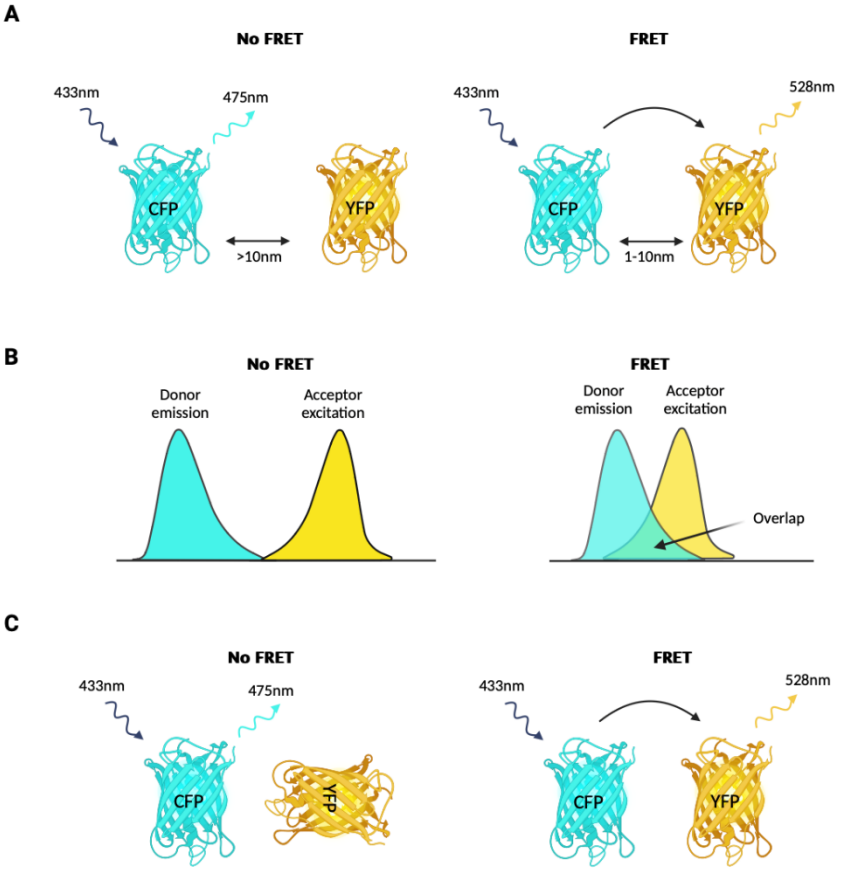


Figure 2.8. Principle of the FRET phenomenon. **A.** If two fluorescent proteins, e.g., cyan fluorescent protein (CFP) and yellow fluorescent protein (YFP), are too far apart (>10nm), no FRET occurs. When they are within range (1-10nm), excitation of the donor is propagated to the acceptor, resulting in emission from the acceptor being observed. **B.** For FRET to occur, the donor's emission spectrum must overlap with the excitation spectrum of the acceptor. **C**. FRET occurs when the dipole orientation of the donor and acceptor are parallel; otherwise, no FRET can be measured (figure created with BioRender).

2.10.2 Plasma Membrane Epac2 (pmEPAC2) FRET Sensor for cAMP Measurement

The Epac2 FRET sensor, a fluorescent indicator for cAMP that is based on the cAMP-binding domains of Epac and is expressed throughout the cytosol, was developed by Prof. Viacheslav Nikolaev. This development was achieved by fusing the cAMP-binding domain of Epac to CFP and YFP (Nikolaev et al., 2004). The pmEPAC2 FRET sensor was designed based on the Epac2 FRET sensor. The construction of the pmEPAC2 sensor involved the modification of the Epac2

sensor at its N-terminus, by adding the 'SH4' motif (MGCINSKRKD) from Lyn kinase (Wachten et al., 2010) (Figure 2.9). Lyn kinase is a protein known for its ability to anchor to the plasma membrane through post-translational modifications, specifically myristoylation and palmitoylation (Zacharias et al., 2002). These modifications involve the addition of myristate and palmitate fatty acids to the protein, which facilitates its localisation to the plasma membrane and also its preferential localisation to caveolin-rich domains.

When unbound to cAMP, the proximity of CFP and YFP allows for energy transfer from CFP to YFP, thereby increasing the FRET signal. Binding with the cAMP leads to a conformational change within the pmEPAC2 FRET sensors, increasing the distance between CFP and YFP. Consequently, the energy no longer transfers between them, decreasing the FRET signal (Figure 2.9).

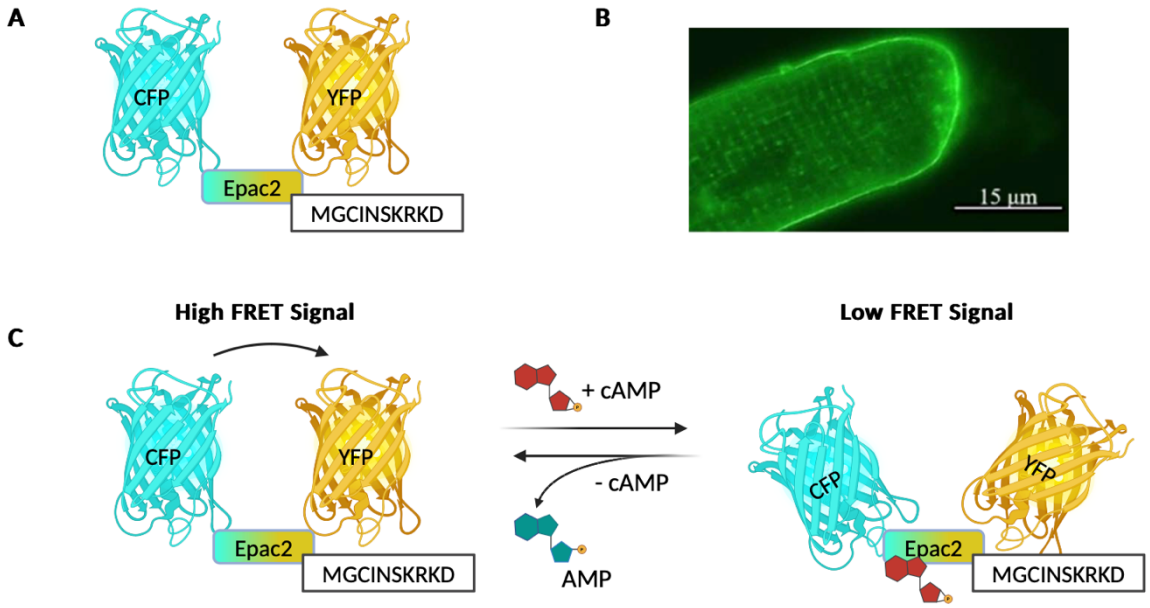


Figure 2.9. Overview of the pmEpac2 Sensor. A. The pmEpac2 sensor is based on the Epac2 sensor and is combined with the SH4 motif (MGCINSKRKD) from the Lyn Kinase. **B.** A representative image shows how pmEpac2 is expressed in an isolated adult rat left ventricular cardiomyocytes. **C.** When the pmEpac2 sensor is activated by cAMP, there's a decrease in the FRET signal (figure created with BioRender).

2.10.3 Cardiomyocyte FRET Sensor Infection Protocol

Isolated Cardiomyocytes were centrifuged at 10,000RPM for 1 min and resuspended in MEM media (composed of 10.74 g/L MEM with Hank's salts, 9mM $NaHCO_3$, 1% Glutamine, and 1% Antibiotic Antimycotic, all dissolved in culture grade water), supplemented with 10% FBS. Approximately 10,000 cells were then plated on a laminin-coated 25mm glass slide. Following 1h attachment, cells were washed with serum-free MEM media to remove the non-adherent cells or dead cells and cultured for 48h at 37 ℃, 5% CO_2 in MEM media, in the presence of adenoviral vectors encoding the pmEPAC2 FRET sensor, at a multiplicity of infection (MOI) of 200.

2.10.4 Multi-cell FRET Microscopy for Measurement of cAMP Activity

The high-throughput Multi-cell FRET Microscopy system was developed by Dr Masoud Ramuz (Ramuz et al., 2019). An overview of the FRET Microscopy setup is shown in Figure 2.10A. This system includes a CMOS camera connected to an inverted Nikon TE2000 microscope, complemented by a 430nm LED light source and a long pass 455nm dichroic mirror. The fluorescence emitted can be split into YFP and CFP channels by passing through a beam splitter equipped with 480/30 and 525/30 emission filters, allowing the acquisition of cyan and yellow light, respectively. Additionally, the system has a mechanised stage, which enables the positioning of cells in the X and Y coordinates. Visualisation of cells was carried out using a Plan Apo 60X/1.40 oil objective, and real-time ratiometric FRET signals could be analysed using an integrated Micro-manager (Icy 1.4), based on the data acquired by moving the mechanical stage between cells and capturing images of each at set intervals (Figure 2.10B).

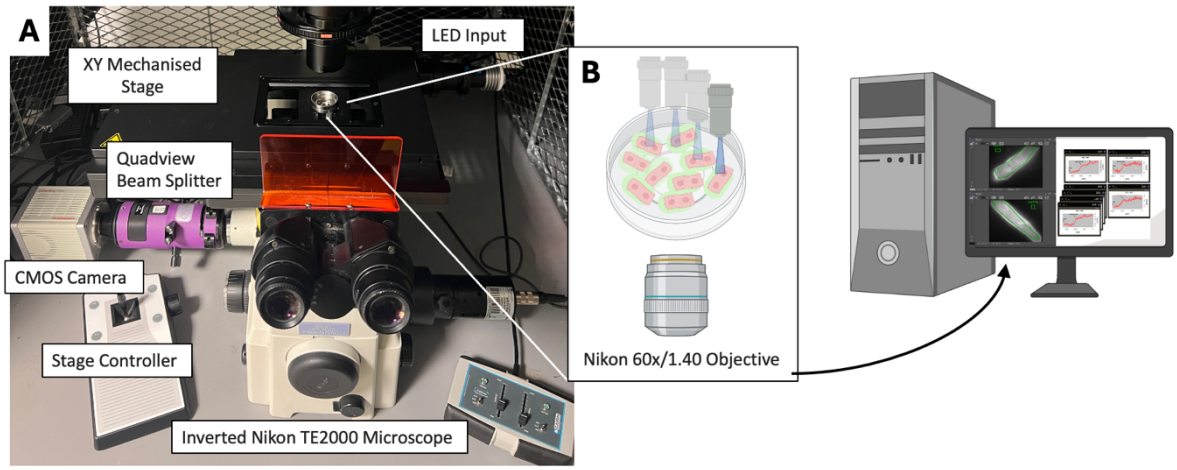


Figure 2.10. Overview of FRET Microscopy system. A. FRET Microscopy system setup. **B**. The system is capable of simultaneously capturing and analysing multiple cells in real time. During each set time interval, the mechanical stage automatically cycles through all pre-selected cells, capturing and analysing data for each cell. This cycle is consistently repeated at each interval (panel B created with BioRender).

Baseline FRET measurement was measured with either iso- or hypoosmotic solution in the presence of β_1 (100nM CGP 20712A) or β_2 blocker (50nM ICI 118,551), and cells were perfused with 100nM isoprenaline (Schobesberger et al., 2017). Following this phase, 100µM IBMX, a non-selective PDE inhibitor and 10µM Forskolin, a adenylyl activator, were perfused onto the cells to cause the maximum stimulation of cAMP activity, which allows normalisation of the βAR-cAMP response to the maximum cAMP responses (Kwan et al., 2023). A detailed protocol was described in each chapter, and an illustration diagram was shown in Figure 2.11A.

When data acquisition is completed, it will automatically export as an Excel file. The mean FRET ratios from the last 10 acquisitions before adding the first stimulant were determined as baseline. The mean FRET ratios for each subsequent stimulant were calculated in a similar manner, using the last 10 acquisitions before introducing the new stimulant or saturator. These mean values are used to determine the FRET ratio shift from the baseline induced by

each stimulant. This change is then normalised to the saturator, which gives us the total cAMP response to the stimulant stimulation (Figure 2.11B).

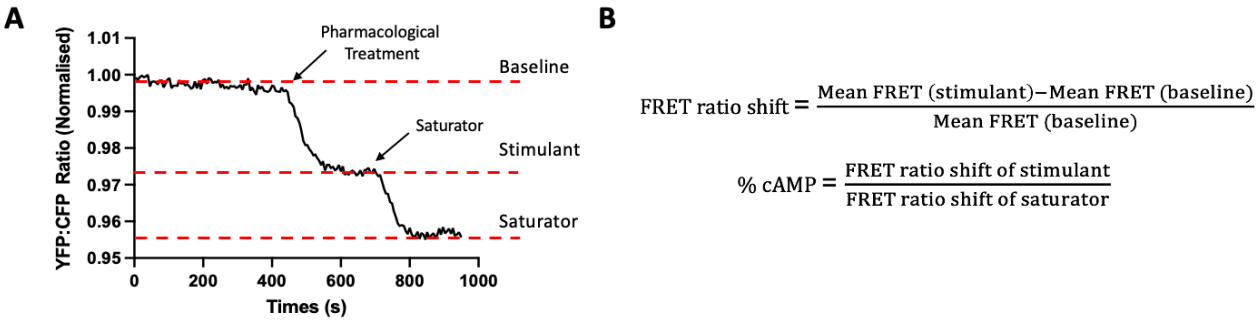


Figure 2.11. Illustration of FRET experiment calculation. A. An example FRET trace, which will vary depending on different protocols. **B**. Calculation of the FRET ratio shift given by each treatment and also the maximum cAMP release.

2.11 CytoCypher

2.11.1 Introduction of CytoCypher

CytoCypher/IonOptix MultiCell System™ is a high-throughput system that can simultaneously measure the contractility and calcium transient of living myocytes (Wright et al., 2020). A schematic of the system is shown in Figure 2.12. It has a static high-resolution MyoCam-S3 digital camera, combined with a scanning microscope that can rapidly position along the x-y-z axes. The system is connected to a fluorescence system interface device equipped with a HyperSwitch Light Source for dual excitation ratiometric fluorescence recordings. The cells are placed in a chamber that maintains a constant temperature of 37℃, and are stimulated to contract via a MyoPacer-EP cell stimulator through a pair of electrodes at a frequency of 1.0Hz (20V for rat cells, 40V for human cells, with a 10ms pulse width). Figure 2.13 shows a large mosaic field measuring approximately 3500μm by 1600μm, from which a specific area of interest can be chosen. Once an individual cell is chosen from this area, its orientation and

focus are adjusted to facilitate the measurement of sarcomere length. Subsequently, the recording is made. The software then marks out this cell with a green rectangle for future assessment. Following this, the same process is repeated with the next cell.

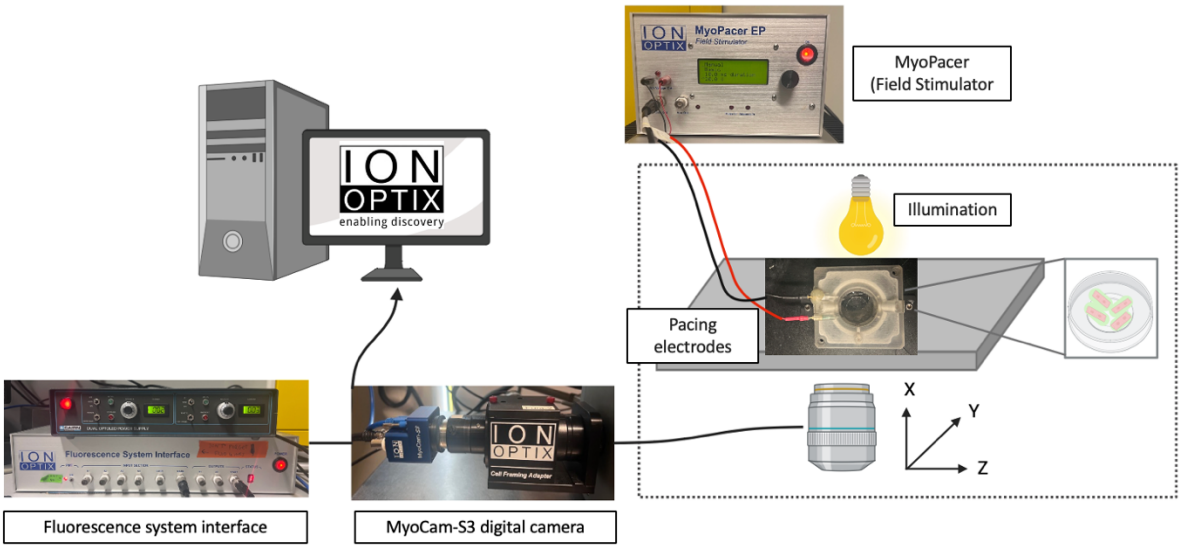


Figure 2.12. Overview of CytoCypher setup

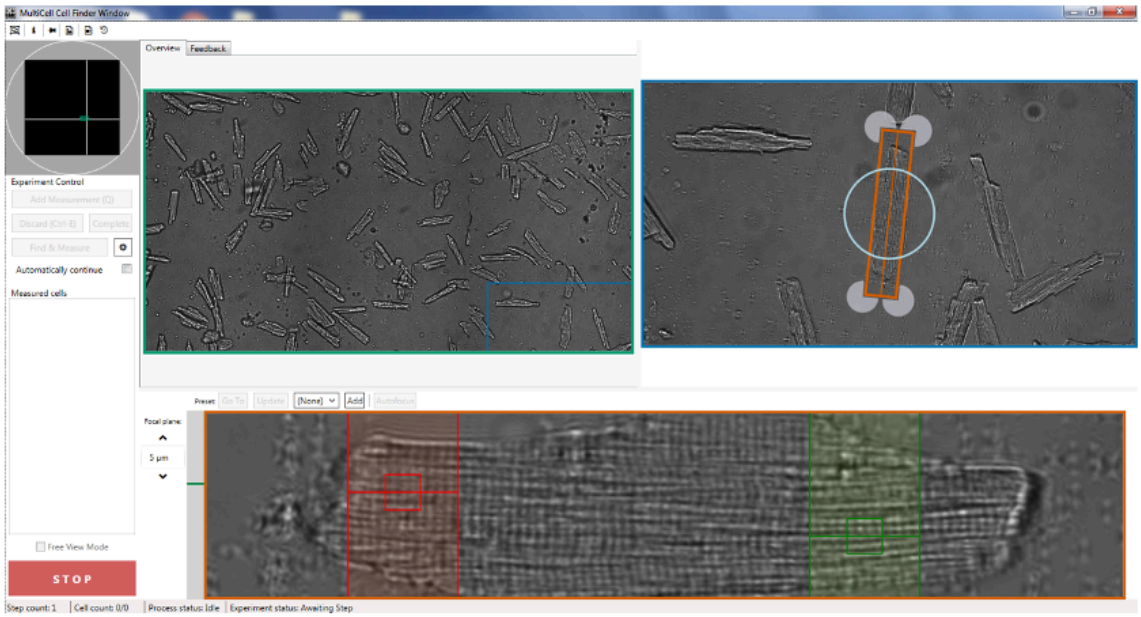


Figure 2.13. Illustration of the acquisition screen of the CytoCypher system.

Data were analysed using the Cytosolver (IonOptix LLC, United States). In this study, we analysed three key parameters of sarcomere-shortening magnitude and speed: percentage of sarcomere shortening, time to 90% peak (TTP90) and time to 10% above baseline (TTB90). TTP90, the time taken to reach 90% of the peak, measures the speed of contraction. TTB90, the time from peak to 10% above baseline, measures the speed of relaxation. For the calcium transients and speed, the following parameters were measured: calcium transient F/F0, TTP90 and TTB90. A summary of the measured parameters is shown in Figure 2.14.

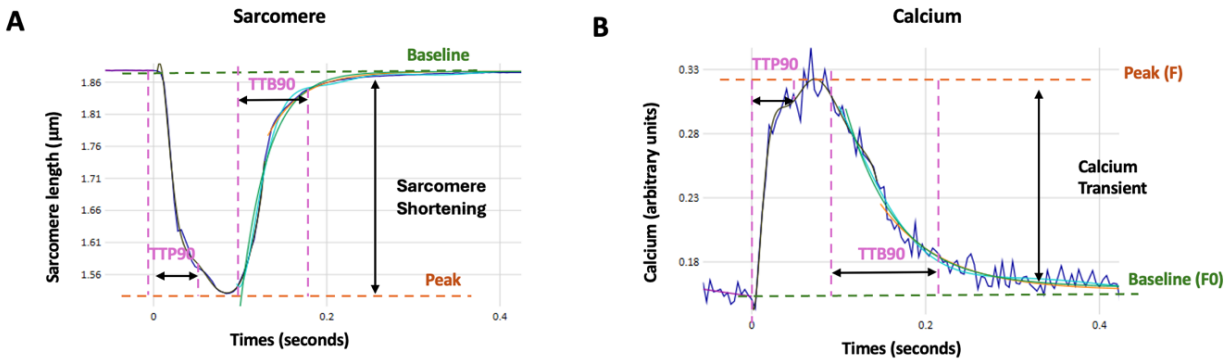


Figure 2.14. Illustration shows a single transient of sarcomere and calcium produced in a cardiomyocyte. A. The initial length of the cell, measured during the diastolic period before the application of the pacing current, is referred to as the baseline cell length. The cell undergoes transient shortening, referred to as the systole phase. Sarcomere shortening is determined by the difference in cell length between systole and diastole, and this parameter is used as an indicator of the strength of sarcomere contractility. TTP90 represents the time taken to reach 90% of peak contraction from baseline, indicating the cell's inotropic ability. TTB90 is the time taken for the cell to relax and restore 90% of the shortening produced by the pacing current, which reflects the cell's lusitropic ability. **B.** The amplitude of the calcium transient was defined as peak (F) divided by the baseline (F0). The time to reach 90% of the peak is represented as the calcium transient rise time, while the time from peak to 10% of the baseline is represented as the calcium decay time.

In addition to functional studies, the CytoCypher system can also capture thumbnail images of cells, providing two-dimensional morphological information (Kartasalo et al., 2015). A segmentation mask is created using a custom macro in FIJI (Figure 2.15), which is subsequently used in conjunction with CytoSpectre, a freeware image analysis software. Data are extracted into Excel, where the cell minor axis represents cell width, and the major axis represents the cell length (Figure 2.15).

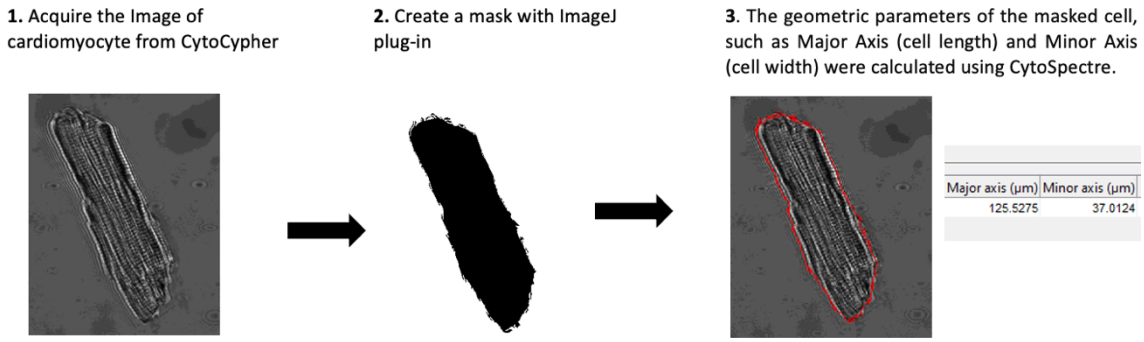


Figure 2.15. Overview of the cardiomyocyte morphology analysis using CytoSpectre software. The image of the cardiomyocytes is masked using Fiji, and the marks are applied to identify cell edges. The masks and original images are then analysed using CytoSpectre to identify cell length, width and sarcomere regularity.

2.11.2 CytoCypher Protocol

Isolated cardiomyocytes at a density of 100 cells/µl were plated on laminin-coated MatTek™ (MatTek Corp, United States) dishes and left for 1h at room temperature to allow attachment. Following this, the cells were perfused with Hank's Buffered Salt Solution (HBSS), 1mg/ml BSA, and 1µM Fura-2AM, a calcium-sensitive fluorescent indicator, for 45min (5% CO_2, 37°C). After incubation, cells were washed with HBSS and BSA and incubated for another 20 minutes.

The cardiomyocytes were transferred to the CytoCypher chamber and stabilised for 15min in the iso/hypoosmotic solution. Pacing was set at 1Hz, and 10-15 cells were randomly chosen for baseline measurement. Selection and analysis criteria included a rod shape with clear

striations, being quiescent before pacing, and showing no arrhythmic activity throughout the experiment. The timeline of the overall CytoCypher experiment is shown in Figure 2.16.

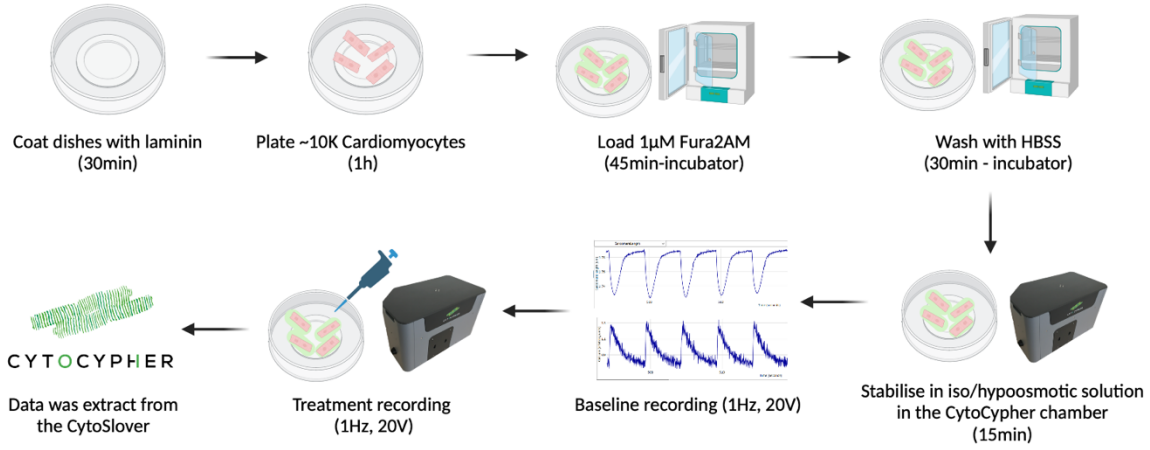


Figure 2.16. Summary of the cell preparation study protocol for CytoCypher experiment (figure created with BioRender).

2.12 Langendorff-Optical Mapping

While a deep understanding of cellular and molecular mechanisms is crucial for comprehending physiological and pathological electrophysiological processes, it is also important to place these cellular findings in the context of whole-heart electrophysiology.

2.12.1 Introduction and Principle of Langendorff-Optical Mapping Approach

The isolated perfused heart model has been used in cardiovascular research for over a century. The foundational concepts of perfusing a heart ex vivo were first introduced by Oskar Langendorff in 1895; known as Langendorff perfusion, which involves delivering an oxygen and glucose-rich perfusate into the aorta in a retrograde way under constant hydrostatic pressure (Langendorff, 1895). This reverse flow causes the aortic valve to close and directs the perfusate into the coronary arteries, supplying the myocardium with oxygen and nutrients via

the pulmonary artery. With this approach, the heart could be kept alive ex vivo for several hours.

Perfusion can be maintained using two main ways: constant pressure or constant flow rate (Skrzypiec-Spring et al., 2007). The original constant pressure method developed by Langendorff has the advantages of being physiologically relevant and simple to implement. In this method, the aortic cannula is connected to a reservoir of perfusate held at a height that creates a perfusion pressure of around 80-100mmHg. This system allows the coronary vessels to maintain their autoregulatory function, adjusting coronary blood flow in response to local physiological conditions through vasoconstriction or vasodilation. However, a limitation of this method arises when precise drug dosing is required, as changes in heart rate or myocardial contractility can affect coronary perfusion. In this study, perfusion was maintained using the constant flow rate method, where a peristaltic pump delivers the perfusate at a steady rate. This approach overrides local autoregulatory processes, ensuring a constant volume of perfusate or dose of the drug is delivered, regardless of changes in contractility and heart rate (Katz et al., 1939).

Optical mapping is a non-contact imaging technique that provides high spatiotemporal resolution and is used to record biological data from whole hearts, allowing us to map the propagation of heterogeneous electrical signals across the myocardium. Potentiometric dyes were used to monitor transmembrane voltage changes, and calcium-sensitive fluorescent probes were used to study cellular calcium transients. Optical mapping experiments involve several key steps. First, the isolated, perfused hearts are stained with potentiometric dyes that bind to the cell membrane's phospholipid bilayer, while the calcium-sensitive dye crosses the cell membrane and binds to cytosolic Ca^{2+}. A specific light wavelength is then directed

onto the heart to excite the fluorescent dye. This excitation prompts the dye to transition from its resting state to an excited state, during which it emits photons. These photons are captured and focused through a system of optical lenses, filters, and mirrors onto a photodetector, which measures the changes in the fluorescence signal. Each pixel of the resulting data represents the spatial average of transmembrane potential changes for the group of cells within that specific field of view (O'Shea et al., 2020).

2.12.2 Protocol for Langendorff-Optical Mapping Experiments

Male Sprague Dawley rats (250-350g) were first deep anaesthetised (5% isoflurane, 95% oxygen) and then humanely killed with cervical dislocation. Death of the rats was confirmed by exsanguination from the carotid artery. Thoracotomy was performed to expose the chest cavity, and the heart was taken along with the surrounding tissue such as lungs, thymus, and trachea. The heart was then transferred to the cold oxygenated Krebs-Henseleit buffer, which contained (mmol/L): NaCl 118.5, KCl 4.6, $CaCl_2$ 1.4, $MgCl_2$ 1.2, $NaHCO_3$ 25, $NaH_2PO_4.2H_2O$ 1.2 and glucose 11, pH=7.4) with 5000 units/ml of unfractionated heparin (Wockhardt UK Ltd) to prevent the internal blood clot and limit the effects of hypoxia. To avoid air embolism of the coronary arteries, the heart was gently submerged, and the lungs, trachea, thymus, and aortic arch were excised. The aorta was held by the arch and cut horizontally just below the branch. The heart was then ligated on the metal cannula via the aorta and held temporality in place with a clip. A silk 4-0 suture (Ethicon, UK) was used to secure the aorta to the cannula. The aorta is cannulated above the sinus of Valsalva where the coronary opstia originate, and coronary flow of the perfusate was established. After successful cannulation, the pulmonary artery was cut open to provide drainage. The heart was placed in a custom-made chamber to maintain the temperature surrounding the heart and also allow light transmission. The heart

was retrogradely perfused with oxygenated KHB solution with a flow rate of 15ml/min using a Peri-Star Pro peristaltic pump (World Precision Instruments-Europe, UK) at a temperature of 37℃ and was allowed to stabilise for 15min. An electrode was placed in the epicardial layer of the basal portion of the left ventricle for pacing the heart and another electrode connected to the cannula with a crocodile clip to create a closed circuit. The pacing wires were connected to a clinical pacing system (Micropace, MicropaceEP Ltd, UK). Three separate electrodes were connected to a Bioamplifier (AD Instruments, USA) and a data acquisition system (Powerlab 8/35, AD Instruments, USA), where the realtime ECG was displayed in the LabChart 7 (AD Instruments, USA).

2.12.3 Mechanical Stretch Model

Ventricular ballooning is a widely used model to investigate the physiological effects of stretch at the whole heart level. In this setup, a deflated latex balloon (Harvard Apparatus), connected to a pressure transducer and syringe is inserted into the left ventricular lumen via an incision in the left atrium, along with a separate tube of 0.9 mm outer diameter. Both the balloon and tube are secured by attaching them to a stand. The balloon is then inflated with 1 ml of distilled water to achieve a pressure of 60 mmHg, creating a stretch model in the heart (Li et al., 1997). For the control model, the balloon is inserted without inflation. An illustration of the stretched model is shown in Figure 2.17.

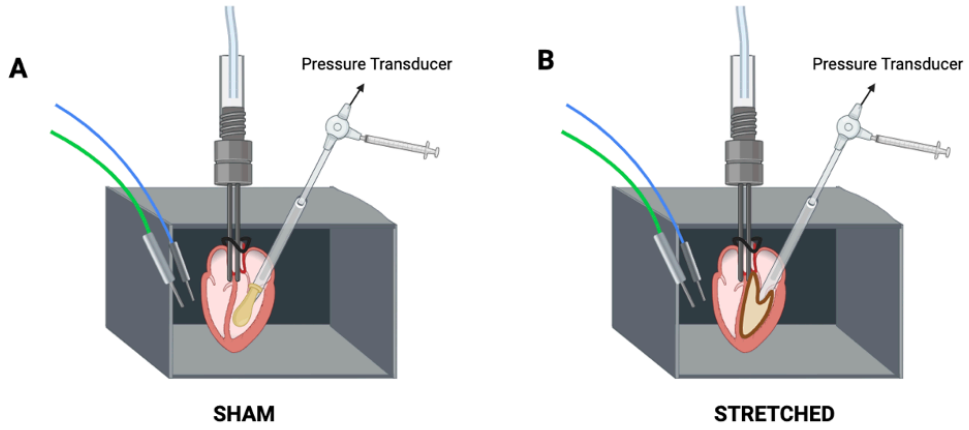


Figure 2.17. Illustration of the balloon stretched model. A. Sham condition: the balloon is inserted into the left ventricular lumen without inflation.**B**, Stretched condition: the balloon is inserted and inflated, stretching the left ventricle. Both setups include a pressure transducer for monitoring (figure created with BioRender).

2.12.3 Optical Mapping Set Up

Optical Mapping experiments were performed using two custom-made complementary metal oxide semiconductor (CMOS) optical mapping camera systems (Cairns Research Lab, UK). The dual-camera set-up allowed for simultaneous mapping of the transmembrane potential and calcium transient.

An array of four LEDs (Cairn, Faversham, UK) with 525/36nM filters (green) were used for the excitation of dye on the stained heart. The light emitted from the epicardial surface of the heart passed through a 0.65x objective lens (Nikon, UK) and a macroscope (x0.63 – x6.3, MVX10, Olympus, UK) to allow light to be finely focused. The light was then passed through a dichroic mirror which splits the light into two perpendicular light beams passing to two FastCMOS-128X cameras (Redshirt LLC, Georgia, USA), with the 620LP filter for voltage

imaging and 585/40nm filter for calcium imaging. The CMOS cameras have a 128X80 pixels sensor resolution and for all the experiments in this study, a sampling rate of 1KHz was used.

The Langendorff-Optical Mapping set up was demonstrated in Figure 2.18.

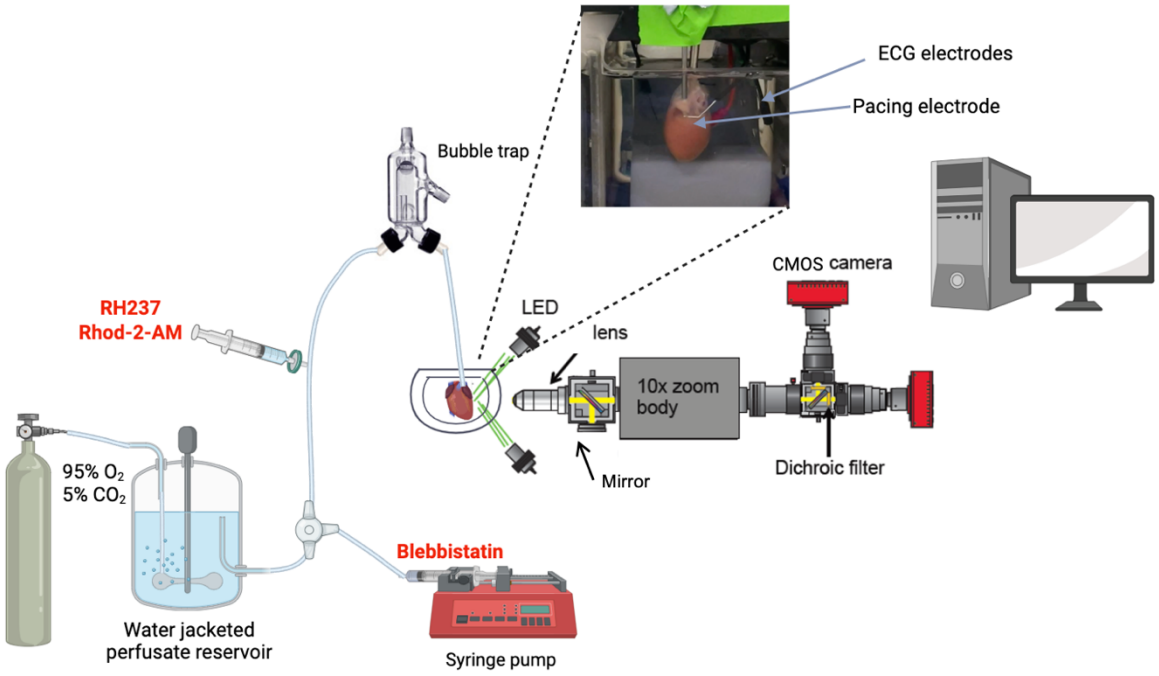


Figure 2.18. Illustration of Langendorff-optical mapping set up. The heart was explanted from an SD rat (300-350g) and rapidly cannulated on the Langendorff perfusion apparatus. The heart was perfused with a Krebs-Henseleit buffer (composed of, in mmol/L: NaCl 118.5, Glucose 11.1, MgSO4 2.5, NaH2PO4:1.4, KCL 4.5, CaCl2 1.85, NaHCO3 25.0; 37°C, 95% O2 and 5% O2) with a constant flow rate of 15ml/min. A deflated latex balloon (connected to a pressure transducer and an air-filled syringe) was placed in the left ventricular lumen via the mitral valve and opening created by an incision in the left atrium. The LV was stretched by 1ml air inflation of the balloon (60mmHg). An electrode was placed in the epicardial layer of the basal part of the left ventricle for pacing and stimulating the heart. ECG signal was continuously recorded and displayed on the computer. 10µmol/l Blebbistatin, an excitation-contraction uncoupler, was used to prevent motion artefacts during the recording. The potentiometric dye RH237 was used to map transmembrane voltage, while Rhod-2-AM was used for imaging calcium transients. Our optical mapping is performed using two CMOS cameras with the following combination of filters: 525/36 for excitation, 700nm dichroic mirror with 620LP for RH237, and 585/40 for Rhod-2AM (figure created with BioRender).

2.12.4 Dye Loading

In this study, the potentiometric dye RH237 (Invitrogen, UK) was used to record transmembrane voltage. RH237 is a fast-response, voltage-sensitive probe that binds to the cardiomyocyte membrane, where changes in membrane potential cause shifts in the intramolecular charge distribution of the dye, resulting in an alteration in its emission fluorescence. For the optical mapping experiment, the heart was loaded with 50µl of KHB prepared from a stock solution of 5mg/ml RH237 dissolved in DMSO. RH237 was injected over five minutes at a rate of 0.2ml/minute through a side port near the aortic cannula, using a 22G needle attached to a 1ml syringe, with care taken to minimise the risk of introducing air bubbles.

Calcium transients were imaged by loading the heart with the calcium-sensitive dye Rhod-2AM (Invitrogen, UK). Rhod-2AM belongs to the Rhod family of long-wavelength calcium indicators, which increase in fluorescence intensity when bound to Ca^{2+}. The combination of Rhod-2AM and RH237 was selected due to their narrow excitation spectrum, both peaking at 540nm, but with different peak emission wavelengths, 585nm for Rhod-2AM and 650nm for RH237. Therefore, this combination allows us to measure the intracellular calcium at 585nm without interference from RH237 fluorescence, enabling simultaneous recordings of both membrane potential and calcium transient (Choi and Salama, 2000).

For each experiment, 200µl of Rhod-2AM (Invitrogen, UK), prepared from 1mg stock in 1ml DMSO and mixed with 1ml of 20% Pluronic F-127 (Invitrogen, UK), a non-ionic detergent that aids in dye solubilisation and uptake, was dissolved in 2ml KHB. The Rhod-2AM was loaded into two 1ml syringes and administered over 5-10mins via a side port. Images were taken via the camera 25-30 minutes after infusion to ensure adequate dye loading.

Since RH237 is entirely membrane-bound and does not need to transit to the cytoplasm, its fluorescence signal can be visualised immediately after administration. And because RH237 exhibits a slight degree of photobleaching with prolonged exposure to LED light, therefore Rhod-2AM was administered first, followed by RH237.

2.12.5 Acquisition of Optical Mapping Data

After the dyes and excitation-contraction uncoupler were administered, data recording was started once all visible cardiac movements had stopped. The data were captured using the Turbo-SM software (RedshirtImaging LLC, USA). Before starting data acquisition, four LED lights were arranged around the heart to provide optimal illumination across the recording region, the epicardial surface of the left ventricle. The objective lens and macroscope were then focused, and the zoom was adjusted to maximise the recording area.

Baseline recordings were obtained with the heart paced at a rate faster than its sinus rhythm, with a cycle length of 200ms and a sampling rate of 250 frames per second with 4ms exposure time. Afterwards, 100nM of the β_1 blocker CGP was injected, and recordings were taken at a cycle length of 200ms. Subsequently, 100nM of Isoprenaline was administered, and recordings were made at a cycle length of 150ms.

All data were analysed using a custom-written Matlab (Matlab v2023b, Mathworks, USA). In this study, we analysed the following parameters: action potential duration 50, 70 and 90, calcium transient duration 50, 80 and 90 and conduction velocity (Figure 2.19).

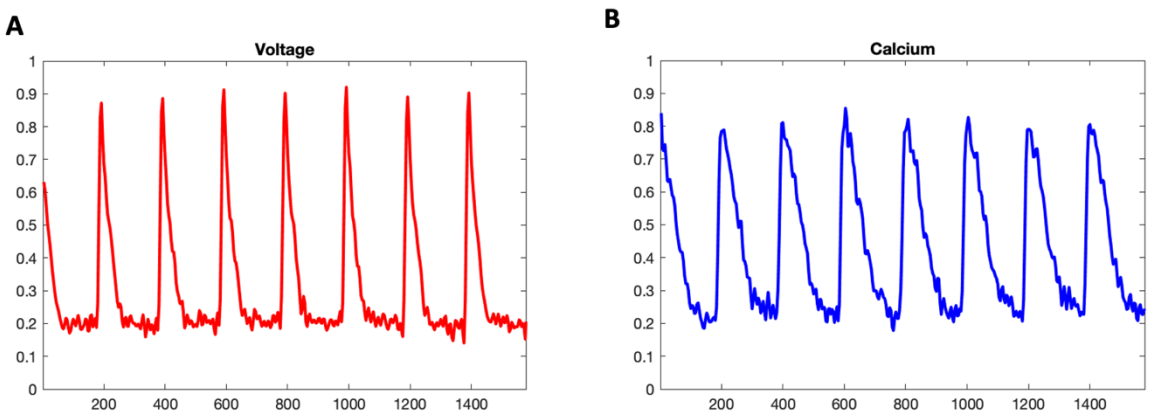


Figure 2.19. Examples of voltage and calcium traces.

2.13. Statistics

All statistical analyses were performed using Prism 10 (GraphPad). Data are presented as mean ± standard error of the mean (SEM), unless otherwise specified. The number of animals/patients is represented by 'N', while the number of cells is represented by 'n'. Statistical comparisons on histograms are indicated between columns tested, with asterisks used to denote the significance levels: *p<0.05, **p<0.01, and ***p<0.001. A value of p<0.05 was considered statistically significant. Normality was assessed using the Shapiro-Wilk test. For data sets with normally distributed, parametric analyses were used. When at least one data set did not pass the normality test, non-parametric statistical tests were applied.

An unpaired T-test is used when comparing the means of two independent groups. When we compare the means of three or more independent groups to determine if there are any statistically significant differences among them, One-way ANOVA is used. Two-way ANOVA is used to compare the mean differences between groups on two independent factors. Mixed-effects analysis is used when there is nesting or repeated measurements, as it will account for within-group variability. If multiple measurements are made from the same samples, mixed-effects analysis is used instead of Two-way ANOVA. A post hoc multiple comparisons

test, e.g. Tukey's or Šidák's multiple comparisons test, is used to determine specific differences between the groups.

Nested T-test is used to compare the means of two groups where data are hierarchically structured, while Nested One-way ANOVA is applied to compare three or more groups in hierarchically structured data. A nested test considers potential variability within clusters and, therefore, is highly recommended for high-throughput techniques.

Power calculations were done prior to the experiment using the WebPower, based on published data or pilot studies, which ensured appropriate sample sizes for multiple analyses. For example, in comparison of the number of caveolae between isosmotic and hypoosmotic groups, the effect size, which gives an idea of how big or small the difference between two groups, was calculated using the means and standard deviations of the isosmotic and hypoosmotic groups (Kozera et al., 2009). In this case, the effect size was 1.43, and with a significant level of 0.05 and a desired power of 0.9, a minimum of 9 samples was required. For two-way ANOVA, the effect size was calculated from marginal means and a common variance estimate. Marginal means are the average values for each level of a factor, regardless of other factors. For instance, when comparing the effects of solution (isosmotic vs hypoosmotic) and region (apex vs base), the marginal mean for the isosmotic group would be the average of all isosmotic samples, regardless of region. The common variance is a pooled measure of variability across all groups and was derived by averaging the squared standard deviations from each condition. These values with the desired power and significant level were entered into WebPower, which estimates the sample size needed. For repeated-measures ANOVA, power calculations need to consider the number of repeated measurements, the effect size, and the nonsphericity correction. Sphericity is the condition where the variances of the

differences between all pairs of repeated measurements are similar. Violation of sphericity will lead to an increase in the Type I error rate. Therefore, nonsphericity correction (e.g. Geisser-Greenhouse) is needed to apply to decrease the degrees of freedom.

Chapter 3 The Effect of Membrane Stretch and The Role of Caveolae on β-adrenoceptor Signalling in Cardiomyocytes

3.1 Introduction

Acute myocardial stretch has been shown to elevate cAMP levels in isolated perfused dog hearts (Todaka et al., 1998) and ferret papillary muscles (Calaghan et al., 1999a), though the underlying mechanism remains unclear. The acute stretch from hemodynamic overload presents a significant challenge to the myocardium, occurring in various physiological and pathological conditions such as exercise, myocardial ischemia, hypertensive crises, and heart failure (Neves et al., 2016). The heart, being a mechanosensitive organ, adjusts cardiac output in response to acute stretch through intrinsic mechanosiganlling pathways (Nóbrega et al., 1995, Kohl et al., 1999). Failure to develop this response and improve diastolic function in response to acute myocardial stretch contributes to heart failure pathogenesis. Thus, understanding the mechanosensation and mechanotransduction pathways involved in the cardiac stretch response is vital for developing new cardiovascular disease therapies.

Cardiomyocytes have highly regulated subcellular signalling microdomains. β-adrenoceptor (βARs) in these cells modulate intracellular levels of cyclic adenosine monophosphate (cAMP). The β_1AR subtype is located in transverse tubules (TT) and on the sarcolemmal membrane, increasing cAMP levels via the stimulatory G-protein (G_s). The β_2AR subtype is predominantly found in TT and caveolae, where it can activate both G_s and the inhibitory G protein (G_i), which inhibits cAMP production (Macdougall et al., 2012, Wright et al., 2014, Zhu et al., 2001). The concurrent coupling to G_i proteins can completely negate the G_s-mediated contractile response, providing a cardioprotective effect following β_2AR stimulation.

Caveolae, small membrane invaginations (50-100nM) in cardiomyocytes, play a crucial role as signalling microdomains (Balijepalli and Kamp, 2008) . These structures are rich in cholesterol and sphingolipids, with their integrity maintained by the protein Caveolin-3 (Cav3) (Parton et al., 2020). Caveolae serve as membrane reserves that integrate with the surface area and protect the membrane from rupture (Sinha et al., 2011). They also contain various receptors and ion channels, therefore structural changes in caveolae during stretch may impact associated signalling pathways. Studies have indicated that caveolae are necessary for stretch-induced electrophysiological changes, for example, slowed conduction velocity in ventricular tissue (Pfeiffer et al., 2014) or activation of swelling-induced chloride ion channels in ventricular myocytes (Kozera et al., 2009). In this current study, we aim to explore the role of caveolae in mediating βAR signalling in response to stretch.

3.2 Hypothesis and Aims

Given that caveolae are mechanosensitive nanodomains in cardiomyocytes that regulate β_2-adrenoceptor signalling during the stretch, membrane stretch induced by hypoosmotic swelling will cause structural changes in caveolae, disrupting G_i signalling and thereby enhancing the β_2-adrenoceptor-mediated inotropic response.

Aim 1: Investigate the effect of hypoosmotic swelling on the morphology of cardiomyocytes.

- Objective 1: Assess the number of caveolae in cardiomyocytes maintained in iso- or hypoosmotic solutions using electron microscopy.
- Objective 2: Measure cell size (width and length) in both iso- and hypoosmotic cells using CytoCypher.
- Objective 3: Assess T-tubule density, regularity and directionality via Di-8-ANEPPS staining in healthy and MβCD-treated cardiomyocytes maintained in iso- or hypoosmotic solutions, using confocal microscopy.
- Objective 4: Determine Caveolin-3 density and regularity of healthy and MβCD-treated cardiomyocytes maintained in iso- or hypoosmotic solutions using confocal microscopy.

Aim 2: Investigate the effect of hypoosmotic swelling (membrane stretch) on β_1 and β_2-adrenoceptor signalling pathways in healthy cardiomyocytes.

- Objective 1: Use CytoCypher to assess the contractility of control cardiomyocytes maintained in iso-or hypoosmotic solutions following isoprenaline stimulation in the presence of either β_1 or β_2 blocker.

- Objective 2: Use FRET microscopy to assess the cAMP response of control cardiomyocytes following either β_1 or β_2AR stimulation.

Aim 3: Investigate the role of caveolae in contractility and cAMP response following β_1 and β_2-adrenoreceptor stimulation.

- Objective 1: Assess the contractility and cAMP response of control and MβCD-treated cardiomyocytes with hypoosmotic swelling using CytoCypher and FRET microscopy, respectively.

Aim 4: Investigate the effect of membrane stretch on β_2AR induced G_i response.

Objective 1: Assess the contractility of PTX pre-treated cardiomyocytes using CytoCypher.

3.3 Method

3.3.1 Solutions and Drugs

To study the impact of hypoosmotic swelling in cardiomyocytes, cells were suspended in either isosmotic (osmolarity: 290 mOsm/L) or hypoosmotic (osmolarity: 214 mOsm/L) solutions for 15min.

Solutions	Composition
Isosmotic solution	NaCl 118; KCl 5.3; $MgCl_2$ 0.5; $CaCl_2$ 1; Glucose 10; Na_2HPO_4 7.5; $NaH_2PO_4.H_2O$ 2.5
Hypoosmotic solution	NaCl 81; KCl 5.3; $MgCl_2$ 0.5; $CaCl_2$ 1; Glucose 10; Na_2HPO_4 7.5; $NaH_2PO_4.H_2O$ 2.5
MEM media	MEM with Hank's salts, 9mM $NaHCO_3$, 1% glutamine and 1% antibiotic/antimycotic (AA)
Blocking solution	5% BSA, 20% Tween 20, 10% goat serum and PBS

Table 3.1. The list of solutions and their compositions used in the experiments for Chapter 3.

β_1AR blocker CGP20712A, β_2AR blocker ICI 118,551 and non-selective βAR agonist isoprenaline HCl, Cholesterol depletion agent cyclodextrin, muscarinic acetylcholine receptor agonist carbachol and non-selective PDE inhibitor IBMX were supplied by Sigma Aldrich. G_i protein inhibitor pertussis toxin and adenylyl cyclase activator forskolin were obtained from Tocris Bioscience.

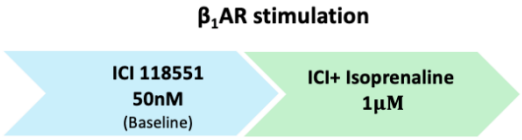
3.3.2 CytoCypher

CytoCypher (IonOptix LLC, Westwood, MA, USA). is a high throughput system which was used for the contractility study of the LV cardiomyocyte. Cardiomyocytes were isolated according to the procedure described in section 2.3 and around 10K cells were plated on laminin-coated MatTek dishes. After 1 hour, cells were washed with HBSS and were loaded with 1μM of Fura-

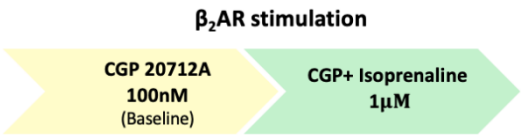
2AM in HBSS in the dark for 45 min at 37°C. The cells were washed and kept in HBSS for an additional 20 min in the dark at 37°C. The cells were stabilised in iso- or hypoosmotic solution for 15min in the CytoCypher chamber. Cells were paced at 1Hz, 20V, and after confirming that the cells were contracted rhythmically in sync with the stimulation and without any arrhythmic episodes, cells were selected and recorded by the IonOptix software. Sarcomere shortening, Ca^{2+} transients and cell size were recorded for each cell selected as detailed in the section 2.12. Recordings were taken from approximately 15 cells per dish. The data was analysed using CytoSolver (IonOptix LLC, Westwood, MA, USA).

3.3.2.1 Investigation of the Contractile Response of Cardiomyocytes to βAR Stimulation Following Hypoosmotic Swelling

Baseline contractility was first recorded and then βAR stimulation was achieved using 100nM Isoprenaline. For selective β_1AR stimulation, 1µM Isoprenaline was added in the presence of 50nM ICI 118,551 (Tocris Bioscience).



For selective β_2AR stimulation, 1µM Isoprenaline was added in the presence of 100nM CGP 20712A (Sigma-Aldrich) (Wright et al., 2018a).



3.3.2.2 Investigation of the Role of Caveolae in Contractile Response of Cardiomyocytes to Selective βAR Stimulation Following Hypoosmotic Swelling

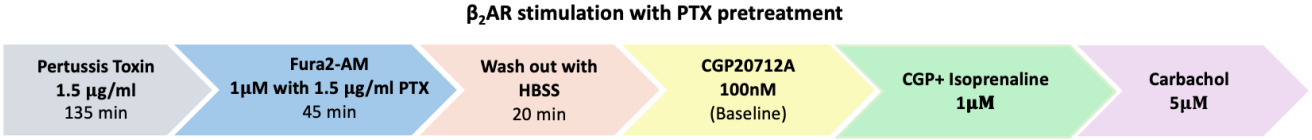
Caveolae depletion was achieved by pre-treating the cells with methyl-β-cyclodextrin (MβCD, 13.1 mg/ml diluted in HBSS and Fura2AM and incubated 37°C, 95% O_2, 5% CO_2) for 45min (Balijepalli et al., 2006). They were then assessed as above.

3.3.2.3 Investigation of the Effect of Adenylyl Cyclase Activity Following Hypoosmotic Swelling

After baseline recording in either iso- or hypoosmotic solution, cells were treated with 10µM Forskolin, an adenylyl cyclase activator and the sarcomere shortening and calcium transient were recorded from the same cells that were chosen already.

3.3.2.4 Investigation of the effect of G_i on β_2AR induced Contractile Response Following Hypoosmotic Swelling

Cardiomyocytes were incubated in the presence of with 1.5 µg/ml pertussis toxin (PTX) for 3h at 37°C (Paur et al., 2012, Xiao et al., 1999a). Effective removal of Gi activity was confirmed with 5uM of carbachol, a muscarinic acetylcholine receptor agonist which stimulates the activation of G_i.



3.3.3 Multi-cell FRET Microscopy

Around 10K of Isolated cardiomyocytes were plated onto laminin-coated coverslips and were cultured at 37℃ for 48 hours with MEM in the presence of adenovirus containing pmEPAC2 FRET sensor (MOI 200). 48h post-infection, a coverslip on which infected cardiomyocytes were attached was washed with either iso- or hypoosmotic solution and fastened into a coverslip holder. This was placed on the stage of an inverted microscope. The FRET response was recorded by an ORCA-ER CCD camera, and data were acquired using an integrated Micro-manager ICY1.4. The region of interest (ROI) and background were manually selected. Following the selection of cells, images of the cells of interest were acquired once every 5 seconds, and the change in fluorescent signal was tracked in real-time using the high-throughput MultiFRET software. After a satisfactory baseline measurement in the presence of β_1AR (100nM CGP 20712A) or β_2AR blocker (50nM ICI 118.551) was achieved, 100nM Isoprenaline was applied to give either β_1AR or β_2AR stimulation. After the β_2AR response had plateaued, 100µM IBMX (non-selective PDE inhibitor) and 10µM Forskolin (adenylyl cyclase activator) were perfused onto the cells to cause the maximum cAMP response, which allowed normalisation of the βAR-cAMP response to the maximum cAMP responses. An example of FRET response and analysis stages is shown in Figure 3.1.

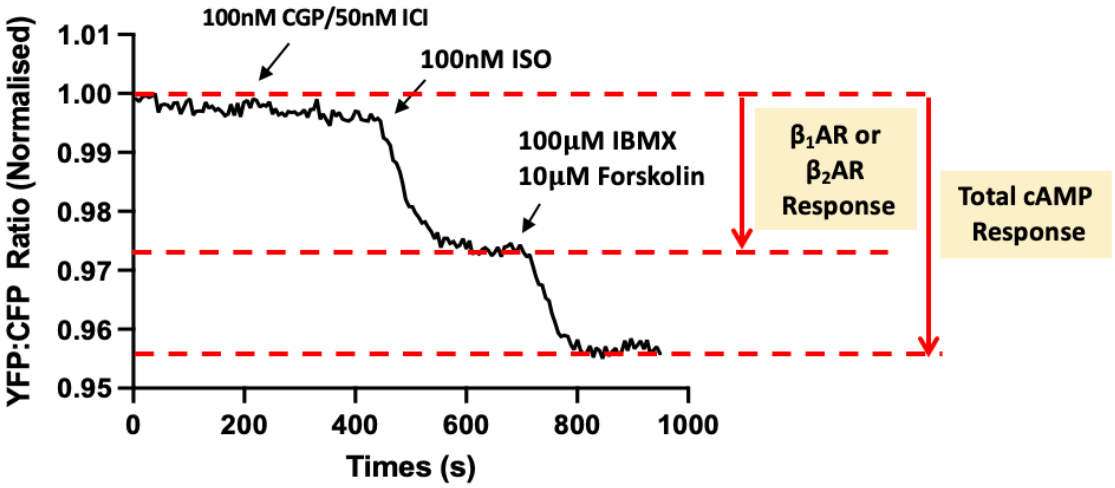


Figure 3.1. Examples of FRET Response and analysis stages demonstrating the role of different pharmacological stimuli in enhancing cellular cAMP responses.

3.3.4 Live Cell T-tubule Staining via Di-8-ANNEPPS

Cells were stained with 10µM Di-8-ANNEPS, which was prepared beforehand in FRET buffer and sonicated for 20 minutes at 50°C. Cells were washed twice with FRET buffer after 3min staining and were then stabilised in 2ml iso/hypoosmotic solution before imaging. Cells were imaged using a Zeiss LSM-78- inverted confocal microscope. The obtained images were analysed using Image J and MatLab. Detailed analysis protocol can be found in section 2.8.2.

3.3.5 Confocal Microscopy of LV Cardiomyocytes Following Caveolin-3 Staining

Isolated Cardiomyocytes were plated onto the coverslip and perfused with either iso- or hypoosmotic solution for 15 minutes and then fixed with 4% PFA. 0.1% Triton-X was used to permeabilise the cells, while a blocking buffer containing PBS, 5% bovine serum albumin, 20% Tween20 and 10% goat serum was used to prevent non-specific binding. Cells were incubated in blocking solution in a humidified dish for 24H at 10 °C with caveolin-3 primary antibody in 1:100 dilution (purified mouse anti-caveolin-3, BD Bioscience). Slides were then incubated

with blocking solution containing 1:500 Alexa Fluor 488 conjugated donkey anti-mouse IgG (Thermo Scientific) for 2H at room temperature in the dark. Subsequently, the coverslips were mounted onto slides using Prolong gold mounting with the nuclear stain DAPI, the edges of the coverslips were sealed with nail varnish. Detailed Staining protocol can be found in section 2.9.1.

3.3.6 Quantification of Caveolae Number in LV Cardiomyocytes Using Transmission Electron Microscopy

LV cardiomyocytes were fixed in 2.5% glutaraldehyde in PBS, centrifuged, and left in fixative overnight. Further experiments were performed by Ivan Diakonov. They were then washed in cacodylate buffer, fixed with 1% osmium tetroxide, and briefly rinsed with distilled water. 2% liquid agar was added, solidified, dehydrated with alcohols and propylene oxide, and embedded in Araldite. Sections of 0.1µm were cut and stained with uranyl acetate and lead citrate for TEM. Images of cell membranes were taken. Ten cells from each region were randomly selected, with 10 fields of view per cell. This was repeated multiple times. Caveolae-like structures were counted, and their density per 1µm of membrane was calculated. Detailed TEM protocol can be found in section 2.7.

3.3.7 Statistics

All graphs and statistical analyses were performed using Prism10 (GraphPad).

Normality was assessed using the Shapiro-Wilk test. Data sets with normally distributed variables were statistically tested using parametric analyses. Non-parametrical statistical test was applied when at least one data set assessed failed the normality tests.

Cell size, number of caveolae, T-tubule and Caveolin-3 assessment were analysed using un-paired T-test.

CytoCypher experiment (cell contractility) and FRET Microscopy experiment (cAMP response) were analysed using Nested T-test, which allows comparison of the means of the two groups with large data sets and hierarchical clustering. Nested one-way ANOVA was applied when comparing the means of three groups. Two-way ANOVA with Šídák's multiple comparisons test was used when there were two independent variables and a nested analysis could not be performed.

3.4 Results

3.4.1 Impact of Hypoosmotic Swelling Model on Isolated Cardiomyocytes

The hypoosmotic swelling model was used in isolated left ventricular rat cardiomyocytes to replicate the membrane stretch during the acute cardiac stretch. To evaluate the effect of hypoosmotic swelling on the number of caveolae, cells were maintained in either isosmotic or hypoosmotic solution for 15 minutes. The number of caveolae was assessed using transmission electron microscopy, and the longitudinal membrane sections of cardiomyocytes were captured. There was a significant decrease of ~ 50% in the number of caveolae in the hypoosmotic solution compared to the cells exposed to the isosmotic solution (Figure 3.2).

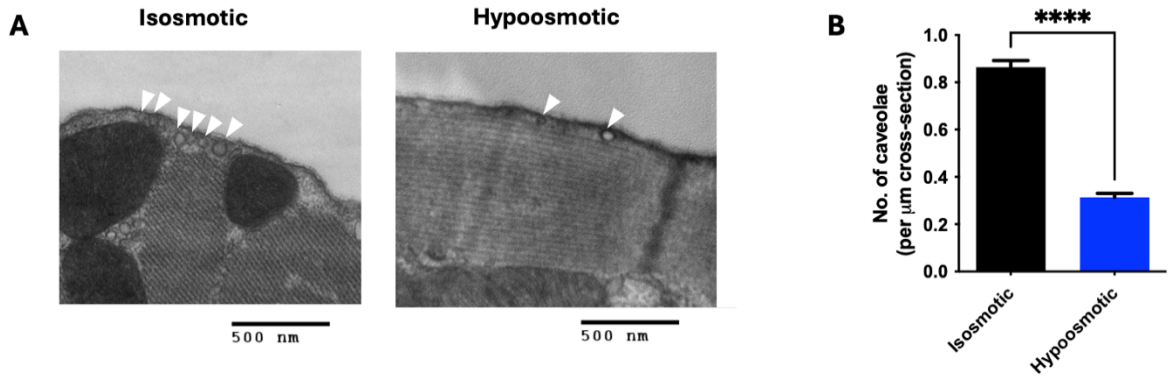


Figure 3.2. Hypoosmotic swelling reduces the number of caveolae in cardiomyocytes. A. Representative electron microscopy images of cardiomyocyte membrane showing the caveolae (white arrows) in isosmotic solution (290 mOsmol/L) and hypoosmotic solution (214 mOsmol/L). Scale bars: 500nm. **B**. Quantification of the number of caveolae per µm cross-section of the membrane. N=2, n=20 cells (178-189 frames), **** $p<0.0001$, Mann Whitney test, Error bars indicate SEM.

To address the effect of hypoosmotic swelling on cell size, cells were stabilised in either iso- or hypoosmotic solution for 15 minutes in IonOptix CytoCypher. Single-cell images were then captured using IonOptix IonWizard software. Results indicated a significant increase in average

cell width in hypoosmotic solution compared to isosmotic solution, while cell length remained unchanged (Figure 3.3).

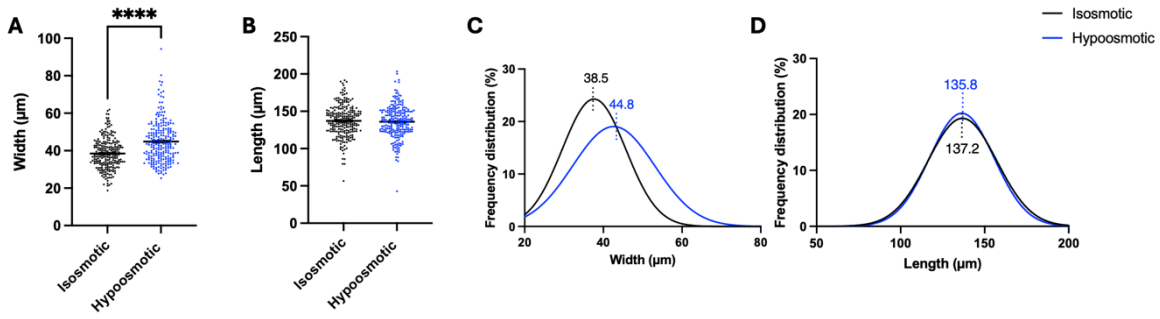


Figure 3.3. Hypoosmotic swelling increases the width of rat left ventricular cardiomyocytes rather than cell length. **A**, Length and **(B)** width from cardiomyocytes in isosmotic (black) and hypoosmotic (blue) solution. Frequency distribution of **(C)** width and **(D)** length of individual cardiomyocyte dimensions with mean shown. Control: N=9, n= 235, **** p<0.0001, Unpaired T-test. All data are presented as mean ± SEM.

To assess the T-tubule (TT) organisation in rat left ventricular cardiomyocytes during hypoosmotic swelling, TT membranes were labelled with Di-8-ANEPPS and imaged using confocal microscopy. Hypoosmotic swelling did not significantly affect TT density, regularity and directionality (Figure 3.4 and Figure 3.5), indicating the TT network remained intact under the hypoosmotic swelling model.

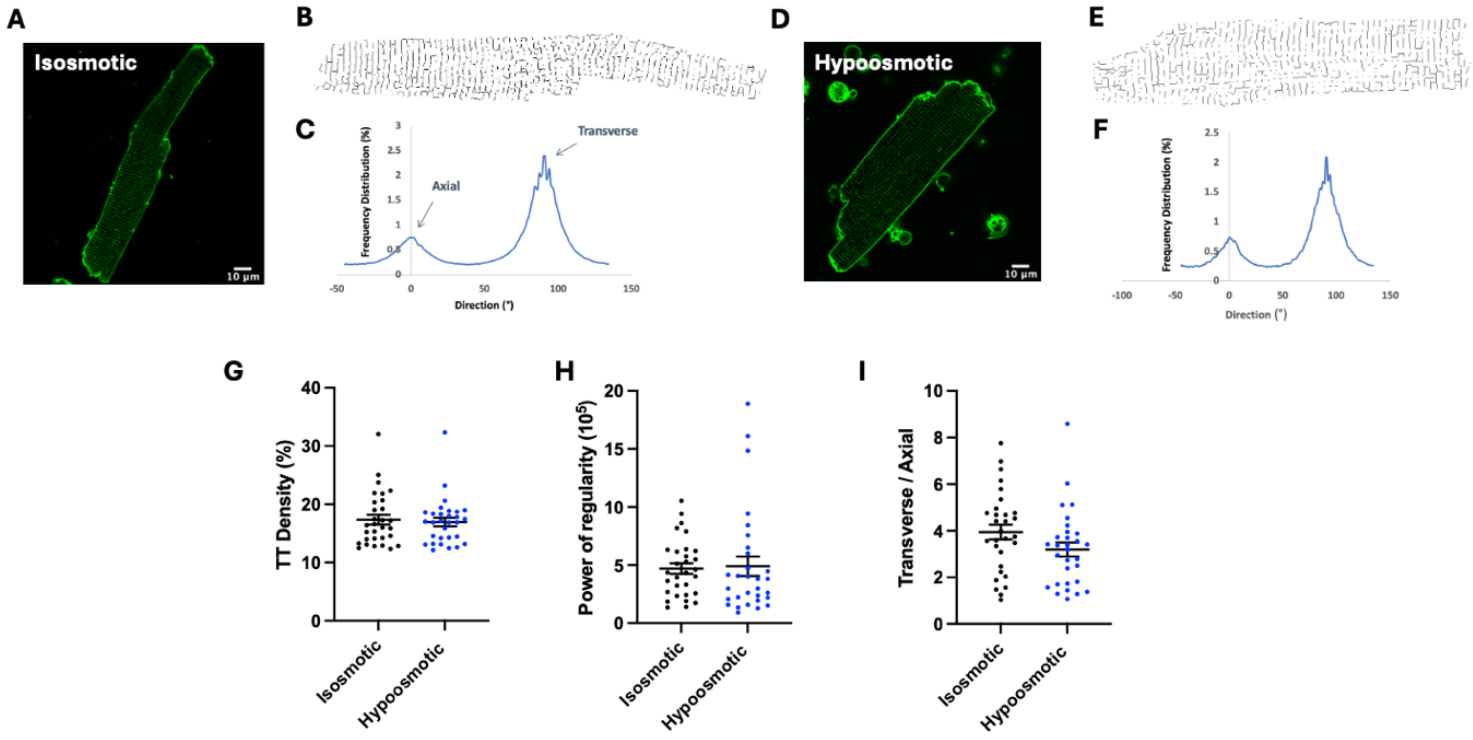


Figure 3.4. The T-tubule of cardiomyocytes does not alter in hypoosmotic swelling. Representative confocal image of rat left ventricular cardiomyocytes showing membrane stained with Di-8-ANEPPS in **(A)** iso- and **(D)** hypoosmotic solution. Scale bar: 10 µm. Representative images of cells showing skeletonised Transverse-Axial Tubule network in **(B)** isosmotic and **(E)** hypoosmotic solution. Directionality histograms of **(C)** isosmotic and **(F)** hypoosmotic were generated from skeletonised images of the T-tubule. Gaussian fitting shows axial (0°) and transverse (90°) components. Mean **(G)** T-tubular density; **(H)** power of regularity and **(I)** directionality of T-tubular structure in the iso- and hypoosmotic solution. N=3; n=30, Unpaired T-test. Data are presented as mean ± SEM.

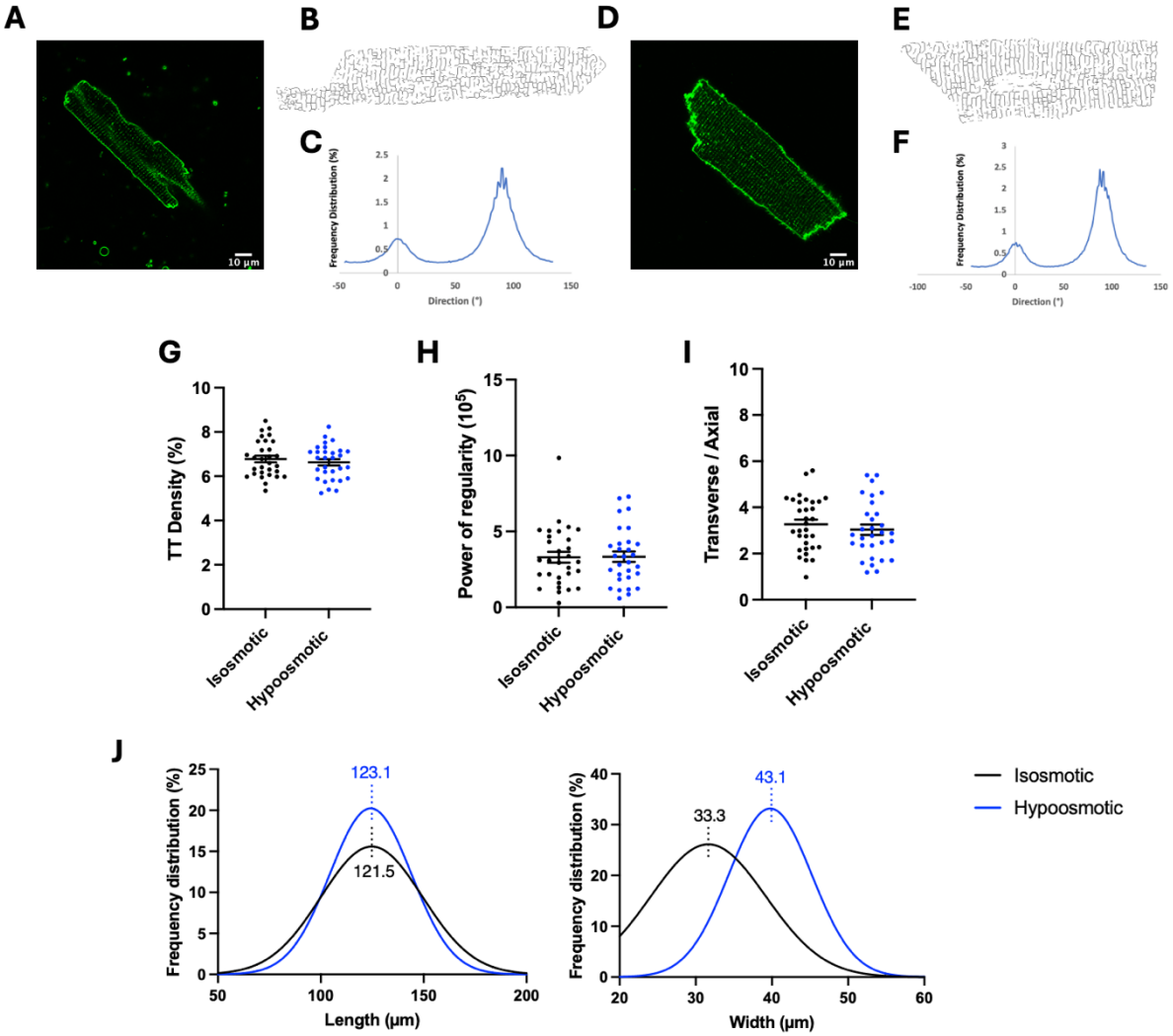


Figure 3.5. The Transverse-Axial Tubule network in MβCD treated did not alter in hypoosmotic swelling. Confocal image examples of cyclodextrin-treated rat left ventricular cardiomyocytes showing membrane stained with Di-8-ANEPPS in **(A)** iso- and **(D)** hypoosmotic solution. Scale bar: 10µm. Representative images of cells showing skeletonised Transverse-Axial Tubule network in **(B)** isosmotic and **(E)** hypoosmotic solution. Directionality histograms of **(C)** isosmotic and **(F)** hypoosmotic were generated from skeletonised images of T-tubular system. Gaussian fitting shows axial (0°) and transverse (90°) components. Mean **(G)** T-tubular density; **(H)** power of regularity and **(I)** directionality of T-tubular structure in the iso- and hypoosmotic solution. N=3; n=30, Unpaired T-test. Data are presented as mean ± SEM **(J)** Frequency distribution graphs showing mean cell length and cell width. N=6, n=110.

Additionally, we examined the Cav3 protein density in TTs following hypoosmotic swelling. Cardiomyocytes were stained with Cav3 antibody, and the density and regularity were evaluated in iso-and hypoosmotic solution via confocal microscopy (Figure 3.6). There were no observed differences in Cav3 density and regularity between iso-and hypoosmotic conditions.

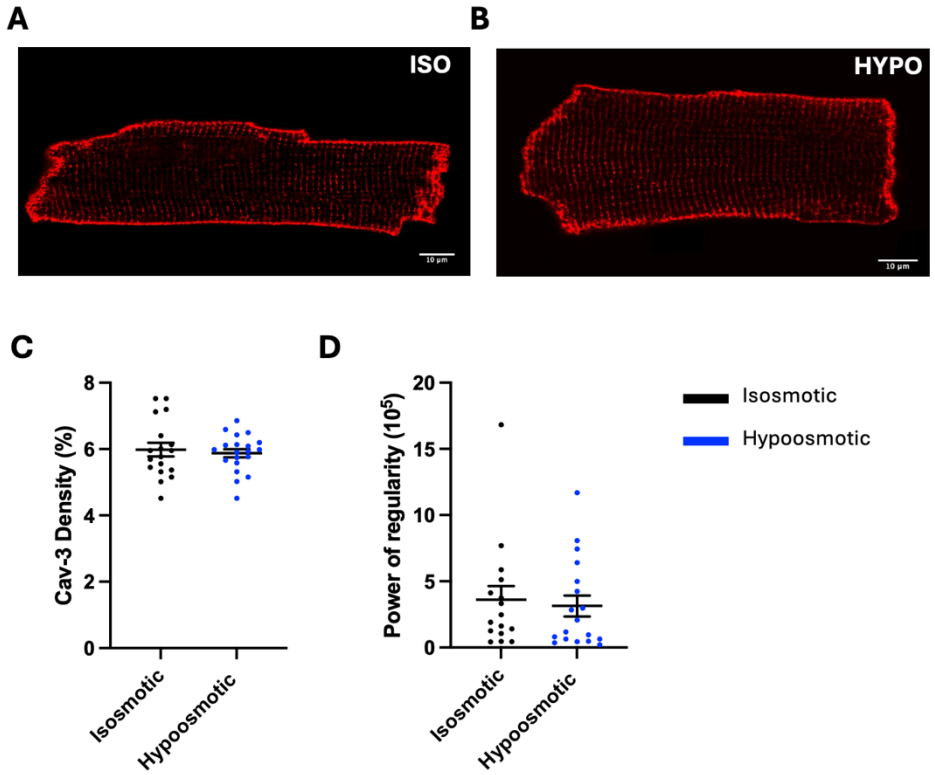


Figure 3.6. Caveolin-3 distribution was not altered after hypoosmotic swelling. Representative confocal images of caveolin-3 staining from rat left ventricular cardiomyocytes in **(A)** iso- and **(B)** hypoosmotic solution. **C**, Mean caveolin-3 density and **(D)** caveolin-3 regularity in both iso-and hypoosmotic solution. N=3; n=18-20. Data are presented as mean ± SEM. Data was analysed by either Unpaired t-test or Mann-Whitney test.

3.4.2 Hypoosmotic swelling of isolated cardiomyocytes causes an increase in β_2-adrenoceptor induced cAMP release

To investigate the impact of hypoosmotic swelling on the functionality of βAR subtypes, FRET microscopy along with membrane localised pmEPAC2 sensor was used to detect the cAMP signal on the plasma membrane. Non-selective βAR agonist isoprenaline was used along with 50nM β_2AR blocker ICI 118,551 to show the β_1AR response, and 100nM β_1AR CGP 20712A was used to show the β_2AR response.

Representative traces are shown in Figure 3.7 A and B, which illustrate the β1AR and β2AR-cAMP responses in isosmotic (black line) and hypoosmotic (blue line) solutions following treatment with isoprenaline and saturators (IBMX and Forskolin). The traces indicate that cAMP responses for both β_1AR and β_2AR stimulation increased upon the addition of isoprenaline, reaching maximum cAMP release after the addition of IBMX and forskolin. Hypoosmotic swelling resulted in a significant increase in β_2AR-specific cAMP release, while no change was observed following β_1AR stimulation (Figure 3.7 C and D).

To ensure that the specific β_2AR effect was not due to differences in NaCl between isosmotic and hypoosmotic solutions, experiments were done using an isosmotic solution with 81mM NaCl and 75mM Mannitol (Figure 3.8). No differences in β_1AR and β_2AR responses were observed between the two isosmotic solutions: high NaCl (118nM) and low NaCl (81mM) with 75mM mannitol, confirming that the difference in NaCl levels did not influence the observed differences in β_1AR and β_2AR responses.

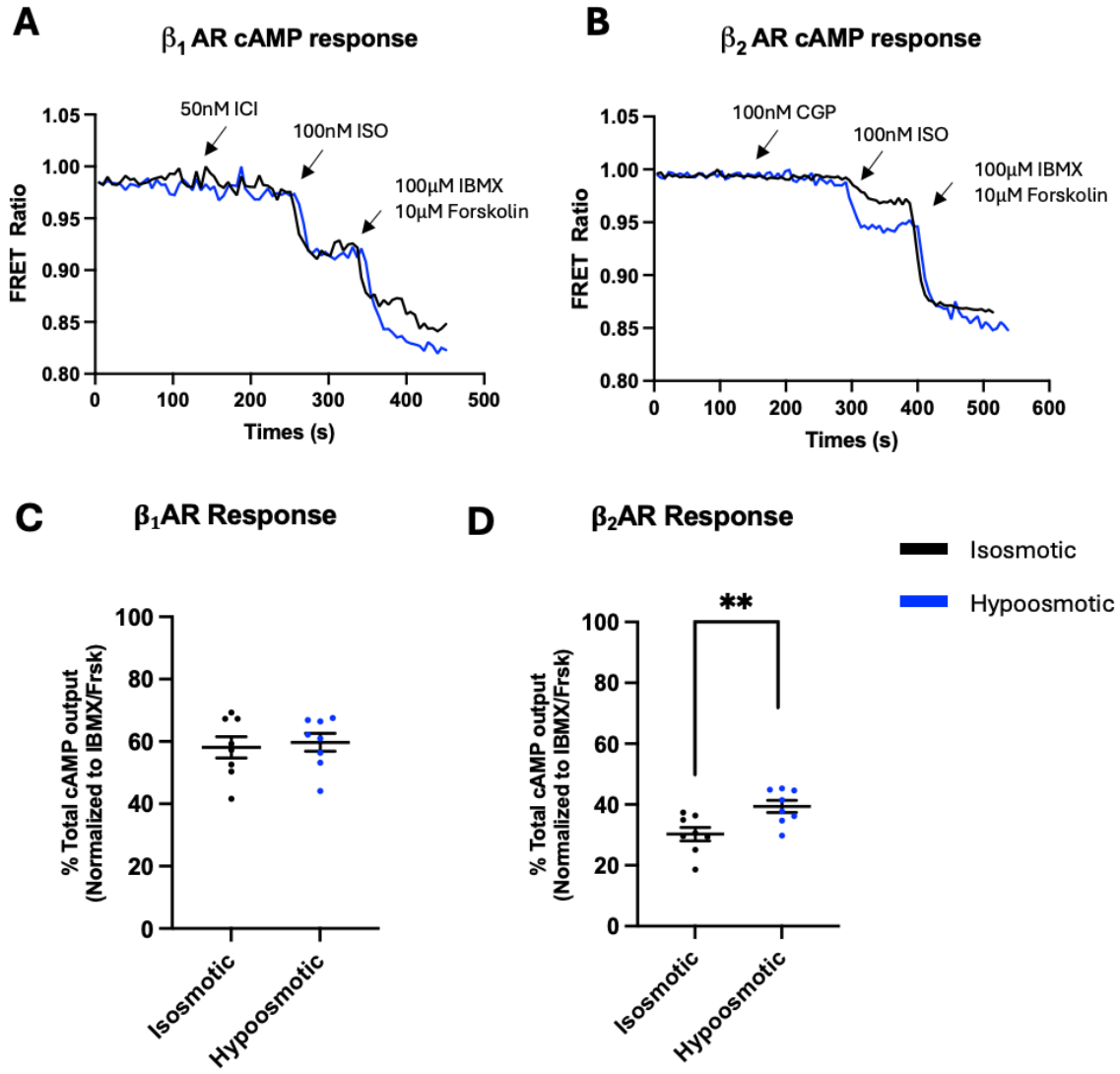


Figure 3.7. Hypoosmotic swelling causes an increase in β_2-adrenoceptor induced cAMP release. Representative FRET trace following **(A)** β_1 or **(B)** β_2AR-specific stimulation with isoprenaline (100nM) in the presence of selective β_2AR antagonist ICI 118,551 (50nM) or β_1AR antagonist CGP 20712A (100nM); adenylyl cyclase agonist Forskolin (10μM) and phosphodiesterase antagonist IBMX (100μM) were later added to elicit maximal cAMP production. Calculation of the amount of cAMP production after **(C)** β_1 or **(D)** β_2AR-specific stimulation relative to absolute maximum of production after stimulation with Forskolin and IBMX. N=8; ** $p<0.01$, Nested T-test. Data are presented as mean ± SEM.

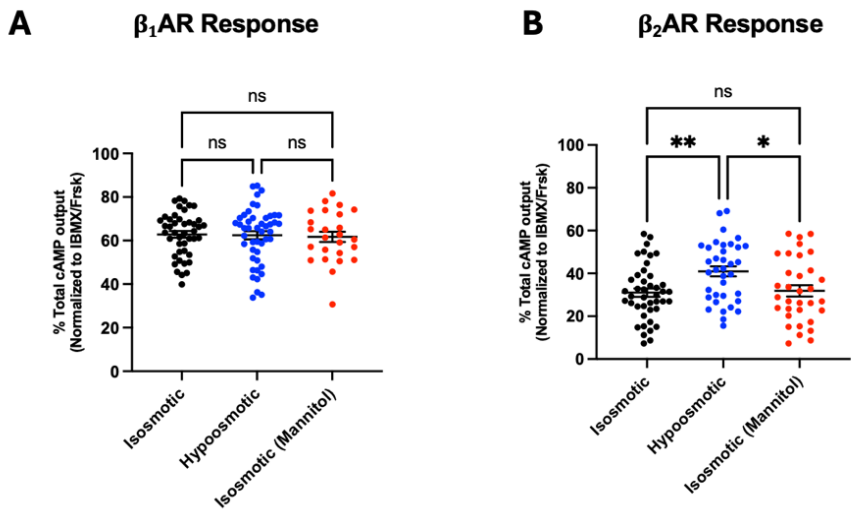


Figure 3.8. No difference of %total cAMP output in two isosmotic solutions (118mM NaCl vs 81mM NaCl + 75mM Mannitol). Calculation of the amount of cAMP production after **(A)** β_1AR and **(B)** β_2AR stimulation relative to absolute maximum of production after stimulation with Forskolin and IBMX. N=3, n=33-43, One way ANOVA with Šídák's multiple comparisons test. Data are presented as mean ± SEM.

3.4.3 Hypoosmotic swelling causes an increase in sarcomere shortening following β_2-adrenoceptor stimulation.

We then explored the impact of hypoosmotic swelling on cardiomyocyte contractility following selective βAR stimulation. Measurements of sarcomere shortening and calcium transients were taken at baseline and following selective βAR with 1μM isoprenaline (Figure 3.8). Representative traces are shown in Figure 3.9 A and B, which illustrate the sarcomere shortening and calcium transient, respectively, in isosmotic (black) and hypoosmotic solution (blue) in baseline (dashed line) and following stimulation (solid line).

Stimulation of β_1AR showed no difference in sarcomere shortening between isosmotic and hypoosmotic cells, while the sarcomere shortening in hypoosmotic cells was significantly enhanced following β_2AR stimulation (Figure 3.9E and H). However, there is no difference

between iso- and hypoosmotic cells in calcium transient following both β_1AR and β_2AR stimulation (Figure 3.10 E and H).

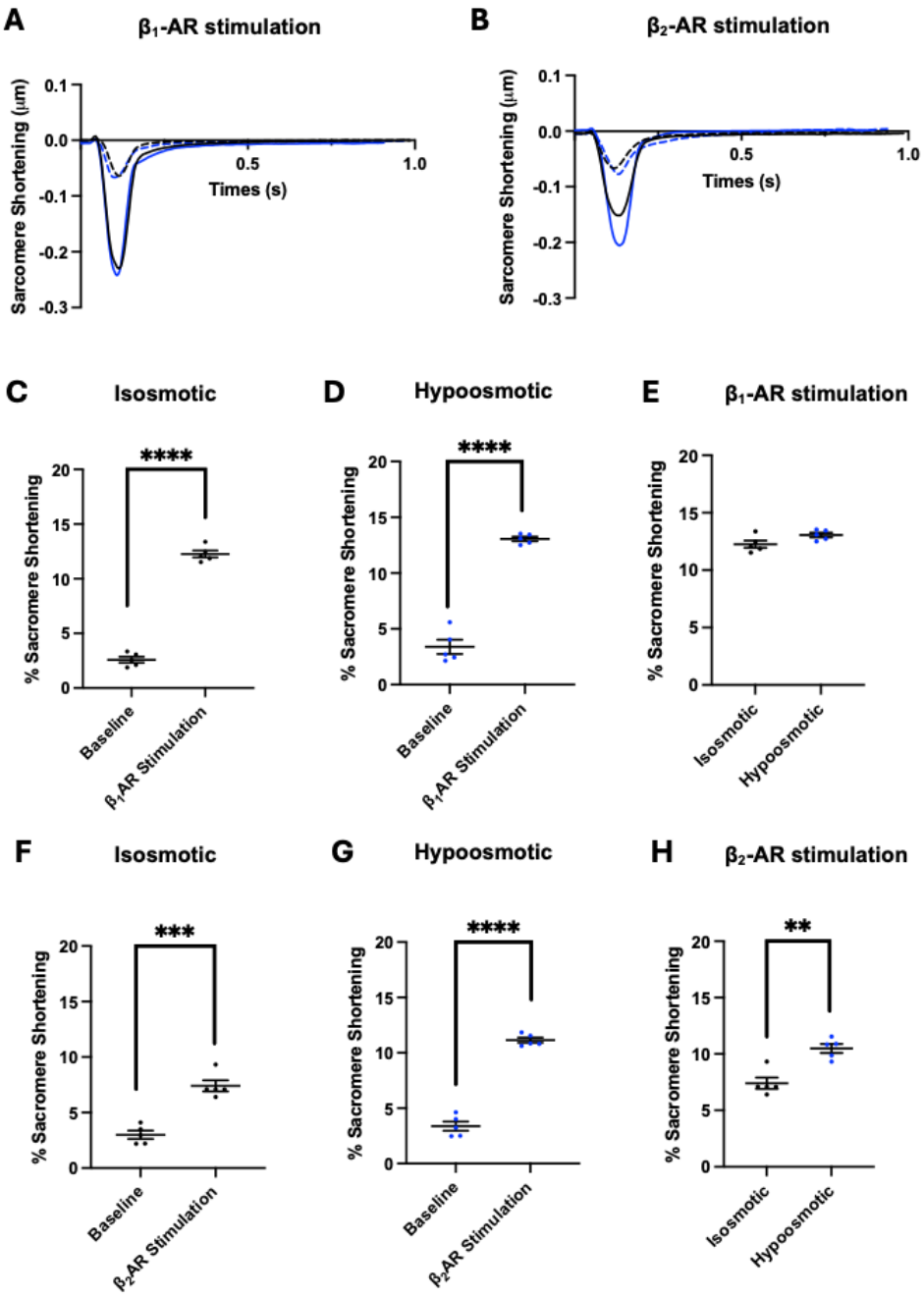


Figure 3.9. Hypoosmotic swelling increases β_2AR but not β_1AR-induced contractility. Representative traces of sarcomere shortening following **(A)** β_1AR and **(B)** β_2AR stimulation in iso- (black) and hypoosmotic (blue) cells. Percentage sarcomere shortening at baseline and following stimulation with 1µM isoprenaline in the presence of the β_2AR blocker ICI or the β_1AR blocker CGP in **(C,F)** iso- and **(D,G)** hypoosmotic solution. **(E,H)** Comparison of percentage sarcomere shortening following β_1AR and β_2AR stimulation in iso- and hypoosmotic solution. N=5,**P<0.01, ** p<0.001, ***P<0.0001, Nested T test.

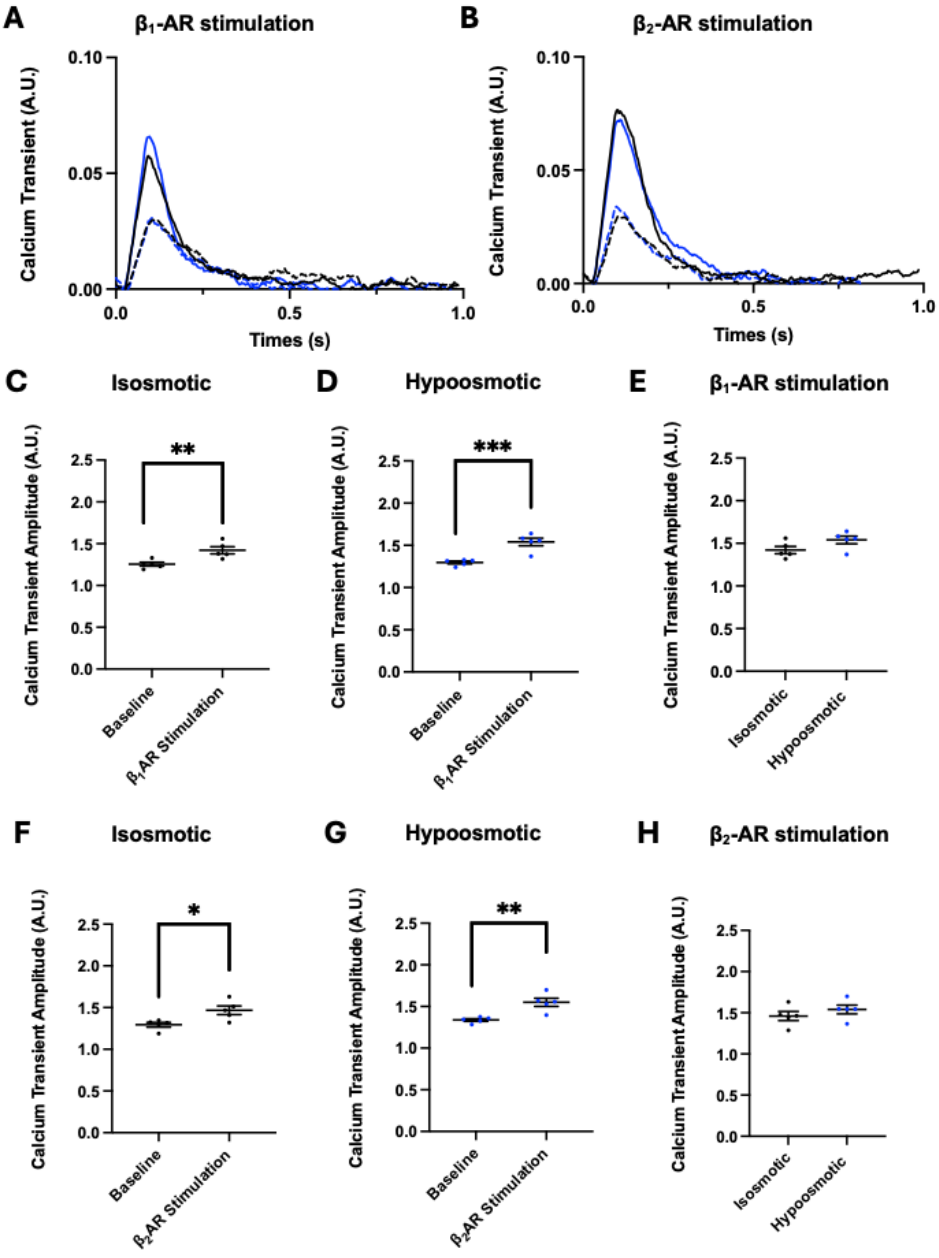


Figure 3.10. Hypoosmotic swelling did not alter the calcium transient following β_1AR and β_2AR stimulation. Representative traces of calcium transient following **(A)** β_1AR and **(B)** β_2AR stimulation in iso- (black) and hypoosmotic (blue) cells. Calcium transient amplitude at baseline and following stimulation with 1μM isoprenaline in the presence of the β_2AR blocker ICI or the β_1AR blocker CGP in **(C,F)** iso- and **(D,G)** hypoosmotic solution. **(E,H)** Comparison of calcium transient amplitude following β_1AR and β_2AR stimulation in iso- and hypoosmotic solution. N=5, * P<0.05, **P<0.01, ***P<0.001, Nested T test.

3.3.4 Dependence of increased β_2AR activity on functional caveolae following hypoosmotic swelling

To investigate the role of caveolae in βAR signalling following hypoosmotic swelling, MβCD was used to disrupt caveolae, and cAMP response was measured using the FRET microscopy. Representative traces are shown in Figure 3.11 A and B, which illustrate the control and MβCD treated cells following β_2AR stimulation in isosmotic (black line) and hypoosmotic (blue line) conditions. Hypoosmotic swelling resulted in a significant increase in β_2AR-specific cAMP release, while no change was observed in MβCD treated cells (Figure 3.11C).

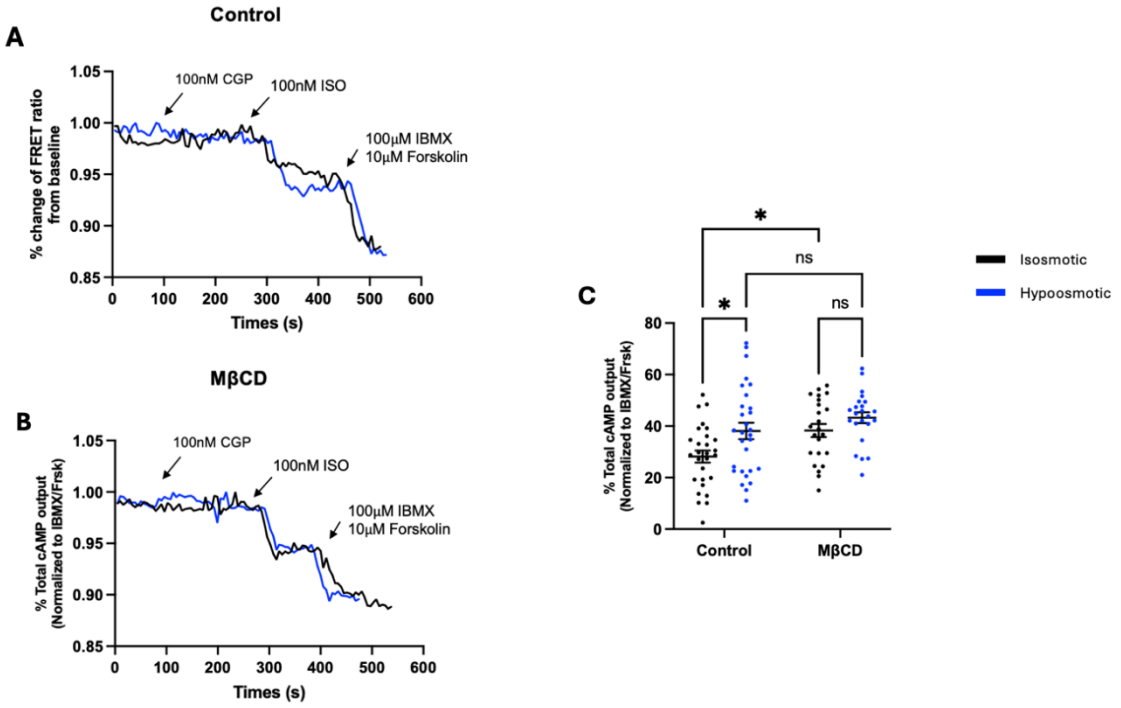


Figure 3.11. the increased in β_2AR induced cAMP release following hypoosmotic swelling is lost in MβCD treated cells. Representative FRET trace of **(A)** control and **(B)** MβCD treated cells following β_2AR-specific stimulation with isoprenaline (100nM) in the presence of selective β_1AR antagonist CGP 20712A (100nM); adenylyl cyclase agonist Forskolin (10μM) and phosphodiesterase antagonist IBMX (100μM) were later added to elicit maximal cAMP production. **C.** Calculation of the amount of cAMP production in control and MβCD treated cells after β_2AR-specific stimulation relative to absolute maximum of production after stimulation with Forskolin and IBMX. N=3; n=23~30. *p<0.05, Two-way ANOVA with Šídák's multiple comparisons test. All data are presented as mean ± SEM.

Sarcomere shortening and calcium transients were also recorded in both iso- and hypoosmotic solutions following MβCD treatment. There was no difference in sarcomere shortening between isosmotic and hypoosmotic cells in both control and MβCD-treated groups after β_1AR stimulation. However, the increased β_2AR response observed after hypoosmotic swelling was eliminated following MβCD treatment (Figure 3.12), indicating that the enhanced β_2AR activity following hypoosmotic swelling relies on the functional integrity of caveolae. Furthermore, no differences in calcium transients between isosmotic and hypoosmotic conditions were detected in MβCD-treated (Figure 3.13).

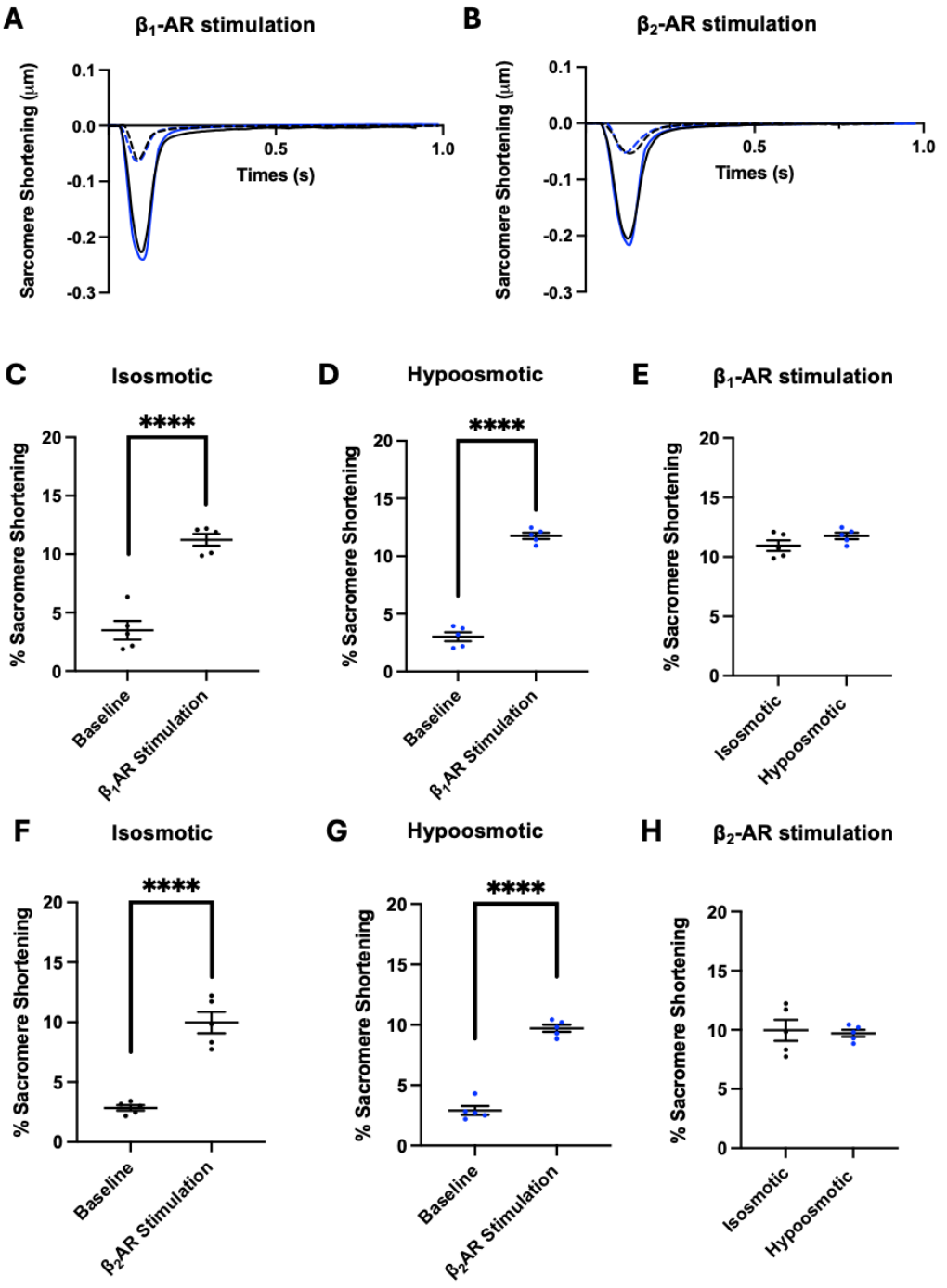


Figure 3.12. Hypoosmotic swelling did not alter the sarcomere shortening in MβCD treated cells following both β_1AR and β_2AR stimulation. Representative traces of sarcomere shortening following **(A)** β_1AR and **(B)** β_2AR stimulation in iso- (black) and hypoosmotic (blue) cells. Percentage sarcomere shortening at baseline and following β_1AR and β_2AR stimulation in **(C,F)** iso- and **(D,G)** hypoosmotic solution. **(E,H)** Comparison of percentage sarcomere shortening following β_1AR and β_2AR stimulation in iso- and hypoosmotic solution. N=5, ***P<0.0001, Nested T test.

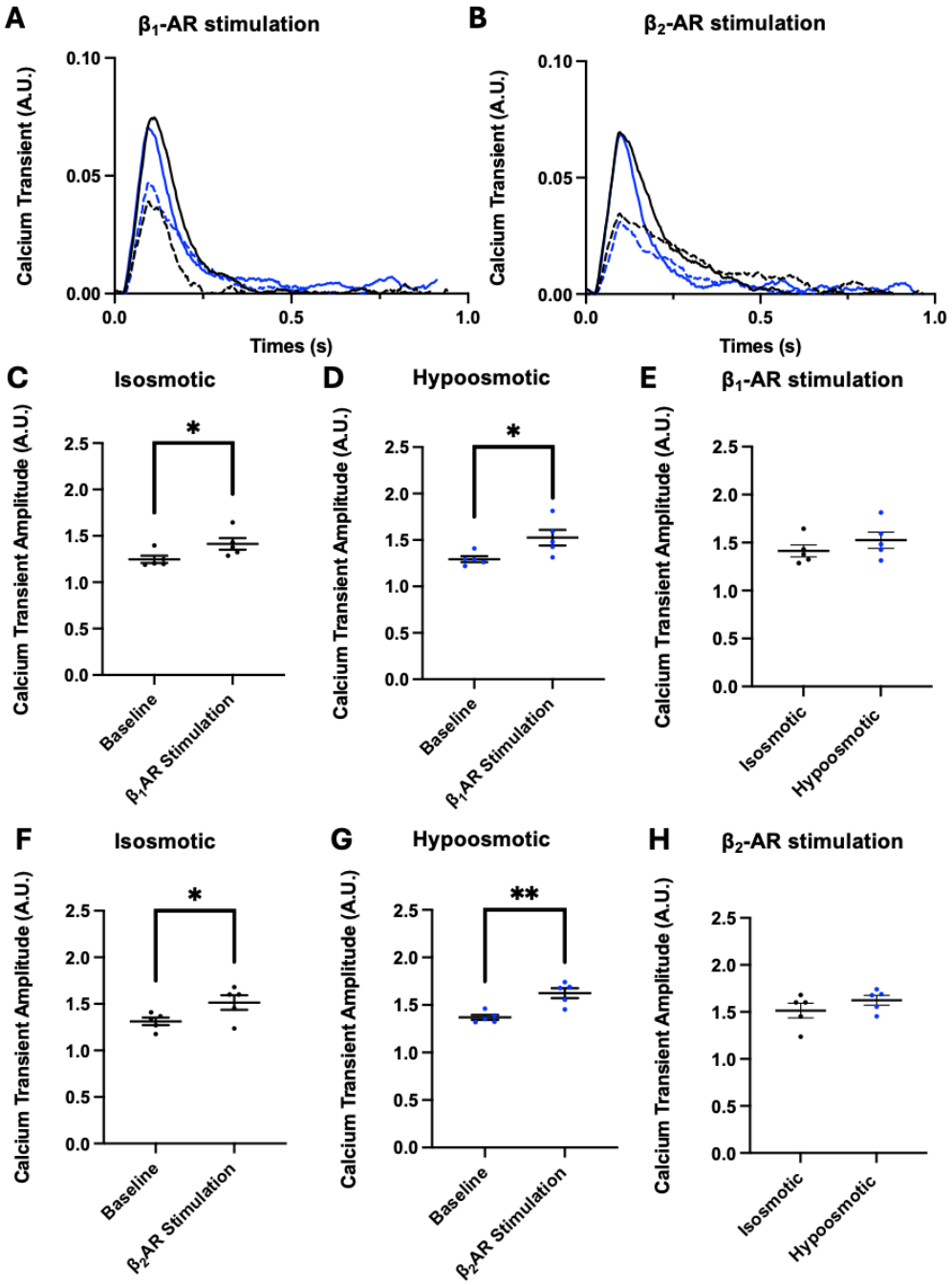


Figure 3.13. Hypoosmotic swelling did not alter the calcium transient in MβCD treated cells following β_1AR and β_2AR stimulation. Representative traces of calcium transient following **(A)** β_1AR and **(B)** β_2AR stimulation in iso-(black) and hypoosmotic (blue) cells. Calcium transient amplitude at baseline and following β_1AR or β_2AR stimulation in **(C,F)** iso- and **(D,G)** hypoosmotic solution. **(E,H)** Comparison of calcium transient amplitude following β_1AR and β_2AR stimulation in iso- and hypoosmotic solution. N=5, * P<0.05, **P<0.01, Nested T test.

3.4.5 Increased β_2AR Activity Following Hypoosmotic Swelling is Lost in PTX-Treated Cells

β_2AR can couple to both G_s and G_i proteins, with G_i exerting a negative inotropic effect in cardiomyocytes. To determine if the increased β_2AR response observed after hypoosmotic swelling is influenced by G_i protein, cells were pre-treated with 1.5 μg/ml pertussis toxin (PTX) for 3 hours. The effectiveness of PTX treatment in inhibiting G_i activity was confirmed using 5 μM Carbachol, which activates G_i. Carbachol was administered following β_2AR stimulation by CGP and isoprenaline. Without PTX treatment, Carbachol activation of G_i reduced sarcomere contractility to baseline levels, an effect not seen in PTX pre-treated cells. Representative traces of sarcomere shortening transient in isosmotic (black) and hypoosmotic (blue) cells, without and with PTX pretreatment could be found in Figure 3.14.

In isosmotic conditions, PTX treatment significantly increased sarcomere shortening. However, there was no difference in sarcomere shortening between PTX-treated and untreated cells following hypoosmotic swelling (Figure 3.15). Furthermore, the enhanced sarcomere shortening in response to β_2AR stimulation observed after hypoosmotic swelling was absent in PTX-treated cells (Figure 3.15 C and F).

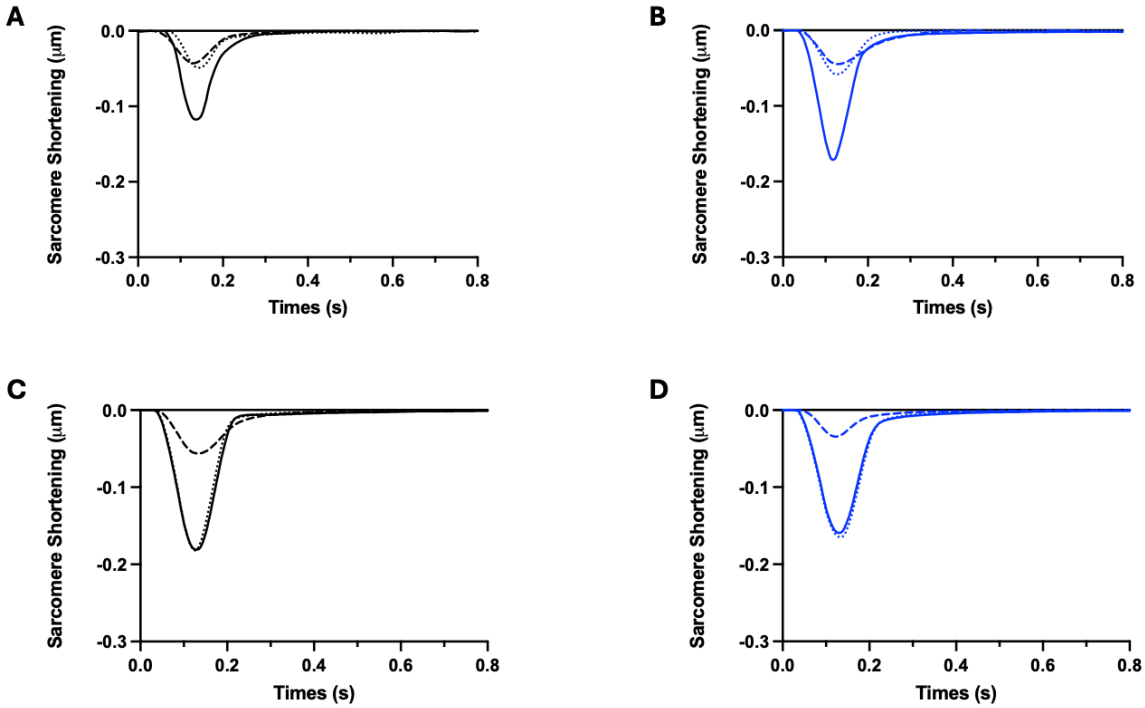


Figure 3.14. Representative traces of sarcomere shortening in isosmotic (black) and hypoosmotic (blue) cells, (A) (B) without and (C) (D) with PTX pretreatment. The solid line represents the baseline, the dashed line represents isoprenaline treatment, and the dotted line represent carbochol treatment.

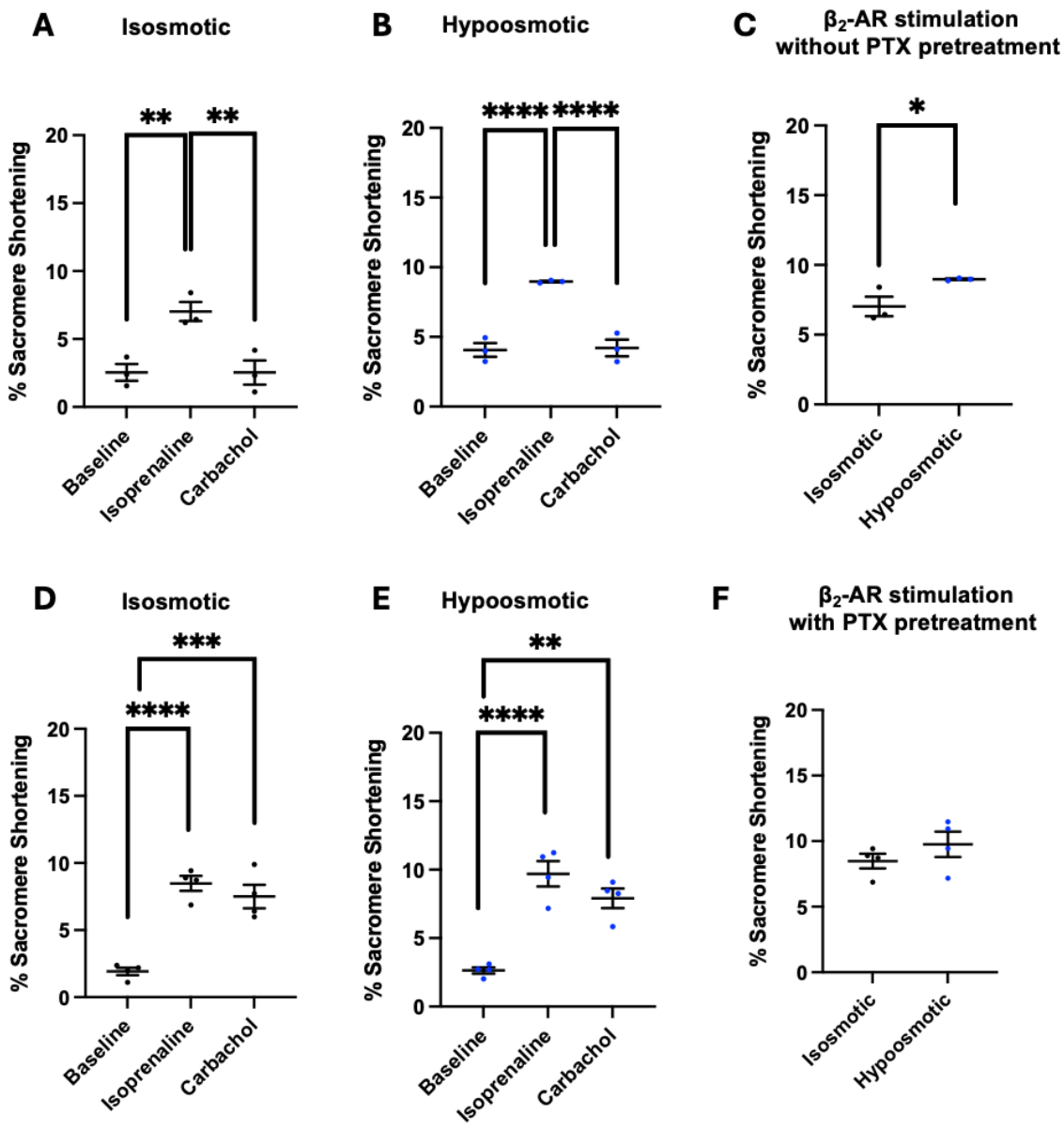


Figure 3.15. PTX treatment abolishes increased β_2AR activity following hypoosmotic swelling. Percentage sarcomere shortening **(A,B,C)** without PTX pretreatment and **(D,E F)** with PTX treatment at baseline, following β_2AR stimulation and carbachol treatment in **(A,D)** iso- and **(B,E)** hypoosmotic solution. **(C,F)** Comparison of percentage sarcomere shortening following β_1AR and β_2AR stimulation in iso- and hypoosmotic solution. N=3~4, * P<0.05, **P<0.01, ***P<0.001, ****P<0.0001, Nested One-way ANOVA with Šídák's multiple comparisons test and Nested- T test.

3.5 Discussion

In this chapter, we investigated the effect of membrane stretch on βAR signalling and the role of caveolae in regulating this effect in cardiomyocytes. Additionally, we explored how membrane stretch influences the β_2AR-G_i pathway. The key findings from this chapter can be summarised as follows:

- Hypoosmotic swelling reduces the number of caveolae in cardiomyocytes and increases cell size by widening the cells without affecting their length.
- Hypoosmotic swelling does not alter the structure of the T-tubule and density of Cav3 in cardiomyocytes.
- Hypoosmotic swelling causes an increase in sarcomere shortening and cAMP production following β_2AR stimulation, but not β_1AR stimulation.
- Increased β_2AR activity following hypoosmotic swelling is dependent on functional caveolae.
- PTX treatment abolishes the increased β_2AR-induced sarcomere shortening observed after hypoosmotic swelling.

3.5.1 The Effect of Hypoosmotic Swelling on Cardiomyocyte Structure

In this study, we used hypoosmotic swelling as a model to mimic membrane stretch. During hypoosmotic swelling, caveolae undergo conformational changes, flattening and integrating into the surface membrane, leading to a reduced number of caveolae in the plasma membrane (Kozera et al., 2009). This finding was confirmed by our electron microscopy results, which showed a significant reduction in caveolae in hypoosmotic cells compared to isosmotic

cells. Hypoosmotic swelling may affect the observed cell surface area, as the cell surface expands due to swelling, parts of the membrane may move out of the imaging plane, therefore less of the membrane is captured, resulting in an underestimation of caveolae numbers. However, the reduction in caveolae and Cav3 density in the membrane fraction following hypoosmotic swelling has been consistently demonstrated in multiple studies using different techniques, including total internal reflection fluorescence microscopy and immunoblot analysis (Sinha et al., 2011, Kozera et al., 2009). Consistent with previous reports (Gonano et al., 2014), we demonstrated that maintaining cardiomyocytes in hypoosmotic solution for 15 minutes increases the width without affecting cell length. Certain mechanical stress can disrupt the T-tubule structure, leading to impaired excitation-contraction coupling and consequently affecting cell contraction (Nikouee et al., 2018). In addition, the protein Caveolin-3 (Cav3) is not only essential for caveolae formation but also contributes to T-tubule formation and is required for the functional LTCC-β_2 Complex in the t-tubule (Sanchez-Alonso et al., 2023). Our results showed that hypoosmotic swelling did not cause any significant change in T-tubule density, regularity, or directionality, nor did it affect Cav3 density. This suggests that the observed effects are due to alterations in caveolae conformation rather than due to TT deformation.

3.5.2 The Effect of Hypoosmotic Swelling on βAR Signalling

Acute myocardial stretch has been shown to elevate cAMP levels in both isolated perfused dog hearts and ferret papillary muscles (Todaka et al., 1998) (Calaghan et al., 1999a), though the underlying mechanism remains unclear. The study from Dr Wright has demonstrated that

chronic partial mechanical unloading of the heart suppresses the β_2AR-cAMP response, indicating that βAR-cAMP signalling is influenced by mechanical loads (Wright et al., 2018b).

We investigated the effect of membrane stretch on cAMP production via β_1AR and β_2AR subtypes. At both iso-and hypoosmotic conditions, higher cAMP release and sarcomere shortening were seen in response to β_1AR compared to β_2AR, consistent with the higher abundance of β_1ARs in the heart. Following β_2AR stimulation, hypoosmotic cells showed a significantly higher cAMP production and sarcomere shortening compared to the isosmotic cells. This increase in cAMP release following hypoosmotic swelling was not seen with β_1AR stimulation, indicating a stronger dependence of the β_2AR response on stretch. One of the possible explanations could be due to caveolae recruitment to the sarcolemma, thus leading to β_2ARs translocating to the membrane and becoming more accessible for activation. As mentioned in the introduction, β_2AR-cAMP signalling is more localised to the sarcolemmal region while β_1AR-cAMP signalling spreads throughout the cells. Therefore, following hypoosmotic swelling, the changes in the membrane structure are more likely to influence the β_2ARs.

It is well established that calcium triggers muscle contraction. An increase in cytoplasmic calcium binds to myofilaments or sarcoplasmic proteins, initiating a cascade of events that result in actin and myosin interaction, leading to contraction (Ebashi and Endo, 1968). Various studies, including on rat cardiac muscle, have shown that calcium transients precede contraction, with calcium rising before force generation and decreasing before force relaxation (Allen and Kurihara, 1982). In our study, we observed that sarcomere shortening following either β_1AR or β_2AR stimulation was accompanied by an increase in calcium

transients. However, in the case of enhanced β_2AR-induced sarcomere shortening following hypoosmotic swelling, we did not observe a corresponding increase in calcium transients. Previous studies have shown that stretching cat papillary muscle during contraction has either no effect on calcium transients (Allen and Kurihara, 1982) or a much smaller effect compared to the muscle release (Ridgway and Gordon, 1984). This lack of observed increase might be due to the minor differences in calcium transients post-stretch, making them undetectable by the used methods, or it could be due to stretch altering a combination of calcium-dependent and calcium-independent mechanisms or stretch increasing myofilament sensitivity without altering calcium.

3.5.3 The Role of Caveolae in β_2AR Signalling Following Hypoosmotic Swelling

Caveolae are invaginations of the plasma membrane, playing a crucial role in β_2AR compartmentation and signalling. Previous studies on adult rat ventricular cardiomyocytes have shown that caveolae depletion using methyl-β-cyclodextrin (MβCD) enhances sarcomere shortening, calcium transients, and L-type calcium channel activity following β_2AR but not β_1AR simulation (Calaghan and White, 2006, Wright et al., 2014). Additionally, Calaghan and colleagues showed that disrupting caveolae alters β_2AR compartmentation, dampening the positive inotropic response without affecting the β_1AR response (Calaghan et al., 2008). Unpublished data from our group further supports the role of caveolae in β_2AR signalling, showing that Caveolin-3 Knockout in cardiac trabeculae increases β_2AR-induced cAMP release but not β_1AR.

In our study, we further investigated the role of caveolae in βAR signalling under stretch conditions. Cells were treated with 1.3mg/ml MβCD for 45 minutes, and we found that

hypoosmotic swelling did not cause major disruption to the T-tubule as well as Cavoelin-3 density in MβCD treated cells. Additionally, Caveolae depletion with MβCD abolished the enhanced sarcomere shortening response during hypoosmotic swelling following β_2AR stimulation, but not β_1AR simulation. This indicates that the increased response observed following hypoosmotic swelling is dependent on functional caveolae. The distinct responses between β_1AR and β_2AR may be due to their differential distribution.

β_2AR are primarily located in caveolae, while β_1AR are distributed across the plasma membrane. During hypoosmotic swelling, caveolae flatten and integrate into the plasma membrane, potentially causing β_2AR to relocate to the plasma membrane, where they become more accessible to agonists like isoprenaline, leading to increased contractility. Unpublished data from our lab also demonstrated that stretching cardiac trabeculae increases β_2AR-induced cAMP release, an effect lost with Caveolin-3 Knockout. This finding aligns with our results, further confirming the involvement of caveolae in the stretch-dependent regulation of β_2AR signalling. These observed effects of caveolae depletion on β_2AR-mediated contractility suggest that, despite their low numbers, caveolae provide an important signalling platform that enables localised, spatially restricted β_2AR activation.

3.5.4 The Effect of Hypoosmotic Swelling on β_2 mediated G_i-Pathway

β_2AR are pleiotropic receptors, in addition to coupling with G_s proteins to stimulate cAMP production, also couple with G_i proteins, which inhibit the cAMP production and confine the cAMP signal to the surface membrane (Nikolaev et al., 2010, Kuschel et al., 1999a). Most G_i proteins, along with β_2AR, are located in buoyant caveolar fractions of cardiomyocytes (Head et al., 2005). In our study, we found that pertussis toxin (PTX) treatment significantly

enhanced sarcomere shortening in isosmotic cells following β_2AR stimulation. This is consistent with findings from the Calaghan group, which observed an enhanced contractile response to β_2AR stimulation in PTX-treated cells. This indicated that in unstretched cells, G_i signalling typically counteracts G_s activation, thereby balancing β_2AR signalling at high activity levels (Calaghan and White, 2006). However, this effect was not observed in hypoosmotic cells, as there was no difference in sarcomere shortening between PTX-treated and untreated groups. Additionally, the increased sarcomere contractility following β_2AR stimulation during hypoosmotic swelling was absent in PTX-treated cells, similar to the effect of caveolae depletion on the response to β_2AR stimulation. These results suggest that the conformational change of caveolae during stretch disrupts G_i signalling, potentially leading to a switch to G_s coupling. Consequently, this shift causes positive inotropic effects when stimulated with isoprenaline.

3.6 Conclusions

In conclusion, membrane stretch via hypoosmotic swelling causes increased cardiomyocyte volume by increasing the cell width but not cell length and reduces the number of caveolae without affecting TT organisation and Cav3 density. Hypoosmotic swelling causes an increase in sarcomere shortening and cAMP production following β_2AR stimulation, but not β_1AR stimulation and this increased β_2AR activity following hypoosmotic swelling is dependent on functional caveolae. Furthermore, increased β_2AR activity following hypoosmotic swelling is lost in PTX-treated cells, suggesting a disrupted G_i signalling following hypoosmotic swelling.

Chapter 4 The Effect of Phosphodiesterase 4 on β-adrenoceptor Signalling in Cardiomyocytes Following Membrane Stretch

4.1 Introduction

cAMP is a widely distributed second messenger that translates the action of neurotransmitters into cellular responses. In the cardiomyocytes, cAMP mediates the inotropic and lusitropic effects of βAR stimulation by catecholamines (Zaccolo et al., 2021). cAMP signalling is compartmentalised; proteins involved in cAMP signalling, including GPCRs, adenylyl cyclase (AC) and protein kinase A (PKA), are organised into distinct multi-protein complexes(Lissandron and Zaccolo, 2006). Cyclic nucleotide Phosphodiesterase (PDE) are enzymes which hydrolyse and inactivate cAMP and are key components of these complexes, limiting and regulating the cAMP levels within specific compartments (Fischmeister et al., 2006). PDEs are derived from 21 distinct genes and are categorised into 11 families (PDE1-PDE11). PDE4 is the largest PDE family with high affinity in the heart, they regulate the PKA-mediated modulation of β_{1-} and β_2AR, L-type calcium channels (LTCC), cardiac ryanodine receptors (RYR2), the phospholamban/sarcoplasmic reticulum calcium ATPase (PLB/SERCA) complex, and troponin I (Houslay et al., 2007, Kerfant et al., 2007, Leroy et al., 2008a, Lehnart et al., 2005b). Inhibition of PDE4 significantly increases βAR induced PKA-dependent phosphorylation, substantially impacting the function of the associated signalling proteins in isolated cardiomyocytes. (Mongillo et al., 2004, Nikolaev et al., 2006).

PDE4 family consists of four homologous genes – PDE4A, PDE4B, PDE4C and PDE4D – each of which generates multiple transcript variants, which differ in their regulatory properties and subcellular localisation (Conti et al., 2003). Richter et al. conducted immunoprecipitation studies using PDE4-selective antibodies, and they found unlike in rats, where PDE4A, PDE4B,

and PDE4D are expressed at similar levels, PDE4D appears to be more prominently expressed in humans (Richter et al., 2011). A study from Wright et al. showed that both PDE4B and PDE4D are apparent in caveolae-enriched buoyant membrane fractions of cardiomyocytes (Wright et al., 2018a). In addition, PDE4B and PDE4D are the most similar among the PDE4 subfamilies. Nearly all the residues involved in inhibitor binding in PDE4B and PDE4D share the same conformation, with only minor positional variations (Wang et al., 2007). A study by Xiang et al. demonstrated that PDE4D plays a crucial role in regulating βAR-mediated contractile response in neonatal cardiac myocytes (Xiang et al., 2005).

PDE4D5 is one of the nine different isoforms encoded by the PDE4D gene and is found in a variety of cell types, including cardiomyocytes (Lynch et al., 2007). PDE4D5 is distinguished from other PDE4D isoforms by the presence of a unique amino-terminal region of 88 amino acids, which is highly conserved among mammals (Bolger et al., 2003). In the cardiomyocytes, PDE4D5 is primarily associated with β-arrestin, a crucial factor in limiting the GPCR signalling and is specifically recruited from the cytosol to the β_2AR upon agonist stimulation, providing dual desensitisation of β_2AR (Lynch et al., 2005, Houslay et al., 2007, De Arcangelis et al., 2009a). Stimulation of the β_2AR by isoprenaline leads to coupling to G_s, resulting in activation of AC and an increase in cAMP levels. This rise in cAMP results in PKA phosphorylation of the β_2AR, enabling its coupling to G_i, and thus activating ERK. In the meantime, the activation of G_s facilitates the recruitment of G protein-coupled receptor kinase (GRK) to the β_2AR, leading to its phosphorylation. This phosphorylation signals the recruitment of a β-arrestin–PDE4D5 complex to the β_2AR, leading to dual desensitisation. β-arrestin reduces the coupling of β_2AR to G_s, reduces the AC activation, and consequently decreases cAMP generation. Whereas

PDE4D5 creates a localised cAMP sink and reduces the levels of PKA-phosphorylated β_2AR (Lynch et al., 2005) (Figure 4.1).

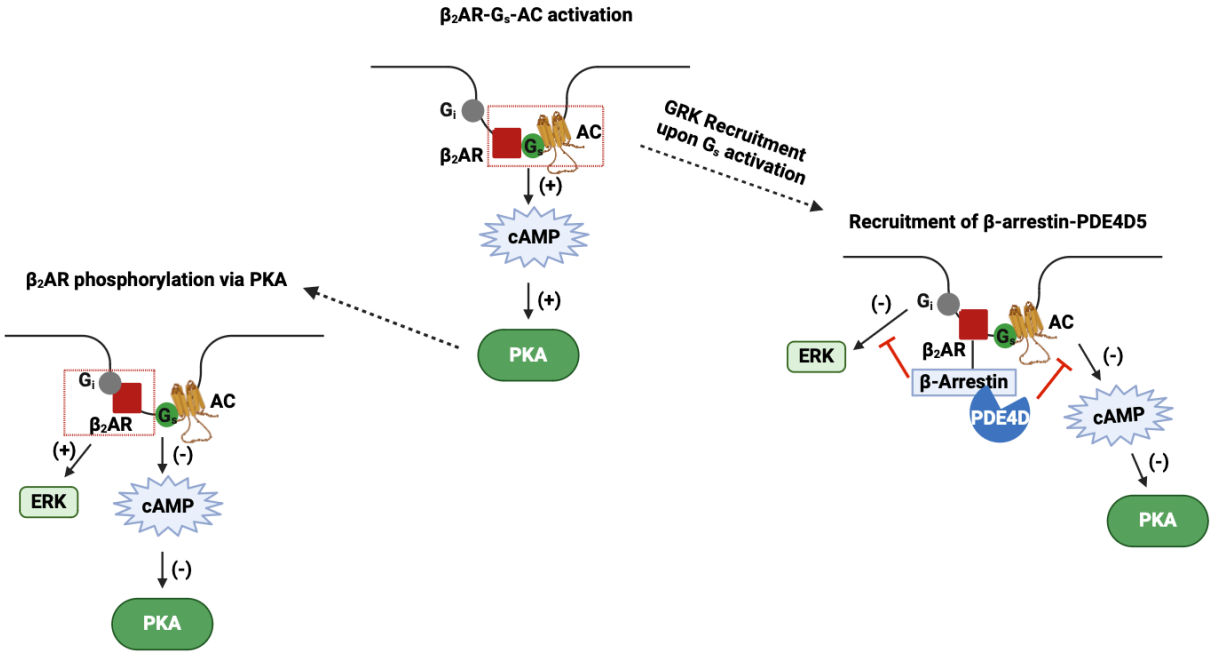


Figure 4.1. Schematic diagram of β_2AR regulation. In the upper panel, agonist stimulation of β_2AR coupled with G_s leads to the activation of adenylyl cyclase (AC), which in turn increases cAMP production and PKA phosphorylation. Following PKA-mediated phosphorylation of the β_2AR (lower left panel), the receptor switches from the G_s to G_i coupling, resulting in ERK activation, therefore, reducing cAMP production and PKA phosphorylation. G_s activation can also recruit GRK, which then facilitates the recruitment of β-arrestin along with bound PDE4D5 (lower right panel). This complex achieves dual desensitisation of β_2AR signalling through both its G_s and G_i-coupled pathways (figure created with BioRender).

While PDE4 families can be selectively inhibited, the identical catalytic within the sub-family, along with the close homology between the sub-family, make it challenging to use active site-directed inhibitors to study the functional roles of individual isoforms. The PDE4D5 isoform exhibits preferential interaction with β-arrestin as its unique N-terminal region contains a β-arrestin-binding site. Here, we used cell-permeable peptide reagents based upon the N-terminal region of PDE4D5 that allow for the selective disruption of PDE4D5 targeting to β-arrestin (Smith et al., 2007), which enables us to identify PDE4D5- β-arrestin complex as

playing a unique role in regulating the β_2AR mediated response following membrane stretch. Mutational analysis and peptide array studies showed that several residues within the 38-m34 peptide play key roles in the binding of PDE4D5 to β-arrestin; for example, Glu27Ala mutations individually serve to ablate β-arrestin binding in the intact PDE4D5 (Bolger et al., 2006). Thus, in this current study, cognate peptide with a Glu27Ala substitution was used as a scrambled peptide.

4.2 Hypothesis and Aims

Caveolae restructuring induced by membrane stretch disrupts the regulation of PDE4 and its subtypes, including PDE4D and PDE4B, leading to increased sarcomere shortening and cAMP production. This disruption also interferes with β-arrestin-mediated recruitment of PDE4D5 following β_2AR stimulation, further enhancing cardiomyocyte contractility

Aim 1: Investigate the role of PDE4 on β_2AR-cAMP signaling pathway during membrane stretch in the rat left ventricular cardiomyocytes.

- Objective 1: Use CytoCypher to assess the sarcomere shortening of cardiomyocytes maintained in iso- or hypoosmotic solutions following isoprenaline and rolipram (PDE4 inhibitor) stimulation in the presence of β_1 blocker.
- Objective 2: Measure β_2-cAMP response in cardiomyocytes by FRET following β_2 stimulation and PDE4 inhibition (rolipram).

Aim 2: Investigate the role of PDE4 subtypes (PDE4D and PDE4B) on β_2-AR/cAMP signalling pathway during membrane stretch in the rat left ventricular cardiomyocytes.

- Objective 1: Use CytoCypher to assess the sarcomere shortening of cardiomyocytes maintained in iso- or hypoosmotic solutions following isoprenaline, GEBR-7b (PDE4D inhibitor)/ A33 (PDE4B inhibitor) and rolipram (PDE4 inhibitor) stimulation in the presence of β_1 blocker.
- Objective 2: Measure β_2AR-cAMP response in cardiomyocytes by FRET following β_2 stimulation, PDE4D (GEBR-7b)/ PDE4B (A33) inhibition and PDE4 inhibition (rolipram).

Aim 3: Investigate the colocalisation of PDE4D and PDE4B with Cav3 in adult rat cardiomyocytes under membrane stretch.

- Objective 1: Double immunostaining of isolated rat LV cardiomyocyte with iso and hypo-osmotic solution, using Cav 3 and PDE4D or PDE4B antibodies
- Objective 2: Identify and quantify Cav 3 and PDE4D/B colocalisation using Pearson's correlation and Mander's coefficient

Aim 4: To investigate the effect of β-arrestin-PDE4D5 complex on β_2AR mediated contractility during membrane stretch in rat left ventricular cardiomyocytes.

- Objective 1: Measure β_2AR mediated contractile response following either scrambled peptide (Glu27-Ala) or disruptive peptide (Val12-Ser) treatment using CytoCypher.

4.3 Methods

4.3.1 Solutions and Drugs

Solutions	Composition
Isosmotic solution	NaCl 118; KCl 5.3; $MgCl_2$ 0.5; $CaCl_2$ 1; Glucose 10; Na_2HPO_4 7.5; $NaH_2PO_4.H_2O$ 2.5
Hypoosmotic solution	NaCl 81; KCl 5.3; $MgCl_2$ 0.5; $CaCl_2$ 1; Glucose 10; Na_2HPO_4 7.5; $NaH_2PO_4.H_2O$ 2.5
MEM media	MEM with Hank's salts, 9mM $NaHCO_3$, 1% glutamine and 1% antibiotic/antimycotic (AA)
Blocking solution	5% BSA, 20% Tween 20, 10% goat serum and PBS

Table 4.1. The list of solutions and their compositions used in the experiments for Chapter 4.

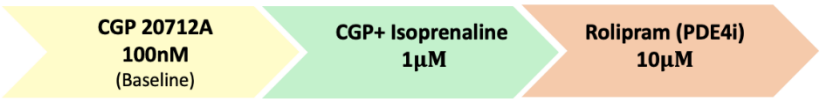
Cells were suspended in either isosmotic (osmolarity: 290 mOsm/L) or hypoosmotic (osmolarity: 214 mOsm/L) solutions for 15min. Selective inhibitors of PDE4 Rolipram, PDE4B A33 and PDE4D GEBR-7b were obtained from Tocris Bioscience.

4.3.2 CytoCypher

The high throughput system CytoCypher (IonOptix LLC, Westwood, MA, USA) was used to assess the shortening of isolated cardiomyocytes as an indicator of contractility, as described in earlier chapters. A number of protocols were used in this chapter and the role of PDE4 and its subtypes PDE4D and PDE4B were investigated, as well as the role β-arrestin-PDE4D5 complex to β_2AR mediated contractility following membrane stretch. The protocols for these various treatments are detailed below.

4.3.2.1 Investigation of the Role of PDE4 on β_2AR Mediated Contractile Response of Cardiomyocytes Following Membrane Stretch

Cells were maintained in either iso- and hypoosmotic solution for 15min with β_1AR blocker 100nM CGP. After recording the baseline measurement, 1000nM isoprenaline was added to the dishes to stimulate β_2AR. Following this, 10μM rolipram, a PDE4 inhibitor was added to inhibit PDE4 activity (MacKenzie and Houslay, 2000).



4.3.2.2. Investigation of the Role of PDE4B/D on β_2AR Mediated Contractile Response of Cardiomyocytes Following Membrane Stretch

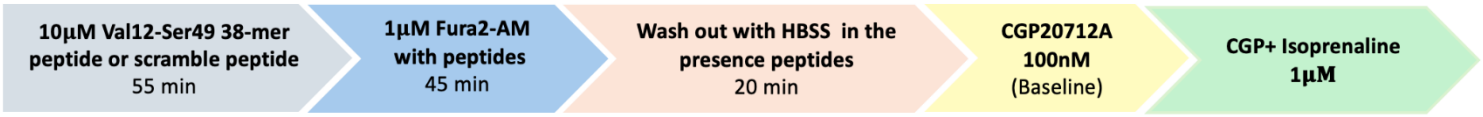
Sarcomere shortening and calcium are transient upon the addition of either PDE4B (A33, 10μM) or PDE4D inhibitor (GEBR-7b, 10μM) was measured after β_2AR stimulation and before rolipram. This allowed us to assess the function of PDE4B/D compared to the remaining PDE4 subtypes.



4.3.2.3. Investigation of the Effect of β-arrestin-PDE4D5 Complex on β_2AR Mediated Contractile Response During Membrane Stretch

Isolated cardiomyocytes were treated with either a 10μM membrane-permeable Val12-Ser49 38-mer peptide or a scramble peptide with a Glu27Ala substitution for 2h at 37°C prior to the experiment (Smith et al., 2007). Peptides were dissolved in DMSO at a stock concentration of

10mM and added 1:1000 v/v with MEM. 45min Fura2Am treatment and a 30min washout period were done in the last 75min of incubation in that 3h incubation.



4.3.3 Multi-cell FRET Microscopy

FRET microscopy was conducted as described in Chapter 2. These experiments were carried out on cells transfected with a pmEPAC2 FRET sensor. To measure cAMP induced by β_2AR, cells were stimulated with 100nM CGP (β_1AR blocker) followed by 100nM Isoprenaline (βAR agonist). Quantifying the cAMP release upon addition of PDE4 (Rolipram, 10 μM, PDE4 inhibitor) was measured after β_2AR stimulation. Assessing the role of PDE4B and PDE4D was completed using 10μM A33 (PDE4B) and 10μM GEBR-7b (PDE4D). Treatment to inhibit PDE4B or PDE4D was given after β_2AR stimulation and before rolipram treatment. Finally, 100μM IBMX, a non-specific PDE inhibitor and 10μM Forskolin, an adenylyl cyclase activator, were applied to assess the maximal cAMP release (Figure 4.2).

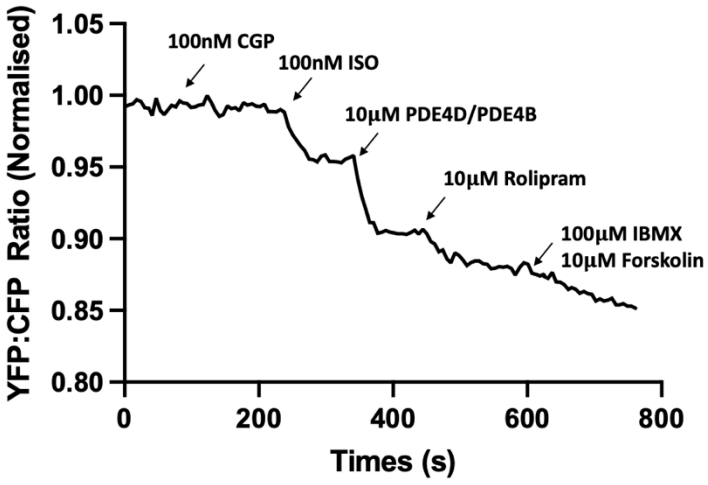


Figure 4.2. Example of FRET response and drug protocol used in the FRET microscopy experiment.

4.3.4 Confocal Microscopy Double Immunostaining

Isolated Cardiomyocytes were maintained in iso- or hypoosmotic solution for 15min, fixed with 4% PFA, permeabilised with 0.1% Triton X-100 and blocked with blocking buffer (PBS with 5% BSA, 20% Tween20 and 10% goat serum). Cells were incubated overnight at 4℃ with primary antibodies: mouse anti Caveolin-3 (1:100, BD Bioscience) and sheep anti-PDE4D antibodies (1:200, non-commercial and from Baillie, Glasgow) or sheep anti-PDE4B (1:200, Invitrogen). Secondary antibodies used were Alexa Fluor 488 conjugated donkey anti-mouse IgG (1:500, Invitrogen) and Alexa fluor 546 conjugated donkey anti-sheep (1:500, Invitrogen). Cells were mounted with DAPI and sealed with nail polish.

4.3.5 Statistics

All graphs and statistical analyses were performed using Prism10 (GraphPad).

Cell contractility (CytoCypher experiments) was analysed using either Two-way ANOVA with Šidák's multiple comparisons test or mixed-effects analysis followed by Tukey's multiple comparisons test. cAMP output (FRET microscopy experiments) was analysed using Two-way ANOVA with Šidák's multiple comparisons test. Protein colocalisation studies were quantified and tested using an unpaired T-test.

4.4 Results

4.4.1 PDE4 Inhibition Enhances β_2AR Responses and Equilibrates Cell Contractile Responses to β_2AR Stimulation Following Hypoosmotic Swelling

Hypoosmotic swelling model was used in isolated left ventricular rat cardiomyocytes to mimic membrane stretch that occurs during cardiac stretch. Our findings from the previous chapter demonstrated that hypoosmotic swelling enhances the β_2AR-meidated response. Previous studies have highlighted the significant role of PDE4 in regulating the β_2AR-mediated contractile response (Xiang et al., 2005). To investigate whether the increased β_2AR response in cardiomyocytes following hypoosmotic swelling is linked to PDE4 activity, we measured sarcomere shortening at baseline, after β_2AR stimulation, and following the application of the PDE4-specific inhibitor Rolipram using CytoCypher.

Activation of β_2ARs in left ventricular cardiomyocytes led to a significant increase in sarcomere shortening in hypoosmotic cells compared to isosmotic cells. The application of Rolipram enhanced the sarcomere shortening in isosmotic cells, but not in hypoosmotic cells. In addition, inhibition of PDE4 equilibrates the sarcomere shortening between iso- and hypoosmotic cells (Figure 4.3).

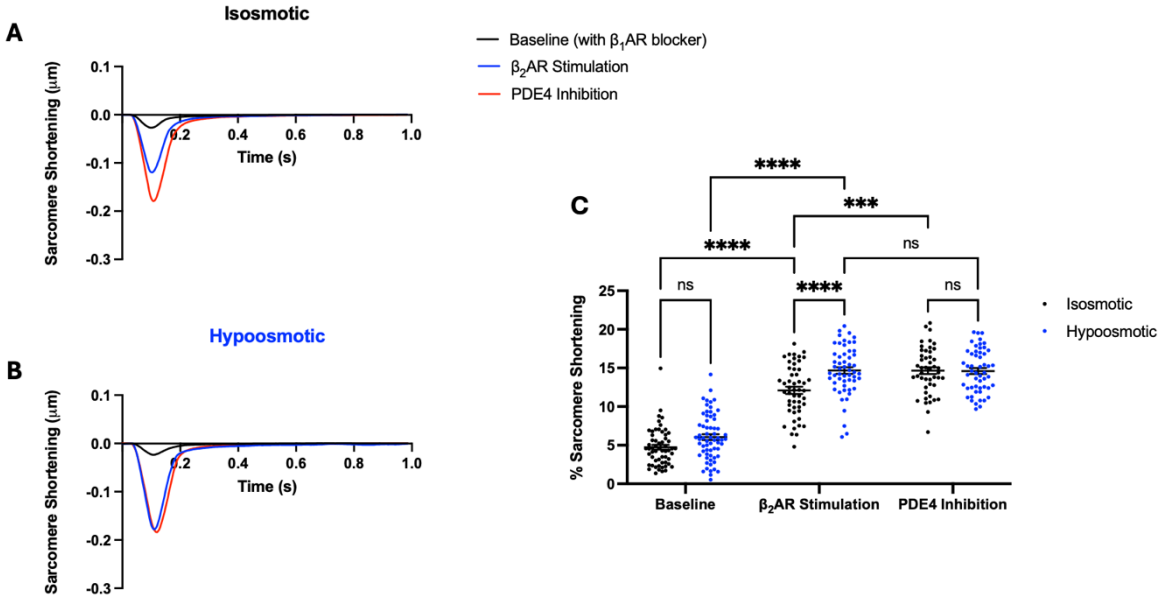


Figure 4.3. PDE4 Inhibition Enhances β_2AR Responses and Equilibrates Cell Contractile Responses to β_2AR Stimulation Following Hypoosmotic Swelling. Representative traces of sarcomere shortening in **(A)** isosmotic and **(B)** hypoosmotic cells during the contraction cycle at baseline with the presence of β_1AR blocker (100nM CGP) (black line) after β_2AR stimulation (1µM Isoprenaline) (blue line) and after PDE4 inhibition (10µM Rolipram). **C.** Percentage of sarcomere shortening in iso-(black) and hypoosmotic (blue) cells following β_2AR stimulation and PDE4 inhibition. N=3, n=46~64. Data are presented as means ± SEM. ***, ****P<0.001, 0.0001 receptively, Two-way ANOVA followed by Šídák's multiple comparisons test.

4.4.2 Inhibition of PDE4 Further Enhances β_2AR Induced cAMP Production Following Hypoosmotic Swelling

We investigate the effect of PDE4 on β_2AR mediated cAMP response. Figure 4.4A shows representative traces illustrating the cAMP response following PDE4 inhibition with the selective PDE4 blocker Rolipram in β_2AR-stimulated cardiomyocytes under both isosmotic (black line) and hypoosmotic (blue line) conditions. β_2AR stimulation leads to significantly higher cAMP production in hypoosmotic cells compared to isosmotic cells and the difference between them becomes non-significant after PDE4 inhibition with Rolipram. However, unlike

the contractility study, we found that the cAMP level was further increased in both iso- and hypoosmotic cells following PDE4 inhibition.

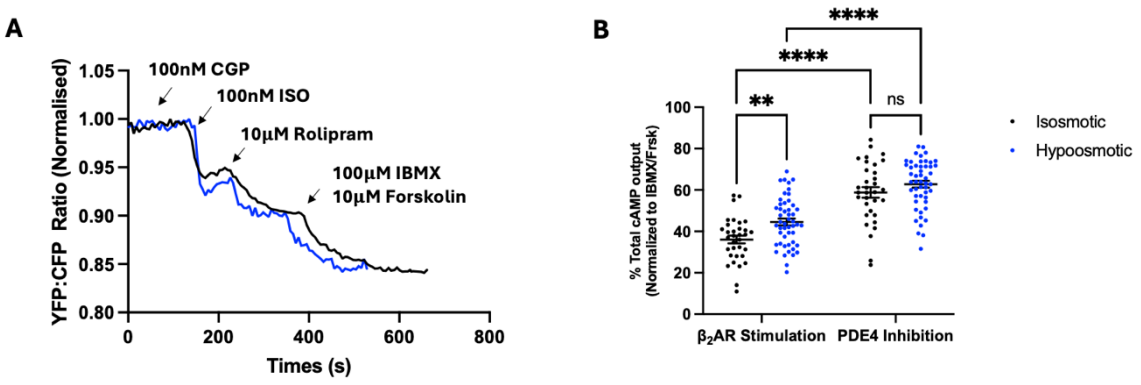


Figure 4.4. PDE4 Inhibition enhances β_2AR-cAMP activity in both iso-and hypoosmotic cells. A. A representative trace illustrating the β_2AR-specific FRET response measured by the plasma membrane cAMP sensor pmEPAC2-camp in left ventricular cardiomyocytes under iso-osmotic (black line) and hypoosmotic (blue line) conditions. Responses were recorded after the application of CGP (β_1AR blocker, 100nM), isoprenaline (a non-selective βAR agonist, 100nM), and Rolipram (a PDE4 inhibitor, 10μM). **B.** Quantification of cAMP production following β_2AR stimulation and PDE4 inhibition, relative to the maximum cAMP production achieved with IBMX and forskolin stimulation. N=3, n=35-50. Data are expressed as means ± SEM. **P<0.01, ****P<0.0001, Two-way ANOVA followed by Šídák's multiple comparisons test.

4.4.3 PDE4D is Predominately Involved in β_2AR Signalling for Sarcomere Shortening Response and cAMP Production

PDE4D has been shown to play an essential role in mediating β_2AR-specific signalling in rat neonatal cardiomyocytes (Xiang et al., 2005). We then investigated the role of PDE4D in the β_2AR-mediated response following hypoosmotic swelling in adult rat cardiomyocytes. To assess this, we used the PDE4D-selective inhibitor GEBR-7b. The inhibitor was applied after β_2AR stimulation but before the administration of rolipram, allowing us to determine the specific contribution of PDE4D in relation to the other PDE4 subtypes. In line with our previous finding, activation of β_2ARs expressed in rat left ventricular cardiomyocytes resulted in a robust increase in sarcomere shortening following hypoosmotic swelling. In isosmotic cells,

the increase in sarcomere shortening after β_2ARs stimulation was further enhanced by PDE4D inhibition, whereas this effect was not observed in the hypoosmotic cells. In addition, inhibition of the remaining PDE4 activity with rolipram did not elicit any additional response in either isosmotic or hypoosmotic cells (Figure 4.5C). These data provide an indication that PDE4D is the major PDE4 subtype regulating the β_2AR signalling that controls the sarcomere shortening.

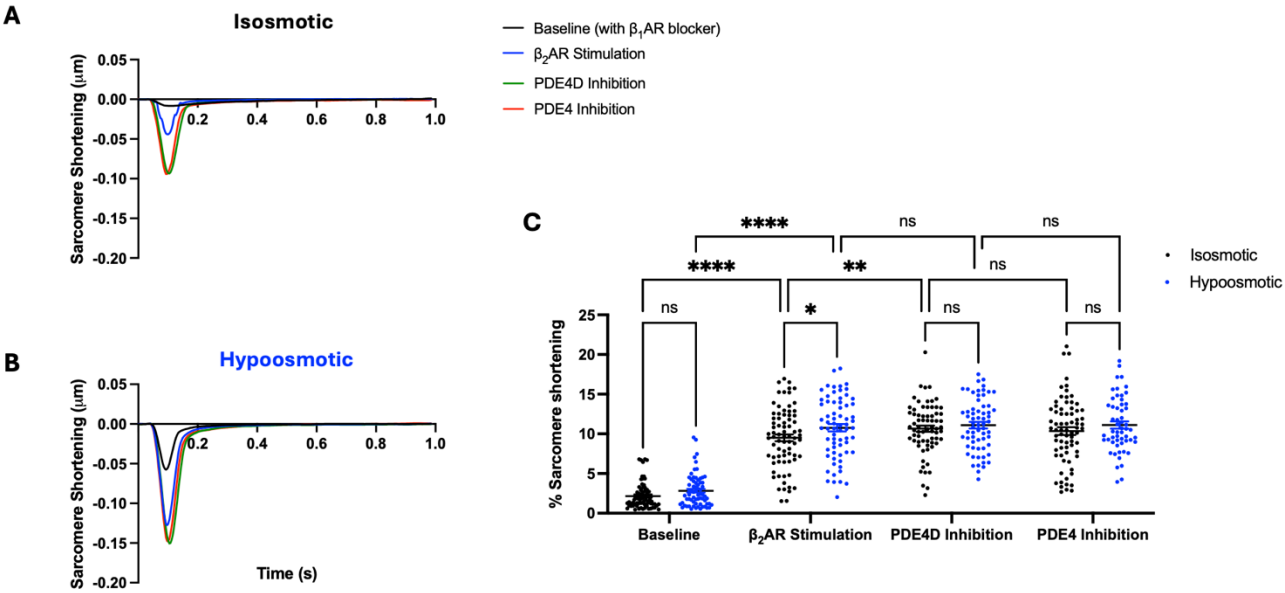


Figure 4.5 PDE4D predominately contributes to β_2AR signalling in sarcomere shortening response in Adult Rat LV cardiomyocytes. (A) and (B) show representative traces of sarcomere shortening in isosmotic and hypoosmotic cells, respectively, throughout the contraction cycle. Traces are shown at baseline with the presence of CGP (black line), after the addition of 1µM isoprenaline (blue line), following the application of 10µM GEBR-7b (green line), and after 10µM Rolipram. **C.** Percentage of sarcomere shortening in iso-(black) and hypoosmotic (blue) cells following treatment with 1µM isoprenaline, 10µM GEBR-7b and 10µM Rolipram. N=5, n=56~70. Data are presented as means ± SEM. *, **,****P<0.05, 0.01, 0.0001 respectively, Mixed-effects analysis followed by Tukey's multiple comparisons test.

We then assessed the impact of PDE4D on the cAMP activity following β_2AR signalling pathway stimulation. To induce a β_2AR response, 100nM isoprenaline was added in the presence of 100nM CGP, while 10µM GEBR-7b and 10µM rolipram were used to inhibit PDE4D and PDE4,

respectively. To achieve maximum cAMP stimulation, 100µM IBMX and 10µM Forskolin were also applied. A representative FRET trace is shown in Figure 4.6A.

Hypoosmotic cells exhibited a significant increase in cAMP output following β_2AR stimulation compared to isosmotic cells, with further enhancement in cAMP output observed in both cells after PDE4D inhibition. Additionally, PDE4 inhibition led to an increase in cAMP output in isosmotic cells, but not in hypoosmotic cells. Following inhibition of PDE4D and PDE4, the difference in cAMP output between iso-and hypoosmotic conditions was eliminated (Figure 4.6B).

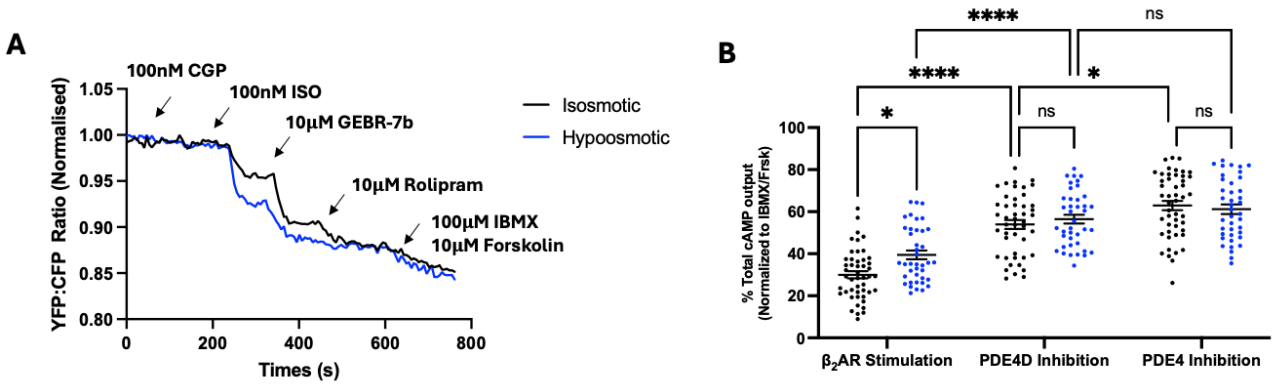


Figure 4.6 PDE4D inhibition enhances β_2AR-cAMP activity in both iso-and hypoosmotic cells and doesn't have any further elevation after PDE4 inhibition. A. Representative FRET trace following β_2AR-specific stimulation (100nM isoprenaline in the presence of 100nM CGP) and PDE4D (10µM GEBR-7b) and PDE4 (10µM Rolipram) inhibition in isosmotic (black) and hypoosmotic (blue) cells. **B.** % of the total cAMP output of β_2AR-specific response in iso- and hypoosmotic cells. N=4, n=40~47. Data are presented as means ± SEM. *, **** P<0.05, 0.0001 respectively, Two-way ANOVA followed by Šídák's multiple comparisons test.

Since there was still an increase in cAMP production following PE4D inhibition in hypoosmotic cells, we then plotted a graph showing the percentage change in two conditions. We found that hypoosmotic cells had a smaller increase in β_2AR-mediated cAMP production compared to isosmotic cells following PDE4D inhibition (Figure 4.7), suggesting that the PDE4D regulation was disrupted under hypoosmotic swelling.

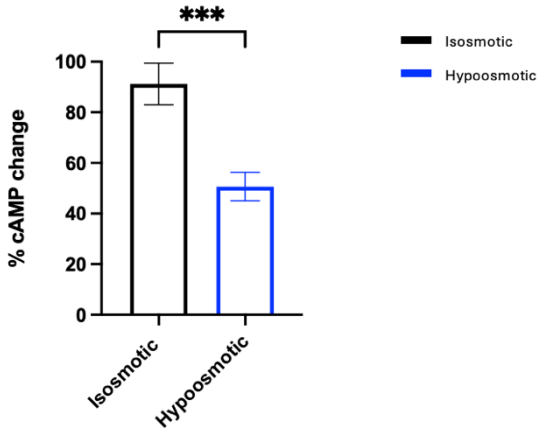


Figure 4.7. Decrease in β_2AR-mediated cAMP production in hypoosmotic cells following PDE4D inhibition. The percentage change of β_2AR-mediated cAMP production following PDE4D inhibition in iso- and hypoosmotic cells. N=4, n=40~47, Data are presented as means ± SEM. *** P<0.001, Mann Whitney test.

4.4.4 Hypoosmotic Swelling Disrupts Colocalisation of Cav3 and PDE4D in Adult Rat Ventricular Cardiomyocytes

We have established the role of PDE4D in the β_2AR-mediated response following hypoosmotic swelling. Since caveolae undergo conformational changes under these conditions, we aimed to investigate whether Cav3, the primary scaffold protein in cardiomyocyte caveolae, colocalises with PDE4D and if hypoosmotic swelling affects their colocalisation. Cardiomyocytes were treated with iso- and hypoosmotic solutions for 15 minutes before being fixed with 4% PFA. The proteins Cav3 and PDE4D were then double-stained. Figure 4.8A shows the representative immunofluorescence images of Cav3 and PDE4D in isosmotic and hypoosmotic conditions.

There was a significant reduction in Pearson's coefficient (PC) under hypoosmotic conditions, indicating that hypo-osmotic stretch disrupts the colocalisation between Cav3 and PDE4D in

cardiomyocytes (Figure 4.9B). Manders' coefficient was also used to confirm the impact of hypoosmotic swelling on the colocalisation of Cav3 and PDE4D proteins. Unlike Pearson's coefficient, which measures the linear correlation between two proteins, Manders' coefficient quantifies the proportion of one protein that colocalises with another relative to their total presence, assessing the overlap ratio. M1 represents the proportion of Cav3 overlap with PDE4D, while M2 indicates the proportion of PDE4D overlap with Cav3. Figure 4.8C and D show that both M1 and M2 were significantly reduced in cardiomyocytes under hypoosmotic conditions compared to the isosmotic group. This decrease in M1 and M2 suggests a marked reduction in the overlap of Cav3 and PDE4B, supporting the notion that hypoosmotic stretching disrupts their colocalisation in cardiomyocytes.

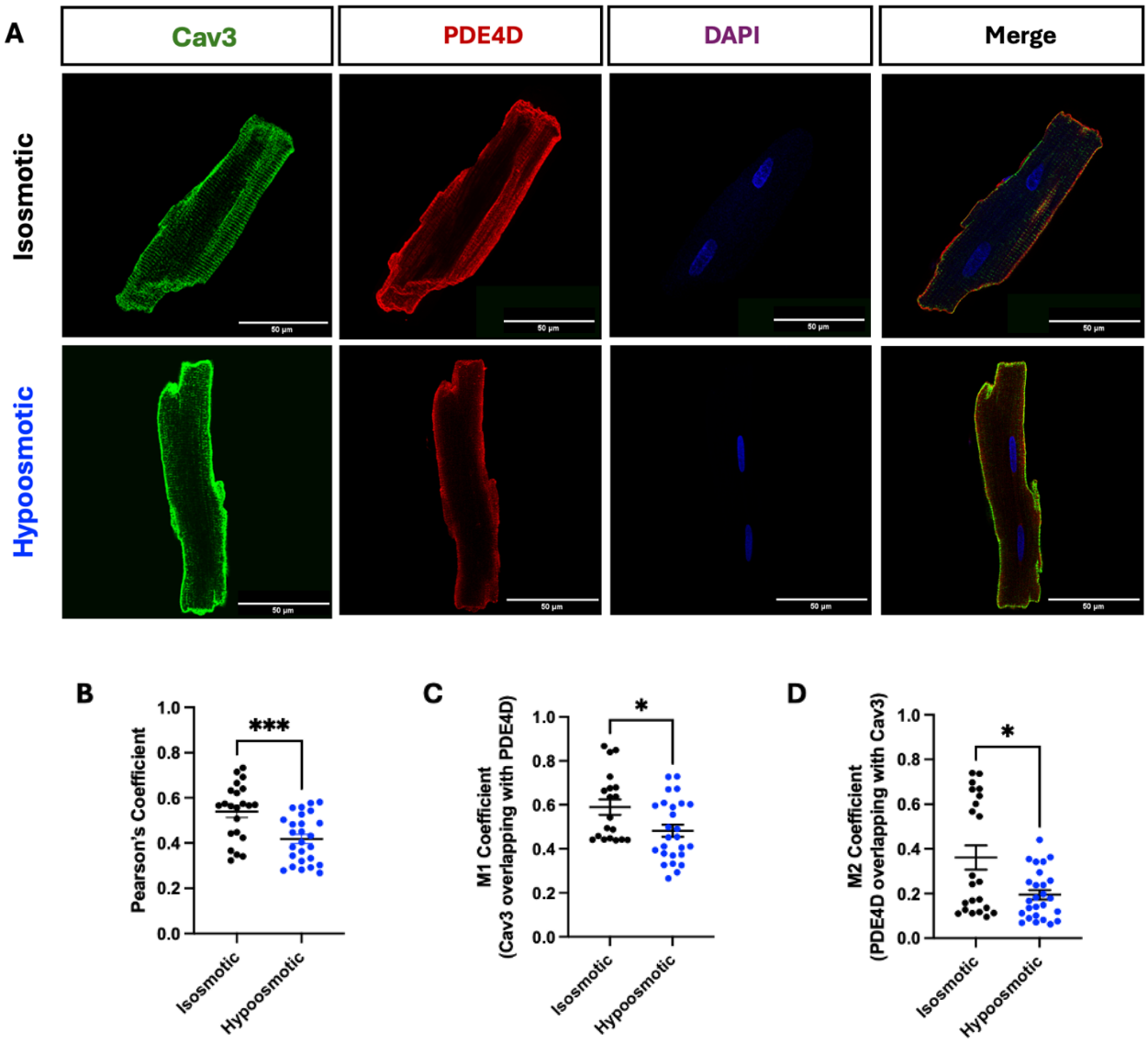


Figure 4.8. Cav3 colocalises with PDE4D, but the colocalisation is disrupted following hypoosmotic swelling. A. Representative immunofluorescence images illustrating the colocalisation of Cav3 (green, monoclonal), PDE4D (red, polyclonal), and DAPI (nucleus, blue) in cells exposed to iso- and hypoosmotic conditions. **B.** Pearson's correlation coefficients and Mander's coefficients **(C)** M1 and **(D)** M2 quantifying the colocalisation of Cav3 and PDE4D in iso- and hypoosmotic cells. **C.** N=3, n=25. Data are presented as means ± SEM. *, ***P<0.05,0.001, unpaired t-test. Scale bars = 50µm

4.4.5 PDE4B is Involved in β_2AR Signalling for Sarcomere Shortening Response and cAMP Production

To evaluate the role of PDE4B in regulating β_2-mediated cardiomyocyte contraction, the PDE4B-selective inhibitor A33 was used following β_2AR stimulation. The non-selective PDE4 inhibitor rolipram was applied after PDE4B inhibition, enabling us to determine the specific contribution of PDE4B compared to other PDE4 subtypes. Representative traces in Figure 4.9 A and B show sequential changes in sarcomere shortening under different treatments: baseline with 100nM β_1 blocker CGP (black), 1μM non-selective β-agonist isoprenaline (blue), 10μM selective PDE4B inhibitor A33 (green), and 10μM PDE4 inhibitor rolipram (red).

β_2 stimulation resulted in a significant increase in sarcomere shortening in both iso- and hypoosmotic cells, with further enhancement observed following PDE4B inhibition. Surprisingly, no additional increase in sarcomere shortening was detected after PDE4 inhibition, similar to the one shown following PDE4D inhibition. As previously noted, hypoosmotic cells exhibited a greater sarcomere shortening compared to isosmotic cells following β_2 stimulation, and this difference was maintained after PDE4B inhibition. However, the difference in sarcomere shortening between the two conditions was eliminated after PDE4 inhibition (Figure 4.9C). This suggested that the stretch-sensitive mechanism is still preserved following PDE4B inhibition, indicating that other PDE4 isoforms, in addition to PDE4B, may contribute to the regulation of contractile responses following hypoosmotic swelling.

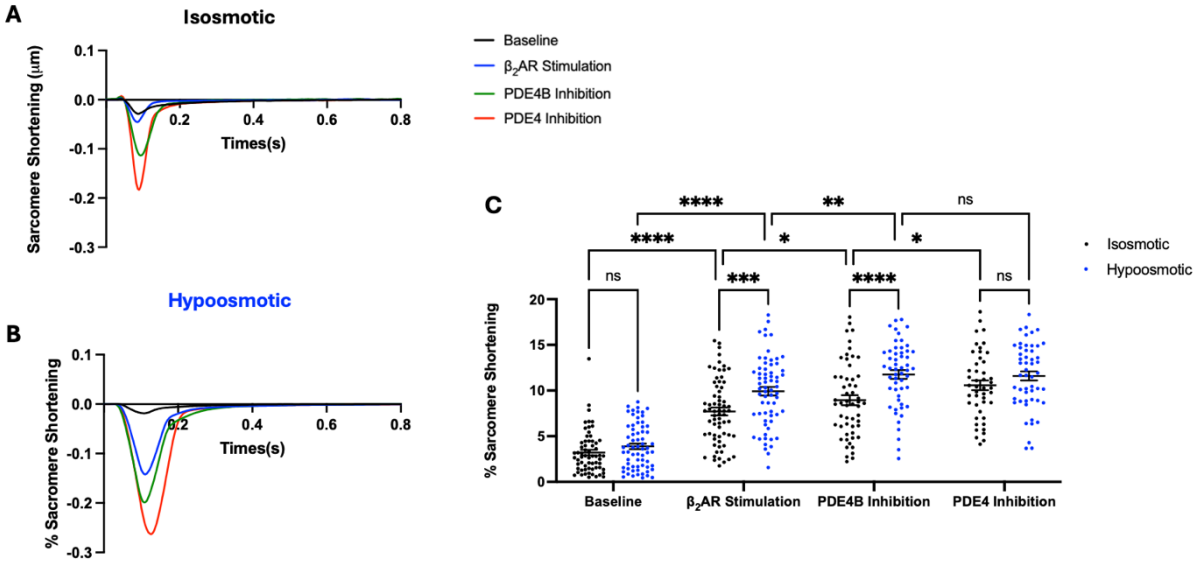


Figure 4.9. PDE4B contributes to β_2AR signalling in sarcomere shortening response in adult rat LV cardiomyocytes. **(A) and (B)** show representative traces of sarcomere shortening in isosmotic and hypoosmotic cells, respectively, throughout the contraction cycle. Traces are shown at baseline with the presence of CGP (black line), after the addition of 1µM isoprenaline (blue line), following the application of 10µM A33 (green line), and after 10µM Rolipram. **C.** Percentage of sarcomere shortening in iso-(black) and hypoosmotic (blue) cells following treatment with 1µM isoprenaline, 10µM GEBR-7b and 10µM Rolipram. N=5, n=47~69. Data are presented as means ± SEM. *, **, ***,**** P<0.05, 0.01, 0.001, 0.0001, respectively. Mixed-effects analysis followed by Tukey's multiple comparisons test.

To further investigate the PDE4B response to β_2AR mediated cAMP under hypoosmotic conditions, A33, a selective PDE4B inhibitor, was added following CGP and isoprenaline treatment. Rolipram was then added to compare the effects of PDE4B inhibition with the remaining PDE4 subtypes. Finally, IBMX and forskolin were added to standardise individual responses against maximal cAMP production (Figure 4.10A).

Under β_2AR stimulation, cAMP levels were significantly elevated in hypoosmotic cells compared to isosmotic cells. When a specific inhibitor for PDE4B was applied, there was an increased trend in hypoosmotic cells compared to isosmotic cells ($p<0.0839$), though this

increase was not statistically significant. Upon general PDE4 inhibition, no significant difference in cAMP output was observed between isosmotic and hypoosmotic conditions (Figure 4.10B). These results suggest that PDE4B inhibition does not fully account for the elevated cAMP response under hypoosmotic conditions, although additional data are needed to confirm this finding.

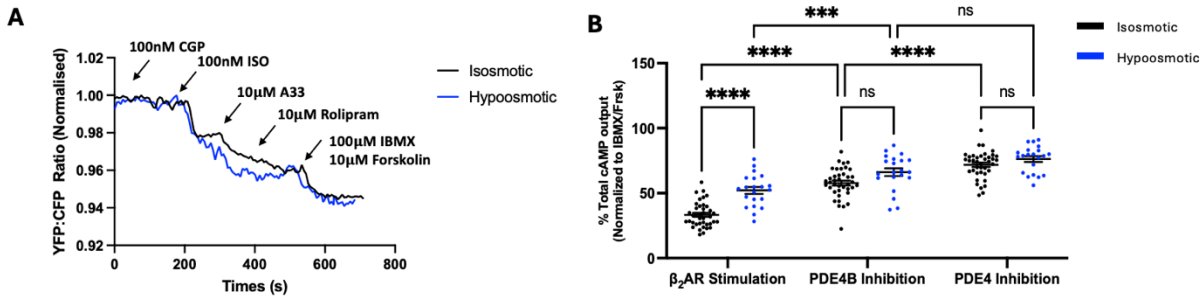


Figure 4.10. PDE4B inhibition enhances β_2AR-cAMP activity in both iso-and hypoosmotic cells and only isosmotic cells have further elevation after PDE4 inhibition. **A.** Representative FRET trace following β_2AR-specific stimulation (100nM isoprenaline in the presence of 100nM CGP) and PDE4B (10μM A33) and PDE4 (10μM Rolipram) inhibition in isosmotic (black) and hypoosmotic (blue) cells. **B.** % of the total cAMP output of β_2AR-specific response in iso- and hypoosmotic cells. N=3~4, n=23~39. Data are presented as means ± SEM. ***, **** P<0.001, 0.0001 respectively, Two-way ANOVA followed by Šídák's multiple comparisons test.

4.4.6 Hypoosmotic swelling decreases colocalisation of Cav3 and PDE4B in Adult Rat Ventricular Cardiomyocytes

To assess the impact of hypoosmotic swelling on the colocalisation of Cav3 and PDE4B. Isolated left ventricular cardiomyocytes from healthy rats were exposed to a hypoosmotic solution to induce membrane stretch, while a control group of cardiomyocytes was maintained under an isosmotic solution. The cells were double stained using Cav3 and PDE4B

antibodies, and imaging was done using confocal microscopy with FIJI software for analysis. Figure 4.11A shows representative immunofluorescence images of cells under these different conditions.

As shown in Figure 4.11B, Pearson's coefficients for both groups were above 0.5, indicating colocalisation of the two proteins in both iso- and hypoosmotic conditions. However, a notable decrease in Pearson's coefficient was observed under hypoosmotic conditions, implying that hypoosmotic swelling disrupts the colocalisation between Cav3 and PDE4B in cardiomyocytes. M1 reflects the percentage of Cav3 colocalising with PDE4B, whereas M2 represents the percentage of PDE4B colocalising with Cav3. Figures 4.11C and D further show that both M1 and M2 were significantly lower in cardiomyocytes subjected to hypoosmotic conditions compared to those in the isosmotic group. This reduction in M1 and M2 values supports the hypothesis that hypoosmotic stretching interferes with the colocalisation of Cav3 and PDE4B in cardiomyocytes.

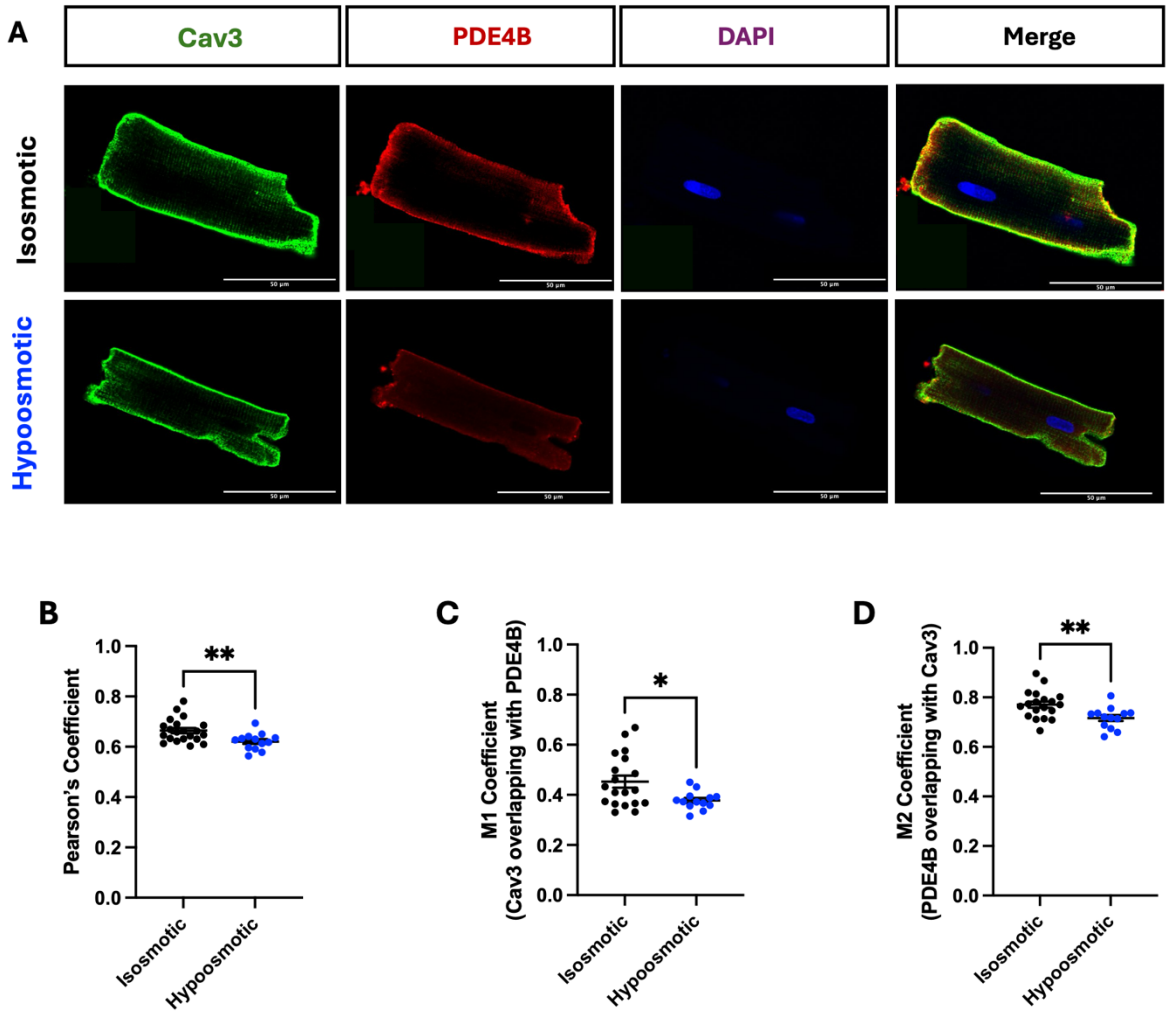


Figure 4.11 Hypoosmotic swelling decreases colocalisation of Cav3 and PDE4B in adult rat ventricular cardiomyocytes. A. Representative immunofluorescence images illustrating the colocalisation of Cav3 (green, monoclonal), PDE4B (red, polyclonal), and DAPI (nucleus, blue) in cells exposed to iso- and hypoosmotic conditions. **B.** Pearson's correlation coefficients and Manders' coefficients **(C)** M1 and **(D)** M2 quantifying the colocalisation of Cav3 and PDE4B in iso- and hypoosmotic cells. **C.** N=4~5, n=13~21. Data are presented as means ± SEM. **P<0.01, unpaired t-test. Scale bars = 50µm

4.4.7 PDE4D5 β-arrestin Disruptive Peptide Removes the Enhanced β_2AR induced Contractility Following Hypoosmotic Swelling

To investigate the role of β-arrestin in regulating the PDE4D5-mediated sarcomere shortening response following β_2AR stimulation, we treated isolated left ventricular cardiomyocytes with a PDE4D5 β-arrestin disruptive peptide and compared the effects to a control scramble peptide. As shown in Figure 4.12, cardiomyocytes under hypoosmotic conditions displayed significantly greater sarcomere shortening compared to those under hypoosmotic conditions when treated with the scramble peptide. However, when cells were treated with the PDE4D5 β-arrestin disruptive peptide, the difference in sarcomere shortening between isosmotic and hypoosmotic cells was abolished, with no significant difference observed (Figure 4.12). This suggests that disruption of the interaction between PDE4D5 and β-arrestin negates the stretch-induced increase in sarcomere shortening. Although there was a trend for the increase, there was no significant difference in sarcomere shortening found between the scramble and disrupted peptide-treated groups in isosmotic cells (P=0.0945). In addition, there was no difference found in hypoosmotic cells, suggesting that hypoosmotic swelling disrupts the PDE4D5-β-arrestin mediated regulation in β_2AR contractile response.

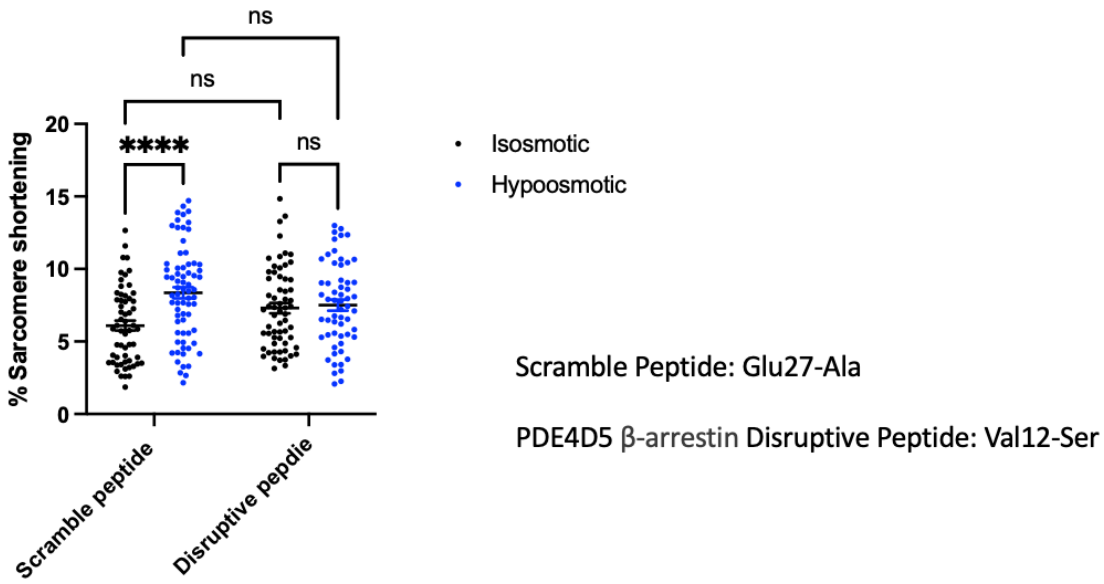


Figure 4.12. PDE4D5-β-arrestin disruptive peptide removes the enhanced β_2AR induced contractility following hypoosmotic swelling. Cells were pre-treated with either scrambled peptide (Glu27-Ala) or disruptive peptide (Val12-Ser) for 2h prior to the experiment. Percentage of sarcomere shortening following β_2AR stimulation under both osmotic conditions is shown. N=5, n=58~71, **** p<0.0001. Two-way ANOVA followed by Šídák's multiple comparisons test.

4.5 Discussion

In this chapter, we investigated the role of PDE4 and their subtypes PDE4D and PDE4DB on β_2AR-mediated response during hypoosmotic swelling in the rat left ventricular cardiomyocytes. The key findings from this chapter can be summarised as follows:

- PDE4 inhibition enhances β_2AR responses and equilibrates cell cAMP activity and contractile responses to β_2AR stimulation following hypoosmotic swelling.
- Both PDE4D and PDE4B inhibitions increase the β_2AR responses, whereas only PDE4D inhibition eliminates the differences between iso- and hypoosmotic cells.
- Cardiomyocytes subjected to hypoosmotic conditions show a decreased colocalisation of Cav3 and PDE4D/PDE4B on the membrane when compared to iso-osmotic cells.
- PDE4D5 β-arrestin disruptive peptide removes the enhanced β_2AR induced contractility following hypoosmotic swelling.

The βAR signalling pathway enhances cAMP production, leading to increased cell contractility. However, chronic stimulation can contribute to cardiac remodelling. PDEs are critical regulatory enzymes that degrade cAMP, tightly regulating the signalling pathway (Boularan and Gales, 2015). In the rat heart, PDE4 accounts for 52% of total PDE activity and is the predominant cAMP-specific PDE (Richter et al., 2011). A previous study by Xiang et al. demonstrated that PDE4D plays a key role in modulating the β_2AR contractile response in neonatal rat ventricular cardiomyocytes (Xiang et al., 2005). Our findings extend this concept to adult rats, showing that PDE4D inhibition significantly enhances β_2AR-induced sarcomere shortening and cAMP production.

Furthermore, the β_2AR-dependent contractile responses following PDE4D inhibition are equilibrated in both isosmotic and hypoosmotic cells, which is reminiscent of the effects seen with MβCD treatment, as shown in the previous chapter. Furthermore, inhibiting the remaining PDE4 activity did not produce any additional effect on the β_2AR-mediated response, suggesting that PDE4D is the predominant isoform associated with the β_2AR response. One thing that needs to be noted is that after hypoosmotic swelling, there is no further increase in β_2AR mediated sarcomere shortening following PDE4D inhibition. This suggests that PDE4D regulation is disrupted in the hypoosmotic swelling, limiting its effect on β_2AR mediated contractility with its inhibition. However, we observed elevated cAMP levels following PDE4D inhibition in hypoosmotic cells. When comparing the percentage change in cAMP production, hypoosmotic cells showed a smaller increase compared to isosmotic cells, suggesting that PDE4D regulation is impaired but not entirely abolished. This partial disruption may indicate that membrane stretch from hypoosmotic swelling also affects downstream signalling that contributes to contractility and is regulated by PDE4D, thereby negating the contractile response.

A study by Wright et al. showed that both PDE4B and PDE4D are expressed with Cav3 in both buoyant and heavy membrane fractions (Wright et al., 2018a). Therefore, we examined the β_2AR-mediated response following PDE4B inhibition. Inhibiting PDE4B enhanced the β_2AR-induced sarcomere shortening and cAMP production. Further inhibition of remaining PDE4 activity led to additional increases in sarcomere shortening and cAMP production, whereas this was not observed in hypoosmotic cells. PDE4B inhibition did not abolish the stretch-induced increase in the β_2AR-mediated response. These suggest that while both PDE4D and PDE4B tightly regulate cAMP hydrolysis following β_2AR stimulation, membrane stretch has a greater influence on PDE4D than PDE4B.

Studies indicate that PDE4B colocalises with the LTCC along T-tubules, and PDE4B knockout mice significantly increased the Ca^{2+} transients, cell contraction and spontaneous Ca^{2+} release upon βAR stimulation (Leroy et al., 2011). This suggests that PDE4B may play a more prominent role in the t-tubule rather than in the caveolae. In our colocalisation study, we observed decreased colocalisation of Cav3 and PDE4B in hypoosmotic cells. However, as Cav3 is present not only in the caveolae but also in the T-tubules, we cannot determine in which region the colocalisation of Cav3 and PDE4B is decreased.

Caveolae, which play a crucial mechanotransduction role in the heart, organise the compartmentalisation of signalling proteins such as adenylyl cyclase, PDE4B, and PDE4D (Timofeyev et al., 2013). These invaginated nanodomains also contribute to the spatial organisation of β_2AR signalling within ventricular cardiomyocytes (Calaghan and White, 2006). In our earlier investigation, we observed a notable increase in sarcomere contractility and cAMP production following β_2AR stimulation under hypoosmotic swelling. One possible explanation is that caveolae recruitment to the sarcolemma facilitates the translocation of β_2ARs to the membrane surface, making them more accessible to agonists. Moreover, our current results show reduced colocalisation of both Cav3 with PDE4D and Cav3 with PDE4B, which may impair the ability of PDE4D and PDE4B to regulate cAMP signalling through their hydrolytic activity. This disruption could explain the elevated cAMP production and enhanced sarcomere shortening observed under hypoosmotic conditions. Under membrane stretch induced by hypoosmotic swelling, β_2AR agonists stimulate receptors that are not fully compartmentalised due to the reduction in membrane complexity. As a result, cAMP is less effectively regulated by PDE4s, particularly PDE4D, allowing persistent β_2AR-cAMP signalling to penetrate PKA-RII compartments, thereby enhancing the phosphorylation of proteins involved in excitation-contraction coupling.

β_2ARs form complexes with various PDE4D isoforms in cardiomyocytes, with PDE4D9 and PDE4D8 preferentially binding to β_2AR under resting conditions. These isoforms regulate both β2AR-induced contraction rate responses and cAMP accumulation (De Arcangelis et al., 2009b). The same study revealed that β_2AR stimulation causes the dissociation of PDE4D9 from the receptor while recruiting PDE4D8 and PDE4D5. This recruitment is mediated by β-arrestin, a crucial factor in limiting GPCR signalling. Research has shown that β-arrestin facilitates the recruitment of PDE4D3 and PDE4D5 to β_2AR, acting as an adaptor for the translocation of PDE4Ds to activated receptors, thereby enhancing cAMP degradation at the plasma membrane (Perry et al., 2002). The recruitment of PDE4D regulates receptor activity, uncouples G_s signalling, and enhances G_i-coupled receptor inhibition of cAMP production, effectively compartmentalising the cAMP signal within a subsarcolemmal microdomain (Baillie et al., 2003). From our results, we found that treating cells with the PDE4D5 β-arrestin disruptive peptide abolished the stretch-induced increase in the β_2AR-mediated response. Our previous findings demonstrated that the enhanced sarcomere shortening observed during β_2AR stimulation under hypoosmotic conditions was eliminated in PTX-treated (G_i inhibitor) cells. Taken together, our results suggest that caveolae restructuring induced by hypoosmotic swelling (membrane stretch) disrupts β-arrestin-mediated recruitment of PDE4D to β_2ARs, preventing the switch from G_s to G_i. This disruption leads to increased cAMP production and enhanced contraction.

A recent study investigated the effect of hypoosmotic swelling on βAR signalling, and they found neither cholesterol depletion via MβCD nor PDE inhibition via IBMX abolished the swelling-induced increase in cAMP (Sirbu et al., 2023). In contrast, instead of general βAR, our study specifically focuses on β_2AR signalling within caveolar compartments, as β_2AR is predominantly localised in caveolae, whereas β_1ARs are more widely distributed across the

plasma membrane and are less dependent on caveolae. In addition, β_1AR is far more abundant than β_2AR in cardiomyocytes. Even if β_2AR signalling is significantly affected by hypoosmotic swelling and PDE4 regulation, the total βAR-mediated response still largely depends on β_1AR signalling. This might explain the difference in our findings, as their study did not distinguish between β_1AR and β_2AR, any β_2AR specific changes may be masked by the β_1AR-driven response. Therefore, they observed no significant impact of hypoosmotic swelling, caveolae depletion and PDE inhibition on overall βAR signalling, whereas we found an enhanced β_2AR response under those conditions. However, the same study used fluorescently tagged nanobody 80 (Nb80) and Nb37, for β_2AR and β_2AR-G_s activation respectively, and they found that hypoosmotic swelling enhances β_2AR-G_s coupling, leading to increased receptor activation. Furthermore, they found enhanced recruitment of β-arrestin-2 following hypoosmotic swelling without affect the receptor internalisation (Sirbu et al., 2023). However, our study indicates that hypoosmotic swelling disrupts β-arrestin-mediated recruitment of PDE4D to β_2AR, impairing its ability to regulate cAMP levels, suggesting that the β-arrestin recruitment alone does not guarantee PDE4D localication, β-arrestin might still bind to the β_2AR, but fail to bring the PDE4D into this complex.

4.6 Conclusion

In conclusion, caveolae restructuring induced by stretch disrupts the regulation of PDE4s, particularly PDE4D, leading to enhanced sarcomere shortening and cAMP production. Moreover, treatment with the PDE4D5 β-arrestin disruptive peptide abolished the stretch-induced increase in the β_2AR-mediated response. This suggests that hypoosmotic swelling interferes with the β-arrestin-mediated recruitment of PDE4D, which in turn disrupts the compartmentalisation of β_2AR signalling. As a result, this disruption contributes to the observed increase in sarcomere shortening and cAMP production.

Chapter 5 The Regional Differences in Cardiomyocytes β_2AR Response Following Hypoosmotic Swelling

5.1 Introduction

The left ventricular apex is located at the bottom of the left ventricle, is sharply angular or forms a sector of a sphere, whereas the base of the left ventricle begins at the left atrioventricular valve and extends downward toward the apex of the heart (McAlpine, 1975). The thickness of the left ventricular (LV) wall gradually decreases from the base to the apex (Sengupta et al., 2006b). There is limited knowledge regarding regional differences across the myocardium. An early study in canine hearts revealed a gradient in βAR density within the ventricular myocardium, showing a higher concentration of βARs in the apical myocardium and a lower concentration in the basal myocardium (Mori et al., 1993). This variation in distribution resulted in a more pronounced contractile response to catecholamine stimulation in the apical myocardium, compensating for the relatively sparse sympathetic innervation in this region, thereby maintaining balanced responsiveness throughout the left ventricular myocardium.

Paur et al. further distinguished the distribution of β_1ARs and β_2ARs within the heart, reporting that apical cardiomyocytes exhibit a higher amount of β_2ARs. They also observed that the contractile response of apical cardiomyocytes following β_2AR stimulation was greater compared to that of basal cardiomyocytes (Paur et al., 2012). Additionally, they discovered that high levels of epinephrine stimulation induce stimulus trafficking, where β_2AR switches from coupling with G_s protein to G_i protein, which is caused by the phosphorylation of G protein-coupled receptor kinase 2 (GRK2) and the translocation of β-arrestin to the receptor

(Freedman and Lefkowitz, 1996). This receptor internalisation protects from the overactivation of PKA. The overactivation of PKA via cAMP from G_s activation enhances the contractile response, while elevated cyclic AMP levels also lead to the generation of free radicals, which trigger the expression of stress response genes and initiate apoptosis (Litvinov et al., 2009) . This βAR-G_i activation leads to a negative inotropic effect in human ventricular cardiomyocytes, a phenomenon observed in Takotsubo cardiomyopathy, an acute yet reversible left ventricular dysfunction, which was first described in Japan in the 1980s. In Takotsubo cardiomyopathy, the apical myocardium loses inotropy due to elevated epinephrine concentrations, resulting in the characteristic apical ballooning appearance (Paur et al., 2012).

A more recent study by Wright et al. also reported that the β_2AR-dependent cAMP production is more pronounced in the apex at the whole heart level (Wright et al., 2018a). They used a Langendorff-perfused mouse heart, with a fluorescence resonance energy transfer (FRET)-based cAMP sensor to explore the differences in β_2AR-cAMP responses between the apex and the base. The results revealed stronger FRET responses at the apex compared to the base following CGP (a β_1 blocker) and isoprenaline stimulation. The same study also suggested that cardiomyocytes in the basal region of the heart possess more organised membranes, with a higher density of caveolae and t-tubules (Wright et al., 2018a). They also found that basal cells have more restricted β_2AR-cAMP compartmentalisation. This phenomenon can be attributed to the increased membrane complexity and enhanced phosphodiesterase 4 (PDE4) -mediated cAMP hydrolysis in the basal myocardium, leading to tighter control of β_2AR-cAMP signalling. Therefore, in this study, we aim to investigate how the effect of membrane stretch on β_2AR signalling differs in different regions of the heart.

Electrical heterogeneity within the ventricular myocardium has also been demonstrated in several studies. Depolarisation has been shown to initiate at the apical subendocardium, with a significant delay in reaching the LV base, while repolarisation occurs in the reverse direction, propagating from the base to the apex (Sengupta et al., 2006a). Variations in action potential and calcium dynamics across regions have also been reported, with the apex typically has a shorter action potential duration (APD) and calcium transient duration (CaD) compared to the base, which are attributed to the differences in ion currents and channel density (Szentadrassy et al., 2005, Choi and Salama, 2000). Therefore, in this study, we will investigate the effect of mechanical stretch on action potential and calcium dynamics using the Langendorff-perfused heart. Our aim is to determine whether mechanical loading differentially affects the apex and base, which in turn alter the action potential properties and calcium handling.

5.2 Hypothesis and Aims

The enhanced sarcomere shortening and cAMP activity following β_2-adrenoreceptor stimulation depend to a greater proportion on the basal cardiomyocytes rather than the apical cardiomyocytes. Hypoosmotic swelling equilibrates apical and basal cell contractile responses to β_2AR stimulation.

Aim 1: Explore the impact of hypoosmotic swelling (membrane stretch) and the role of caveolae on membrane structure, cell size and the transverse/axial-tubule system in apical and basal cardiomyocytes.

- Objective 1: Assess the number of caveolae in healthy and MβCD-treated apical and basal cardiomyocytes using electron microscopy.
- Objective 2: Measure cell size (width and length) in healthy and MβCD-treated apical and basal cardiomyocytes using CytoCypher.
- Objective 3: Evaluate T-tubule density, the power of regularity and directionality in healthy and MβCD-treated apical and basal cardiomyocytes using confocal microscopy.
- Objective 4: Evaluate caveolin-3 density and the power of regularity in healthy and MβCD-treated apical and basal cardiomyocytes using confocal microscopy.

Aim 2: Examine the effects of hypoosmotic swelling (membrane stretch) on contractility in apical and basal cardiomyocytes following β_2AR stimulation.

- Objective 1: Measure the contractility in apical and basal rat cardiomyocytes using CytoCypher.

Aim 3: Investigate the influence of the removal of caveolae on contraction and cAMP response following hypoosmotic swelling in isolated apical and basal cardiomyocytes following β_2AR stimulation.

- Objective 1: Assess cell contractility and cAMP output in control and MβCD-treated conditions in apical and basal cardiomyocytes using CytoCypher and FRET microscopy, respectively.

Aim 4: Investigate the β_2AR response in a Langendorff-perfused rat heart following stretch within left ventricle (Apex and base).

- Objective 1: Perform Langendorff perfusion system using CGP with isoprenaline, with an inflated balloon with optical mapping system to test the Calcium transient and Voltage.

5.3 Methods

5.3.1 Solutions

Solutions	Composition
Isosmotic solution (mM)	NaCl 118; KCl 5.3; $MgCl_2$ 0.5; $CaCl_2$ 1; Glucose 10; Na_2HPO_4 7.5; $NaH_2PO_4.H_2O$ 2.5
Hypoosmotic solution (mM)	NaCl 81; KCl 5.3; $MgCl_2$ 0.5; $CaCl_2$ 1; Glucose 10; Na_2HPO_4 7.5; $NaH_2PO_4.H_2O$ 2.5
MEM media	MEM with Hank's salts, 9mM $NaHCO_3$, 1% glutamine and 1% antibiotic/antimycotic (AA)
FRET Buffer (mM)	NaCl 144, HEPES 10, $MgCl_2$ 1, KCl_2 5
Blocking solution	5% BSA, 20% Tween 20, 10% goat serum and PBS

Table 5.1 The list of solutions and their compositions used in the experiments for Chapter 5

Cells were suspended in either isosmotic (osmolarity: 290 mOsm/L) or hypoosmotic (osmolarity: 214 mOsm/L) solution for 15min. β_1AR blocker CGP20712A and non-selective βAR agonist isoprenaline HCl, cholesterol depletion agent cyclodextrin were supplied. The potentiometric dye RH237 was used for voltage-sensitive ratiometric imaging, while Rhod-2-AM was used for imaging calcium transients.

5.3.2 CytoCypher

The contractile response of apical and basal cardiomyocytes was evaluated using the CytoCypher system, as described in section 2.11. This system measured cell shortening and calcium transients as indicators of contractility, as discussed in previous chapters. This approach allowed us to investigate the effects of hypoosmotic swelling (membrane stretch) on contractility in apical and basal cardiomyocytes following β_2AR stimulation. The protocols used were the same as those in section 3.3.2, except that apical and basal cardiomyocytes were studied instead. Briefly, 100nM CGP combined with 1μM isoprenaline was used to

selectively stimulate β_2AR. To examine the role of caveolae in β_2AR-induced contractility following hypoosmotic swelling in isolated apical and basal cardiomyocytes.

5.3.3 FRET Microscopy

Approximately 10K cardiomyocytes were plated onto laminin-coated coverslips and cultured at 37°C for 48 hours in MEM, with the pmEPAC2 FRET sensor (MOI 200) present. The experiments were done after 48 hours of transfection, following a protocol similar to that described in Chapter 3, but using apical and basal cells. Briefly, the cells were first stimulated with 100 nM CGP (a β1AR blocker), followed by 100 nM isoprenaline (a βAR agonist). 100 µM IBMX, a non-specific PDE inhibitor, and 10 µM forskolin, an adenylyl cyclase activator, were subsequently applied to achieve the maximum cAMP release.

5.3.4 Live Cell T-tubule Staining via Di-8-ANNEPPS

Apical and basal cardiomyocytes were stained with 10 µM Di-8-ANNEPPS, prepared in FRET buffer and sonicated for 20 minutes at 50°C. After 3 minutes of staining, cells were washed twice with FRET buffer and stabilised in 2 ml of iso- or hypo-osmotic solution prior to imaging. Imaging was performed using a Zeiss LSM-78 inverted confocal microscope, and the images were analysed using ImageJ and MATLAB. For detailed analysis, refer to Section 2.82.

5.3.5 Confocal Microscopy of Apical and Basal Cardiomyocytes Following Caveolin-3 Staining

Apical and basal cardiomyocytes were plated onto coverslips, perfused with iso- or hypo-osmotic solution for 15 minutes, and fixed with 4% PFA. Cells were permeabilised, blocked, and incubated with a caveolin-3 primary antibody (1:100 dilution) for 24 hours at 10°C, followed by Alexa Fluor 488-conjugated donkey anti-mouse IgG (1:500) for 2 hours at room

temperature in the dark. Coverslips were mounted using ProLong Gold with DAPI. Detailed staining protocol is provided in Section 2.9.1.

5.3.6 Quantification of Caveolae in Apical and Basal Cardiomyocytes Using Transmission Electron Microscopy

Cardiomyocytes were fixed in 2.5% glutaraldehyde in PBS overnight, washed in cacodylate buffer, and further processed with 1% osmium tetroxide. The samples were dehydrated, embedded in Araldite, sectioned (0.1 µm), and stained with uranyl acetate and lead citrate. TEM images were taken of the cell membranes. Ten cells from each region (apex and base) were randomly selected, with 10 fields of view per cell. Caveolae were counted, and their density per 1 µm of membrane was calculated. For the detailed TEM protocol, refer to Section 2.7.

5.3.7 Balloon Stretched Isolated Rat Heart

Sprague-Dawley rats, each weighing between 300-400 grams, were anesthetised with isoflurane in an induction chamber. Once the rats were fully anesthetised, they were euthanised via cervical dislocation to facilitate heart extraction. The excised hearts were placed in Krebs-Henseleit buffer (118.5 NaCl, 1.4 $CaCl_2.2H_2O$, 11 Glucose, 25 $NaHCO_3$, 1.2 $MgSO_4.7H_2O$, 1.2 $NaH_2PO_4.2H_2O$, 4.5 KCl) and supplemented with Heparin to prevent blood clotting before cannulation.

The heart was then perfused *ex vivo* on a Langendorff apparatus at a steady coronary flow rate of 15 ml/min. The perfusion medium, Krebs-Henseleit buffer, was maintained at 37°C and balanced with a gas mixture of 95% O_2 and 5% CO_2 to achieve a pH of 7.4. A deflated latex balloon (Harvard Apparatus) attached to a pressure transducer and a syringe was inserted into

the left ventricular lumen through an incision made in the left atrium, along with a separate 0.9 mm outer diameter tube. Both the balloon and the tube were secured by attaching them to the stand. The balloon was inflated with 1 ml of distilled water to reach a pressure of 60 mmHg, creating a stretch model in the heart (Li et al., 1997). The heart was then submerged into water bath inside a customised water-jacket chamber that allows temperature control and optical transmission. During 15 minutes of equilibriltion, volume-conducted electrocardiogram (ECG) was used to monitor cardiac function. ECG signals were recorded using needle electrodes connected to a Dual Bio Amp system (ADInstruments, Australia).

5.3.8 Isolated Heart Optical Mapping

Myocardium was stained with potentiometric probe RH237 (Invitrogen, 1mg/ml, 2M) and calcium non-ratiometric dye Rhod-2AM (Invitrogen, 1mg/ml, 0.9M). Epicardium of left ventricle was excited with four high-power LEDs (CAIRN Research, UK) at 530 nm. Emission signals was recorded by two CMOS cameras (128 x 80 pixels, Sci-measure, USA). Emission light from the heart was divided by a dichroic mirror and passed through a 585/40 nm and 620LP filters to monitor action potentials and calcium transients. To minimise motion artifacts during recording, the excitation-contraction uncoupler blebbistatin (10 µmol/L, 10M) was administered into the heart.

Selectively activation of β_2AR can be achieved by injecting β_1AR blockers CGP, followed by administration of βAR agonist, isoprenaline. During the experiments, signals were recorded while pacing of the left ventricle using a Micro-Pace stimulator. Pacing was conducted with a cycle length of 200ms for baseline and CGP treatment and a cycle length of 150ms for isoprenaline.

5.3.9 Statistics

All graphs and statistical analyses were performed using Prism10 (GraphPad).

Cell size, number of caveolae, T-tubule and Caveolin-3 assessment were analysed using Two-way ANOVA with Šidák's multiple comparisons test.

CytoCypher experiment (cell contractility) and FRET Microscopy experiment (cAMP response) were analysed using Two-way ANOVA followed by either Šidák's multiple comparisons test or Uncorrected Fisher's LSD test.

Optical mapping experiments (voltage and calcium transient) were analysed by Two-way ANOVA followed by uncorrected Fisher's LSD test.

5.4 Result

5.4.1 Effect of Hypoosmotic Swelling Model on Apical and Basial Cardiomyocytes

In earlier chapters, we have shown that hypoosmotic swelling decreases the number of caveolae, and previous research has demonstrated that basal cardiomyocytes contain more caveolae compared to apical cardiomyocytes (Wright et al., 2018a). Transmission electron microscopy was first used to assess the impact of hypoosmotic swelling on caveolae numbers in cardiomyocytes from the apical and basal regions. As illustrated in Figure 5.1, hypoosmotic conditions led to a significant reduction in caveolae numbers compared to isosmotic conditions in both apical and basal regions. Furthermore, basal cardiomyocytes exhibited a higher number of caveolae than apical cells under isosmotic conditions. Consistent with the results from the previous chapter, cardiomyocytes exposed to hypoosmotic solution showed a significantly increased width compared to those in the isosmotic solution, while no notable difference in cell length was observed (Figure 5.2). The width-to-length ratio of each cell was also calculated, with similar results indicating that hypoosmotic swelling increases cell width without affecting length. In addition, there was no significant difference in cell size between cardiomyocytes from the apical and basal regions of the heart under both isosmotic and hypoosmotic conditions.

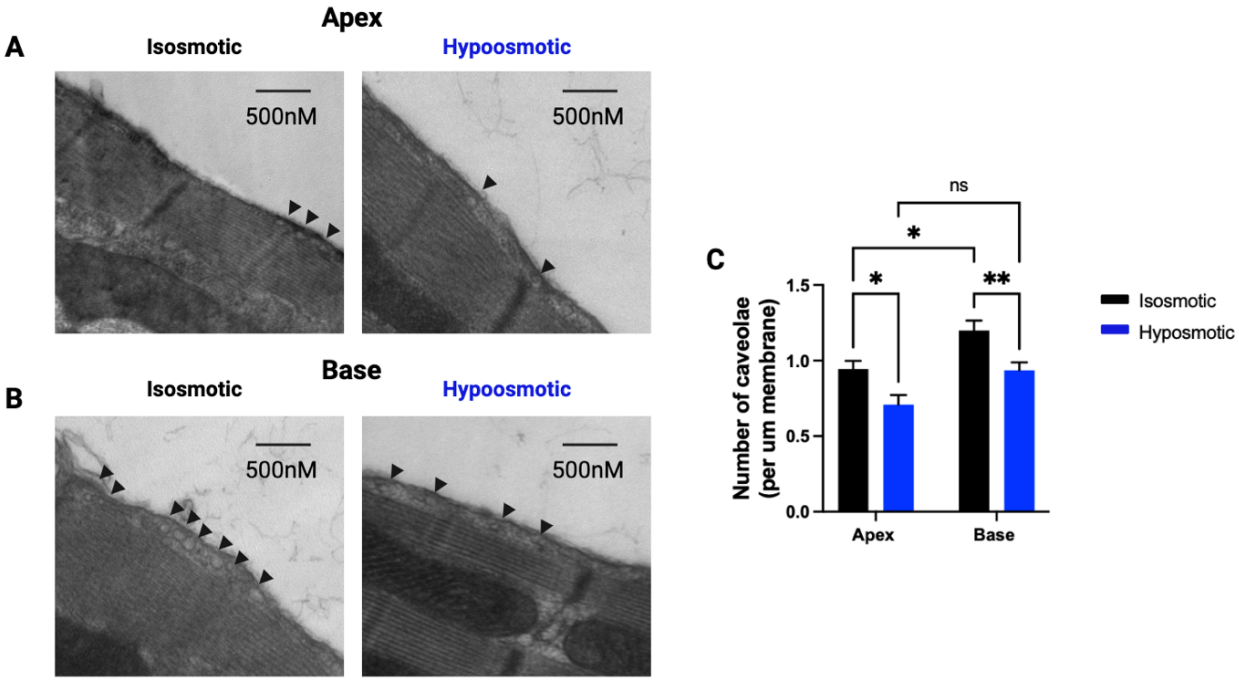


Figure 5.1 Hypoosmotic swelling reduces the number of caveolae in both apical and basal cardiomyocytes. Transmission electron microscope images show **(A)** apical and **(B)** basal cardiomyocytes under isosmotic and hypoosmotic conditions. **C.** Quantification of caveolae numbers across the four groups. N=4, n=70-88. Data were analysed through Two-way ANOVA, followed by Šídák's multiple comparisons test. Data are presented as mean ± SEM. *, ** indicates statistically significant differences at $p<0.05$ and $p<0.01$, respectively.

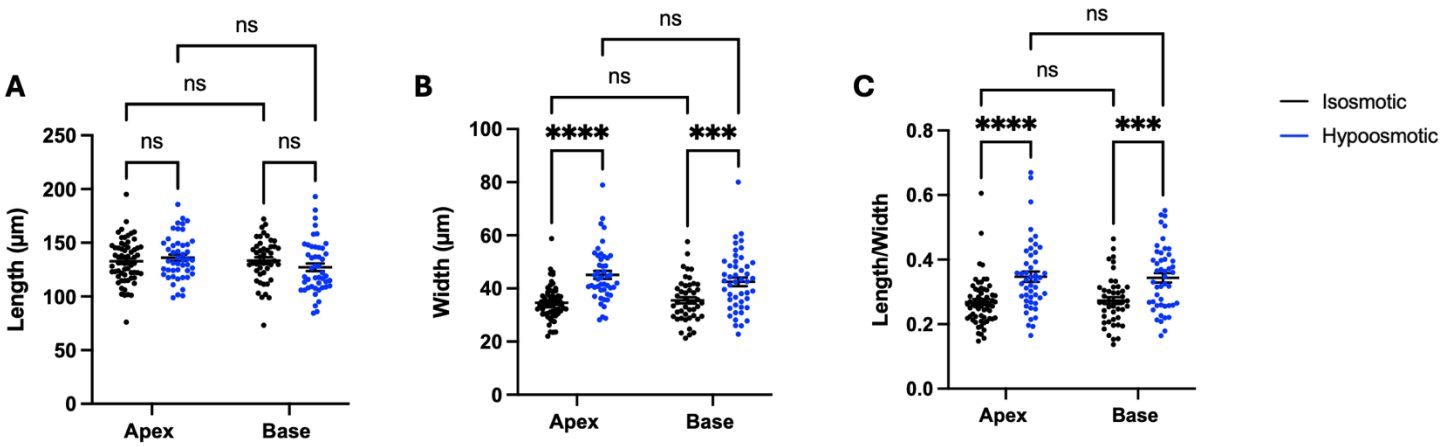


Figure 5.2. Hypoosmotic swelling increases the width, rather than the length, of rat left ventricular cardiomyocytes in both the apical and basal regions. A. Width; **B.** Length; and **C.** the width/length ratio of apical and basal cardiomyocytes in iso-osmotic (black) and hypoosmotic (blue) conditions. N=3, n=46-62. Data were analysed using Two-way ANOVA, followed by Šídák's multiple comparisons test. Data are presented as mean ± SEM, with ***, and **** indicating statistically significant differences at $p<0.001$ and $p<0.0001$, respectively.

We then evaluated the intrinsic structural differences between apical and basal cardiomyocytes under isosmotic and hypoosmotic conditions. Cells were stained with di-8-ANEPPS and examined using confocal microscopy. The green fluorescence indicated the distribution of T-tubules. As shown in Figure 5.3, T-tubule density and regularity were significantly higher in basal cells compared to apical cells, suggesting that basal cardiomyocytes have a denser and more organised T-tubular network than apical cells. Furthermore, no differences in T-tubule density or regularity were observed between isosmotic and hypoosmotic conditions, indicating that hypoosmotic swelling did not affect T-tubule organisation (Figure 5.3).

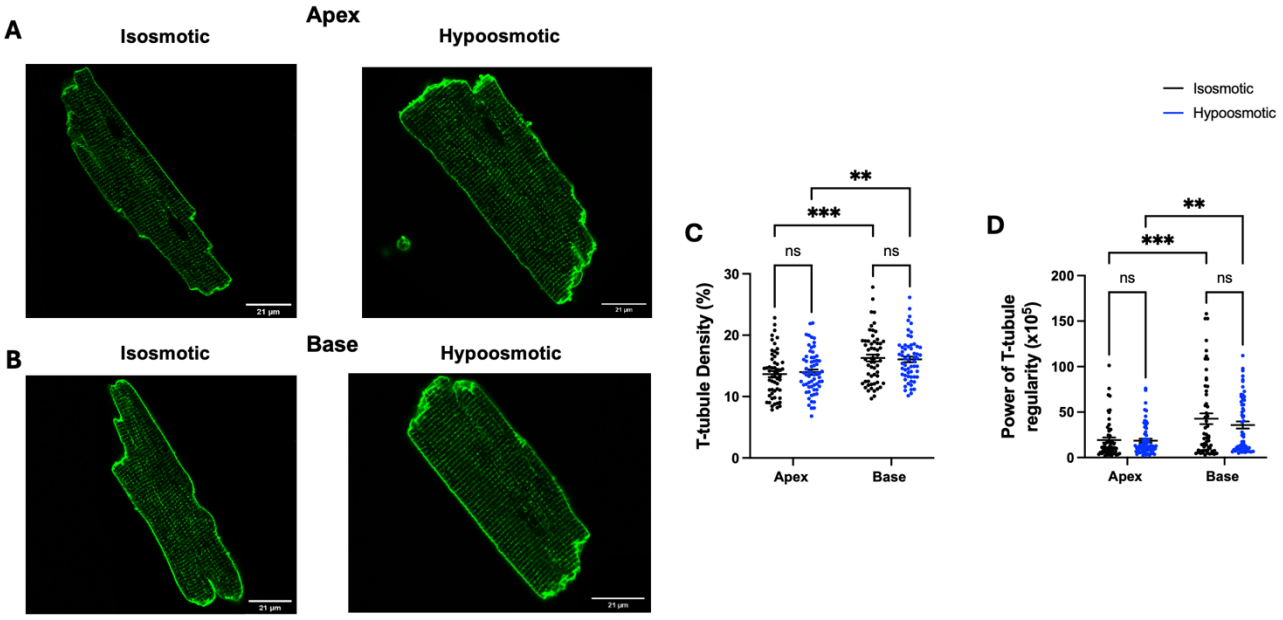


Figure 5.3. Basal cardiomyocytes show higher T-tubule organisation than apical cells, while hypoosmotic solution has no effect on T-tubules. Representative immunostaining images of **(A)** apical and **(B)** basal cardiomyocytes in isosmotic and hypoosmotic conditions. **C.** T-tubule density and **(D)** regularity stained with di-8-ANEPPS. N=4, n=56-63. Data were analysed using Two-way ANOVA, followed by Šídák's multiple comparisons test. Data are presented as mean ± SEM, with **, and *** indicating statistically significant differences at $p<0.01$ and $p<0.001$, respectively.

Immunostaining was done to determine whether hypoosmotic swelling affects caveolin-3 distribution, and confocal microscopy was used to measure the density and regularity of caveolin-3. Similar to the findings for T-tubules, neither iso- nor hypoosmotic solutions had an effect on caveolin-3 density or regularity (Figure 5.4). In addition, caveolin-3 was found to have a significantly higher density in basal cardiomyocytes compared to apical cardiomyocytes (Figure 5.4C). Although the power of regularity for caveolin-3 appeared to be higher in basal cells compared to apical cells, this trend was not statistically significant (Figure 5.4D). These findings suggest hypoosmotic conditions do not alter the Cav3 distribution in both apical and basal cardiomyocytes.

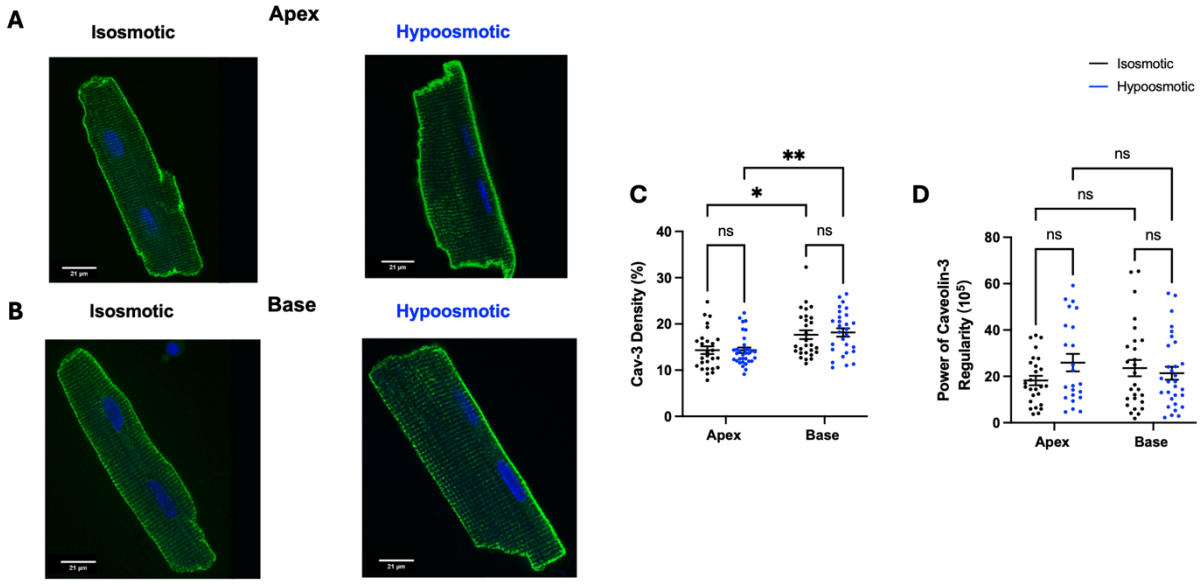


Figure 5.4. Basal cardiomyocytes show higher caveolin-3 density than apical cells, while hypoosmotic solution does not affect caveolin-3. Representative images of **(A)** apical and (B) basal cardiomyocytes under isosmotic and hypoosmotic conditions. **C.** Caveolin-3 density and **(D)** regularity across the four groups. N=4, n=27-34. Data were analysed using Two-way ANOVA, followed by Šídák's multiple comparisons test. Data are presented as mean ± SEM, with *, and ** indicating statistically significant differences at $p<0.05$ and $p<0.01$, respectively.

5.4.2 Hypoosmotic Swelling Increases β_2AR-cAMP Activity and Sarcomere Shortening in Basal Cardiomyocytes

To assess the functional impact of hypoosmotic swelling, we first used FRET microscopy to measure the β_2AR–dependent cAMP production in apical and basal cardiomyocytes. Representative traces are shown in Figure 5.5A and B, illustrating the β_2AR-cAMP cAMP response in isosmotic (black line) and hypoosmotic (blue line) solution for both apical and basal cardiomyocytes following treatment with CGP, isoprenaline and saturators. Our results indicated that hypoosmotic swelling increased cAMP production following β_2AR stimulation in basal cardiomyocytes, but not in apical cells (Figure 5.5). Furthermore, FRET responses were higher at the apex in comparison with the base, indicating a greater β_2AR response in the apex.

However, following hypoosmotic swelling, the cAMP response in basal cardiomyocytes was elevated to a level comparable with that of apical cardiomyocytes.

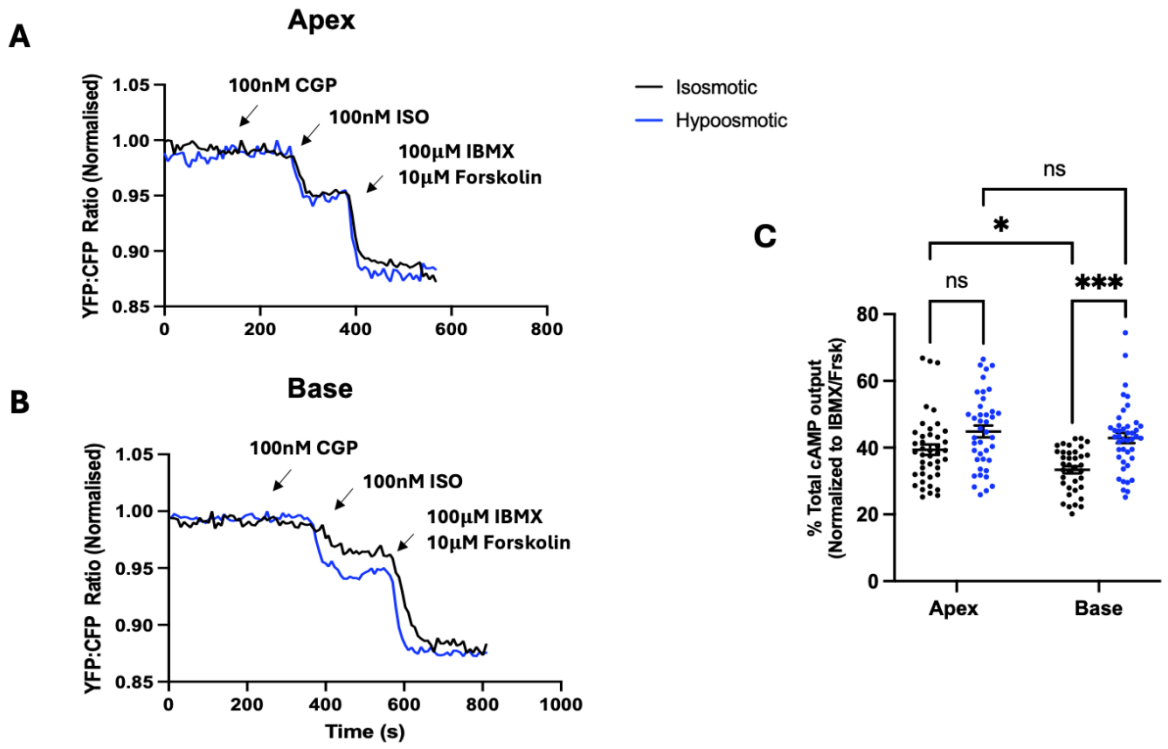


Figure 5.5. Hypoosmotic swelling enhances β_2AR-cAMP activity in basal cardiomyocytes. Representative trace illustrating the β_2AR-specific FRET response measured by the plasma membrane cAMP sensor pmEPAC2-camp in **(A)** apical and **(B)** basal ventricle cardiomyocyte under iso-(black line) and hypoosmotic (blue line) conditions following application of CGP (β_1AR antagonist, 100nM), Isoprenaline (βAR non-specific agonist,100nM), IBMX (non-selective PDE inhibition, 100 µM) and Forskolin (adenylyl cyclase activator, 10µM). **C**, Quantification of cAMP production after β_2AR-specific stimulation relative to the maximum production achieved with IBMX and Forskolin stimulation. N=3, n=35~50. Data are presented as means ± SEM. *,***P<0.05, 0.001 respectively, Two way ANOVA followed by Šídák's multiple comparisons test.

Contraction was measured under stimulation (1Hz, 20V). Representative traces are shown in Figure 5.6 A and B, which illustrate the sarcomere shortening in isosmotic (black) and hypoosmotic solution (blue) at baseline (black line) and after stimulation (blue line) in cardiomyocytes from both the apex and base. Apical cardiomyocytes demonstrated a greater increase in their shortening after β_2AR stimulation compared to basal cardiomyocytes, revealing a significant difference between the two regions. Consistent with cAMP response, we found that hypoosmotic swelling enhances sarcomere shortening following β_2 stimulation in basal, but not apical cells. Furthermore, after hypoosmotic swelling, the contractile response in basal cells to β_2AR stimulation is equilibrated with that of apical cells (Figure 5.6C).

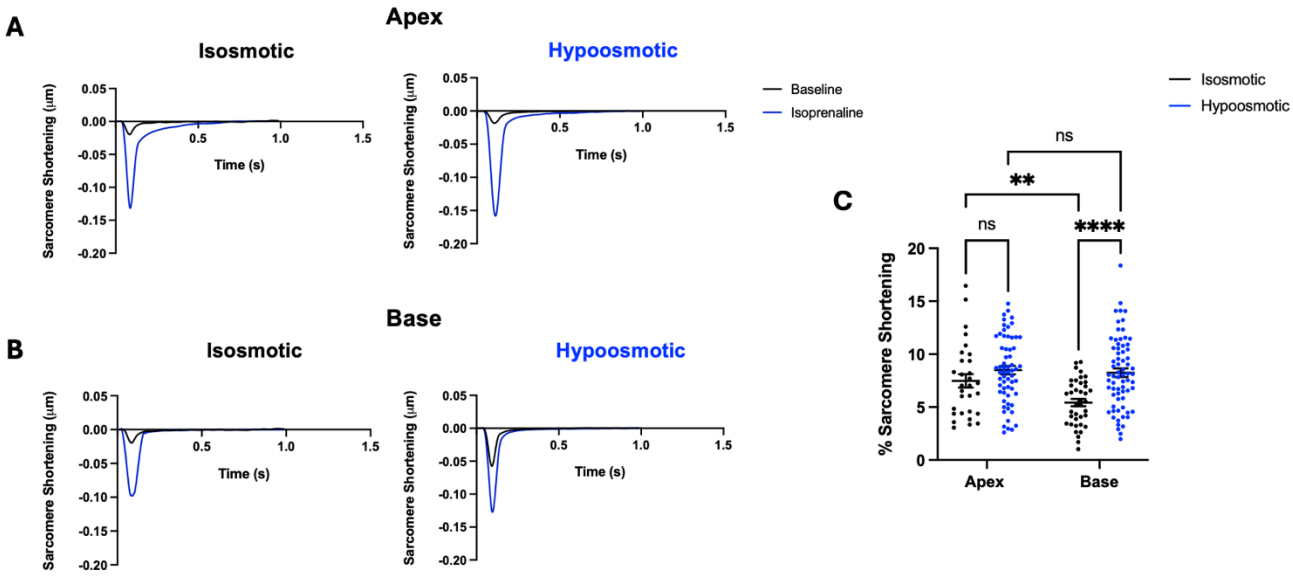


Figure 5.6. Hypoosmotic swelling enhances sarcomere shortening following β_2 stimulation in basal, but not apical, cardiomyocytes. A. Representative trace of sarcomere shortening in apical cells and **(B)** in basal cells under isosmotic and hypoosmotic conditions during the contraction cycle, recorded at baseline with CGP (black line), and after the addition of 1µM isoprenaline (blue line). **C.** Percentage of sarcomere shortening in apical and basal cardiomyocytes under isosmotic (black) and hypo-osmotic (blue) conditions following 1µM isoprenaline. N=4, n=35-70. Data are presented as mean ± SEM, with ** and **** indicating significance at P<0.01 and P<0.0001, respectively, as determined by two-way ANOVA followed by Uncorrected Fisher's LSD test.

5.4.3 Differential Responses to Cardiac Stretch following β_2AR stimulation on Action Potential Duration

To investigate the impact of mechanical stretch at the whole-heart level, we developed a model in which an inflated balloon was used to stretch the left ventricular myocardium, linking cellular responses to overall heart function. We used high-resolution dual optical mapping on Langendorff-perfused rat hearts, allowing for detailed observation of cardiac electrical activity. The voltage-sensitive dye RH237 and the Ca^{2+} indicator Rhod-2-AM were used to measure transmembrane potentials and calcium transients, respectively. Throughout the experiment, recordings were taken during epicardial pacing of the left ventricle, initially at a cycle length (CL) of 200ms for baseline measurements and after adding CGP, a β_1AR blocker. Following the administration of isoprenaline, a β-AR agonist, the heart was paced at a CL of 150ms.

Representative voltage traces of sham and stretched heart at the apex and the base during baseline and following β_2AR stimulation are shown in Figure 5.7A and C. Our results revealed that mechanical stretch did not significantly affect APD50, APD70, or APD90 at baseline in either the apex or base regions. However, the basal myocardium exhibited significantly higher APD50, APD70, and APD90 compared to the apical myocardium under sham conditions, as well as higher APD50 and APD70 under stretched conditions. Stretch caused a significant increase in APD50, APD70 and APD90 in the apex following β_2AR stimulation. While the base showed a significant increase in APD50 and APD70 following stretch. (Figure 5.8).

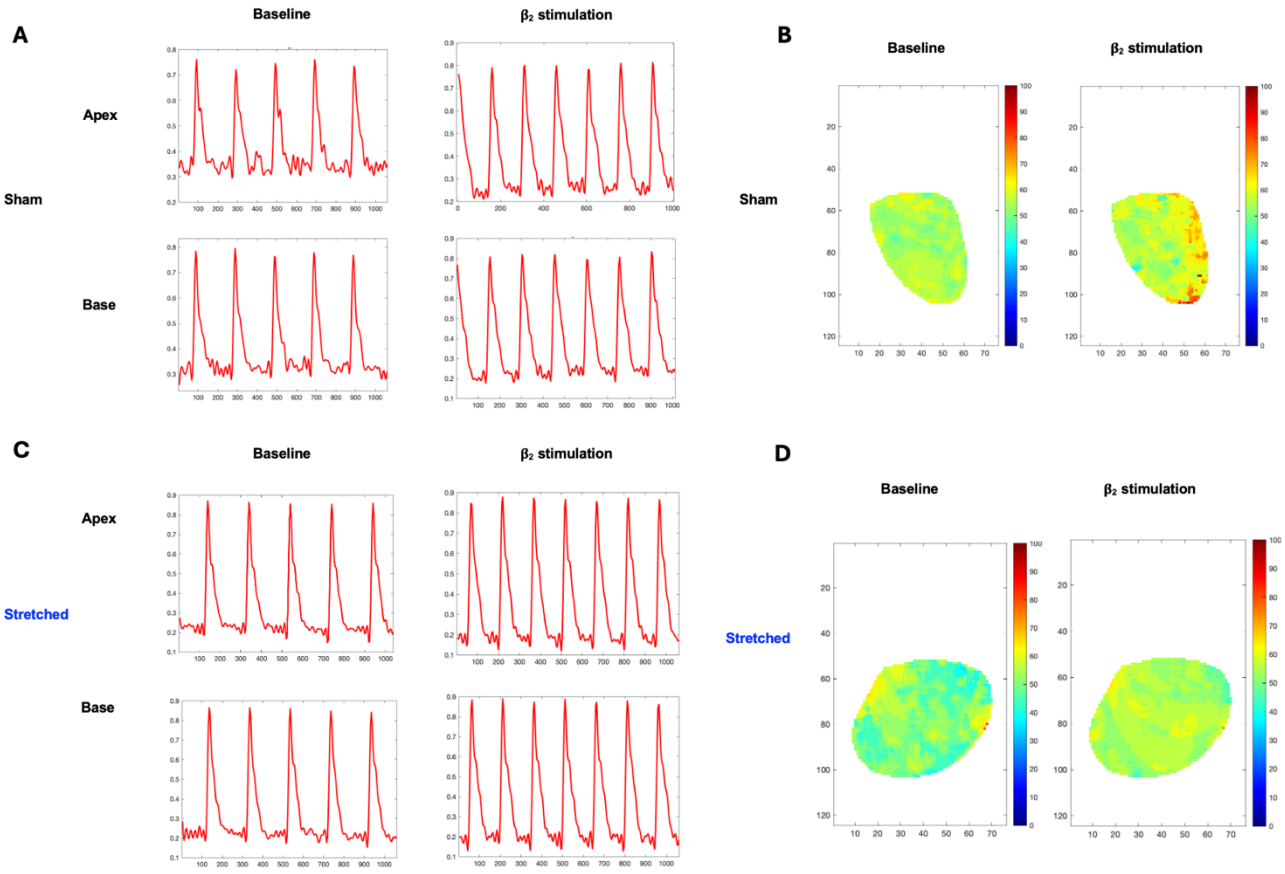


Figure 5.7 Illustration of optical mapping of transmembrane voltage in sham and stretched rat hearts. Representative voltage traces from **(A)** sham and **(C)** stretched hearts at the apex and base during baseline and following β_2AR stimulation. Action potential duration at 70% repolarisation (APD70) maps of **(B)** sham and **(D)** stretched heart at baseline and following β_2AR stimulation.

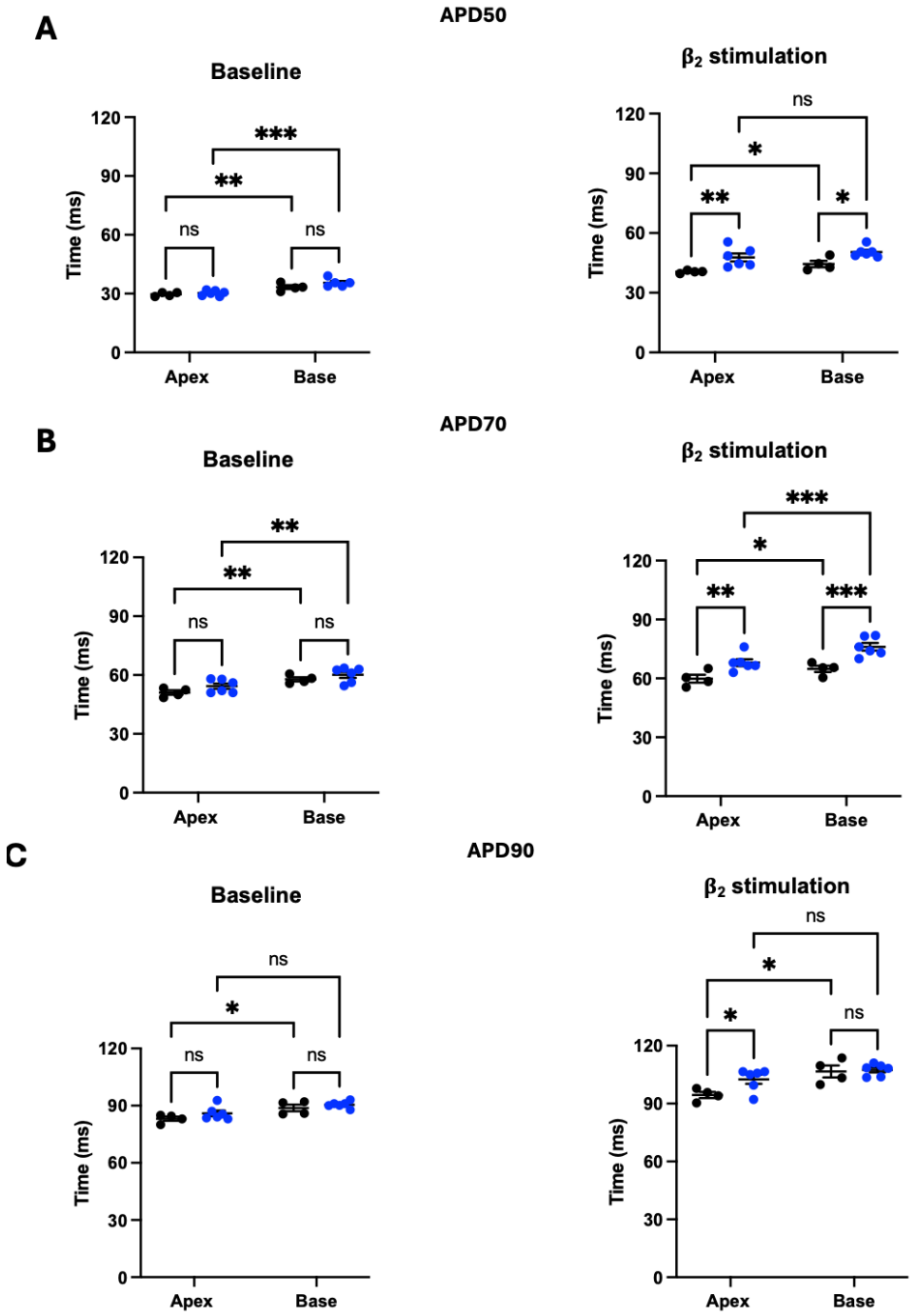


Figure 5.8. Optical mapping of transmembrane voltage in sham and stretched rat hearts. A. APD50, **(B)** APD70, and **(C)** APD90 across left ventricle apex and base. Control N= 4; Stretched N= 6. Data are presented as mean ± SEM, with *, **, and *** indicating statistically significant differences at $p<0.05$, $p<0.01$ and $p<0.001$, respectively, as assessed by two-way ANOVA test followed by uncorrected Fisher's LSD test.

We recorded calcium transients simultaneously with the action potential. Representative calcium traces for sham and stretched hearts at apex and base during baseline and following β_2AR stimulation are shown in Figure 5.9A and C. The calcium transient duration (CAD) at 50% (CAD50), 70% (CAD70), and 90% (CAD90) repolarisation across the apex and base of sham (black) and stretched (blue) hearts at baseline and following β_2AR stimulation (Figure 5.10A, B and C). At baseline, there were no statistically significant differences in CAD50, CAD70, or CAD90 between sham and stretched hearts, either at the apex or base. Following β_2AR stimulation, no significant changes were observed in CAD50, CAD70, or CAD90 in either the apex or base for both sham and stretched conditions. Additionally, comparisons between the apex and base regions within the same condition (sham or stretched) also showed no significant differences in any CAD.

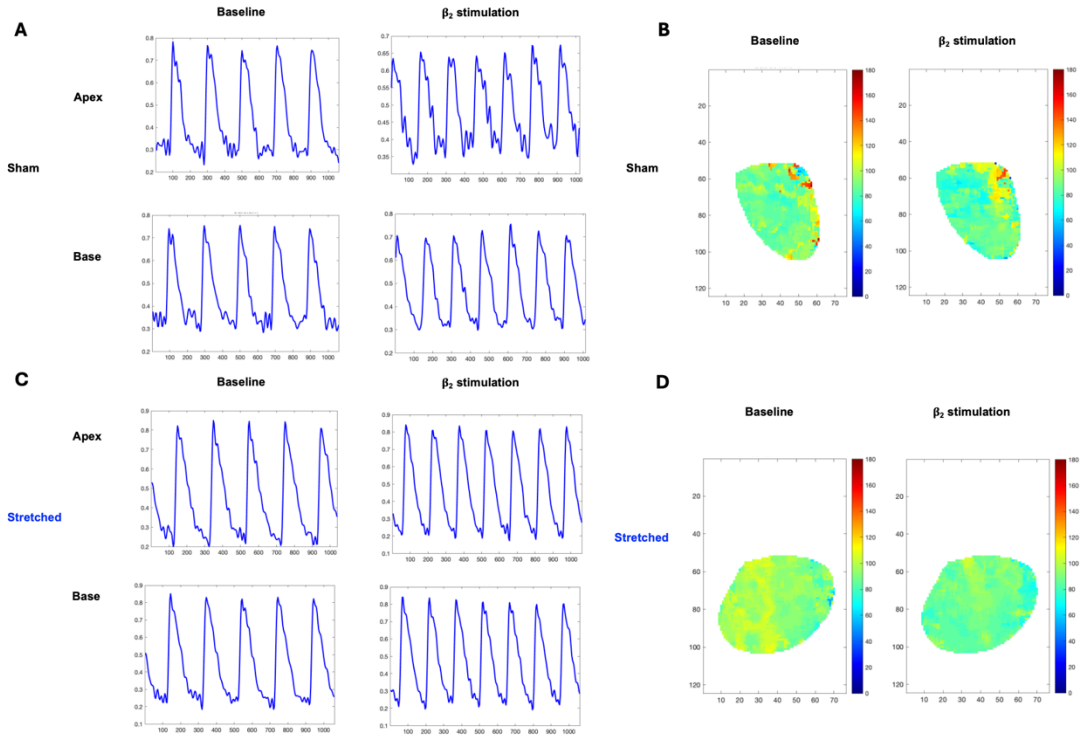


Figure 5.9 Illustration of optical mapping of intracellular calcium transient in sham and stretched rat hearts. Representative voltage traces from **(A)** sham and **(C)** stretched hearts at the apex and base during baseline and following β_2AR stimulation. Calcium transient duration at 70% repolarisation (CAD70) maps of **(B)** sham and **(D)** stretched heart at baseline and following β_2AR stimulation.

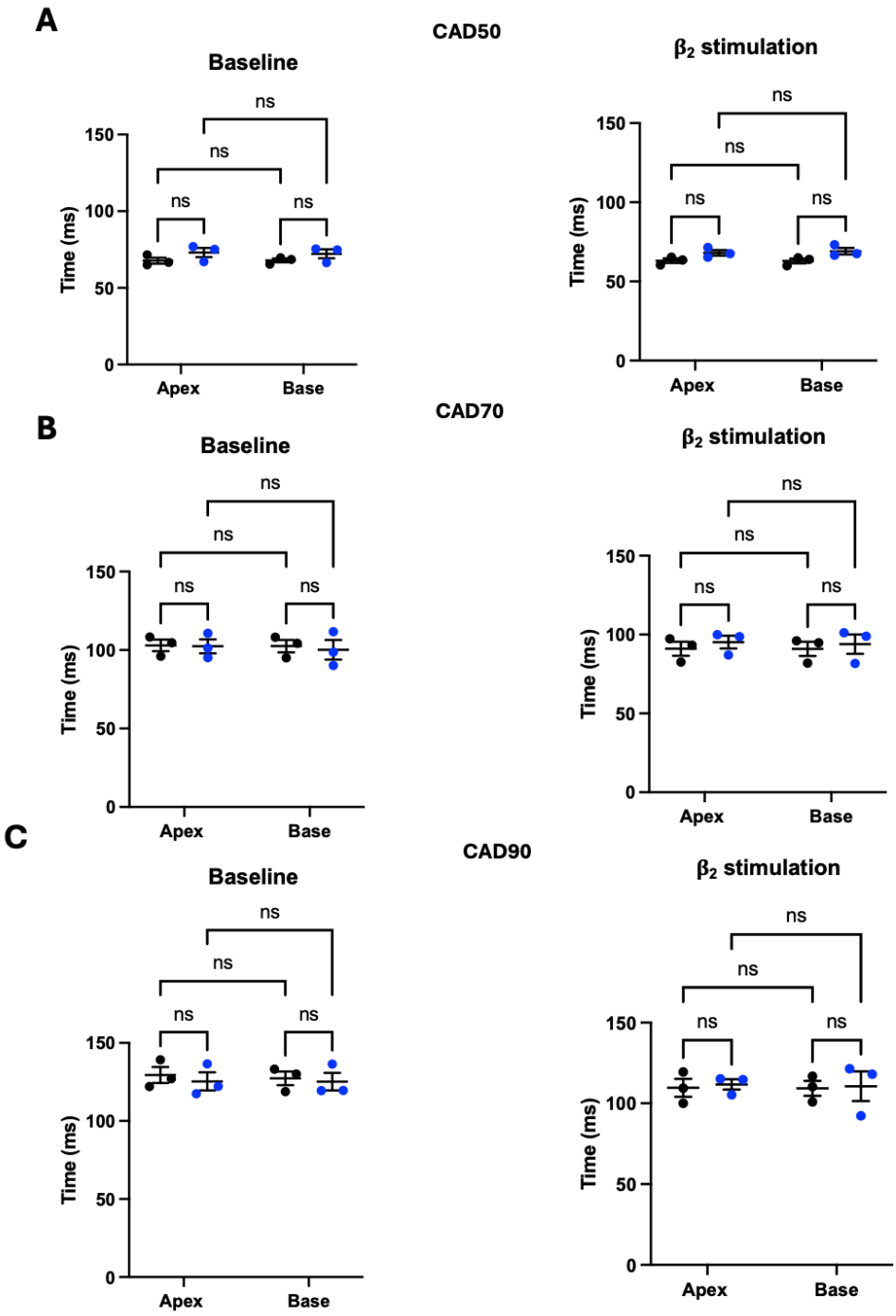


Figure 5.10 Optical mapping of intracellular calcium transient in sham and stretched rat hearts. A. CAD50, **(B)** CA70, and **(C)** CAD90 across left ventricle apex and base. Control N= 3; Stretched N= 3. Data are presented as mean ± SEM, data assessed using two-way ANOVA test followed by uncorrected Fisher's LSD test.

We also measured the time to peak (TTP) of calcium transients, which is the time from initiation of calcium departure to peak fluorescence. Our results showed that at baseline, stretch significantly shortened TTP at the base, with a decreasing trend at the apex as well, although the latter was not statistically significant. No significant difference in TTP was observed between the apex and base in either sham or stretched hearts (Figure 5.11A). Following β_2AR stimulation, TTP showed a decreasing trend in stretched hearts compared to sham hearts, although this was not statistically significant. Additionally, TTP was significantly longer at the base compared to the apex in sham hearts, but this difference was not observed in stretched hearts (Figure 5.11B).

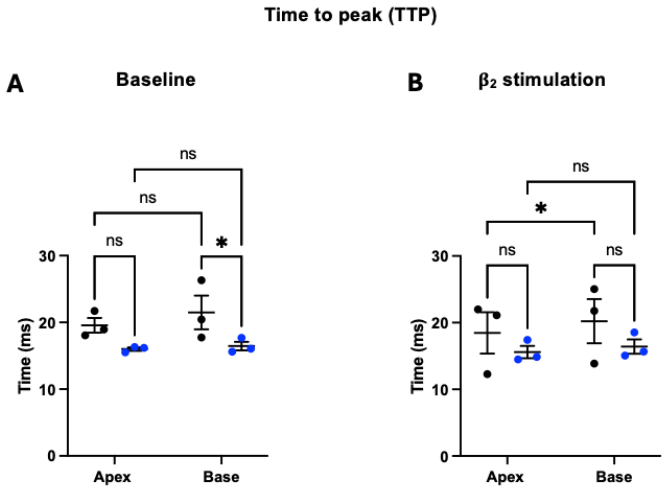


Figure 5.11 Time to peak (TTP) of calcium transients in sham and stretched rats. Quantification of TTP in sham and stretched heart at the apex and base during **(A)** baseline and following **(B)** β_2AR stimulation.

5.5 Discussion

In this chapter, we investigated the regional differences in β_2AR-mediated responses across the rat left ventricular myocardium following hypoosmotic swelling in isolated cardiomyocytes, as well as after mechanical stretch in the isolated rat heart. The key findings from this chapter are summarised as follows:

- Basal cardiomyocytes contain more caveolae than apical cardiomyocytes; hypoosmotic swelling reduces the number of caveolae in both regions.
- Hypoosmotic swelling increases cell width, with no significant difference between apical and basal cardiomyocytes.
- Basal cardiomyocytes exhibit higher T-tubule and Cav3 organisation compared to apical cells, and the hypo-osmotic solution has no effect on these structures.
- Hypoosmotic swelling enhances sarcomere shortening and cAMP production following β_2 stimulation in basal cardiomyocytes, but not in apical cells.
- Basal myocardium shows a longer action potential duration compared to apical myocardium at baseline and following β_2 stimulation. Mechanical stretch increases APD50 and APD70 in both the apex and base after β_2 stimulation.
- Mechanical stretch did not significantly alter calcium transient duration at baseline or following β_2AR stimulation in either the apex or base. However, stretch significantly shortened the time to peak at the base at baseline, and there was a decreasing trend following β_2AR stimulation.

The compartmentalisation of β_2AR signalling in cardiomyocytes is closely linked to their structural organisation, particularly the abundance of caveolae and the density and regularity

of T-tubules. Consistent with previous studies, our findings indicate that cardiomyocytes from different regions of the myocardium respond differently to β_2AR stimulation, with apical cells demonstrating a stronger contractile response compared to basal cells (Wright et al., 2018a). This heightened response in apical cells may be attributed to their reduced number of caveolae and less organised T-tubular network. The lower membrane complexity in apical cardiomyocytes allows for more diffuse cAMP signalling, resulting in more efficient phosphorylation of downstream targets, including proteins involved in excitation-contraction coupling, thereby enhancing contractility.

In contrast, basal cardiomyocytes exhibit greater membrane complexity, which leads to more tightly regulated cAMP activity. Our results further demonstrated that hypoosmotic swelling amplifies the β_2AR response in basal cardiomyocytes but does not significantly affect the response in apical cells. This effect essentially brings the contractile response of basal cells to a level comparable with that of apical cells, suggesting that the enhanced sarcomere shortening and increased cAMP production observed after β_2AR stimulation during hypo-osmotic swelling are predominantly due to changes in basal cardiomyocytes.

These findings align with the observation that basal cells have a higher caveolae density, making them more sensitive to the effects of hypoosmotic swelling. The increased caveolar abundance in basal cardiomyocytes likely creates a greater potential for membrane stretch to influence β_2AR signalling, leading to an amplification of the contractile response in these cells. Therefore, our study shows the critical role of structural differences between apical and basal cardiomyocytes in modulating their β_2AR responsiveness, particularly under conditions of membrane stretch.

To translate these findings to a more integrated organ level, we used a whole-heart Langendorff optical mapping system to record the action potential duration (APD) at 50%, 70%, and 90% repolarisation (APD50, APD70, APD90). APD is primarily determined by the balance between inward (depolarising) and outward (repolarising) currents, with each APD parameters reflecting the contribution of specific ion currents activity to different phases of repolarisation. APD50 is mainly influenced by L-type calcium current ($I_{Ca,L}$) activity, as calcium influx is dominant in the early repolarisation phase. APD 70 is more affected by the transient outward potassium current (I_{to}) and the rapid delayed rectifier potassium current (I_{kr}). APD90 is closely associated with the slow delayed rectifier potassium current (I_{ks}) and the Na^+/Ca^{2+} exchanger (NCX), which are involved in the final phase of repolarisation and the restoration of resting membrane potential. There are well-documented differences in action potential configuration and the density of underlying transmembrane ion currents along the apical-basal axis of the heart in various species, including rats (Bryant et al., 1999), rabbits (Cheng et al., 1999), and ferrets (Brahmajothi et al., 1997). Previous studies have reported regional differences in APD within the heart, with APD being shorter at the apex and lengthening toward the base (Watanabe et al., 1983, Efimov et al., 1994). In our study, we found that APD50 was prolonged in the basal region of the myocardium compared to the apex at baseline. This may be due to the higher expression of L-type calcium channels (LTCCs) at the base, leading to increased $I_{Ca,L}$ influx, however, further experiment, such as western blot are needed to confirm LTCC expression levels at the apex and base. Similarly, APD70 was also prolonged in the basal region compared to the apex, which can be attributed to regional differences in repolarising K^+ currents. Studies have shown that the transient outward K^+ current (I_{to}) and the delayed rectifier K^+ current (I_K) are significantly larger in apical than in basal cardiomyocytes

(Szentadrassy et al., 2005). Both I_{to} and I_{ks} are the main currents responsible for ventricular repolarisation (Zeng et al., 1995) (Huo et al., 2014). The larger I_{to} and I_K in the apical region, relative to the basal region, likely underlie these observations. In addition, we observed that APD90 was prolonged in the basal region, and this might be due to increased NCX at the base, facilitating a greater inward Na^+ current during late repolarisation. However, further experiments are needed to confirm whether NCX expression levels differ between the apex and base.

The prolonged action potential durations (APD50, APD70, APD90) observed following β_2AR stimulation (CGP with isoprenaline treatment) in our study highlight the complex and context-dependent effects of isoprenaline on cardiac electrophysiology. Previous research has shown that the impact of isoprenaline on action potential duration (APD) varies significantly across species and experimental conditions. In studies involving pig and human cardiac preparations, isoprenaline typically shortens APD (Szentandrássy et al., 2012, Dorian et al., 2002). However, in our study, as well as in other studies using guinea pig and rat models, isoprenaline exposure led to APD prolongation (Rocchetti et al., 2006, Ogura et al., 2007). This difference may be due to the greater susceptibility of larger mammals to repolarisation abnormalities, which has been linked to the increased expression of the I_K in these species (Rocchetti et al., 2006). For example, Harmati et al. investigated the effect of βAR stimulation on delayed rectifier potassium currents in canine ventricular cardiomyocytes and found that, following β_1AR inhibition with CGP, I_{Kr} showed no significant change with isoprenaline administration, whereas I_{Ks} increased, suggesting that β_2AR plays a key role in regulating I_{Ks} and, consequently, APD (Harmati et al., 2011).

The application of mechanical stretch led to an increase in active force development, which could provide a trigger for changes in the electrical function of cardiac myocardium. Regarding the effects of mechanical stretch, our findings align with those of Youganda et al., who reported significant increases in APD50 and APD70 in cardiomyocytes from caveolin-3 (Cav3) knockout models (Markandeya et al., 2023). This supports our observation of increased APD in both the apex and base regions of the heart under mechanical stretch conditions. These results suggest that caveolae, regulated by Cav3, may play a critical role in modulating action potential duration during stress in the heart.

Cardiac electrical activation and myocyte contraction are tightly coupled through calcium handling. Calcium is essential for coordinating contraction by propagating electrical signals as waves through the myocardium, ensuring synchronised contraction and relaxation (Ladeiras-Lopes et al., 2009). Mechanical stretch has been shown to impact calcium handling, as Tsai et al. demonstrated that stretch decreases SECRA2a expression and slows diastolic calcium decay in atrial myocytes (Tsai et al., 2011). Similarly, a study in isolated rabbit ventricular myocytes reported that stretch regulates calcium signalling by increasing systolic calcium transients and slowing relaxation (Shimkunas et al., 2021). In human left ventricular slices, high mechanical preload was found to increase diastolic myocardial length and enhanced contractility, though it significantly slowed relaxation and did not affect calcium sequestration. In contrast, βAR stimulation significantly increased the amplitude of calcium and accelerated relaxation in calcium (Sun et al., 2024). Lyon et al. also differentiated the effects of acute βAR stimulation and cardiomyocyte stretch on calcium transient dynamics and force generation (Lyon et al., 2020). They demonstrated that βAR activation enhances force amplitude, reflecting positive inotropy, while also increasing calcium transient amplitude and shortening calcium transient

duration, thereby facilitating faster relaxation. In contrast, stretch produced similar positive inotropic effects as βAR stimulation but had different lusitropic effects, with longer sarcomere length resulting in prolonged calcium transient duration and slower relaxation. Simulations combining acute βAR activation and increased sarcomere length showed an increase in peak calcium concentration and faster calcium transient relaxation. These findings suggest that the interplay between βAR activation and sarcomere length, rather than their independent effects, is essential in maintaining diastolic function during exercise-like conditions by enhancing both force generation and relaxation.

Regarding regionality, Choi et al. identified a gradient of ventricular relaxation, showing that calcium transients were shorter at the apex and progressively longer towards the base (Choi and Salama, 2000). In this study, we explored regional differences of β_2AR response in left ventricle following stretch. We observed a reduction in CAD90 following β_2AR stimulation in both the apex and base under sham and stretched conditions, consistent with previous studies. However, no significant differences were detected between sham and stretch conditions or between the apex and base in any CAD measurements. The lack of observed differences may be due to the slow exposure rate and the rapid dynamics of calcium transients or the lower sample size. Therefore, additional experiments are needed to draw a more definitive conclusion.

In our calcium transient measurements, the time to peak (TTP), reflects the kinetics of calcium release from the sarcoplasmic reticulum (SR) via ryanodine receptors (RyR) (Jaimes et al., 2016). RyR plays a critical role in excitation-contraction coupling by mediating the rapid release of calcium into the cytosol. Mechanical stretch has been shown to enhance RyR

sensitivity, facilitating faster calcium release (Zhang et al., 2020, Jian et al., 2014), which is consistent with our results showing shortened TTP. Following β_2AR stimulation, TTP was longer in the base compared to the apex in the sham group, suggesting regional heterogeneity in calcium dynamics. This may be linked to variations in RyR density; indeed, a previous study found higher RyR density in the apex than in the base, although this finding was based on rabbit left ventricular epicardium (Papp et al., 2017). Interestingly, mechanical stretch appeared to homogenise these regional differences, eliminating the variation in TTP between the apex and base. However, our results showed a large variation, more experimental repeats are needed to draw a conclusion.

5.6 Conclusion

In conclusion, hypoosmotic swelling amplifies the β_2AR response in basal cardiomyocytes but does not significantly alter the response in apical cells, which equilibrates the apical and basal response. This observation suggests that the enhanced sarcomere shortening and cAMP production following β_2AR stimulation following hypoosmotic swelling was mainly due to the effect on the basal region of the heart. This is consistent with the fact that the basal cells have more caveolae, thereby being more susceptible to the effect of hypoosmotic swelling. In addition, we used the whole heart Langendorff optical mapping approach, showing that mechanical stretch increases the action potential duration in both apical and basal regions following β_2AR stimulation. Further work is needed to investigate the regional differences in channel activity between the apex and base.

Chapter 6 The Effect of Membrane Stretch on β_1 and β_2AR Signalling in Failing Rat and Human Ventricular Cardiomyocytes

6.1 Introduction

Chronic heart failure (HF) is a progressive condition resulting from structural or functional abnormalities in the heart, leading to reduced cardiac output. It is a major cause of morbidity and mortality worldwide, imposing a substantial burden on global healthcare systems. The causes of HF include myocardial diseases (such as ischaemic heart disease and genetic disorders), abnormal loading conditions (like hypertension and myocardial stretch), and arrhythmias (both tachyarrhythmias and bradyarrhythmias) (Ponikowski et al., 2016).

Key contributors to HF include alterations in cellular signalling processes within ventricular cardiomyocytes at the subcellular level. In HF, the T-tubule network undergoes remodelling, with reduced T-tubule density observed in failing rat cardiomyocytes (Schobesberger et al., 2017). Additionally, increased separation between the T-tubule membrane and the sarcoplasmic reticulum delays excitation-contraction coupling, leading to diminished and prolonged cardiac contraction (Heinzel et al., 2008). Similarly, studies on human heart samples from patients with ischaemic, idiopathic dilated, and hypertrophic cardiomyopathy also revealed significant reductions in T-tubule density (Lyon et al., 2009).

Cavolin-3 (Cav3), the principal protein component of caveolae and a key structural protein in the T-tubule, is closely associated with HF. Studies in Cav-3 knockout mice and Cav-3 null mice showed a significant reduction in caveolae number associated with t-tubule disorganisation and cardiac hypertrophy. Additionally, decreased Cav-3 expression has been reported in

various cardiovascular diseases, including left ventricular dysfunction, cardiac hypertrophy, and myocardial infarction (Feiner et al., 2011, Woodman et al., 2002). In contrast, studies using transgenic mice with overexpressing Cav-3 revealed attenuation in cardiac hypertrophy progression (Horikawa et al., 2011). Cav3 also associates with the L-type calcium channel (LTCC), particularly Cav1.2, which plays a crucial role in the β_2AR-LTCC complex within the T-tubule. A study by Dr Sanchez-Alonso et.al. demonstrated that this complex is disrupted in heart failure, leading to impaired compartmentalisation of β_2AR (Sanchez-Alonso et al., 2023).

HF is also linked to changes in β-adrenergic receptor (βAR) populations in the ventricular myocardium. Specifically, there is a decrease in β_1AR density, while β_2AR levels remain unchanged (Bristow et al., 1986). Research from Dr Nikolaev further demonstrated that in cardiomyocytes derived from a rat model of HF, β_2ARs redistribute from T-tubules to the cell surface, altering β_2AR-cAMP signalling from a localised pattern to a more diffuse distribution, similar to β_1AR signalling (Nikolaev et al., 2010). Understanding the compartmentalisation of βAR signalling and how structural alterations in HF affect its molecular mechanisms is, therefore, a crucial area of investigation. Stretch occurs both under physiological conditions, such as exercise, and pathophysiological conditions like HF. However, these types of stretch are not the same: in HF, the stretch is largely passive and pathological, rather than active, which may significantly impact the βAR signalling. In this study, in addition to exploring how structural changes affect the βAR signalling, we aim to investigate whether the effects of stretch on β_2AR signalling, as we previously observed, are preserved or disrupted in failing cardiomyocytes. This could help us assess the capacity for further stretch in HF, as structural and functional changes in the heart may limit the heart's ability to respond to additional

stretch. By examining how HF affects β_2AR signalling and how stretch in the context of HF influences this pathway, we hope to better understand the role of altered mechanical signalling in the progression of heart failure.

Importantly, most studies have focused on animal models, with less emphasis on human ventricular myocytes. Dilated cardiomyopathy (DCM), a leading cause of heart failure, is characterised by left ventricular dilation and impaired contractility, often due to genetic mutations or acquired factors such as infections, toxins and tachyarrhythmias that weaken the cardiac muscle (Heymans et al., 2023). Certain conditions can also act as modifiers, worsening cardiomyopathy even if they are not direct causes. For example, the hemodynamic changes can trigger the clinical onset of previously asymptomatic dilated cardiomyopathy. In DCM, the βAR receptor desensitisation reduces intracellular cAMP levels, which subsequently decreases protein kinase A (PKA)-mediated phosphorylation of sarcomeric proteins such as troponin I and troponin C. This reduction in phosphorylation results in increased calcium sensitivity and preserves maximal force generation (van der Velden et al., 2000, Wolff et al., 1996). A recent study by Dr. Sanchez-Alonso highlighted that different HF phenotypes exhibit specific functional aberrations. For instance, in patients with ischemic cardiomyopathy (ICM), L-type calcium channel (LTCC) activity increased in T-tubules, whereas in DCM patients, LTCC activity was elevated in the cell crest (Sanchez-Alonso et al., 2020). These underlying pathophysiological differences suggest that HF subtypes may have varying responses to therapeutic interventions. Therefore, investigating subcellular signalling processes in HF, particularly in human ventricular myocytes, is essential for advancing potential therapies and guiding optimal treatment strategies.

6.2 Hypothesis and Aims

In heart failure, alterations in membrane nanodomains, such as caveolae, disrupt the stretch-sensitivity of β_2-adrenoceptor signalling, leading to impaired β_2-adrenergic responses in failing cardiomyocytes. Additionally, β_1- and β_2-adrenoceptor signalling differs between healthy and failing human ventricular cardiomyocytes, potentially due to structural and functional remodelling in heart failure.

Aim 1: Explore the impact of hypoosmotic swelling (membrane stretch) on cell size and the transverse/axial-tubule system failing (16 weeks post-myocardial infarction) cardiomyocytes.

- Objective 1: Measure cell size (width and length) in failing cardiomyocytes using CytoCypher.
- Objective 3: Evaluate T-tubule density, the power of regularity and directionality in failing cardiomyocytes using confocal microscopy.
- Objective 4: Evaluate caveolin-3 density and the power of regularity in failing cardiomyocytes using confocal microscopy.

Aim 2: Investigate the effect of hypoosmotic swelling (membrane stretch) in β_1 and β_2-adrenoceptor/cAMP signalling in failing rat ventricular cardiomyocytes.

- Objective 1: Assess contractility (sarcomere shortening) and cAMP response in failing rat left ventricular cardiomyocytes by using CytoCypher and FRET microscopy.

Aim 3: Investigate the β_1 and β_2-adrenoceptor response in human donor and failing (dilated cardiomyopathy) ventricular cardiomyocytes.

- Objective 1: Measure the sarcomere shortening and cAMP response in human donor and DCM ventricular cardiomyocytes by using CytoCypher and FRET microscopy.

6.3 Methods

6.3.1 Solutions

Solutions	Composition
Isosmotic solution	NaCl 118; KCl 5.3; $MgCl_2$ 0.5; $CaCl_2$ 1; Glucose 10; Na_2HPO_4 7.5; $NaH_2PO_4.H_2O$ 2.5
Hypoosmotic solution	NaCl 81; KCl 5.3; $MgCl_2$ 0.5; $CaCl_2$ 1; Glucose 10; Na_2HPO_4 7.5; $NaH_2PO_4.H_2O$ 2.5
MEM media	MEM with Hank's salts, 9mM $NaHCO_3$, 1% glutamine and 1% antibiotic/antimycotic (AA)
FRET Buffer	
Blocking solution	5% BSA, 20% Tween 20, 10% goat serum and PBS

Table 6.1 The list of solutions and their compositions used in the experiments for Chapter 6.

β_1AR blocker CGP20712A, β_2AR blocker ICI 118,551 and non-selective βAR agonist isoprenaline HCl, non-selective PDE inhibitor IBMX were supplied by Sigma Aldrich. Adenylyl cyclase activator forskolin were obtained from Tocris Bioscience.

6.3.2 Animal Ethics Approval

All animal procedures were carried out in accordance with UK Home Office guidelines (ASPA1986 and EU directive 2010/83) and approved by Animal Welfare and Ethics Review Board of Imperial College London.

6.3.3 Rat Heart Failure Model

Adult male Sprague-Dawley rats (Charles River, UK) were used for operation once their body weight reach 250g. Myocardial infarction (MI) was induced via ligation of the left anterior descending (LAD) coronary artery. Briefly, Rats were first anaesthetised with 3% isoflurane and antibiotic enrofloxacin (5mg/kg), 0.9% saline (10ml/kg) and buprenorphine (0.05 mg/kg) were

given subcutaneously for pain relief. Chest and pericardium were opened, and a suture was go through the LAD coronary artery and then tied to reduce the blood flow (Schobesberger et al., 2017). Experiments were also performed in failing cardiomyocytes from rats that had undergone MI 16 weeks before isolation. Detailed protocol can be found in section 2.2.

6.3.4 Human Ethics Approval

All experiments involving isolated human cardiomyocytes were done with approval from the Imperial College Institutional Review Board, and informed consent was obtained from each patient. Heart tissue samples from donor hearts which were unsuitable for transplantation were used with approval from NHSBT, under REC approval reference 16/LO/1568. In addition, samples from patients with end-stage heart failure were provided with the authorisation of the Brompton Harefield & NHLI Ethics Committee under Biobank REC approval reference 09/H0504/104+5.

6.3.5 Human Study Population

The Donor ventricular was obtained from samples of left ventricles taken from donor hearts unsuitable for transplantation (n=8, average age 47±4.6, six females and two males). None of the donors had a history of hypertension, cardiothoracic disease, or diabetes. Three of them presented a history of smoking. The reasons for these hearts being rejected for transplantations were heart size; age; and logistics. Failing ventricular cardiomyocytes were prepared from the hearts of patients with end-stage heart failure caused by dilated cardiomyopathy (DCM) who were undergoing transplantation (N=5 patients, average age 38 ± 6.2, five males). Clinical characteristics of the heart failure patients used in this work can be found in Table 6.2.

CHARACTERISTICS	
AGE, YEAR (MEAN ± SEM)	38 ± 6.2
MEN, N (%)	5 (100)
WOMEN, N (%)	0
MEDICAL HISTORY	
HYPERTENSION	1 (20)
MYOCARDITIS	1 (20)
DIABETES MELLITUS	1 (20)
EX-SMOKER	1 (20)
ALCOHOL	3 (60)
MEDICATIONS	
β-BLOCKERS	3 (60)
DIURETICS	2 (40)
ANTIPLATELET	2 (40)
ACE/ARB	2 (40)
ARRHYTHMIC	1 (20)
ALDOSTERONE ANTAGONIST	2 (40)

Table 6.2. Clinical characteristics of heart failure patient.

Values are the total number of patients with percentages in parentheses. ACE, Angiotensin-converting enzyme inhibitors: ARB, Angiotensin II receptor blocker.

6.3.6 Human Cardiomyocytes Isolation

Failing ventricular cardiomyocytes were isolated from the hearts of patients with end-stage heart failure (HF) due to ischemic or dilated cardiomyopathies who were undergoing

transplantation. Healthy cardiomyocytes were prepared from donor hearts that were unsuitable for transplantation. Small pieces of the left ventricle (LV) were excised, with fat and connective tissue carefully removed. The tissue was then washed three times in calcium-free Krebs-Ringer solution containing the following (in g/L): NaCl 7.012, KCl 0.402, $MgSO_4$ 1.332, pyruvate 0.55, glucose 3.603, taurine 2.502, HEPES 2.383 (pH 7.4) at 37°C. The samples were agitated for 25 minutes at 37°C in 10 ml of Krebs-Ringer solution with 0.36 mg/ml protease. The samples were then shaken in Krebs-Ringer solution with 1 mg/ml collagenase for 10-15 minutes. Cardiomyocytes were released after the first collagenase digestion. After each digestion step, the solution was centrifuged at 600 rpm for 3 minutes, and the resulting pellets were re-suspended in Krebs-Ringer solution. Detailed protocol can be found in section 2.5.

6.3.7 Confocal Microscopy Following Di-8-ANNEPS and Caveolin-3 Staining

Rat failing cardiomyocytes were stained with 10 µM Di-8-ANNEPPS in FRET buffer, then sonicated for 20 minutes at 50°C. After 3 minutes of staining, the cells were washed twice with FRET buffer and stabilised in 2 ml of iso- or hypoosmotic solution before imaging. Imaging was carried out using a Zeiss LSM-78 inverted confocal microscope, and images were analysed with ImageJ and MATLAB. For more details, refer to Section 2.8.

For the caveolin-3 staining, rat failing cardiomyocytes were plated on coverslips, perfused with iso- or hypoosmotic solution for 15 minutes, and fixed with 4% PFA, permeabilised and blocked. Cells were incubated with a caveolin-3 primary antibody (1:100) in blocking buffer for 24 hours at 10°C, followed by Alexa Fluor 488-conjugated donkey anti-mouse IgG (1:500) for 2 hours at room temperature. Coverslips were mounted using ProLong Gold with DAPI. The full staining protocol can be found in Section 2.9.1

6.3.8 Functional Study – CytoCypher & FRET Microscopy

The contractile response of cardiomyocytes from both rats and humans was measured using the CytoCypher system, as explained in Section 2.11. This system measured cell shortening and calcium transients to assess contractility, as discussed in previous chapters. This allowed us to examine the effects of hypoosmotic swelling (membrane stretch) on contractility following β_1AR and β_2AR stimulation in rat heart failure model as well as in human donor cells. However, due to low cell counts and low viability rate, we unable to apply hypoosmotic swelling in the human failing cells. Therefore, in this chapter, we compared the differences between β_1AR and β_2AR responses in human failing cells and donor cells. The same protocols as in Section 3.3.2 were followed. In brief, 50nM ICI and 1 μM isoprenaline were used to selectively stimulate β_1AR, while 100 nM CGP and 1 μM isoprenaline were used to selectively stimulate β_2AR.

To study the cAMP dynamics, we used FRET microscopy. Cells were transfected with pmEPAC2 FRET sensor (MOI 200) and the experiments were performed after 48 hours, following the same protocol to that in Chapter 3. The cells were first treated with either 60nM ICI (β_2AR blocker) or 100nM CGP (a β_1AR blocker), followed by 100nM isoprenaline (a βAR agonist). To maximise cAMP release, 100 μM IBMX (a non-specific PDE inhibitor) and 10 μM forskolin (an adenylyl cyclase activator) were applied. Detailed analysis could be found in Section 2.10.

6.3.9 Statistics

All graphs and statistical analyses were performed using Prism 10 (GraphPad).

The biometric data was analysed using unpaired t-test. Cell size, T-tubule and Caveolin-3 assessment were analysed using Two-way ANOVA with Šidák's multiple comparisons test.

CytoCypher experiment (cell contractility) and FRET Microscopy experiment (cAMP response) were analysed using Two-way ANOVA followed by Šidák's multiple comparisons test.

6.4 Results

The heart weight/body weight ratio and heart weight/lung weight ratio were assessed to confirm the success of the MI model. We also visually confirmed the presence of an infarct transmural region of the LV on the isolation day. In the few cases where the infarct area was minimal and restricted to the epicardium, those cells were not included in the study. The heart weight-to-body weight ratio (g/kg) and the heart-to-lung weight ratio were significantly increased, indicating a pronounced hypertrophy phenotype (Figure 6.1).

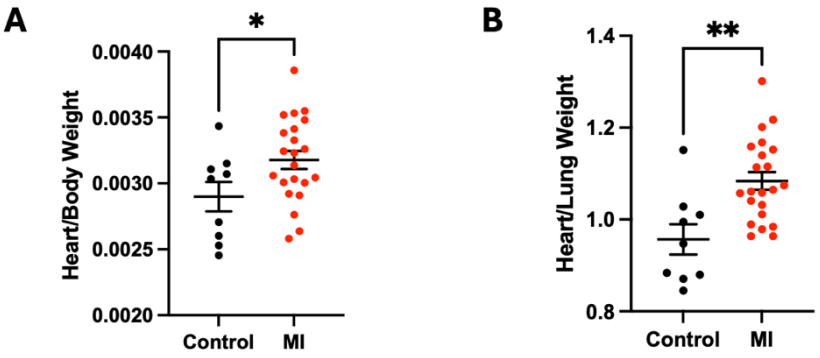


Figure 6.1. Biometric data in rat age-matched control hearts and hearts with myocardial infarction. **A.** Heart weight/body weight ratios and **(B)** heart weight/lung weight ratios in control and MI rats. N=9-22, Unpaired T-test, * $p<0.05$, ** $p<0.01$.

6.4.1 Hypoosmotic Swelling Increases the Width but Not the Length of Rat Left Ventricular Cardiomyocytes in Both Control and Failing Cells

To assess the impact of hypoosmotic swelling on cell size, both control and failing cardiomyocytes were stabilised in isosmotic and hypoosmotic solutions for 20 minutes using the IonOptix CytoCypher system. Images of individual cells were captured with the IonOptix IonWizard software. Failing cardiomyocytes exhibited a significant increase in cell dimensions, consistent with the hypertrophic remodelling characteristic of these cells. In response to hypoosmotic swelling, the cells increased in volume by increasing in width rather than length, a trend observed in both the control and failing groups. There was a significant increase in the average width of cardiomyocytes in the hypoosmotic solution compared to the isosmotic solution, while cell length remained unchanged (Figure 6.2).

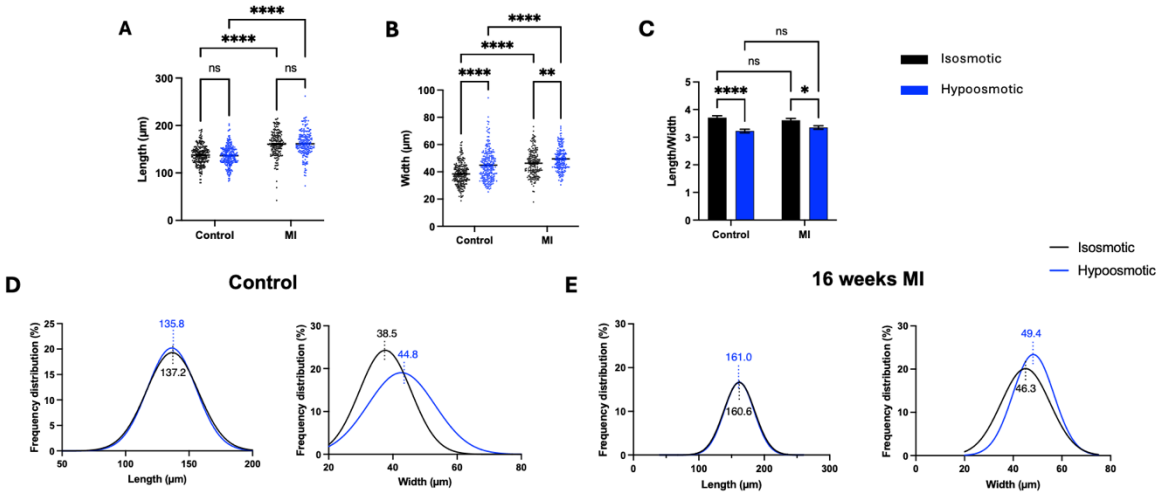


Figure 6.2 Hypoosmotic swelling increases the width of rat left ventricular cardiomyocytes but not length in both control and MI group. A, Length; **(B)**, width and **(C)** their ratio, from cardiomyocytes in isosmotic (black) and hypoosmotic (blue) solution in control and 16 weeks MI group. **D**, Histograms of frequency distribution of individual cardiomyocyte dimensions with mean shown. Control: N=9; n= 235; MI: N=6; n=190. *, **, **** p<0.05, 0.01, 0.0001 respectively, Two-way ANOVA followed by Šídák's multiple comparisons test.

6.4.2 Hypoosmotic Swelling Does Not Alter T-Tubule (TT) Structure in Both Control and Failing Cardiomyocytes

To investigate the organisation of T-tubules (TT) in rat left ventricular cardiomyocytes during hypoosmotic swelling, we labelled the TT membranes with Di-8-ANEPPS and imaged the cells using confocal microscopy. Representative images of TT structures in both control and failing cardiomyocytes under isosmotic and hypoosmotic conditions are shown in Figure 6.3A-D. In both control and failing groups, hypoosmotic swelling did not result in any significant changes in TT density, regularity, or directionality, indicating that the TT network remained intact under hypoosmotic swelling in our model (Figure 6.3). Failing cardiomyocytes showed a significant reduction in TT density and regularity compared to controls in both iso- and hypoosmotic conditions. Although there was a trend towards decreased directionality in hypoosmotic failing cells, these changes were not statistically significant.

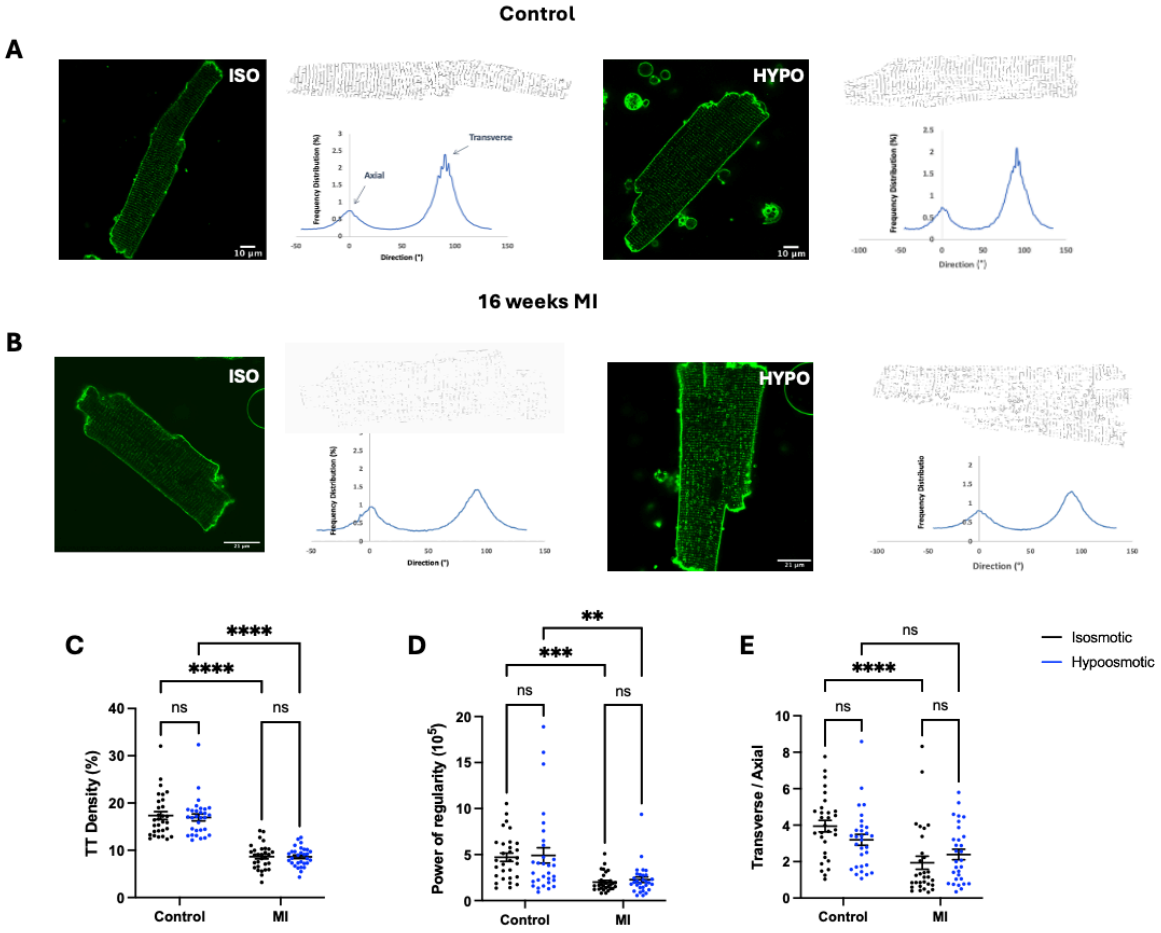


Figure 6.3. Hypoosmotic stress did not alter the T-tubule (TT) network in control and failing cardiomyocytes. Di-8-ANEPPS membrane staining showing the TT network in a representative healthy **(A)** and **(B)** failing left ventricular cardiomyocytes in iso-and hypoosmotic solution. Scar bar: 10µm. Representative images of control and failing cells showing skeletonised TT network and directionality histograms of iso and hypoosmotic cells were generated from skeletonised images of TT. Gaussian fitting show axial (0^0) and transverse components (90^0). Mean **(C)** TT density; **(D)** Power of Regularity; and **(E)** Directionality of TT structure in control and failing cardiomyocytes in iso-and hypoosmotic solution. Control: N=3, n=30; MI: N=3; n=30. Data are presented as mean ± SEM. **,***, ****p<0.01, 0.001 and 0.0001 respectively. Two-way ANOVA followed by Šídák's multiple comparisons test.

6.4.3 Caveolin-3 (Cav3) Density is Increased in Failing Cardiomyocytes

We also examined the effect of hypoosmotic swelling on Cav3 protein density in heart failure. Adult rat ventricular cardiomyocytes, both control and failing, were stained with a Cav3 antibody, and Cav3 density was assessed under isosmotic and hypoosmotic conditions using confocal microscopy (Figure 6.4). The results showed that Cav3 density was significantly higher in failing cardiomyocytes compared to control. However, no difference was observed in Cav3 density between isosmotic and hypoosmotic conditions in either the healthy or failing groups.

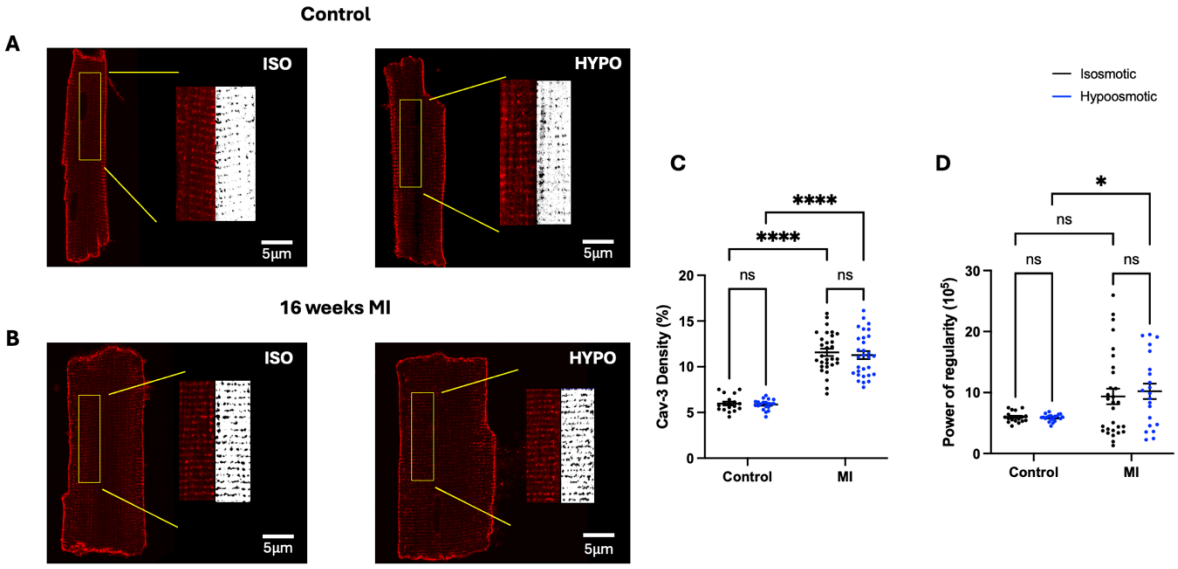


Figure 6.4. Cav3 Density was increased in the failing cardiomyocytes. Representative confocal images taken from **(A)** control and **(B)** failing cardiomyocytes. Scar bars: 5μm. Left insets in confocal images: zoom of 40 × 5 μm area of confocal image; right insets: binarised image represented in the corresponding left inset, used to determine Cav3 density. **(C)** Density and **(D)** regularity of Cav3 calculated from binarised images of control and failing cardiomyocytes in iso- (black) and hypoosmotic (blue) solution. Control: N=3, n=20; MI: N=3, n=30. N, number of animals; n, number of cells. Data are presented as mean ± SEM. * p<0.05, ****P<0.0001. Two-way ANOVA followed by Šídák's multiple comparisons test.

6.4.4 Hypoosmotic Swelling Enhances cAMP Production and Sarcomere Shortening Following β_2AR Stimulation, but These Effects Are Lost in MI Cells

To evaluate the functional effects of hypoosmotic swelling in failing cardiomyocytes derived from 16-week post-MI rats, we used FRET microscopy to measure cAMP production following both β_1AR and β_2AR stimulation. Representative traces are shown in Figure 6.5A and C, illustrating the β_1AR and β_2AR cAMP response in isosmotic (black) and hypoosmotic (blue) solutions for both control and 16-week MI cells.

There is a significant reduction in the total cAMP output in the failing group compared to the control group following β_1AR stimulation, in both isosmotic and hypoosmotic conditions (Figure 6.5B). No significant difference was observed between isosmotic and hypoosmotic conditions within either group, indicating that β_1AR response is compromised in MI, and hypoosmotic swelling does not seem to affect cAMP production following β_1AR stimulation in both the control and MI groups. Conversely, following β_2AR stimulation, the total cAMP output in the MI group increased compared to the control group (Figure 6.5D). In addition, the increase in cAMP production observed under hypoosmotic swelling in the control group was lost in the MI group.

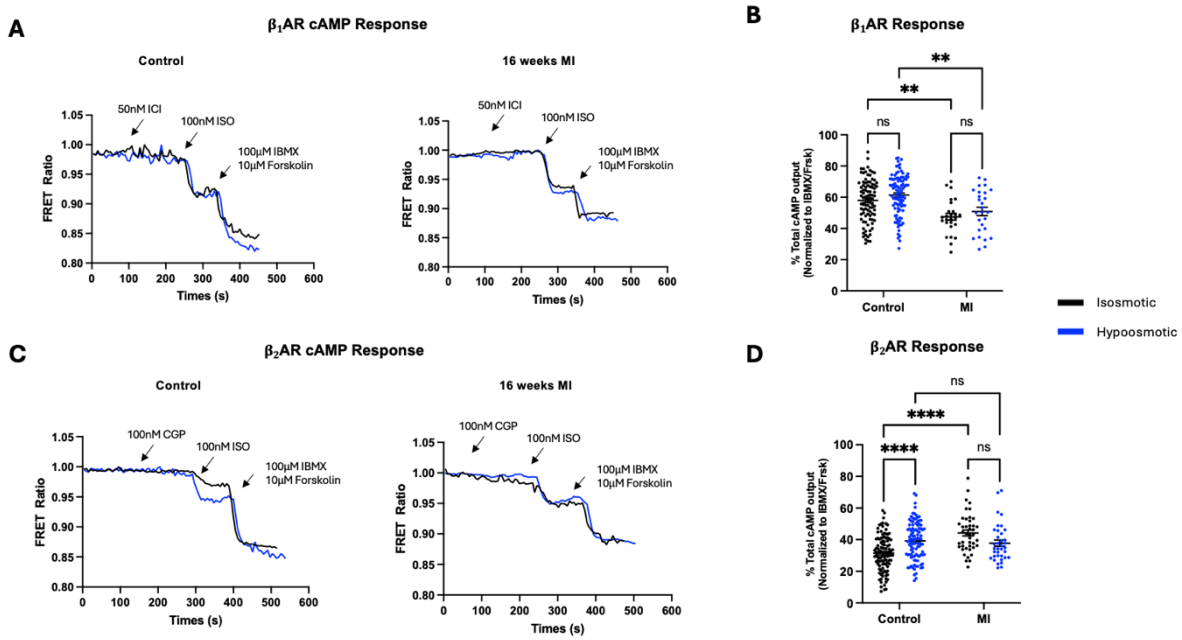


Figure 6.5 Hypoosmotic swelling enhances cAMP production following β2AR stimulation, but the effect is lost in MI cells. Representative trace illustrating the **(A)** β1AR- and **(C)** β2AR-specific FRET response measured by the plasma membrane cAMP sensor pmEPAC2-camp in control and failing ventricle cardiomyocyte under iso-(black line) and hypoosmotic (blue line) conditions following application of ICI (β2AR antagonist, 50nM) or CGP (β1AR antagonist, 100nM), Isoprenaline (βAR non-specific agonist,100nM), IBMX (non-selective PDE inhibition, 100μM) and Forskolin (adenylyl cyclase activator, 10μM). Quantification of cAMP production after **(B)** β1AR- and **(D)** β2AR-specific stimulation relative to the maximum production achieved with IBMX and Forskolin stimulation. Control N=8; n=101-108, MI N=3~4, n=26~43. Data are presented as means ± SEM. ****P<0.0001, Two way ANOVA followed by Šídák's multiple comparisons test.

Next, we assessed the cell contractility in both control and failing cells using CytoCypher. Following β1AR stimulation, no significant difference in sarcomere shortening was observed between isosmotic and hypoosmotic conditions (Figure 6.6C). Under hypoosmotic swelling, there was an increase in sarcomere shortening following β2AR stimulation in control cells. However, following β2AR stimulation of failing cells, there was also no difference in sarcomere shortening in the hypoosmotic condition as compared to the isosmotic condition, although it was an increased trend (Figure 6.6D). Furthermore, it is also important to note that in

isosmotic conditions, the contractile response to β_2AR stimulation in failing cells showed a higher trend compared to control cells, which may imply that it is already quite deregulated in failing cells.

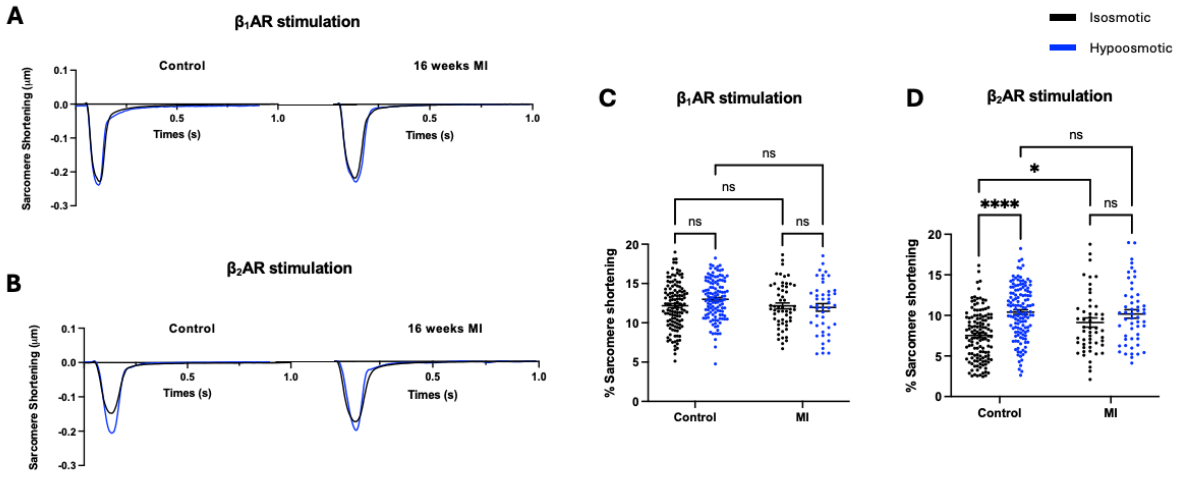


Figure 6.6 Hypoosmotic swelling enhances sarcomere shortening following β_2AR stimulation, but the effect is lost in MI cells. Representative traces of sarcomere shortening in control and failing cardiomyocytes following **(A)** β_1AR and **(B)** β_2AR stimulation in iso- (black) and hypoosmotic (blue) cells. Percentage sarcomere shortening in control and failing cardiomyocytes following **(C)** β_1AR stimulation and **(D)** β_2AR stimulation in isosmotic (black) and hypoosmotic (blue) solution. Control: N=5, n=121~133. MI: N=45~56. Data are presented as mean ± SEM, with * and **** indicating significance at P<0.05 and P<0.0001, respectively, as determined by Two-way ANOVA followed by Šídák's multiple comparisons test.

6.4.5 Sarcomere Shortening is Greater Following β_1AR Stimulation, but Hypoosmotic Swelling Does Not Affect β_2AR-Induced Shortening in Human Donor Cardiomyocytes

Following our investigations in rat cardiomyocytes, we next examined the effect of β_1AR and β_2AR in human donor cardiomyocytes to explore whether similar responses following hypoosmotic swelling would be observed.

Representative traces of sarcomere shortening following β_1AR and β_2AR stimulation were shown in Figure 6.7A and B, with comparisons between isosmotic (black) and hypoosmotic (blue) conditions. Sarcomere shortening is significantly increased following β_1AR stimulation compared to baseline under both isosmotic and hypoosmotic conditions (Figure 6.7C). However, hypoosmotic swelling did not induce a significant difference in sarcomere shortening when compared to the isosmotic condition for β_1AR stimulation. Similarly, after β_2AR stimulation, sarcomere shortening was significantly enhanced compared to baseline, but there was no significant difference between iso- and hypoosmotic conditions (Figure 6.7D).

When comparing the effects of β_1AR and β_2AR stimulation, sarcomere shortening was greater following β_1AR stimulation than β_2AR stimulation in both isosmotic conditions, with no significant differences in hypoosmotic conditions (Figure 6.7E). These findings suggest that while both β_1AR and β_2AR stimulation increase sarcomere shortening in human donor cardiomyocytes, hypoosmotic swelling does not significantly affect the contractile response in either β_1AR or β_2AR stimulation.

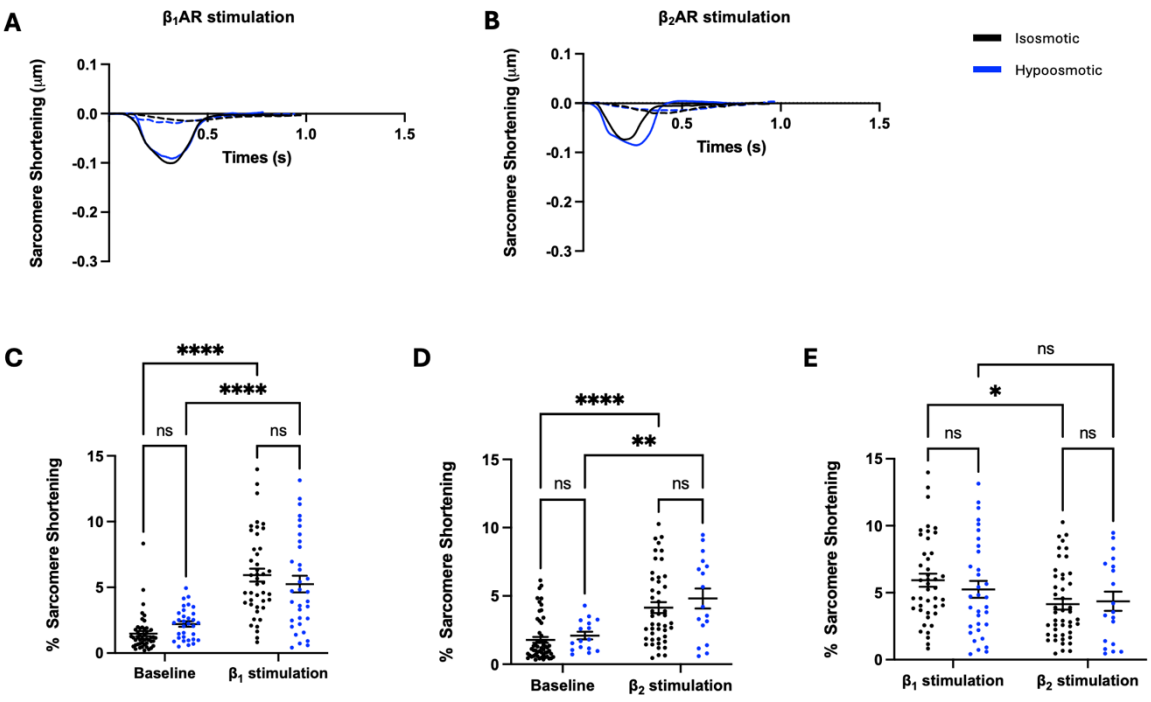


Figure 6.7. Sarcomere shortening is greater following β1AR stimulation, while hypoosmotic swelling does not affect sarcomere shortening following β2AR stimulation in human donor cardiomyocytes. Representative traces of sarcomere shortening in human donor cardiomyocytes at baseline (dashed line) and following **(A)** β1AR and **(B)** β2AR stimulation (solid line) in iso- (black) and hypoosmotic (blue) cells. Percentage sarcomere shortening in human donor cardiomyocytes following **(C)** β1AR stimulation and **(D)** β2AR stimulation in isosmotic (black) and hypoosmotic (blue) solution. **E.** Comparison of sarcomere shortening of human donor cardiomyocytes following β1AR and β2AR stimulation in iso- and hypoosmotic conditions. N=3~6, n=17~56. Data are presented as mean ± SEM, with ** and **** indicating significance at P<0.01 and P<0.0001, respectively, as determined by Two-way ANOVA followed by Šídák's multiple comparisons test.

6.4.6 Decreased Sarcomere Shortening Following β1AR Stimulation in DCM Cardiomyocytes

We next examined the sarcomere shortening following β1AR and β2AR stimulation in human dilated cardiomyopathy (DCM) cardiomyocytes. Representative traces of sarcomere shortening at baseline (dashed line) and following β1AR or β2AR stimulation (solid line) are shown in Figures 6.8A and 6.8B, comparing donor (black) and DCM (red) cells.

There is a significant increase in sarcomere shortening after β_1AR stimulation in both donor and DCM cardiomyocytes, compared to baseline. The sarcomere shortening following β_1AR stimulation is significantly reduced in the DCM group compared to the donor group (Figure 6.8C). β_2AR stimulation also resulted in a marked increase in sarcomere shortening in both donor and DCM cells, without significant differences between the groups (Figure 6.8D).

When comparing the effects of β_1AR and β_2AR stimulation within the same cell populations, DCM cardiomyocytes showed a similar degree of sarcomere shortening for both receptor types (Figure 6.8E). In donor cells, sarcomere shortening following β_1AR stimulation was significantly higher compared to β_2AR stimulation, whereas in DCM cells, the responses were comparable.

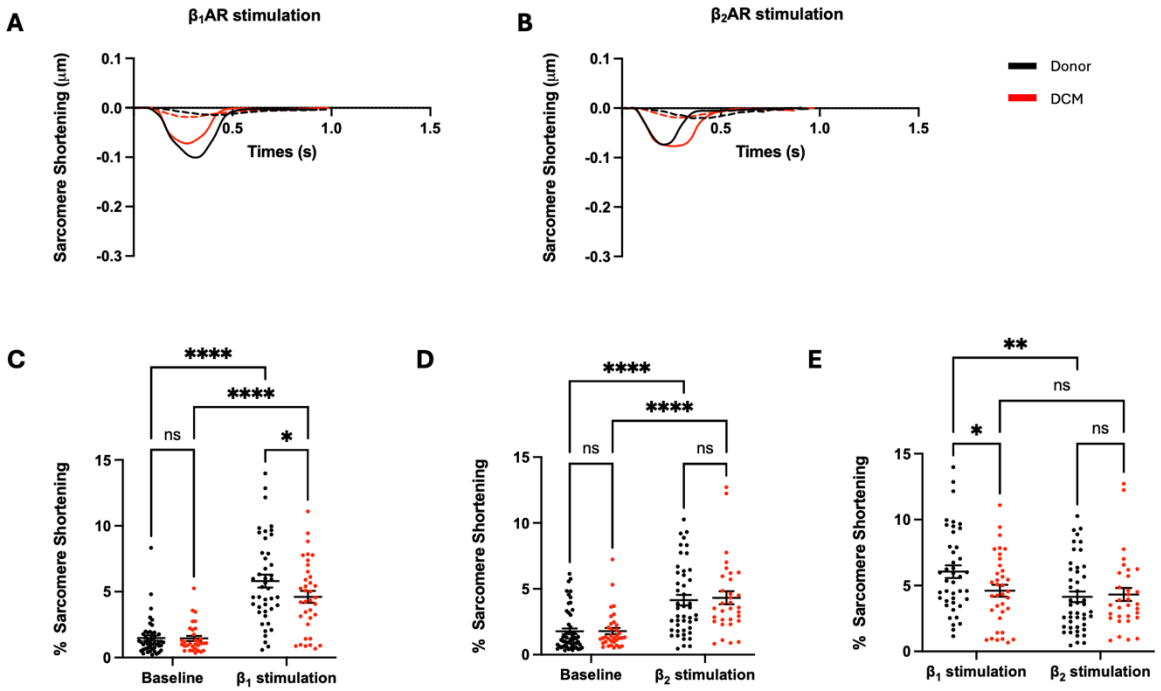


Figure 6.8. Sarcomere shortening following β_2AR stimulation is equal to that produced by the β_1AR stimulation in human DCM cardiomyocytes. Representative traces of sarcomere shortening at baseline (dashed line) following **(A)** β_1AR and **(B)** β_2AR stimulation (solid line) in the donor (black) and DCM (red) cells. Percentage sarcomere shortening following **(C)** β_1AR stimulation and **(D)** β_2AR stimulation in the human donor (black) and DCM (red) cells. **E.** Comparison of sarcomere shortening following β_1AR and β_2AR stimulation in human donor and DCM cardiomyocytes. Donor: N=3~6, n=17~56. DCM: N=4, n=32~36. Data are presented as mean ± SEM, with ** and **** indicating significance at P<0.01 and P<0.0001, respectively, as determined by Two-way ANOVA followed by Šídák's multiple comparisons test.

6.4.7 Increased cAMP Response in DCM Cardiomyocytes Following β_2AR Stimulation

We assessed the cAMP production in donor and DCM cardiomyocytes following β_1AR- and β_2AR-specific stimulation. The cAMP response was measured using the plasma membrane cAMP sensor pmEPAC2-camp in both groups. Figures 6.9A and 6.9 illustrate the FRET traces of cAMP production after β_1AR and β_2AR stimulation in donor (black) and DCM (red) cells, respectively. In the β_2AR response, there is a tendency towards reducing the cAMP output in the Donor samples compared to the β_1AR response, but the spread of data is high, and the

number of observations is perhaps too small for us to conclude. While β_1AR-mediated cAMP production was not significantly different between donor and DCM cells, β_2AR stimulation led to significantly higher cAMP production in DCM cells compared to donor cells (Figure 6.9C).

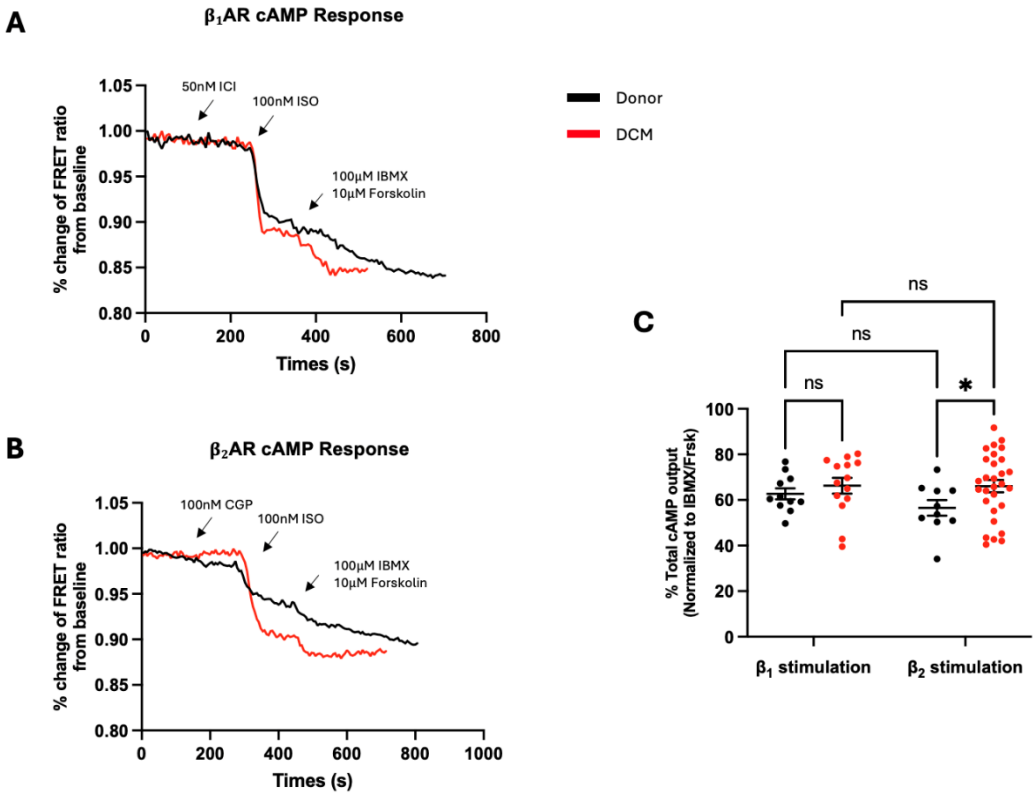


Figure 6.9. Enhanced cAMP production in DCM cardiomyocytes following β_2AR stimulation. Representative trace illustrating the **(A)** β_1AR- and **(C)** β_2AR-specific FRET response measured by the plasma membrane cAMP sensor pmEPAC2-camp in donor and DCM ventricle cardiomyocyte following application of ICI (β_2AR antagonist, 50nM) or CGP (β_1AR antagonist, 100nM), Isoprenaline (βAR non-specific agonist,100nM), IBMX (non-selective PDE inhibition, 100μM) and Forskolin (adenylyl cyclase activator, 10μM). **C.** Quantification of cAMP production after β_1AR- and β_2AR-specific stimulation relative to the maximum production achieved with IBMX and Forskolin stimulation. Donor: N=2~3, n=10-11. DCM: N=2~3, n=15~33. Data are presented as means ± SEM. *P<0.05, Two-way ANOVA followed by Uncorrected Fisher's LSD.

6.5 Discussion

In this chapter, we investigated the effect of membrane stretch in rat cardiomyocytes from heart failure model (16 weeks post-MI) following β_1AR and β_2AR stimulation. In addition, we have also used the cells taken from human donors and DCM patients, comparing the β_1AR and β_2AR response in those two populations and also evaluate the effect of membrane stretch on β_1AR and β_2AR response in human cells. The key findings from this chapter are summarised as follows:

- Failing rat left ventricular contained larger cell dimensions and hypoosmotic swelling increases the width of rat left ventricular cardiomyocytes but not length in both control and MI groups.

- T-tubule network was distorted in failing LV with decreased T-tubule density and regularity; hypoosmotic swelling did not disorganise the T-tubule structure.

- Caveolin-3 density in T-tubule was increased in failing LV but was not altered after hypoosmotic swelling.

- The increase in the in β_2AR response due to hypoosmotic swelling is lost in failing cells.

- Sarcomere shortening was greater following β_1AR stimulation compared with β_2AR stimulation; hypoosmotic swelling does not affect both β_1AR- and β_2AR-induced shortening in human donor cardiomyocytes.

- Sarcomere shortening was decreased following β_1AR stimulation in DCM cardiomyocytes, while there was increased cAMP response in DCM cardiomyocytes following β_2AR stimulation.

A well-known phenotype of heart failure (HF) is cardiomyocyte hypertrophy, which was also observed in our failing cardiomyocytes. Hypoosmotic swelling increased cell volume by expanding cell width but not cell length in both healthy and failing cardiomyocytes. These changes in cell shape were accompanied by significant structural changes, particularly in the transverse tubule network. T-tubule density and regularity were significantly reduced in failing cardiomyocytes, consistent with findings by Schobesberger (Schobesberger et al., 2017). Similarly, our study showed a significant reduction in T-tubule density, regularity and directionality in MI cardiomyocytes. However, hypoosmotic swelling did not cause significant changes in T-tubule organisation, suggesting that the observed changes in β_2AR responses were likely due to changes in caveolae structure, rather than T-tubule deformation.

Cardiac Cav3 expression has been shown to decrease in hypertrophy and heart failure (Feiner et al., 2011), while Cav3 overexpression has been reported to attenuate the progression of cardiac hypertrophy (Horikawa et al., 2011). However, we observed an increase in Cav3 density in failing cardiomyocytes at 16 weeks post-MI, consistent with findings by Schobesberger et al. who reported that Cav3 dissociated from the membrane into the cytosol in early heart failure (8 weeks post-MI) followed by increased Cav3 protein levels at 16 weeks post-MI. A similar trend was observed by Wagner's group, who reported a significant increase in Cav3 expression at 8 weeks post-MI (Wagner et al., 2012). This rise in Cav3 has been suggested as a compensatory response during hypertrophic remodelling, and these conflicting

findings regarding Cav3 expression may be explained by differences in species, models, measured parameters, and the severity of heart failure. However, despite the increase in Cav3 density, this did not correspond with increased functional caveolae. Although Cav3 is a key component of the caveolar β_2AR signalling complex, the redistribution of β_2ARs suggests that the increased Cav3 density may not support the functionality of the signalling complex. Furthermore, we did not observe any differences in Cav3 expression between isosmotic and hypoosmotic conditions in either control or failing cardiomyocytes. This suggests that changes in membrane structure conformation did not alter Cav3 protein expression.

HF is associated with altered βAR populations in the human ventricular myocardium, characterised by a decrease in β_1AR and an unchanged β_2AR population (Bristow et al., 1986). In the failing heart, β_2ARs become crucial mediators of inotropic support in response to nonselective βAR agonist stimulation. Our findings indicate an increased β_2AR response in failing cardiomyocytes compared to controls, aligning with the work of Nikolaev and colleagues (Nikolaev et al., 2010). They demonstrated that β_2ARs redistribute from the T-tubules to the cell crest, leading to a more diffuse β_2AR-cAMP signalling pattern, similar to that seen in β_1ARs. Although the difference in β_2AR response between stretched and unstretched cells in failing cardiomyocytes diminishes, we observed a trend toward increased β_2AR activity following stretch. This suggests that cardiomyocytes in HF retain a stretch-sensitive mechanism. However, due to changes in membrane stiffness, failing cardiomyocytes may have reduced resistance to stretching, likely because of decreased caveolae mechanosensitivity, potentially impairing stretch-regulated β_2AR signalling.

Most previous studies have focused on rodents, and less is known about the compartmentation of βAR in human cardiomyocytes or its alteration in the HF. In nonfailing human hearts, β_1AR and β_2AR populations account for 77% and 23% of total βARs, respectively (Bristow et al., 1986). Moreover, β_1AR was shown to mediate 66% of the total contractile response following β_1AR stimulation. Our findings are consistent with this, as β_1AR-induced sarcomere shortening in human donor cardiomyocytes was significantly greater than that mediated by β_2ARs. However, the stretch-induced increase in β_2AR response observed in rats was not reproduced in human cells. This discrepancy could be due to the small sample size or donor sample heterogeneity.

HF significantly alters the proportion of βAR subtypes. In failing hearts, the β_1AR to β_2AR ratio shifts from 77:23 to 60:38, primarily due to a selective downregulation of the β_1AR rather than an increase in β_2AR concentration (Bristow et al., 1986). In our study, we found a significant decrease in β_1AR-induced contractile response in DCM samples. However, this reduction was not observed in β_1AR-induced cAMP production. In fact, we saw a significant increase in β_2AR-induced cAMP production in DCM samples.

Interestingly, previous studies have shown that in human βARs, β_2AR is more effective than β_1AR in stimulating adenylyl cyclase, indicating a lower efficacy parameter for β_1AR compared to β_2AR (Levy et al., 1993). Moreover, β_2AR stimulation leads to the phosphorylation of phospholamban, a response not observed in rodent hearts, and equal to that produced by β_1AR. In failing hearts, β_2AR activation increases phosphorylase activity, highlighting the role of the β_2AR-Gs protein pathway in the human heart (Molenaar et al., 2007). This may explain why there was no significant difference between β_1AR and β_2AR-induced cAMP production in

both donor and failing samples, as well as the observed increase in β_2AR-induced cAMP production in failing samples. However, more sample numbers should be given to draw definitive conclusions.

However, we noticed that there is a lack of correlation between contraction and cAMP production in human donors and failing cardiomyocytes. This could be due to the differing sensitivities of the β_1AR and β_2AR signalling pathways in HF. In HF, β_1AR are downregulated, which could lead to reduced sarcomere shortening even if some cAMP is produced. In contrast, β_2ARs are less affected by desensitisation and may be redistributed, leading to increased cAMP production in failing cells. However, the increased β_2AR-induced cAMP production may not fully compensate for the diminished β_1AR signalling in terms of contractile function. In addition, sarcomere shortening is dependent on intracellular calcium dynamics. In HF, calcium handling is often impaired, even when cAMP levels are elevated. If β_2ARs are producing cAMP but calcium handling proteins like the sarcoplasmic reticulum calcium ATPase (SERCA) are not functioning properly, this could explain why cAMP production is increased without a corresponding increase in sarcomere shortening. In addition, β_2ARs form a functional complex with L-type Ca^{2+} channels, and this transverse tubule coupling between LTCC and β_2AR was lost in the failing cells (Sanchez-Alonso et al., 2023). In contrast, β_1AR might more effectively stimulate the pathways that impact calcium release and uptake, thus resulting in a more pronounced contractile response under normal conditions. Moreover, in end-stage heart failure patients, a high sympathetic drive might be present due to the use of a clinical β-blocker. Inotropic support with catecholamine in brain-dead donors is also a potential confounding factor for the control group. Furthermore, the heterogeneity of donor samples and variations

in disease severity could contribute to the lack of correlation observed. Further investigation with a larger sample size is needed to understand these dynamics fully.

In human DCM samples, many cardiomyocytes may not survive during the isolation, incubation or even the stimulation process. As a result, our analysis is biased toward the surviving and responsive cells, which could explain why there is a lack of significant differences in sarcomere shortening between DCM and donor cardiomyocytes at baseline and also the preserved βAR responsiveness. The contractile response in DCM cells might therefore represent a subset of cells that still maintain functional βAR signalling, rather than being representative of all DCM cardiomyocytes. In addition, in isolated cells, there is an absence of a neurohumoral environment of heart failure, such as chronic exposure to high catecholamine levels, which may affect βAR desensitisation. In other words, the βAR response is not only due to intrinsic defects within the cardiomyocytes but is also influenced by external regulatory factors.

6.6 Conclusion

In conclusion, our study provides insights into the structural and βAR signalling alterations in HF. A characteristic phenotype of HF is hypertrophy, which was observed in our failing cardiomyocytes. Structural remodelling in HF included decreased TT density and regularity, alongside an increase in Cav3 density, suggested as a compensatory response during hypertrophic remodelling. Functionally, the increased β_2AR induced by membrane stretch via hypoosmotic swelling was lost in failing cardiomyocytes, indicating impaired mechanosensitivty in HF. In human donor cardiomyocytes, sarcomere shortening was greater with β_1AR stimulation than β_2AR stimulation, and hypoosmotic swelling did not impact β_1AR- or β_2AR-mediated shortening. This might be due to the lower sample numbers and the heterogeneity of donor samples. However, in dilated cardiomyopathy (DCM) cells, β_1AR-mediated sarcomere shortening was reduced, while β_2AR stimulation produced an increased cAMP response, revealing altered βAR signalling in DCM.

Chapter 7. General Discussion and Conclusions

In this project, the structural and functional roles of caveolae in mediating the βAR signalling following membrane stretch via a hypoosmotic swelling model were investigated in left ventricular (LV) cardiomyocytes. In addition, mechanical stretch was applied at the whole heart level using an inflated balloon, and the Langendorff optical mapping approach was used to investigate the regional difference in voltage and calcium between the apical and basal regions of the heart.

Key findings include:

- Membrane stretch caused an increased β_2AR response, and this increase was dependent on functional caveolae.
- Caveolae restructuring during membrane stretch disrupted β_2AR-G_i signalling and PDE4D regulation, leading to increased cAMP production and enhanced sarcomere shortening.
- Higher β_2AR response was observed in the apex compared to the base, and membrane stretch equalised the difference in β_2AR signalling between the apex and the base.
- Mechanical stretch via an inflated balloon increases the action potential duration in both apical and basal regions of the heart following β_2AR stimulation
- The stretch regulation of β_2AR signalling was lost in heart failure.
- The stretch-induced increase in β_2AR response observed in rats was not reproduced in human cells. In human donor cardiomyocytes, a higher β_1AR response was observed,

while decreased β_1AR response and increased β_2AR response were seen in cells from DCM patients.

7.1 Summary of Findings and Future Works

7.1.1 Caveolae Restructuring Following Membrane Stretch Decompartmented the β_2ARs Signalling and Disrupting the β_2AR-G_i Signalling

In Chapter 3, we first clarify the effect of membrane stretch on βAR signalling. We adapted the osmotic solutions from the previously published paper and modified them to be suitable for our contraction study. The model was validated, as we observed a significant reduction in the number of caveolae and an increase in cell size in hypoosmotic cells. cAMP production and cell contractility were measured using CytoCypher and FRET Microscopy. Our results revealed that membrane stretch caused an increased β_2AR response, including β_2AR-mediated cAMP production and contraction. We showed that this stretch-induced increase in β_2AR response was dependent on functional caveolae rather than T-tubule deformation or differences in sodium concentration between the two solutions. β_2ARs are pleiotropic receptors; in addition to coupling with G_s protein, they also associate with G_i protein, which acts to inhibit cAMP production and restrict the cAMP signal to the cell membrane surface (Nikolaev et al., 2010). A significant portion of G_i proteins, along with β_2AR, has been found in buoyant caveolar fractions of the cardiomyocytes (Head et al., 2005). Moreover, research has indicated that β_2AR-G_i signalling normally offsets the effect of β_2AR-G_s activation, serving as a regulatory mechanism to balance β_2AR activity when its activation levels become excessive (Calaghan and White, 2006). Therefore, we next investigated the effect of membrane stretch on the β_2AR-G_i signalling. We found that caveolae restructuring during membrane stretch disrupted β_2AR-G_i signalling, leading to enhanced sarcomere shortening.

7.1.2 Future Work

β_2AR are coupled to the G_s in an agonist-dependent manner, leading to the activation of adenylyl cyclase (AC) and an increase in intracellular cAMP levels. cAMP in turn activates PKA, which phosphorylates a number of substrates important for cardiac excitation-contraction coupling. These phosphorylation effects lead to positive inotropic and lusitropic effects, strengthening the function of the heart for increased circulatory demands. In this study, we transfected the cells with pmEPAC2 FRET sensor, which allows us to measure the cAMP activity at the plasma membrane. Future studies should measure the effect of stretch on both plasma membrane and cytosolic PKA activity levels following β_2AR stimulation using Lck-AKAR3 FRET sensors, which contain a motif reported to target membrane rafts, whereas AKAR3-NES FRET sensors contain a nuclear export signal that restricts this biosensor to the cytosol (Schott et al., 2016, Koschinski and Zaccolo, 2017) .

β_2AR-G_s activation causes G-protein-coupled receptor kinase 2 (GRK2) recruitment which phosphorylates the β_2AR at the plasma membrane (Madamanchi, 2007). This phosphorylation facilitates the recruitment of β-arrestins from the cytosol, which then interrupt the interaction between β_2AR and G_s, enhancing the G_i-biased β_2AR signalling (Krupnick and Benovic, 1998). In addition to GRK2, PKA could also phosphorylate β_2AR and directly associate with the functional switch from G_s to G_i coupling (Daaka et al., 1997). Previous studies have shown that although PKA and GSK2 β_2AR both target serine residues located in the third intracellular loop and C termini of β_2AR, their phosphorylation site are distinct. GRK phosphorylate at the $Ser^{355/356}$ site, whereas PKA phosphorylate at the $Ser^{261/262}$ site (Fan et al., 2016, Nobles et al., 2011). In our study, we demonstrated that membrane stretch induced by hypoosmotic swelling disrupts the G_i pathway, therefore causing an increase in β_2AR-induced cAMP

production and contraction. Therefore, it would be interesting to investigate the effect of membrane stretch on the β_2AR phosphorylation, to see whether the membrane stretch influences the β_2AR phosphorylation and also from which protein-mediated phosphorylation, either by GRK2 or PKA or both. Western blot will be performed in iso- and hypoosmotic cells, and the β_2AR phosphor-specific antibodies will be used for detection of β_2AR phosphorylation by PKA at Ser(P)$^{261/262}$ and the β_2AR phosphorylation by GRK at Ser(P)$^{355/356}$ (Liu et al., 2009).

β_2AR signalling is well compartmentalised and confined to the subsarcolemmal space, and cannot be transmitted to cytoplasmic and SR PKA target proteins (Nikolaev et al., 2006, Kuschel et al., 1999b). Caveolae restructuring following membrane stretch decompartmentalised the β_2AR-signalling, and in the future, we could identify which cellular compartments are accessible following membrane stretch. There are three main β_2AR mediated PKA-dependent phosphorylation sites that could be targeted. First is the sarcoplasmic protein (SR) phospholamban (PLB), which is phosphorylated by PKA at Ser^{16,} which relieves the inhibition of SR Ca^{2+}ATPase, SERCA, thus promoting the reuptake of Ca^{2+} (Kranias, 1985). RyR2, a protein in the membrane of the SR, is phosphorylated by PKA at Ser^{2809} and Ser^{2030}, increasing the release of Ca^{2+} from the SR (Rodriguez et al., 2003, Xiao et al., 2005). Also at the myofilaments, phosphorylation of cardiac muscle troponin I (CTnI) at Ser^{23} and Ser^{24}, reduces the Ca^{2+} sensitivity (Zhang et al., 1995).

Cardiac protein phosphatases (PP), including PP1, PP2A and PP2B are critical as local terminators of PKA target phosphorylation, which counterbalance the PKA activity (Weber et al., 2015). Most PP1 has been found in the plasma membrane, nucleus or near actin in the cardiomyocyte. While PP2B was predominantly localised to the T-tubule, it is activated by binding of calcium/calmodulin and, therefore, controls the calcium cycling (Chaklader and

Rothermel, 2021). PP2A could be found in the cytosol and nucleus; the study showed that PP2A-mediated dephosphorylation leads to downregulated LTCC activity (Heijman et al., 2013). Study from Kuschel et.al. suggested that phosphatase serves as a key element spatially controlling the β_2AR mediated cAMP/PKA signalling, as they found inhibition of protein phosphatase by calyculin A, enhanced the β_2AR but not β_1AR-mediated contractile response (Kuschel et al., 1999a). Furthermore, a study from MacDougall et.al. also supported the notion that phosphatase makes a major contribution to compartmentalisation of the β_2AR cAMP signalling. Additionally, the authors proposed that this mechanism is dependent on intact caveolae, as they showed that PP inhibition alone was conspicuous in showing robust decompartmentalisation of β_2AR-derived signalling in control cells and a comparatively diminutive effect after cholesterol depletion (Macdougall et al., 2012). Therefore, in future research, we could examine the potential involvement of protein phosphatase in β_2AR-mediated response following membrane stretch.

Prior studies have indicated that the presence of β_2AR signalling components, including β_2ARs, G_s, G_i, AC and LTCCs, in the caveolae-enriched membrane (Head et al., 2005). However, it remains unclear whether β_2AR is directly associated with AC, particularly AC6, which has been shown to be present in the caveolae (Thangavel et al., 2009). It is also unknown if β_2AR physically resides closer to AC under stretched conditions. This spatial reorganisation of signalling complexes might affect the β_2AR signalling. Therefore, it would be of potential interest to study the association between β_2AR and AC in control and stretched conditions.

Furthermore, we could scan the cardiomyocyte topography using Scanning Ion Conductance Microscopy (SICM), a non-optical technique that utilises a glass micropipette as a scanning probe to generate topographic images of cardiomyocytes. This approach allows for precise

characterisation of nanoscale structural features of cardiomyocytes, such as transverse (T) tubules, Z-grooves, and cell crests (Liu et al., 2013). We could measure the Z-groove index to assess cell regularity and evaluate the effect of stretch on the membrane integrity of cardiomyocytes. Additionally, combined nanoscale SICM-FRET could be used to measure the cAMP activity at specific cardiomyocyte nanodomain,s such as transverse T-tubules and caveolin-rich plasmalemma.

Caveolae are not only involved in β_2AR localisation but also play a role in transducing mechanical signals into downstream responses. However, while caveolae contribute to β_2AR compartmentation, the overall number of caveolae in adult ventricular cardiomyocytes is relatively low. Despite their low abundance, caveolae serve as essential microdomains that tightly regulate β_2AR activity, enabling locally confined signalling. The ability for caveolae to organise signalling molecules, modulate receptor trafficking and integrate mechanical signals makes them essential for β_2AR function. Further studies can use super-resolution imaging techniques, for example stimulated emission depletion (STED) microscopy or stochastic optical reconstruction microscopy (STORM), which allow us to analyse the precise colocalisation of β_2AR and Cav3 at 20-50nm resolution. In addition, live cell imaging using β_2AR-GFP to track real-time β_2AR trafficking in response to hypoosmotic swelling (Chen et al., 2013). Therefore, allow us to investigate whether stretch-induced β_2AR redistribution contributes to enhanced β_2AR-mediated contractility.

7.1.3 Caveolae Restructuring Induced by Membrane Stretch Disrupts PDE4D Regulation, Leading to Increased β_2AR Response.

PDEs are enzymes that hydrolyse cAMP, which play a key role in restricting the intracellular concentration gradients of cAMP signalling (Zaccolo, 2006). Among the PDE family, PDE4 has

been shown to play a key role in controlling βAR-mediated cAMP (Leroy et al., 2008a, Nikolaev et al., 2006). In addition, the study showed that PDE4B and PDE4D have been shown to localise in the caveolar membrane fractions and, in particular, PDE4D selectively impacts signalling by β_2AR (Wright et al., 2018a, Xiang et al., 2005). Therefore, in Chapter 4, we investigated how PDE4 and its subtypes PDE4D and PDE4B are involved in β_2AR signalling following membrane stretch. We found that membrane stretch distorted the PDE4 regulation, especially PDE4D, leading to increased cAMP production and enhanced sarcomere shortening. Although the result from the double immunostaining showed that colocalisation between Cav3 and PDE4D or PDE4B was reduced following membrane stretch, PDE4D has a greater influence on the cell function.

Studies have shown that the β-arrestin, a crucial factor in limiting the GPCR signalling, coordinates the β_2AR induced recruitment of PDE4D3 and PDE4D5, serving as adaptors for the translocation of PDE4Ds to activated receptors (Perry et al., 2002). Such recruitment allows β-arrestin to increase the rate of cAMP degradation and also recruits PDE4Ds, which can regulate the activity of PKA at the plasma membrane, thereby affecting the PKA phosphorylation of the β_2AR. In this current study, with the collaboration of Prof George Bailie, we used a PDE4D5- β-arrestin disruptive peptide to investigate whether membrane stretch disrupts the recruitment of β-arrestin mediated recruitment of PDE4D5, thus leading to increased β_2AR response. Our results from the contractility study revealed that membrane stretch enhanced β_2AR mediated contractility, a trend that was abolished by PDE4D5-β-arrestin disruptive peptide, indicating the essential role of the PDE4D5-β-arrestin complex in regulating the β_2AR-cAMP response.

7.1.4 Future Work

In this study, the role of PDE4D was studied using a selective PDE4D inhibitor, GEBR-7b. However, this inhibitor does not distinguish between the catalytic sites of PDE4B and PDE4D (Brullo et al., 2014). Ideally, the use of PDE4DKO transgenic mice would be preferred, alternatively, our collaborator, Professor George Baillie, has developed a novel potent PDE4D inhibitor, PROTAC 184, which is a more economical option. PROTAC (proteolysis targeting chimera) links PDE4D with an E3 ligase, directing PDE4D to the proteasomal degradation machinery inside the cell, resulting in its silencing. Therefore, future studies could be performed using PROTAC 184, with cells pretreated with PROTAC 184 for 24H prior to the experiment, allowing sufficient time for the degradation process to target PDE4D effectively.

During our contraction study, we observed increased arrhythmic events following inhibition of either PDE4D or PDE4B. The RyR2 located on the sarcoplasmic reticulum (SR) is the primary calcium release channel required for excitation-contraction coupling in heart muscles. Previous studies have shown that PDE4D deficiency mice are prone to arrhythmias due to defective regulation of the RyR2 channel. This is associated with PKA hyperphosphorylation of RyR2 and depletion of the RyR2-stabilising protein calstabin2, which normally prevents calcium leak from the SR into the cytosol through RyR (Lehnart et al., 2005a). Furthermore, a study from Kraft et al. showed PDE4B-deficient mice exhibited additional spontaneous afterbeats following isoprenaline stimulation, suggesting that PDE4B regulates cAMP levels near RyR2, thereby controlling calcium leak and isoprenaline-induced ventricular arrhythmias (Kraft et al., 2024). In addition, both PDE4B and PDE4D are tethered to the LTCC, ablation of PDE4B leads to increased $I_{Ca,L}$ during βAR stimulation. Further research could investigate the

effect of membrane stretch on calcium channel open probability, calcium leak and calcium sparks following β_2AR activation.

β_2ARs form complexes with a set of PDE4D isoforms within cardiomyocytes, with the study showing that the PDE4D9 and PDE4D8 isoforms preferentially bind to β_2AR in the neonatal cardiomyocytes. These isoforms regulate the β_2AR induced contraction rate responses and cAMP accumulation (De Arcangelis et al., 2009b). The same study revealed that β_2AR simulation causes PDE4D9 to dissociate from the receptor while facilitating the recruitment of PDE4D8 and PDE4D5 via β-arrestin. It would be interesting to investigate the colocalisation between Cav3 and other PDE4D isoforms, such as PDE4D8 and PDE4D9.

In addition, we could do cell fractionation and subsequently measure the amounts of Cav3, PDE4B, and PDE4D in membrane and cytosolic fractions using Western blot. This would allow us to investigate whether, under membrane stretch, these proteins dissociate from the membrane into the cytosol.

Previous co-immunoprecipitation (Co-IP) results demonstrated that disruption of the PDE4D5 interaction with β-arrestin occurred in HEK-B2 cells when treated with the disruptive peptide. However, similar validation work using co-IP should be done with rat adult ventricular cardiomyocytes. In parallel, proximity ligation assay could be used in cells treated with disruptive peptide and scramble peptide to visualise and quantify the interaction between PDE4D5 and β-arrestin, confirming the model. Furthermore, the interaction of PDE4D and Cav3 following membrane stretch needs to be assessed after treatment with a disruptive peptide. In addition, cAMP production following the disruptive peptide treatment should be measured to understand how this complex contributes to β_2AR mediated cAMP production under membrane stretch conditions. Finally, as our study previously demonstrated that

membrane stretch disrupts the β_2AR-G_i signalling; future studies could investigate the effects of PTX treatment after disrupting the PDE4D5-β-arrestin complex with a disruptive peptide under both osmotic conditions. This would help clarify the role of the PDE4D5-β-arrestin complex in regulating the switch between G_s and G_i protein coupling to activated β_2AR.

7.1.5 Membrane Stretch Equilibrates the Difference in β_2AR Signalling Between the Apex and the Base

There is growing evidence showing the regional differences across the myocardium, and the compartmentalisation of β_2AR signalling is closely linked to the structural organisation within cardiomyocytes. In Chapter 5, we investigated the regional differences in caveolae-based stretch-regulation of β_2 adrenoceptor signalling by studying cells from the apical and basal of the heart. Our study, consistent with prior findings, shows that contractile responses following β_2AR stimulation were higher in the apex compared to the base (Paur et al., 2012, Wright et al., 2018a) . This can be explained by the lower number of caveolae and less organised T-tubules in apical cells, which allows for greater diffusion of cAMP and enhances the phosphorylation of proteins involved in contraction. Whereas basal cardiomyocytes, with their more complex membrane structures, exhibit more regulated cAMP activity. We also found that membrane stretch via hypoosmotic swelling significantly increased the β_2AR response in basal cells but had little effect on apical cells, balancing the responses between the two regions. This suggests that the increase in sarcomere shortening and cAMP production after β_2AR stimulation during membrane stretch is primarily driven by its effects on basal cardiomyocytes, which have more caveolae and are therefore more sensitive to membrane stretch.

In addition to membrane stretch at the cellular level, we also applied mechanical stretch on the intact heart by inflating the left ventricle and assessing cardiac electrical activity at the whole heart level. Our results revealed that the basal myocardium exhibited a prolonged action potential duration (APD) compared to the apical myocardium following β_2AR stimulation, which might be due to the higher abundance of the delayed rectifier K^+ current in the apex than the base (Szentadrassy et al., 2005). Additionally, stretch increases the APD70 in both the apex and base after β_2AR stimulation, potentially due to stretch-induced reduction in outward potassium currents (I_{to}, I_{ss}) and changes in inward currents, including slowed inactivation of I_{Ca},L and increased $I_{Na,L}$.

7.1.6 Future Work

A study by Wright et.al. showed that higher PDE4 activity was observed in basal cells compared with apical cells, leading to tighter control of β_2AR-cAMP signalling (Wright et al., 2018a). Future research should focus on exploring the impact of PDE4 inhibition, especially PDE4B and PDE4D, on β_2AR signalling in apical and basal cardiomyocytes following stretch. Additionally, examining the expression levels of PDE4B and PDE4D proteins in the apex and base and also membrane stretch affects the PDE4B/D protein expression, which would help clarify the molecular basis for these regional differences.

Alongside this, future studies could also characterise the regional differences in ion channel activity under stretch conditions. By analysing the activity of specific ion channels, such as $I_{Ca,L}$, in the apex and base using patch-clamp techniques could better understand the ionic mechanisms that contribute to the observed differences in action potential duration (APD) across the apex and base. In addition, in the Langendorff-optical mapping experiments, in addition to voltage and calcium transient, we could also assess the arrhythmogenicity through

programmed electrical stimulation. Therefore, we could determine whether mechanical stretch influences the incidence of arrhythmias in the heart.

7.1.7 Stretch-sensitivity of β_2-adrenoceptor Signalling was Lost in Falling Cells

Changes in cardiac contractility in response to stretch play a crucial role in maintaining cardiac function over the long term, particularly as demands on the heart change. Heart failure often results in losing the slow force response to stretch (Lookin and Protsenko, 2019). Heart diseases that are associated with changes to mechanical stresses also show a higher risk of arrhythmias, for example, in dilated cardiomyopathy (Meinertz et al., 1984) and hypertension (Hennersdorf and Strauer, 2001), where there is increased ventricular wall stress. Patients with these conditions are known to have reduced exercise capacity and poor tolerance to volume overload (Maeder and Kaye, 2009). Therefore, identifying molecular changes induced by cardiac stretch is essential, as these changes could be potential targets for pharmacological intervention. In Chapter 6, we investigated the effect of membrane stretch on βARs signalling in failing ventricular cardiomyocytes. A decreased T-tubule structure and increased Cav3 density were found in the cells from 16-week MI, which was consistent with the previous findings from Schobesberger et al. (Schobesberger et al., 2017). In addition, the increase we showed in the β_2ARs response following stretch was lost in the failing cells, suggesting a compromised stretch-sensitive β_2AR signalling pathway in heart failure. This loss may indicate that failing cardiomyocytes are less able to adapt their contractile response to mechanical stress, which could contribute to reduced cardiac resilience in heart failure. This diminished response might also be due to the β_2AR signalling already responding at or near its maximal capacity in failing cardiomyocytes, leaving little room for further modulation under stress conditions.

We also explored the effect of membrane stretch in βARs signalling in human donor cardiomyocytes; however, we did not show any effect on either β_1AR or β_2ARs response following membrane stretch, which might be due to the donor sample heterogeneity. Additionally, we observed a decreased β_1AR-mediated contractile response in DCM cardiomyocytes, alongside an increased β_2AR-induced cAMP response, consistent with findings suggesting β_1AR downregulation in heart failure, while β_2AR are redistributed and consequently exhibit a β_1AR-like response.

7.1.8 Future Work

Although the disparity in β_2AR response between stretched and unstretched cells in failing cardiomyocytes diminishes, an increased trend following stretching is noted. This suggests that cardiomyocytes retain a stretch-sensitive mechanism in heart failure. However, due to the changes in membrane stiffness, these cells might show reduced resistance to stretching, potentially impairing stretch-regulated β_2AR signalling. For future research, we could measure the cardiomyocytes stiffness (quantified by the Young's modulus) with the SICM.

Additionally, a study from Schobesberger et al. showed that the progression to a heart failure phenotype is non-linear, with significant changes in T-tubule structure and β_2AR-mediated cAMP signalling observed at 4-week post-MI. At 8 weeks post-MI, β_2AR-mediated cAMP signalling briefly recovers, but by 16 weeks, complete disorganisation of β_2AR-cAMP signalling occurs due to altered receptor localisation and structural changes within the cells (Schobesberger et al., 2017). Therefore, in future studies, we could investigate how the stretch-regulated β_2AR signalling changes throughout the progression of heart failure, using cells isolated from 4-, 8-, and 16-week post-myocardial infarction.

The stretch-induced increase in β_2AR response observed in rats was not reproduced in human donor cells. This could be due to the lower sample number. Therefore, we could increase the n number in future studies.

7.2 Limitations

Studies in this thesis have several limitations. First, the hypoosmotic swelling model was used to induce the membrane stretch and assess its effects on cAMP production, sarcomere shortening and calcium transients. While this model is widely used to investigate stretch-induced responses, it does not fully replicate the mechanical environment of the myocardium. In the intact heart, myocardial stretch during physiological conditions, such as ventricular filling, typically occurs in a longitudinal direction, resulting in increased cell length, rather than width. In contrast, hypoosmotic swelling primarily increases in cell width but not length, suggesting a limitation of this model in mimicking the nature of physiological stretch experienced in the heart. However, despite this limitation, the hypoosmotic swelling model is still valuable for investigating membrane stretch-related mechanisms, particularly the caveolae-associated signalling. While it may not perfectly replicate physiological stretch, it still provides important insights into how caveolae structure regulates the β_2AR signalling in response to membrane deformation.

The key limitation of the hypoosmotic swelling model is the dilution of intracellular ionic composition, which can influence ion channel activity, and in turn, affect calcium transient and contractility. Intracellular Na^+ dilution may inhibit the Ca^{2+} release via NCX, contributing to higher intracellular Ca^{2+}, therefore enhancing contraction. A study from Brette et al. suggested that hypoosmotic swelling induces a biphasic response in cardiomyocytes, where calcium transients and contraction initially increase (50-70s) but subsequently decline after 7-10

minutes of exposure (Brette et al., 2000). In addition, a study from Bewick et al. suggested that swelling-induced Na^+/K^+ pump activation is independent of extracellular Na^+ and Ca^{2+} influx and is mediated by phosphorylation and dephosphorylation events rather than changes in ion concentrations (Bewick et al., 1999). Furthermore, β-agoinst isoprenaline stimulation has been shown to increase phosphorylation of series downstream signalling through the action of protein kinase A (Colyer, 1993) There was no significant difference in sarcomere shortening and calcium transient in hypoosmotic cells compared with isosmotic cells at the baseline measurement. Taken together, these findings suggest that the enhanced β_2AR induced contractile response following 15min exposure to hypoosmotic solution is likely mediated by increased phosphorylation events, and dilution of intracellular ions does not account for that. Our hypoosmotic solution has the same composition as isosmotic solution except for a reduction in NaCI concentration from 118mM to 81mM, which may also have influenced the observed responses. While we have validated that the reduction in NaCI did not influence the cAMP production, whether this reduction in NaCI affects the calcium transients and sarcomere shortening in this model remains unknown. Wong et al. demonstrated that hypoosmotic swelling leads to a rapid and significant increase in intracellular calcium levels, which peaks within seconds and then gradually declines (Wong et al., 1990). Their findings suggest that this increase is driven by calcium influx from the extracellular environment, not mediated by NCX, suggesting that the calcium response is a direct consequence of cell swelling rather than NaCI reduction. In the future study, the patch-clamp technique could be used to measure the channel and current activity, specifically, the LTCC and NCX under isosmotic and hypoosmotic conditions, both at baseline and following β_2AR stimulation, which would help to determine whether cell swelling directly modulates these channels. We could also test whether hypoosmotic swelling increases protein

phosphorylation, such as LTCC, RyR, and PLN following β_2AR stimulation using western blot, which would help to validate whether signalling, rather than ion fluxes, leads to the contractile response.

Culturing cardiomyocytes following isolation has always been a concern, as they may lose their structural integrity. For example, a reduction or even loss of the T-tubular density can occur after prolonged culturing in both rat and human cardiomyocytes (Leach et al., 2005, Louch et al., 2004). This presents challenges for culturing rat cardiomyocytes for FRET experiments, as transfection with FRET sensor requires a 48h incubation period. This culture-induced structural disruption, combined with the potential damage from adenoviral entry, may impair the signalling. Therefore, in the future, it would be advantageous to do experiments using cells from transgenic mice that express the FRET sensor, and we can do experiments directly after isolation.

In this study, we used Fura-2, a ratiometric and highly sensitive indicator dye for measuring intracellular calcium. Several literatures have demonstrated that a reduction in ionic strength can increase the affinity of Fura-2 for calcium (Uto et al., 1991, Wong et al., 1990). Wong et al. showed that a 15% reduction in ionic strength had no effect on the Kd of fura-2, where Kd is the dissociation constant between fura-2 and free Ca^{2+}. However, when the ionic strength was reduced by 30%, the Kd decreased to 40% of its control value (Wong et al., 1990). When cells are exposed to a hypoosmotic solution, the solution enters the cells due to the osmotic gradient, leading to dilution of intracellular ion concentration and a reduction in the intracellular ionic strength. As a result, if the degree of cell swelling leads to intracellular dilution exceeding 15%, there is a possibility that the Kd of fura-2 decreases, which could artificially increase the fura-2 signal for a given intracellular calcium level. Therefore, to ensure

accurate and reliable calcium measurements, future studies need to clarify the change in ionic strength of cardiomyocytes following hypoosmotic swelling and also the Kd of fura-2 following hypoosmotic swelling (Bers, 1982).

CytoCypher is a high-throughput system which allows for the measurement of 15-20 cells at once, which means more time is required to complete a full cycle of measurements. The time between measuring the first cell and the last cell is not the same, which could cause a problem. Sustained isoprenaline stimulation may lead to receptor desensitisation, resulting in inconsistent measurement of cell contractility. In addition, when measuring contractility following a series of pharmacological treatments - as shown in Chapter 4 – we measured responses after treatment with isoprenaline (a βAR-agonist), GEBR-7b (a PDE4D inhibitor), A33 (a PDE4B inhibitor) and Rolipram (PDE4 inhibitor) treatments. These series of treatments along with prolonged stimulation may increase cell mortality and induce arrhythmias. Therefore, as outlined in the future plans, cells could be pretreated with PROTAC 184, and therefore we can examine the role of PDE4D in βAR by administering isoprenaline only during the experiments.

In this study, caveolae depletion was accomplished using the cholesterol-depleting agent, MβCD, as cholesterol is a key component of caveolae. Disruption of lipid rafts via cholesterol depletion leads to the removal of caveolae. While MβCD is commonly used to deplete caveolae, its specificity for caveolae remains unclear. Given that caveolin-3 is a key scaffolding protein for caveolae formation, future studies could be done using Cav-3 knockout mouse cells or Cav-3-specific siRNA transfection to investigate this mechanism further.

In the confocal imaging described in Chapter 3, we did not use Z-stack imaging but instead selected the best single plane, and within that plane, we chose five regions to calculate the

density and regularity of T-tubule and Cav3. A potential limitation is that cardiomyocytes are 3D structures, and the T-tubular or Cav3 protein organisation can vary significantly across different planes. Without Z-stack imaging, variations in density and regularity throughout the full depth of the cells may not be fully captured. This concern was addressed in the following chapter, where images were captured using Z-stack imaging.

In the colocalisation study, first of all, due to the low resolution, it might be difficult to calculate the exact distance between two pixels, which might lead to our results being over concluded. Therefore, as discussed in the previous section, other experimental approaches, such as proximity ligation assay, need to be done to confirm the interaction between two proteins. Additionally, in the present study, homemade primary antibodies of PDE4D and PDE4B were used, which might have lower specificity and therefore increase the risk of false-positive or false-negative results.

In the Langendorff-optical mapping experiment, a balloon pressure of 60mmHg was applied to assess ventricular function, however, it remains unclear whether this pressure induced significant ventricular stretch. The pressure recorded in this setup is the balloon pressure rather than LV end-diastolic pressure, which is around 5mmHg in 4-month rat heart (Pacher et al., 2004). However, in isolated perfused rat hearts, previous studies have demonstrated that balloon inflation up to 150ul generates LV pressures of around 50mmHg, which evoke ectopics (Hurley et al., 2023). In addition, Sung et al. showed that LV filling pressure of 30mmHg leads to epicardial conduction slowing and APD duration prolongation (Sung et al., 2003). Similarly, Li et al. found that balloon inflation to 35mmHg triggered vascular endothelial growth factor via TGF- activation (Li et al., 1997). Moreover, Nakagawa et al. showed that raising left ventricular end diastolic pressure to 60mmHg preconditioned post-ischaemic

myocardial dysfunction, although the exact mechanism of stretch-preconditioning in rats was not yet studied (Nakagawa et al., 1997). Furthermore, Zabel et al. demonstrated that intraventricular balloon inflation from 200 to 750µl produced significant, timing-dependent changes in action potential morphology. Their study showed that stretch applied during late repolarisation or diastole caused transient depolarisation and triggered premature ventricular contractions, while stretch during early systole induced transient repolarisation (Zabel et al., 1996). Therefore, it is reasonable to argue that 60mmHg balloon pressure theoretically induced LV stretch. Studies have also demonstrated that mechanical stretch can induce arrhythmias via Purkinje fibre activation, mediated through mechanosensitive ion channels TRPM4 activation (Hurley et al., 2023). However, they found that arrhythmias occurred as the LV volume was increased and spontaneously ceased within 20s of the onset of LV inflation. In our experiment, we inflated the balloon at the set-up stage, and when we performed the measurement, the heart had already become stable. However, we still need to check whether our hearts have been stretched. To address this limitation, one potential experiment is to slice the LV tissue after the experiment and do the Wheat Germ Agglutinin (WGA) staining, which stains the cardiomyocyte membranes and allows us to measure the cardiomyocyte width and length. By comparing the sham and stretched heart, we can determine whether the myocardium undergoes structural deformation.

We used blebbistatin in our langendorff optical mapping experiment, a commonly used excitation-contraction uncoupler, to remove the motion artefacts. A Study by Kappadan et al. reported that blebbistatin increased action potential duration by 25% (Kappadan et al., 2020). However, the differences between experimental groups may still persist, as all groups were exposed to the same dose of blebbistatin. The ventricular free wall comprises three layers: subendocardium, midmyocardium, and subepicardium (Lang et al., 2015). A Study from Lang

et.al. showed that the action potential duration decreased from the epicardium toward the endocardium following β_2 stimulation. In addition, regarding β_2AR protein expression, there was higher β_2AR expression in the endocardium compared to the epicardium (Lang et al., 2015). However, the transmembrane voltage transients we got from the optical mapping were recorded from the epicardial surface of the heart (Efimov et al., 2004). This limitation may have affected our ability to fully capture the βAR signalling across the ventricular wall. In addition, in this study, we did not measure the calcium transient amplitude because it is influenced by the fluorescence signal of the calcium dye rather than being a direct reflection of calcium concentration. For instance, factors such as poor perfusion or uneven dye loading can result in regions with lower dye fluorescence, leading to an artificially reduced signal amplitude. However, this reduction does not necessarily indicate a lower calcium concentration in those areas; it just reflects insufficient dye presence. As a result, the calcium transient amplitude may not accurately represent the underlying calcium dynamics. Furthermore, the small sample size is another limitation of the optical mapping experiment. We did the power calculation based on the pilot study, and we found that in order to achieve a significance level of 0.05 with a power of 0.9, a minimum of 7 rats would be required. Future studies with a larger sample size would help strengthen our findings.

7.3 Final conclusion

In conclusion, this thesis has expanded the current understanding of stretch-induced regulation in the βAR signalling and revealed the role of mechanosensitive nanodomain-caveolae in this regulation by:

- Demonstrating that membrane stretch, via hypoosmotic swelling, significantly enhances β_2AR signalling in rat cardiomyocytes, leading to increased cAMP production and sarcomere shortening. This enhancement is dependent on functional caveolae and is lost in heart failure.
- Showing that caveolae restructuring due to stretch disrupts the regulation of β_2AR-G_i signalling and PDE4, impairing β_2AR compartmentalisation, promoting a shift toward G_s-mediated signalling and enhancing contractility.
- Revealing regional differences in β_2AR response, where apical cardiomyocytes exhibit a stronger basal response to β_2AR stimulation, while membrane stretch predominantly affects basal cells, equilibrating the β_2AR responses between apical and basal regions.
- Showing that in HF the enhancement of β_2AR response is lost

Taken together, these findings not only contribute to the understanding of how stretch modulates βAR signalling but also highlight the importance of caveolae in maintaining proper βAR function. The study demonstrates that caveolae are critical for maintaining compartmentalised β_2AR signalling and that membrane stretch disrupts this organisation, suggests that restoring or preserving caveolar structure could be a novel approach to enhance βAR function in failing hearts. Therapeutic approaches might include targeting structural components such as Cav3 or modulating key regulatory proteins like PDE4D and β-arrestin.

Since the stretch-induced enhancement of β_2AR signalling is lost in heart failure, reinstating this pathway may help improve contractile reserve. Furthermore, understanding the regional variation in these responses within the heart could help the development of more tailored, nanodomain-specific therapies.

References

ADAPALA, R. K., THOPPIL, R. J., LUTHER, D. J., PARUCHURI, S., MESZAROS, J. G., CHILIAN, W. M. & THODETI, C. K. 2013. TRPV4 channels mediate cardiac fibroblast differentiation by integrating mechanical and soluble signals. Journal of Molecular and Cellular Cardiology, 54**,** 45-52.

AHLES, A. & ENGELHARDT, S. 2014. Polymorphic Variants of Adrenoceptors: Pharmacology, Physiology, and Role in Disease. Pharmacological reviews, 66**,** 598-637.

AKAR, F. G. & ROSENBAUM, D. S. 2003. Transmural Electrophysiological Heterogeneities Underlying Arrhythmogenesis in Heart Failure. Circulation Research, 93**,** 638-645.

AKAR, F. G., YAN, G.-X., ANTZELEVITCH, C. & ROSENBAUM, D. S. 2002. Unique Topographical Distribution of M Cells Underlies Reentrant Mechanism of Torsade de Pointes in the Long-QT Syndrome. Circulation, 105**,** 1247-1253.

ALLEN, D. G. & KENTISH, J. C. 1985. The cellular basis of the length-tension relation in cardiac muscle. J Mol Cell Cardiol, 17**,** 821-40.

ALLEN, D. G. & KURIHARA, S. 1982. The effects of muscle length on intracellular calcium transients in mammalian cardiac muscle. J Physiol, 327**,** 79-94.

ALVAREZ, B. V., PÉREZ, N. G., ENNIS, I. L., CAMILIÓN DE HURTADO, M. C. & CINGOLANI, H. E. 1999. Mechanisms Underlying the Increase in Force and Ca²⁺ Transient That Follow Stretch of Cardiac Muscle. Circulation Research, 85**,** 716-722.

ANTZELEVITCH, C. & FISH, J. 2001. Electrical heterogeneity within the ventricular wall. Basic Res Cardiol, 96**,** 517-27.

AZEVEDO, M. F., FAUCZ, F. R., BIMPAKI, E., HORVATH, A., LEVY, I., DE ALEXANDRE, R. B., AHMAD, F., MANGANIELLO, V. & STRATAKIS, C. A. 2014. Clinical and molecular genetics of the phosphodiesterases (PDEs). Endocr Rev, 35**,** 195-233.

BAHIT, M. C., KOCHAR, A. & GRANGER, C. B. 2018. Post-Myocardial Infarction Heart Failure. JACC: Heart Failure, 6**,** 179-186.

BAILLIE, G. S., MACKENZIE, S. J., MCPHEE, I. & HOUSLAY, M. D. 2000. Sub-family selective actions in the ability of Erk2 MAP kinase to phosphorylate and regulate the activity of PDE4 cyclic AMP-specific phosphodiesterases. Br J Pharmacol, 131**,** 811-9.

BAILLIE, G. S., SOOD, A., MCPHEE, I., GALL, I., PERRY, S. J., LEFKOWITZ, R. J. & HOUSLAY, M. D. 2003. β-Arrestin-mediated PDE4 cAMP phosphodiesterase recruitment regulates β-adrenoceptor switching from G_s to G_i. Proceedings of the National Academy of Sciences, 100**,** 940-945.

BALIJEPALLI, R. C., FOELL, J. D., HALL, D. D., HELL, J. W. & KAMP, T. J. 2006. Localization of cardiac L-type Ca(2+) channels to a caveolar macromolecular signaling complex is required for beta(2)-adrenergic regulation. Proc Natl Acad Sci U S A, 103**,** 7500-5.

BALIJEPALLI, R. C. & KAMP, T. J. 2008. Caveolae, ion channels and cardiac arrhythmias. Prog Biophys Mol Biol, 98**,** 149-60.

BANERJEE, I., FUSELER, J. W., PRICE, R. L., BORG, T. K. & BAUDINO, T. A. 2007. Determination of cell types and numbers during cardiac development in the neonatal and adult rat and mouse. Am J Physiol Heart Circ Physiol, 293**,** H1883-91.

BARONE, I., GIORDANO, C., BONOFIGLIO, D., ANDÒ, S. & CATALANO, S. 2015. Phosphodiesterase type 5 and cancers: Progress and challenges. Oncotarget, 8.

BECA, S., HELLI, P. B., SIMPSON, J. A., ZHAO, D., FARMAN, G. P., JONES, P., TIAN, X., WILSON, L. S., AHMAD, F., CHEN, S. R. W., MOVSESIAN, M. A., MANGANIELLO, V., MAURICE, D. H., CONTI, M. & BACKX, P. H. 2011. Phosphodiesterase 4D regulates baseline sarcoplasmic reticulum Ca2+ release and cardiac contractility, independently of L-type Ca2+ current. Circ Res, 109**,** 1024-1030.

BERS, D. M. 1982. A simple method for the accurate determination of free [Ca] in Ca-EGTA solutions. American Journal of Physiology-Cell Physiology, 242**,** C404-C408.

BEWICK, N. L., FERNANDES, C., PITT, A. D., RASMUSSEN, H. H. & WHALLEY, D. W. 1999. Mechanisms of Na+-K+pump regulation in cardiac myocytes during hyposmolar swelling. American Journal of Physiology-Cell Physiology, 276**,** C1091-C1099.

BOGAERT, J., BOSMANS, H., MAES, A., SUETENS, P., MARCHAL, G. & RADEMAKERS, F. E. 2000. Remote myocardial dysfunction after acute anterior myocardial infarction: impact of left ventricular shape on regional function: a magnetic resonance myocardial tagging study. J Am Coll Cardiol, 35**,** 1525-34.

BOLGER, G. B., BAILLIE, G. S., LI, X., LYNCH, M. J., HERZYK, P., MOHAMED, A., HIGH MITCHELL, L., MCCAHILL, A., HUNDSRUCKER, C., KLUSSMANN, E., ADAMS, D. R. & HOUSLAY, M. D. 2006. Scanning peptide array analyses identify overlapping binding sites for the signalling scaffold proteins, β-arrestin and RACK1, in cAMP-specific phosphodiesterase PDE4D5. Biochemical Journal, 398**,** 23-36.

BOLGER, G. B., MCCAHILL, A., HUSTON, E., CHEUNG, Y.-F., MCSORLEY, T., BAILLIE, G. S. & HOUSLAY, M. D. 2003. The Unique Amino-terminal Region of the PDE4D5 cAMP Phosphodiesterase Isoform Confers Preferential Interaction with β-Arrestins*. Journal of Biological Chemistry, 278**,** 49230-49238.

BOULARAN, C. & GALES, C. 2015. Cardiac cAMP: production, hydrolysis, modulation and detection. Front Pharmacol, 6**,** 203.

BRAHMAJOTHI, M. V., MORALES, M. J., REIMER, K. A. & STRAUSS, H. C. 1997. Regional localization of ERG, the channel protein responsible for the rapid component of the delayed rectifier, K+ current in the ferret heart. Circ Res, 81**,** 128-35.

BRAIDOTTI, N., CHEN, S. N., LONG, C. S., COJOC, D. & SBAIZERO, O. 2022. Piezo1 Channel as a Potential Target for Hindering Cardiac Fibrotic Remodeling. Int J Mol Sci, 23.

BRETTE, F., CALAGHAN, S. C., LAPPIN, S., WHITE, E., COLYER, J. & LE GUENNEC, J. Y. 2000. Biphasic effects of hyposmotic challenge on excitation-contraction coupling in rat ventricular myocytes. Am J Physiol Heart Circ Physiol, 279**,** H1963-71.

BRISTOW, M. R., GINSBURG, R., MINOBE, W., CUBICCIOTTI, R. S., SAGEMAN, W. S., LURIE, K., BILLINGHAM, M. E., HARRISON, D. C. & STINSON, E. B. 1982. Decreased catecholamine sensitivity and beta-adrenergic-receptor density in failing human hearts. N Engl J Med, 307**,** 205-11.

BRISTOW, M. R., GINSBURG, R., UMANS, V., FOWLER, M., MINOBE, W., RASMUSSEN, R., ZERA, P., MENLOVE, R., SHAH, P., JAMIESON, S. & ET AL. 1986. Beta 1- and beta 2-adrenergic-receptor subpopulations in nonfailing and failing human ventricular myocardium: coupling of both receptor subtypes to muscle contraction and selective beta 1-receptor down-regulation in heart failure. Circ Res, 59**,** 297-309.

BRULLO, C., MASSA, M., ROCCA, M., ROTOLO, C., GUARIENTO, S., RIVERA, D., RICCIARELLI, R., FEDELE, E., FOSSA, P. & BRUNO, O. 2014. Synthesis, Biological Evaluation, and Molecular Modeling of New 3-(Cyclopentyloxy)-4-methoxybenzaldehyde O-(2-(2,6-Dimethylmorpholino)-2-oxoethyl) Oxime (GEBR-7b) Related Phosphodiesterase 4D (PDE4D) Inhibitors. Journal of Medicinal Chemistry, 57**,** 7061-7072.

BRUSS, M. D., RICHTER, W., HORNER, K., JIN, S. L. & CONTI, M. 2008. Critical role of PDE4D in beta2-adrenoceptor-dependent cAMP signaling in mouse embryonic fibroblasts. J Biol Chem, 283**,** 22430-42.

BRYANT, S. M., KONG, C. H. T., WATSON, J. J., GADEBERG, H. C., JAMES, A. F., CANNELL, M. B. & ORCHARD, C. H. 2018a. Caveolin 3-dependent loss of t-tubular I(Ca) during hypertrophy and heart failure in mice. Exp Physiol, 103**,** 652-665.

BRYANT, S. M., KONG, C. H. T., WATSON, J. J., GADEBERG, H. C., ROTH, D. M., PATEL, H. H., CANNELL, M. B., JAMES, A. F. & ORCHARD, C. H. 2018b. Caveolin-3 KO disrupts t-tubule structure and decreases t-tubular I(Ca) density in mouse ventricular myocytes. Am J Physiol Heart Circ Physiol, 315**,** H1101-h1111.

BRYANT, S. M., SHIPSEY, S. J. & HART, G. 1999. Normal regional distribution of membrane current density in rat left ventricle is altered in catecholamine-induced hypertrophy. Cardiovascular Research, 42**,** 391-401.

BUSIJA, A. R., PATEL, H. H. & INSEL, P. A. 2017. Caveolins and cavins in the trafficking, maturation, and degradation of caveolae: implications for cell physiology. Am J Physiol Cell Physiol, 312**,** C459-c477.

CALAGHAN, S., KOZERA, L. & WHITE, E. 2008. Compartmentalisation of cAMP-dependent signalling by caveolae in the adult cardiac myocyte. Journal of molecular and cellular cardiology, 45**,** 88-92.

CALAGHAN, S. & WHITE, E. 2006. Caveolae modulate excitation–contraction coupling and β2-adrenergic signalling in adult rat ventricular myocytes. Cardiovascular Research, 69**,** 816-824.

CALAGHAN, S. C., COLYER, J. & WHITE, E. 1999a. Cyclic AMP but not phosphorylation of phospholamban contributes to the slow inotropic response to stretch in ferret papillary muscle. Pflügers Archiv, 437**,** 780-782.

CALAGHAN, S. C., COLYER, J. & WHITE, E. 1999b. Cyclic AMP but not phosphorylation of phospholamban contributes to the slow inotropic response to stretch in ferret papillary muscle. Pflugers Arch, 437**,** 780-2.

CAMELLITI, P., BORG, T. K. & KOHL, P. 2005. Structural and functional characterisation of cardiac fibroblasts. Cardiovascular Research, 65**,** 40-51.

CHAKLADER, M. & ROTHERMEL, B. A. 2021. Calcineurin in the heart: New horizons for an old friend. Cell Signal, 87**,** 110134.

CHEN, M., ZAYTSEVA, N. V., WU, Q., LI, M. & FANG, Y. 2013. Microplate-compatible total internal reflection fluorescence microscopy for receptor pharmacology. Appl Phys Lett, 102**,** 193702.

CHEN-IZU, Y., XIAO, R. P., IZU, L. T., CHENG, H., KUSCHEL, M., SPURGEON, H. & LAKATTA, E. G. 2000. G(i)-dependent localization of beta(2)-adrenergic receptor signaling to L-type Ca(2+) channels. Biophys J, 79**,** 2547-56.

CHENG, J., KAMIYA, K., LIU, W., TSUJI, Y., TOYAMA, J. & KODAMA, I. 1999. Heterogeneous distribution of the two components of delayed rectifier K+ current: a potential mechanism of the proarrhythmic effects of methanesulfonanilideclass III agents. Cardiovascular Research, 43**,** 135-147.

CHIEN, S. 2007. Mechanotransduction and endothelial cell homeostasis: the wisdom of the cell. American Journal of Physiology-Heart and Circulatory Physiology, 292**,** H1209-H1224.

CHOI, B. R. & SALAMA, G. 2000. Simultaneous maps of optical action potentials and calcium transients in guinea-pig hearts: mechanisms underlying concordant alternans. J Physiol, 529 Pt 1**,** 171-88.

CLARK, R. B., BOUCHARD, R. A., SALINAS-STEFANON, E., SANCHEZ-CHAPULA, J. & GILES, W. R. 1993. Heterogeneity of action potential waveforms and potassium currents in rat ventricle. Cardiovasc Res, 27**,** 1795-9.

COLYER, J. 1993. Control of the calcium pump of cardiac sarcoplasmic reticulum. A specific role for the pentameric structure of phospholamban? Cardiovasc Res, 27**,** 1766-71.

CONTI, M., RICHTER, W., MEHATS, C., LIVERA, G., PARK, J. Y. & JIN, C. 2003. Cyclic AMP-specific PDE4 phosphodiesterases as critical components of cyclic AMP signaling. J Biol Chem, 278**,** 5493-6.

COUET, J., LI, S., OKAMOTO, T., IKEZU, T. & LISANTI, M. P. 1997. Identification of Peptide and Protein Ligands for the Caveolin-scaffolding Domain: IMPLICATIONS FOR THE INTERACTION OF CAVEOLIN WITH CAVEOLAE-ASSOCIATED PROTEINS*. Journal of Biological Chemistry, 272**,** 6525-6533.

DAAKA, Y., LUTTRELL, L. M. & LEFKOWITZ, R. J. 1997. Switching of the coupling of the beta2-adrenergic receptor to different G proteins by protein kinase A. Nature, 390**,** 88-91.

DE ARCANGELIS, V., LIU, R., SOTO, D. & XIANG, Y. 2009a. Differential association of phosphodiesterase 4D isoforms with beta2-adrenoceptor in cardiac myocytes. J Biol Chem, 284**,** 33824-32.

DE ARCANGELIS, V., LIU, R., SOTO, D. & XIANG, Y. 2009b. Differential Association of Phosphodiesterase 4D Isoforms with β2-Adrenoceptor in Cardiac Myocytes*. Journal of Biological Chemistry, 284**,** 33824-33832.

DE TOMBE, P. P. 2003. Cardiac myofilaments: mechanics and regulation. Journal of Biomechanics, 36**,** 721-730.

DEL BUONO, M. G., MORONI, F., MONTONE, R. A., AZZALINI, L., SANNA, T. & ABBATE, A. 2022. Ischemic Cardiomyopathy and Heart Failure After Acute Myocardial Infarction. Current Cardiology Reports, 24**,** 1505-1515.

DIFRANCESCO, D. & MCNAUGHTON, P. A. 1979. The effects of calcium on outward membrane currents in the cardiac Purkinje fibre. J Physiol, 289**,** 347-73.

DORIAN, P., DUNNMON, P., ELSTUN, L. & NEWMAN, D. 2002. The effect of isoproterenol on the class III effect of azimilide in humans. J Cardiovasc Pharmacol Ther, 7**,** 211-7.

DREJA, K., VOLDSTEDLUND, M., VINTEN, J., TRANUM-JENSEN, J., HELLSTRAND, P. & SWÄRD, K. 2002. Cholesterol Depletion Disrupts Caveolae and Differentially Impairs Agonist-

Induced Arterial Contraction. Arteriosclerosis, Thrombosis, and Vascular Biology, 22**,** 1267-1272.

DU, X. Y. & SOROTA, S. 1997. Cardiac swelling-induced chloride current depolarizes canine atrial myocytes. Am J Physiol, 272**,** H1904-16.

DULHUNTY, A. F. & FRANZINI-ARMSTRONG, C. 1975. The relative contributions of the folds and caveolae to the surface membrane of frog skeletal muscle fibres at different sarcomere lengths. J Physiol, 250**,** 513-39.

EBASHI, S. & ENDO, M. 1968. Calcium ion and muscle contraction. Prog Biophys Mol Biol, 18**,** 123-83.

EFIMOV, I. R., HUANG, D. T., RENDT, J. M. & SALAMA, G. 1994. Optical mapping of repolarization and refractoriness from intact hearts. Circulation, 90**,** 1469-80.

EFIMOV, I. R., NIKOLSKI, V. P. & SALAMA, G. 2004. Optical Imaging of the Heart. Circulation Research, 95**,** 21-33.

EHARA, T. & HASEGAWA, J. 1983. Effects of hypertonic solution on action potential and input resistance in the guinea-pig ventricular muscle. The Japanese journal of physiology, 33 2**,** 151-67.

FAN, X., GU, X., ZHAO, R., ZHENG, Q., LI, L., YANG, W., DING, L., XUE, F., FAN, J., GONG, Y. & WANG, Y. 2016. Cardiac β2-Adrenergic Receptor Phosphorylation at Ser355/356 Regulates Receptor Internalization and Functional Resensitization. PLoS One, 11**,** e0161373.

FEINER, E. C., CHUNG, P., JASMIN, J. F., ZHANG, J., WHITAKER-MENEZES, D., MYERS, V., SONG, J., FELDMAN, E. W., FUNAKOSHI, H., DEGEORGE, B. R., JR., YELAMARTY, R. V., KOCH, W. J., LISANTI, M. P., MCTIERNAN, C. F., CHEUNG, J. Y., BRISTOW, M. R., CHAN, T. O. & FELDMAN, A. M. 2011. Left ventricular dysfunction in murine models of heart failure and in failing human heart is associated with a selective decrease in the expression of caveolin-3. J Card Fail, 17**,** 253-63.

FIELDING, P. E. & FIELDING, C. J. 1995. Plasma membrane caveolae mediate the efflux of cellular free cholesterol. Biochemistry, 34**,** 14288-92.

FISCHMEISTER, R., CASTRO, L. R., ABI-GERGES, A., ROCHAIS, F., JUREVICIUS, J., LEROY, J. & VANDECASTEELE, G. 2006. Compartmentation of cyclic nucleotide signaling in the heart: the role of cyclic nucleotide phosphodiesterases. Circ Res, 99**,** 816-28.

FORBES, M. S., HAWKEY, L. A. & SPERELAKIS, N. 1984. The transverse-axial tubular system (TATS) of mouse myocardium: its morphology in the developing and adult animal. Am J Anat, 170**,** 143-62.

FORBES, M. S. & SPERELAKIS, N. 1976. The presence of transverse and axial tubules in the ventricular myocardium of embryonic and neonatal guinea pigs. Cell and Tissue Research, 166**,** 83-90.

FŐRSTER, T. 1959. 10th Spiers Memorial Lecture. Transfer mechanisms of electronic excitation. Discussions of The Faraday Society, 27**,** 7-17.

FRANCIS, S. H., BLOUNT, M. A. & CORBIN, J. D. 2011. Mammalian cyclic nucleotide phosphodiesterases: molecular mechanisms and physiological functions. Physiol Rev, 91**,** 651-90.

FRANK, O. 1959. On the dynamics of cardiac muscle. American Heart Journal, 58**,** 282-317.

FRANZ, M. R., CIMA, R., WANG, D., PROFITT, D. & KURZ, R. 1992. Electrophysiological effects of myocardial stretch and mechanical determinants of stretch-activated arrhythmias. Circulation, 86**,** 968-78.

FRANZINI-ARMSTRONG, C., PROTASI, F. & RAMESH, V. 1999. Shape, size, and distribution of Ca(2+) release units and couplons in skeletal and cardiac muscles. Biophys J, 77**,** 1528-39.

FREEDMAN, N. J. & LEFKOWITZ, R. J. 1996. Desensitization of G protein-coupled receptors. Recent Prog Horm Res, 51**,** 319-51; discussion 352-3.

FUHS, S. R. & INSEL, P. A. 2011. Caveolin-3 undergoes SUMOylation by the SUMO E3 ligase PIASy: sumoylation affects G-protein-coupled receptor desensitization. J Biol Chem, 286**,** 14830-41.

FUKUDA, N. & GRANZIER, H. L. 2005. Titin/connectin-based modulation of the Frank-Starling mechanism of the heart. Journal of Muscle Research & Cell Motility, 26**,** 319-323.

GARCÍA-NIÑO, W. R., CORREA, F., RODRÍGUEZ-BARRENA, J. I., LEÓN-CONTRERAS, J. C., BUELNA-CHONTAL, M., SORIA-CASTRO, E., HERNÁNDEZ-PANDO, R., PEDRAZA-CHAVERRI, J. & ZAZUETA, C. 2017. Cardioprotective kinase signaling to subsarcolemmal and interfibrillar mitochondria is mediated by caveolar structures. Basic Research in Cardiology, 112**,** 15.

GILBERT, G., DUCRET, T., MARTHAN, R., SAVINEAU, J.-P. & QUIGNARD, J.-F. 2014. Stretch-induced Ca2+ signalling in vascular smooth muscle cells depends on Ca2+ store segregation. Cardiovascular Research, 103**,** 313-323.

GONANO, L. A., MORELL, M., BURGOS, J. I., DULCE, R. A., DE GIUSTI, V. C., AIELLO, E. A., HARE, J. M. & VILA PETROFF, M. 2014. Hypotonic swelling promotes nitric oxide release in cardiac ventricular myocytes: impact on swelling-induced negative inotropic effect. Cardiovasc Res, 104**,** 456-66.

GORDON, A. M., HUXLEY, A. F. & JULIAN, F. J. 1966. The variation in isometric tension with sarcomere length in vertebrate muscle fibres. J Physiol, 184**,** 170-92.

GORDON, A. M., REGNIER, M. & HOMSHER, E. 2001. Skeletal and cardiac muscle contractile activation: tropomyosin "rocks and rolls". News Physiol Sci, 16**,** 49-55.

GRANT, A. O. 2009. Cardiac Ion Channels. Circulation: Arrhythmia and Electrophysiology, 2**,** 185-194.

HANSEN, D. E., BORGANELLI, M., STACY, G. P., JR. & TAYLOR, L. K. 1991. Dose-dependent inhibition of stretch-induced arrhythmias by gadolinium in isolated canine ventricles. Evidence for a unique mode of antiarrhythmic action. Circ Res, 69**,** 820-31.

HARMATI, G., BÁNYÁSZ, T., BÁRÁNDI, L., SZENTANDRÁSSY, N., HORVÁTH, B., SZABÓ, G., SZENTMIKLÓSI, J. A., SZÉNÁSI, G., NÁNÁSI, P. P. & MAGYAR, J. 2011. Effects of β-adrenoceptor stimulation on delayed rectifier K(+) currents in canine ventricular cardiomyocytes. Br J Pharmacol, 162**,** 890-6.

HEAD, B. P., PATEL, H. H., ROTH, D. M., LAI, N. C., NIESMAN, I. R., FARQUHAR, M. G. & INSEL, P. A. 2005. G-protein-coupled receptor signaling components localize in both sarcolemmal and intracellular caveolin-3-associated microdomains in adult cardiac myocytes. J Biol Chem, 280**,** 31036-44.

HEIJMAN, J., DEWENTER, M., EL-ARMOUCHE, A. & DOBREV, D. 2013. Function and regulation of serine/threonine phosphatases in the healthy and diseased heart. J Mol Cell Cardiol, 64**,** 90-8.

HEINZEL, F. R., BITO, V., BIESMANS, L., WU, M., DETRE, E., WEGNER, F. V., CLAUS, P., DYMARKOWSKI, S., MAES, F., BOGAERT, J., RADEMAKERS, F., D'HOOGE, J. & SIPIDO, K. 2008. Remodeling of T-tubules and reduced synchrony of Ca2+ release in myocytes from chronically ischemic myocardium. Circulation Research, 102**,** 338-346.

HENNERSDORF, M. G. & STRAUER, B. E. 2001. Arterial hypertension and cardiac arrhythmias. J Hypertens, 19**,** 167-77.

HEYMANS, S., LAKDAWALA, N. K., TSCHÖPE, C. & KLINGEL, K. 2023. Dilated cardiomyopathy: causes, mechanisms, and current and future treatment approaches. The Lancet, 402**,** 998-1011.

HIBBERD, M. G. & JEWELL, B. R. 1982. Calcium- and length-dependent force production in rat ventricular muscle. J Physiol, 329**,** 527-40.

HOOP, C. L., SIVANANDAM, V. N., KODALI, R., SRNEC, M. N. & VAN DER WEL, P. C. 2012. Structural characterization of the caveolin scaffolding domain in association with cholesterol-rich membranes. Biochemistry, 51**,** 90-9.

HORIKAWA, Y. T., PANNEERSELVAM, M., KAWARAGUCHI, Y., TSUTSUMI, Y. M., ALI, S. S., BALIJEPALLI, R. C., MURRAY, F., HEAD, B. P., NIESMAN, I. R., RIEG, T., VALLON, V., INSEL, P. A., PATEL, H. H. & ROTH, D. M. 2011. Cardiac-specific overexpression of caveolin-3 attenuates cardiac hypertrophy and increases natriuretic peptide expression and signaling. J Am Coll Cardiol, 57**,** 2273-83.

HOUSLAY, M. D., BAILLIE, G. S. & MAURICE, D. H. 2007. cAMP-Specific Phosphodiesterase-4 Enzymes in the Cardiovascular System. Circulation Research, 100**,** 950-966.

HUANG, C. L.-H. 2017. Murine Electrophysiological Models of Cardiac Arrhythmogenesis. Physiological Reviews, 97**,** 283-409.

HUO, R., SHENG, Y., GUO, W. T. & DONG, D. L. 2014. The potential role of Kv4.3 K+ channel in heart hypertrophy. Channels (Austin), 8**,** 203-9.

HURLEY, M., KAUR, S., WALTON, R., POWER, A., HAÏSSAGUERRE, M., BERNUS, O., WARD, M.-L. & WHITE, E. 2023. Endocardial role in arrhythmias induced by acute ventricular stretch and the involvement of Purkinje fibres, in isolated rat hearts. Current Research in Physiology, 6**,** 100098.

HÜSER, J., LIPSIUS, S. L. & BLATTER, L. A. 1996. Calcium gradients during excitation-contraction coupling in cat atrial myocytes. J Physiol, 494 (Pt 3)**,** 641-51.

IBRAHIM, M., AL MASRI, A., NAVARATNARAJAH, M., SIEDLECKA, U., SOPPA, G. K., MOSHKOV, A., AL-SAUD, S. A., GORELIK, J., YACOUB, M. H. & TERRACCIANO, C. M. 2010a. Prolonged mechanical unloading affects cardiomyocyte excitation-contraction coupling, transverse-tubule structure, and the cell surface. Faseb j, 24**,** 3321-9.

IBRAHIM, M., NAVARATNARAJAH, M., SIEDLECKA, U., MOSHKOV, A. V., GORELIK, J., YACOUB, M. H. & TERRACCIANO, C. M. 2010b. Abstract 17308: Mechanical Unloading of Failing Hearts Normalises Calcium-Induced Calcium Release by Reverse Remodelling of the T-Tubule System. Circulation, 122**,** A17308-A17308.

IBRAHIM, M., SIEDLECKA, U., BUYANDELGER, B., HARADA, M., RAO, C., MOSHKOV, A., BHARGAVA, A., SCHNEIDER, M., YACOUB, M. H., GORELIK, J., KNÖLL, R. & TERRACCIANO, C. M. 2012. A critical role for Telethonin in regulating t-tubule structure and function in the mammalian heart. Human Molecular Genetics, 22**,** 372-383.

IRVING, T. C., KONHILAS, J., PERRY, D., FISCHETTI, R. & TOMBE, P. P. D. 2000. Myofilament lattice spacing as a function of sarcomere length in isolated rat myocardium. American Journal of Physiology-Heart and Circulatory Physiology, 279**,** H2568-H2573.

JAIMES, R., 3RD, WALTON, R. D., PASDOIS, P., BERNUS, O., EFIMOV, I. R. & KAY, M. W. 2016. A technical review of optical mapping of intracellular calcium within myocardial tissue. Am J Physiol Heart Circ Physiol, 310**,** H1388-401.

JAIMES, R., MCCULLOUGH, D., SIEGEL, B., SWIFT, L., HIEBERT, J., MCINERNEY, D. & POSNACK, N. G. 2019. Lights, camera, path splitter: a new approach for truly simultaneous dual optical mapping of the heart with a single camera. BMC Biomedical Engineering, 1**,** 25.

JIAN, Z., HAN, H., ZHANG, T., PUGLISI, J., IZU, L. T., SHAW, J. A., ONOFIOK, E., ERICKSON, J. R., CHEN, Y. J., HORVATH, B., SHIMKUNAS, R., XIAO, W., LI, Y., PAN, T., CHAN, J., BANYASZ,

T., TARDIFF, J. C., CHIAMVIMONVAT, N., BERS, D. M., LAM, K. S. & CHEN-IZU, Y. 2014. Mechanochemotransduction during cardiomyocyte contraction is mediated by localized nitric oxide signaling. Sci Signal, 7**,** ra27.

JOHNS, T. N. & OLSON, B. J. 1954. Experimental myocardial infarction. I. A method of coronary occlusion in small animals. Ann Surg, 140**,** 675-82.

JOUKAR, S. 2021. A comparative review on heart ion channels, action potentials and electrocardiogram in rodents and human: extrapolation of experimental insights to clinic. Lab Anim Res, 37**,** 25.

KAMKIN, A., KISELEVA, I. & ISENBERG, G. 2000. Stretch-activated currents in ventricular myocytes: amplitude and arrhythmogenic effects increase with hypertrophy. Cardiovascular Research, 48**,** 409-420.

KAMKIN, A., KISELEVA, I. & ISENBERG, G. 2003a. Ion selectivity of stretch-activated cation currents in mouse ventricular myocytes. Pflugers Arch, 446**,** 220-31.

KAMKIN, A., KISELEVA, I., ISENBERG, G., WAGNER, K. D., GÜNTHER, J., THERES, H. & SCHOLZ, H. 2003b. Cardiac fibroblasts and the mechano-electric feedback mechanism in healthy and diseased hearts. Progress in biophysics and molecular biology, 82**,** 111-120.

KAPPADAN, V., TELELE, S., UZELAC, I., FENTON, F., PARLITZ, U., LUTHER, S. & CHRISTOPH, J. 2020. High-Resolution Optical Measurement of Cardiac Restitution, Contraction, and Fibrillation Dynamics in Beating vs. Blebbistatin-Uncoupled Isolated Rabbit Hearts. Frontiers in Physiology, 11.

KARAM, S., MARGARIA, J. P., BOURCIER, A., MIKA, D., VARIN, A., BEDIOUNE, I., LINDNER, M., BOUADJEL, K., DESSILLONS, M., GAUDIN, F., LEFEBVRE, F., MATEO, P., LECHÈNE, P., GOMEZ, S., DOMERGUE, V., ROBERT, P., COQUARD, C., ALGALARRONDO, V., SAMUEL, J.-L., MICHEL, J.-B., CHARPENTIER, F., GHIGO, A., HIRSCH, E., FISCHMEISTER, R., LEROY, J. & VANDECASTEELE, G. 2020. Cardiac Overexpression of PDE4B Blunts β-Adrenergic Response and Maladaptive Remodeling in Heart Failure. Circulation, 142**,** 161-174.

KARTASALO, K., PÖLÖNEN, R. P., OJALA, M., RASKU, J., LEKKALA, J., AALTO-SETÄLÄ, K. & KALLIO, P. 2015. CytoSpectre: a tool for spectral analysis of oriented structures on cellular and subcellular levels. BMC Bioinformatics, 16**,** 344.

KATZ, G., PAINE, W. & TILLER, P. 1939. A new method for coronary perfusion of the mammalian heart. Arch Int Pharmacodyn, 61**,** 109-112.

KAYE, D., PIMENTAL, D., PRASAD, S., MÄKI, T., BERGER, H. J., MCNEIL, P. L., SMITH, T. W. & KELLY, R. A. 1996. Role of transiently altered sarcolemmal membrane permeability and basic fibroblast growth factor release in the hypertrophic response of adult rat ventricular myocytes to increased mechanical activity in vitro. J Clin Invest, 97**,** 281-91.

KENTISH, J. C. & WRZOSEK, A. 1998. Changes in force and cytosolic Ca2+ concentration after length changes in isolated rat ventricular trabeculae. J Physiol, 506 (Pt 2)**,** 431-44.

KERFANT, B.-G., ZHAO, D., LORENZEN-SCHMIDT, I., WILSON, L. S., CAI, S., CHEN, S. R. W., MAURICE, D. H. & BACKX, P. H. 2007. PI3Kγ Is Required for PDE4, not PDE3, Activity in Subcellular Microdomains Containing the Sarcoplasmic Reticular Calcium ATPase in Cardiomyocytes. Circulation Research, 101**,** 400-408.

KISELEVA, I., KAMKIN, A., WAGNER, K. D., THERES, H., LADHOFF, A., SCHOLZ, H., GÜNTHER, J. & LAB, M. J. 2000. Mechanoelectric feedback after left ventricular infarction in rats. Cardiovasc Res, 45**,** 370-8.

KLABUNDE, R. E. 2017. Cardiac electrophysiology: normal and ischemic ionic currents and the ECG. Advances in Physiology Education, 41**,** 29-37.

KOCKSKÄMPER, J., VON LEWINSKI, D., KHAFAGA, M., ELGNER, A., GRIMM, M., ESCHENHAGEN, T., GOTTLIEB, P. A., SACHS, F. & PIESKE, B. 2008. The slow force response to stretch in atrial and ventricular myocardium from human heart: functional relevance and subcellular mechanisms. Prog Biophys Mol Biol, 97**,** 250-67.

KOHL, P., COOPER, P. J. & HOLLOWAY, H. 2003. Effects of acute ventricular volume manipulation on in situ cardiomyocyte cell membrane configuration. Progress in Biophysics and Molecular Biology, 82**,** 221-227.

KOHL, P., HUNTER, P. & NOBLE, D. 1999. Stretch-induced changes in heart rate and rhythm: clinical observations, experiments and mathematical models. Prog Biophys Mol Biol, 71**,** 91-138.

KÖHLER, R., HEYKEN, W. T., HEINAU, P., SCHUBERT, R., SI, H., KACIK, M., BUSCH, C., GRGIC, I., MAIER, T. & HOYER, J. 2006. Evidence for a functional role of endothelial transient receptor potential V4 in shear stress-induced vasodilatation. Arterioscler Thromb Vasc Biol, 26**,** 1495-502.

KONG, C. H. T., BRYANT, S. M., WATSON, J. J., ROTH, D. M., PATEL, H. H., CANNELL, M. B., JAMES, A. F. & ORCHARD, C. H. 2019. Cardiac-specific overexpression of caveolin-3 preserves t-tubular I(Ca) during heart failure in mice. Exp Physiol, 104**,** 654-666.

KONHILAS, J. P., IRVING, T. C. & DE TOMBE, P. P. 2002. Frank-Starling law of the heart and the cellular mechanisms of length-dependent activation. Pflugers Arch, 445**,** 305-10.

KOSCHINSKI, A. & ZACCOLO, M. 2017. Activation of PKA in cell requires higher concentration of cAMP than in vitro: implications for compartmentalization of cAMP signalling. Scientific Reports, 7**,** 14090.

KOZERA, L., WHITE, E. & CALAGHAN, S. 2009. Caveolae Act as Membrane Reserves Which Limit Mechanosensitive ICl,swell Channel Activation during Swelling in the Rat Ventricular Myocyte. PLoS ONE, 4**,** e8312.

KRAFT, A. E., BORK, N. I., SUBRAMANIAN, H., PAVLAKI, N., FAILLA, A. V., ZOBIAK, B., CONTI, M. & NIKOLAEV, V. O. 2024. Phosphodiesterases 4B and 4D Differentially Regulate cAMP Signaling in Calcium Handling Microdomains of Mouse Hearts. Cells, 13**,** 476.

KRANIAS, E. G. 1985. Regulation of Ca2+ transport by cyclic 3',5'-AMP-dependent and calcium-calmodulin-dependent phosphorylation of cardiac sarcoplasmic reticulum. Biochim Biophys Acta, 844**,** 193-9.

KRUPNICK, J. G. & BENOVIC, J. L. 1998. The role of receptor kinases and arrestins in G protein-coupled receptor regulation. Annu Rev Pharmacol Toxicol, 38**,** 289-319.

KUSCHEL, M., ZHOU, Y.-Y., CHENG, H., ZHANG, S.-J., CHEN, Y., LAKATTA, E. G. & XIAO, R.-P. 1999a. Gi Protein-mediated Functional Compartmentalization of Cardiac β2-Adrenergic Signaling*. Journal of Biological Chemistry, 274**,** 22048-22052.

KUSCHEL, M., ZHOU, Y. Y., SPURGEON, H. A., BARTEL, S., KARCZEWSKI, P., ZHANG, S. J., KRAUSE, E. G., LAKATTA, E. G. & XIAO, R. P. 1999b. beta2-adrenergic cAMP signaling is uncoupled from phosphorylation of cytoplasmic proteins in canine heart. Circulation, 99**,** 2458-65.

KWAN, Z., PAULOSE NADAPPURAM, B., LEUNG, M. M., MOHAGAONKAR, S., LI, A., AMARADASA, K. S., CHEN, J., ROTHERY, S., KIBREAB, I., FU, J., SANCHEZ-ALONSO, J. L., MANSFIELD, C. A., SUBRAMANIAN, H., KONDRASHOV, A., WRIGHT, P. T., SWIATLOWSKA, P., NIKOLAEV, V. O., WOJCIAK-STOTHARD, B., IVANOV, A. P., EDEL, J. B. & GORELIK, J. 2023. Microtubule-Mediated Regulation of β(2)AR Translation and Function in Failing Hearts. Circ Res, 133**,** 944-958.

KYURKCHIEVA, E. & BAILLIE, G. S. 2023. Short PDE4 Isoforms as Drug Targets in Disease. Front Biosci (Landmark Ed), 28**,** 133.

LAB, M. J. 1978. Mechanically dependent changes in action potentials recorded from the intact frog ventricle. Circ Res, 42**,** 519-28.

LAB, M. J., BHARGAVA, A., WRIGHT, P. T. & GORELIK, J. 2013. The scanning ion conductance microscope for cellular physiology. Am J Physiol Heart Circ Physiol, 304**,** H1-11.

LADEIRAS-LOPES, R., FERREIRA-MARTINS, J. & LEITE-MOREIRA, A. F. 2009. Acute neurohumoral modulation of diastolic function. Peptides, 30**,** 419-425.

LADO, M. G., SHEU, S. S. & FOZZARD, H. A. 1984. Effects of tonicity on tension and intracellular sodium and calcium activities in sheep heart. Circulation Research, 54**,** 576-585.

LANG, D., HOLZEM, K., KANG, C., XIAO, M., HWANG, H. J., EWALD, G. A., YAMADA, K. A. & EFIMOV, I. R. 2015. Arrhythmogenic remodeling of β2 versus β1 adrenergic signaling in the human failing heart. Circulation: Arrhythmia and Electrophysiology, 8**,** 409-419.

LANGENDORFF, O. 1895. Untersuchungen am überlebenden Säugethierherzen. Archiv für die gesamte Physiologie des Menschen und der Tiere, 61**,** 291-332.

LAYLAND, J., SOLARO, R. J. & SHAH, A. M. 2005. Regulation of cardiac contractile function by troponin I phosphorylation. Cardiovasc Res, 66**,** 12-21.

LEACH, R. N., DESAI, J. C. & ORCHARD, C. H. 2005. Effect of cytoskeleton disruptors on L-type Ca channel distribution in rat ventricular myocytes. Cell Calcium, 38**,** 515-26.

LEHNART, S. E. & MARKS, A. R. 2006. Phosphodiesterase 4D and heart failure: a cautionary tale. Expert Opinion on Therapeutic Targets, 10**,** 677-688.

LEHNART, S. E., WEHRENS, X. H., REIKEN, S., WARRIER, S., BELEVYCH, A. E., HARVEY, R. D., RICHTER, W., JIN, S. L., CONTI, M. & MARKS, A. R. 2005a. Phosphodiesterase 4D deficiency in the ryanodine-receptor complex promotes heart failure and arrhythmias. Cell, 123**,** 25-35.

LEHNART, S. E., WEHRENS, X. H. T., REIKEN, S., WARRIER, S., BELEVYCH, A. E., HARVEY, R. D., RICHTER, W., JIN, S. L. C., CONTI, M. & MARKS, A. R. 2005b. Phosphodiesterase 4D Deficiency in the Ryanodine-Receptor Complex Promotes Heart Failure and Arrhythmias. Cell, 123**,** 25-35.

LEROY, J., ABI-GERGES, A., NIKOLAEV, V. O., RICHTER, W., LECHÊNE, P., MAZET, J.-L., CONTI, M., FISCHMEISTER, R. & VANDECASTEELE, G. 2008a. Spatiotemporal Dynamics of β-Adrenergic cAMP Signals and L-Type Ca²⁺ Channel Regulation in Adult Rat Ventricular Myocytes. Circulation Research, 102**,** 1091-1100.

LEROY, J., ABI-GERGES, A., NIKOLAEV, V. O., RICHTER, W., LECHÊNE, P., MAZET, J.-L., CONTI, M., FISCHMEISTER, R. & VANDECASTEELE, G. 2008b. Spatiotemporal Dynamics of β-Adrenergic cAMP Signals and L-Type Ca2+ Channel Regulation in Adult Rat Ventricular Myocytes. Circulation Research, 102**,** 1091-1100.

LEROY, J., RICHTER, W., MIKA, D., CASTRO, L. R., ABI-GERGES, A., XIE, M., SCHEITRUM, C., LEFEBVRE, F., SCHITTL, J., MATEO, P., WESTENBROEK, R., CATTERALL, W. A., CHARPENTIER, F., CONTI, M., FISCHMEISTER, R. & VANDECASTEELE, G. 2011. Phosphodiesterase 4B in the cardiac L-type Ca^{2+} channel complex regulates Ca^{2+} current and protects against ventricular arrhythmias in mice. J Clin Invest, 121**,** 2651-61.

LEVY, F. O., ZHU, X., KAUMANN, A. J. & BIRNBAUMER, L. 1993. Efficacy of beta 1-adrenergic receptors is lower than that of beta 2-adrenergic receptors. Proc Natl Acad Sci U S A, 90**,** 10798-802.

LI, J., HAMPTON, T., MORGAN, J. P. & SIMONS, M. 1997. Stretch-induced VEGF expression in the heart. J Clin Invest, 100**,** 18-24.

LISSANDRON, V. & ZACCOLO, M. 2006. Compartmentalized cAMP/PKA signalling regulates cardiac excitation-contraction coupling. J Muscle Res Cell Motil, 27**,** 399-403.

LITVINOV, I. V., KOTOWYCZ, M. A. & WASSMANN, S. 2009. Iatrogenic epinephrine-induced reverse Takotsubo cardiomyopathy: direct evidence supporting the role of catecholamines in the pathophysiology of the "broken heart syndrome". Clin Res Cardiol, 98**,** 457-62.

LIU, B.-C., LU, X.-Y., SONG, X., LEI, K.-Y., ALLI, A., BAO, H.-F., EATON, D. & MA, H.-P. 2013. Scanning ion conductance microscopy: a nanotechnology for biological studies in live cells. Frontiers in Physiology, 3.

LIU, R., RAMANI, B., SOTO, D., DE ARCANGELIS, V. & XIANG, Y. 2009. Agonist dose-dependent phosphorylation by protein kinase A and G protein-coupled receptor kinase regulates beta2 adrenoceptor coupling to G(i) proteins in cardiomyocytes. J Biol Chem, 284**,** 32279-87.

LOOKIN, O. & PROTSENKO, Y. 2019. The lack of slow force response in failing rat myocardium: role of stretch-induced modulation of Ca-TnC kinetics. J Physiol Sci, 69**,** 345-357.

LOUCH, W. E., BITO, V., HEINZEL, F. R., MACIANSKIENE, R., VANHAECKE, J., FLAMENG, W., MUBAGWA, K. & SIPIDO, K. R. 2004. Reduced synchrony of Ca2+ release with loss of T-tubules-a comparison to Ca2+ release in human failing cardiomyocytes. Cardiovasc Res, 62**,** 63-73.

LYNCH, M. J., BAILLIE, G. S. & HOUSLAY, M. D. 2007. cAMP-specific phosphodiesterase-4D5 (PDE4D5) provides a paradigm for understanding the unique non-redundant roles that PDE4 isoforms play in shaping compartmentalized cAMP cell signalling. Biochem Soc Trans, 35**,** 938-41.

LYNCH, M. J., BAILLIE, G. S., MOHAMED, A., LI, X., MAISONNEUVE, C., KLUSSMANN, E., VAN HEEKE, G. & HOUSLAY, M. D. 2005. RNA silencing identifies PDE4D5 as the functionally relevant cAMP phosphodiesterase interacting with beta arrestin to control the protein kinase A/AKAP79-mediated switching of the beta2-adrenergic receptor to activation of ERK in HEK293B2 cells. J Biol Chem, 280**,** 33178-89.

LYON, A., DUPUIS, L. J., ARTS, T., CRIJNS, H. J. G. M., PRINZEN, F. W., DELHAAS, T., HEIJMAN, J. & LUMENS, J. 2020. Differentiating the effects of β-adrenergic stimulation and stretch on calcium and force dynamics using a novel electromechanical cardiomyocyte model. American Journal of Physiology-Heart and Circulatory Physiology, 319**,** H519-H530.

LYON, A. R., MACLEOD, K. T., ZHANG, Y., GARCIA, E., KANDA, G. K., LAB, M. J., KORCHEV, Y. E., HARDING, S. E. & GORELIK, J. 2009. Loss of T-tubules and other changes to surface topography in ventricular myocytes from failing human and rat heart. Proceedings of the National Academy of Sciences, 106**,** 6854-6859.

LYON, A. R., REES, P. S. C., PRASAD, S., POOLE-WILSON, P. A. & HARDING, S. E. 2008. Stress (Takotsubo) cardiomyopathy—a novel pathophysiological hypothesis to explain catecholamine-induced acute myocardial stunning. Nature Clinical Practice Cardiovascular Medicine, 5**,** 22-29.

MACDOUGALL, D. A., AGARWAL, S. R., STOPFORD, E. A., CHU, H., COLLINS, J. A., LONGSTER, A. L., COLYER, J., HARVEY, R. D. & CALAGHAN, S. 2012. Caveolae compartmentalise β2-adrenoceptor signals by curtailing cAMP production and maintaining phosphatase activity in the sarcoplasmic reticulum of the adult ventricular myocyte. Journal of molecular and cellular cardiology, 52**,** 388-400.

MACKENZIE, S. J., BAILLIE, G. S., MCPHEE, I., MACKENZIE, C., SEAMONS, R., MCSORLEY, T., MILLEN, J., BEARD, M. B., VAN HEEKE, G. & HOUSLAY, M. D. 2002. Long PDE4 cAMP specific phosphodiesterases are activated by protein kinase A-mediated phosphorylation of a single serine residue in Upstream Conserved Region 1 (UCR1). Br J Pharmacol, 136**,** 421-33.

MACKENZIE, S. J. & HOUSLAY, M. D. 2000. Action of rolipram on specific PDE4 cAMP phosphodiesterase isoforms and on the phosphorylation of cAMP-response-element-binding protein (CREB) and p38 mitogen-activated protein (MAP) kinase in U937 monocytic cells. Biochem J, 347**,** 571-8.

MADAMANCHI, A. 2007. Beta-adrenergic receptor signaling in cardiac function and heart failure. Mcgill J Med, 10**,** 99-104.

MAEDER, M. T. & KAYE, D. M. 2009. Heart Failure With Normal Left Ventricular Ejection Fraction. Journal of the American College of Cardiology, 53**,** 905-918.

MARKANDEYA, Y. S., GREGORICH, Z. R., FENG, L., RAMCHANDRAN, V., T, O. H., VAIDYANATHAN, R., MANSFIELD, C., KEEFE, A. M., BEGLINGER, C. J., BEST, J. M., KALSCHEUR, M. M., LEA, M. R., HACKER, T. A., GORELIK, J., TRAYANOVA, N. A., ECKHARDT, L. L., MAKIELSKI, J. C., BALIJEPALLI, R. C. & KAMP, T. J. 2023. Caveolin-3 and Caveolae regulate ventricular repolarization. J Mol Cell Cardiol, 177**,** 38-49.

MARKANDEYA, Y. S., PHELAN, L. J., WOON, M. T., KEEFE, A. M., REYNOLDS, C. R., AUGUST, B. K., HACKER, T. A., ROTH, D. M., PATEL, H. H. & BALIJEPALLI, R. C. 2015. Caveolin-3 Overexpression Attenuates Cardiac Hypertrophy via Inhibition of T-type Ca2+ Current Modulated by Protein Kinase Cα in Cardiomyocytes. Journal of Biological Chemistry, 290**,** 22085-22100.

MARTIN, S. S., ADAY, A. W., ALMARZOOQ, Z. I., ANDERSON, C. A. M., ARORA, P., AVERY, C. L., BAKER-SMITH, C. M., GIBBS, B. B., BEATON, A. Z., BOEHME, A. K., COMMODORE-MENSAH, Y., CURRIE, M. E., ELKIND, M. S. V., EVENSON, K. R., GENEROSO, G., HEARD, D. G., HIREMATH, S., JOHANSEN, M. C., KALANI, R., KAZI, D. S., KO, D., LIU, J., MAGNANI, J. W., MICHOS, E. D., MUSSOLINO, M. E., NAVANEETHAN, S. D., PARIKH, N. I., PERMAN, S. M., POUDEL, R., REZK-HANNA, M., ROTH, G. A., SHAH, N. S., ST-ONGE, M.-P., THACKER, E. L., TSAO, C. W., URBUT, S. M., SPALL, H. G. C. V., VOEKS, J. H., WANG, N.-Y., WONG, N. D., WONG, S. S., YAFFE, K. & PALANIAPPAN, L. P. 2024. 2024 Heart Disease and Stroke Statistics: A Report of US and Global Data From the American Heart Association. Circulation, 149**,** e347-e913.

MCALPINE, W. A. 1975. The Left Ventricle—General Considerations. In: MCALPINE, W. A. (ed.) Heart and Coronary Arteries: An Anatomical Atlas for Clinical Diagnosis, Radiological Investigation, and Surgical Treatment. Berlin, Heidelberg: Springer Berlin Heidelberg.

MCDONAGH, T. A., METRA, M., ADAMO, M., GARDNER, R. S., BAUMBACH, A., BÖHM, M., BURRI, H., BUTLER, J., ČELUTKIENĖ, J., CHIONCEL, O., CLELAND, J. G. F., COATS, A. J. S., CRESPO-LEIRO, M. G., FARMAKIS, D., GILARD, M., HEYMANS, S., HOES, A. W., JAARSMA, T., JANKOWSKA, E. A., LAINSCAK, M., LAM, C. S. P., LYON, A. R., MCMURRAY, J. J. V., MEBAZAA, A., MINDHAM, R., MUNERETTO, C., FRANCESCO PIEPOLI, M., PRICE, S., ROSANO, G. M. C., RUSCHITZKA, F., KATHRINE SKIBELUND, A. & GROUP, E. S. D. 2021. 2021 ESC Guidelines for the diagnosis and treatment of acute and chronic heart failure:

Developed by the Task Force for the diagnosis and treatment of acute and chronic heart failure of the European Society of Cardiology (ESC) With the special contribution of the Heart Failure Association (HFA) of the ESC. European Heart Journal, 42**,** 3599-3726.

MEDVEDEV, R. Y., SANCHEZ-ALONSO, J. L., MANSFIELD, C. A., JUDINA, A., FRANCIS, A. J., PAGIATAKIS, C., TRAYANOVA, N., GLUKHOV, A. V., MIRAGOLI, M., FAGGIAN, G. & GORELIK, J. 2021. Local hyperactivation of L-type Ca2+ channels increases spontaneous Ca2+ release activity and cellular hypertrophy in right ventricular myocytes from heart failure rats. Scientific Reports, 11**,** 4840.

MEDVEDEV, R. Y., TURNER, D. G. P., DEGUIRE, F. C., LEONOV, V., LANG, D., GORELIK, J., ALVARADO, F. J., BONDARENKO, V. E. & GLUKHOV, A. V. 2023. Caveolae-associated cAMP/Ca2+-mediated mechano-chemical signal transduction in mouse atrial myocytes. Journal of Molecular and Cellular Cardiology, 184**,** 75-87.

MEINERTZ, T., HOFMANN, T., KASPER, W., TREESE, N., BECHTOLD, H., STIENEN, U., POP, T., LEITNER, E. R., ANDRESEN, D. & MEYER, J. 1984. Significance of ventricular arrhythmias in idiopathic dilated cardiomyopathy. Am J Cardiol, 53**,** 902-7.

MITCHELL, G. F., LAMAS, G. A., VAUGHAN, D. E. & PFEFFER, M. A. 1992. Left ventricular remodeling in the year after first anterior myocardial infarction: A quantitative analysis of contractile segment lengths and ventricular shape. Journal of the American College of Cardiology, 19**,** 1136-1144.

MOLENAAR, P., SAVARIMUTHU, S. M., SARSERO, D., CHEN, L., SEMMLER, A. B., CARLE, A., YANG, I., BARTEL, S., VETTER, D., BEYERDÖRFER, I., KRAUSE, E. G. & KAUMANN, A. J. 2007. (-)-Adrenaline elicits positive inotropic, lusitropic, and biochemical effects through beta2 -adrenoceptors in human atrial myocardium from nonfailing and failing hearts, consistent with Gs coupling but not with Gi coupling. Naunyn Schmiedebergs Arch Pharmacol, 375**,** 11-28.

MOLINA, C. E., LEROY, J., RICHTER, W., XIE, M., SCHEITRUM, C., LEE, I. O., MAACK, C., RUCKER-MARTIN, C., DONZEAU-GOUGE, P., VERDE, I., LLACH, A., HOVE-MADSEN, L., CONTI, M., VANDECASTEELE, G. & FISCHMEISTER, R. 2012. Cyclic adenosine monophosphate

phosphodiesterase type 4 protects against atrial arrhythmias. J Am Coll Cardiol, 59**,** 2182-90.

MONGILLO, M., MCSORLEY, T., EVELLIN, S., SOOD, A., LISSANDRON, V., TERRIN, A., HUSTON, E., HANNAWACKER, A., LOHSE, M. J., POZZAN, T., HOUSLAY, M. D. & ZACCOLO, M. 2004. Fluorescence Resonance Energy Transfer–Based Analysis of cAMP Dynamics in Live Neonatal Rat Cardiac Myocytes Reveals Distinct Functions of Compartmentalized Phosphodiesterases. Circulation Research, 95**,** 67-75.

MONIER, S., PARTON, R. G., VOGEL, F., BEHLKE, J., HENSKE, A. & KURZCHALIA, T. V. 1995. VIP21-caveolin, a membrane protein constituent of the caveolar coat, oligomerizes in vivo and in vitro. Mol Biol Cell, 6**,** 911-27.

MOORE, G. W., HUTCHINS, G. M., BULKLEY, B. H., TSENG, J. S. & KI, P. F. 1980. Constituents of the human ventricular myocardium: Connective tissue hyperplasia accompanying muscular hypertrophy. American Heart Journal, 100**,** 610-616.

MORI, H., ISHIKAWA, S., KOJIMA, S., HAYASHI, J., WATANABE, Y., HOFFMAN, J. I. E. & OKINO, H. 1993. Increased responsiveness of left ventricular apical myocardium to adrenergic stimuli. Cardiovascular Research, 27**,** 192-198.

MURPHY, S. P., IBRAHIM, N. E. & JANUZZI, J. L., JR 2020. Heart Failure With Reduced Ejection Fraction: A Review. JAMA, 324**,** 488-504.

NAKAGAWA, A., ARITA, M., SHIMADA, T. & SHIRABE, J. 1988. Effects of mechanical stretch on the membrane potential of guinea pig ventricular muscles. Jpn J Physiol, 38**,** 819-38.

NAKAGAWA, C., ASAYAMA, J., KATAMURA, M., MATOBA, S., KEIRA, N., KAWAHARA, A., TSURUYAMA, K., TANAKA, T., KOBARA, M., AKASHI, K., OHTA, B., TATSUMI, T. & NAKAGAWA, M. 1997. Myocardial stretch induced by increased left ventricular diastolic pressure preconditions isolated perfused hearts of normotensive and spontaneously hypertensive rats. Basic Research in Cardiology, 92**,** 410-416.

NAKANO, S., MURAMATSU, T., NISHIMURA, S. & SENBONMATSU, T. 2012. Cardiomyocyte and Heart Failure. InTech.

NEVES, J. S., LEITE-MOREIRA, A. M., NEIVA-SOUSA, M., ALMEIDA-COELHO, J., CASTRO-FERREIRA, R. & LEITE-MOREIRA, A. F. 2016. Acute Myocardial Response to Stretch: What We (don't) Know. Frontiers in Physiology, 6.

NIKOLAEV, V. O., BUNEMANN, M., HEIN, L., HANNAWACKER, A. & LOHSE, M. J. 2004. Novel single chain cAMP sensors for receptor-induced signal propagation. J Biol Chem, 279**,** 37215-8.

NIKOLAEV, V. O., BÜNEMANN, M., SCHMITTECKERT, E., LOHSE, M. J. & ENGELHARDT, S. 2006. Cyclic AMP Imaging in Adult Cardiac Myocytes Reveals Far-Reaching β1-Adrenergic but Locally Confined β2-Adrenergic Receptor–Mediated Signaling. Circulation Research, 99**,** 1084-1091.

NIKOLAEV, V. O., MOSHKOV, A., LYON, A. R., MIRAGOLI, M., NOVAK, P., PAUR, H., LOHSE, M. J., KORCHEV, Y. E., HARDING, S. E. & GORELIK, J. 2010. Beta2-adrenergic receptor redistribution in heart failure changes cAMP compartmentation. Science, 327**,** 1653-7.

NIKOUEE, A., UCHIDA, K., MOENCH, I. & LOPATIN, A. N. 2018. Cholesterol Protects Against Acute Stress-Induced T-Tubule Remodeling in Mouse Ventricular Myocytes. Frontiers in Physiology, 9.

NOBLES, K. N., XIAO, K., AHN, S., SHUKLA, A. K., LAM, C. M., RAJAGOPAL, S., STRACHAN, R. T., HUANG, T.-Y., BRESSLER, E. A., HARA, M. R., SHENOY, S. K., GYGI, S. P. & LEFKOWITZ, R. J. 2011. Distinct Phosphorylation Sites on the β₂-Adrenergic Receptor Establish a Barcode That Encodes Differential Functions of β-Arrestin. Science Signaling, 4**,** ra51-ra51.

NÓBREGA, A. C., WILLIAMSON, J. W. & MITCHELL, J. H. 1995. Left ventricular volumes and hemodynamic responses at onset of dynamic exercise with reduced venous return. J Appl Physiol (1985), 79**,** 1405-10.

NORMAN, R., FULLER, W. & CALAGHAN, S. 2018. Caveolae and the cardiac myocyte. Current Opinion in Physiology, 1**,** 59-67.

O'SHEA, C., KABIR, S. N., HOLMES, A. P., LEI, M., FABRITZ, L., RAJPOOT, K. & PAVLOVIC, D. 2020. Cardiac optical mapping – State-of-the-art and future challenges. The International Journal of Biochemistry & Cell Biology, 126**,** 105804.

OGURA, K., MIAKE, J., SASAKI, N., IWAI, C., BAHRUDIN, U., LI, P., KATO, M., IITSUKA, K., HIROTA, Y., KOSHIDA, T., YAMAMOTO, Y., INOUE, Y., YANO, A., ADACHI, M., IGAWA, O., KURATA, Y., MORISAKI, T., SHIOTA, G., SHIRAYOSHI, Y., HARUAKI, N. & HISATOME, I. 2007. Inhibition of beta-adrenergic signaling by intracellular AMP is independent of cell-surface adenosine receptors in rat cardiac cells. J Mol Cell Cardiol, 43**,** 648-52.

OGURA, T., YOU, Y. & MCDONALD, T. F. 1997. Membrane currents underlying the modified electrical activity of guinea-pig ventricular myocytes exposed to hyperosmotic solution. J Physiol, 504 (Pt 1)**,** 135-51.

OLDHAM, W. M. & HAMM, H. E. 2008. Heterotrimeric G protein activation by G-protein-coupled receptors. Nature Reviews Molecular Cell Biology, 9**,** 60-71.

OLIVER, E., MAYOR JR, F. & D'OCON, P. 2019. Beta-blockers: Historical Perspective and Mechanisms of Action. Revista Española de Cardiología (English Edition), 72**,** 795-886.

OMAR, F., FINDLAY, J. E., CARFRAY, G., ALLCOCK, R. W., JIANG, Z., MOORE, C., MUIR, A. L., LANNOY, M., FERTIG, B. A., MAI, D., DAY, J. P., BOLGER, G., BAILLIE, G. S., SCHWIEBERT, E., KLUSSMANN, E., PYNE, N. J., ONG, A. C. M., BOWERS, K., ADAM, J. M., ADAMS, D. R., HOUSLAY, M. D. & HENDERSON, D. J. P. 2019. Small-molecule allosteric activators of PDE4 long form cyclic AMP phosphodiesterases. Proceedings of the National Academy of Sciences, 116**,** 13320-13329.

ORCHARD, C. & BRETTE, F. 2008. t-Tubules and sarcoplasmic reticulum function in cardiac ventricular myocytes. Cardiovascular research, 77**,** 237-244.

PACHER, P., MABLEY, J. G., LIAUDET, L., EVGENOV, O. V., MARTON, A., HASKÓ, G., KOLLAI, M. & SZABÓ, C. 2004. Left ventricular pressure-volume relationship in a rat model of advanced aging-associated heart failure. American Journal of Physiology-Heart and Circulatory Physiology, 287**,** H2132-H2137.

PACKER, M., ANKER, S. D., BUTLER, J., FILIPPATOS, G. & ZANNAD, F. 2017. Effects of Sodium-Glucose Cotransporter 2 Inhibitors for the Treatment of Patients With Heart Failure: Proposal of a Novel Mechanism of Action. JAMA Cardiol, 2**,** 1025-1029.

PADILLA-PARRA, S. & TRAMIER, M. 2012. FRET microscopy in the living cell: Different approaches, strengths and weaknesses. BioEssays, 34**,** 369-376.

PALADE G, E. 1953. Fine structure of blood capillaries. J Appl Physics, 24**,** 1424-1448.

PAPP, R., BETT, G. C. L., LIS, A., RASMUSSON, R. L., BACZKÓ, I., VARRÓ, A. & SALAMA, G. 2017. Genomic upregulation of cardiac Cav1.2α and NCX1 by estrogen in women. Biology of Sex Differences, 8**,** 26.

PARMLEY, W. W. & CHUCK, L. 1973. Length-dependent changes in myocardial contractile state. Am J Physiol, 224**,** 1195-9.

PARTON, R. G., MCMAHON, K. A. & WU, Y. 2020. Caveolae: Formation, dynamics, and function. Curr Opin Cell Biol, 65**,** 8-16.

PATEL, H. H., MURRAY, F. & INSEL, P. A. 2008. G-protein-coupled receptor-signaling components in membrane raft and caveolae microdomains. Handbook of experimental pharmacology**,** 167-184.

PATTERSON, S. W. & STARLING, E. H. 1914. On the mechanical factors which determine the output of the ventricles. J Physiol, 48**,** 357-79.

PAUR, H., WRIGHT, P. T., SIKKEL, M. B., TRANTER, M. H., MANSFIELD, C., O'GARA, P., STUCKEY, D. J., NIKOLAEV, V. O., DIAKONOV, I., PANNELL, L., GONG, H., SUN, H., PETERS, N. S., PETROU, M., ZHENG, Z., GORELIK, J., LYON, A. R. & HARDING, S. E. 2012. High Levels of Circulating Epinephrine Trigger Apical Cardiodepression in a β2-Adrenergic Receptor/Gi–Dependent Manner. Circulation, 126**,** 697-706.

PERRY, S. J., BAILLIE, G. S., KOHOUT, T. A., MCPHEE, I., MAGIERA, M. M., ANG, K. L., MILLER, W. E., MCLEAN, A. J., CONTI, M., HOUSLAY, M. D. & LEFKOWITZ, R. J. 2002. Targeting of Cyclic AMP Degradation to β₂-Adrenergic Receptors by β-Arrestins. Science, 298**,** 834-836.

PFEFFER, M. A. & BRAUNWALD, E. 1990. Ventricular remodeling after myocardial infarction. Experimental observations and clinical implications. Circulation, 81**,** 1161-72.

PFEIFFER, E. R., WRIGHT, A. T., EDWARDS, A. G., STOWE, J. C., MCNALL, K., TAN, J., NIESMAN, I., PATEL, H. H., ROTH, D. M., OMENS, J. H. & MCCULLOCH, A. D. 2014. Caveolae in ventricular myocytes are required for stretch-dependent conduction slowing. Journal of Molecular and Cellular Cardiology, 76**,** 265-274.

POLLOK, B. A. & HEIM, R. 1999. Using GFP in FRET-based applications. Trends in Cell Biology, 9**,** 57-60.

PONIKOWSKI, P., VOORS, A. A., ANKER, S. D., BUENO, H., CLELAND, J. G. F., COATS, A. J. S., FALK, V., GONZÁLEZ-JUANATEY, J. R., HARJOLA, V.-P., JANKOWSKA, E. A., JESSUP, M., LINDE, C., NIHOYANNOPOULOS, P., PARISSIS, J. T., PIESKE, B., RILEY, J. P., ROSANO, G. M. C., RUILOPE, L. M., RUSCHITZKA, F., RUTTEN, F. H. & VAN DER MEER, P. 2016. 2016 ESC Guidelines for the diagnosis and treatment of acute and chronic heart failure. European Heart Journal, 37**,** 2129-2200.

PRINZEN, F. W., AUGUSTIJN, C. H., ALLESSIE, M. A., ARTS, T., DELHAAS, T. & RENEMAN, R. S. 1992. The time sequence of electrical and mechanical activation during spontaneous beating and ectopic stimulation. Eur Heart J, 13**,** 535-43.

RADEL, C. & RIZZO, V. 2005. Integrin mechanotransduction stimulates caveolin-1 phosphorylation and recruitment of Csk to mediate actin reorganization. Am J Physiol Heart Circ Physiol, 288**,** H936-45.

RAMUZ, M., HASAN, A., GRUSCHESKI, L., DIAKONOV, I., PAVLAKI, N., NIKOLAEV, V. O., HARDING, S., DUNSBY, C. & GORELIK, J. 2019. A Software Tool for High-Throughput Real-Time Measurement of Intensity-Based Ratio-Metric FRET. Cells, 8**,** 1541.

RASMUSSEN, S. G. F., DEVREE, B. T., ZOU, Y., KRUSE, A. C., CHUNG, K. Y., KOBILKA, T. S., THIAN, F. S., CHAE, P. S., PARDON, E., CALINSKI, D., MATHIESEN, J. M., SHAH, S. T. A., LYONS, J. A., CAFFREY, M., GELLMAN, S. H., STEYAERT, J., SKINIOTIS, G., WEIS, W. I., SUNAHARA, R. K. & KOBILKA, B. K. 2011. Crystal structure of the β2 adrenergic receptor–Gs protein complex. Nature, 477**,** 549-555.

RATAJCZAK, P., OLIVIÉRO, P., MAROTTE, F., KOLAR, F., OSTADAL, B. & SAMUEL, J.-L. 2005. Expression and localization of caveolins during postnatal development in rat heart: implication of thyroid hormone. Journal of Applied Physiology, 99**,** 244-251.

REES, S. A., VANDENBERG, J., WRIGHT, A., YOSHIDA, A. & POWELL, T. 1995. Cell swelling has differential effects on the rapid and slow components of delayed rectifier potassium current in guinea pig cardiac myocytes. The Journal of general physiology, 106**,** 1151-70.

REHMAN, I. & REHMAN, A. 2024. Anatomy, Thorax, Heart. StatPearls. Treasure Island (FL): StatPearls Publishing

Copyright © 2024, StatPearls Publishing LLC.

RHODES, S. S., CAMARA, A. K., ALDAKKAK, M., HEISNER, J. S. & STOWE, D. F. 2015. Stretch-induced increase in cardiac contractility is independent of myocyte Ca2+ while block of stretch channels by streptomycin improves contractility after ischemic stunning. Physiol Rep, 3.

RICHTER, W., XIE, M., SCHEITRUM, C., KRALL, J., MOVSESIAN, M. A. & CONTI, M. 2011. Conserved expression and functions of PDE4 in rodent and human heart. Basic Res Cardiol, 106**,** 249-62.

RIDGWAY, E. B. & GORDON, A. M. 1984. Muscle calcium transient. Effect of post-stimulus length changes in single fibers. J Gen Physiol, 83**,** 75-103.

RIZZO, V., SUNG, A., OH, P. & SCHNITZER, J. E. 1998. Rapid Mechanotransduction in Situ at the Luminal Cell Surface of Vascular Endothelium and Its Caveolae*. Journal of Biological Chemistry, 273**,** 26323-26329.

ROCCHETTI, M., FRELI, V., PEREGO, V., ALTOMARE, C., MOSTACCIUOLO, G. & ZAZA, A. 2006. Rate dependency of beta-adrenergic modulation of repolarizing currents in the guinea-pig ventricle. J Physiol, 574**,** 183-93.

RODRIGUEZ, P., BHOGAL, M. S. & COLYER, J. 2003. Stoichiometric phosphorylation of cardiac ryanodine receptor on serine 2809 by calmodulin-dependent kinase II and protein kinase A. J Biol Chem, 278**,** 38593-600.

ROSENBAUM, D. M., RASMUSSEN, S. G. F. & KOBILKA, B. K. 2009. The structure and function of G-protein-coupled receptors. Nature, 459**,** 356-363.

ROTHBERG, K. G., HEUSER, J. E., DONZELL, W. C., YING, Y. S., GLENNEY, J. R. & ANDERSON, R. G. 1992. Caveolin, a protein component of caveolae membrane coats. Cell, 68**,** 673-82.

RUPPERT, M., BÓDI, B., KORKMAZ-ICÖZ, S., LOGANATHAN, S., JIANG, W., LEHMANN, L., OLÁH, A., BARTA, B. A., SAYOUR, A. A., MERKELY, B., KARCK, M., PAPP, Z., SZABÓ, G. & RADOVITS, T. 2019. Myofilament Ca(2+) sensitivity correlates with left ventricular

contractility during the progression of pressure overload-induced left ventricular myocardial hypertrophy in rats. J Mol Cell Cardiol, 129**,** 208-218.

RUUD, M., FRISK, M., MELLEBY, A. O., NORSENG, P. A., MOHAMED, B. A., LI, J., ARONSEN, J. M., SETTERBERG, I. E., JAKUBICZKA, J., VAN HOUT, I., COFFEY, S., SHEN, X., NYGÅRD, S., LUNDE, I. G., TØNNESSEN, T., JONES, P. P., SJAASTAD, I., GULLESTAD, L., TOISCHER, K., DAHL, C. P., CHRISTENSEN, G. & LOUCH, W. E. 2024. Regulation of cardiomyocyte t-tubule structure by preload and afterload: Roles in cardiac compensation and decompensation. J Physiol.

RUWHOF, C. & VAN DER LAARSE, A. 2000. Mechanical stress-induced cardiac hypertrophy: mechanisms and signal transduction pathways. Cardiovascular Research, 47**,** 23-37.

RUWHOF, C., VAN WAMEL, A. E., VAN DER VALK, L. J., SCHRIER, P. I. & VAN DER LAARSE, A. 2001. Direct, autocrine and paracrine effects of cyclic stretch on growth of myocytes and fibroblasts isolated from neonatal rat ventricles. Arch Physiol Biochem, 109**,** 10-7.

SALIEZ, J., BOUZIN, C., RATH, G., GHISDAL, P., DESJARDINS, F., REZZANI, R., RODELLA, L. F., VRIENS, J., NILIUS, B., FERON, O., BALLIGAND, J. L. & DESSY, C. 2008. Role of caveolar compartmentation in endothelium-derived hyperpolarizing factor-mediated relaxation: Ca2+ signals and gap junction function are regulated by caveolin in endothelial cells. Circulation, 117**,** 1065-74.

SANCHEZ-ALONSO, J. L., FEDELE, L., COPIER, J. S., LUCARELLI, C., MANSFIELD, C., JUDINA, A., HOUSER, S. R., BRAND, T. & GORELIK, J. 2023. Functional LTCC-β(2)AR Complex Needs Caveolin-3 and Is Disrupted in Heart Failure. Circ Res, 133**,** 120-137.

SANCHEZ-ALONSO, J. L., LOUCKS, A., SCHOBESBERGER, S., VAN CROMVOIRT, A. M., POULET, C., CHOWDHURY, R. A., TRAYANOVA, N. & GORELIK, J. 2020. Nanoscale regulation of L-type calcium channels differentiates between ischemic and dilated cardiomyopathies. EBioMedicine, 57**,** 102845.

SANTANA, L. F., CHENG, E. P. & LEDERER, W. J. 2010. How does the shape of the cardiac action potential control calcium signaling and contraction in the heart? J Mol Cell Cardiol, 49**,** 901-3.

SAPNA, F., RAVEENA, F., CHANDIO, M., BAI, K., SAYYAR, M., VARRASSI, G., KHATRI, M., KUMAR, S. & MOHAMAD, T. 2023. Advancements in Heart Failure Management: A Comprehensive Narrative Review of Emerging Therapies. Cureus, 15**,** e46486.

SARGIACOMO, M., SCHERER, P. E., TANG, Z., KÜBLER, E., SONG, K. S., SANDERS, M. C. & LISANTI, M. P. 1995. Oligomeric structure of caveolin: implications for caveolae membrane organization. Proceedings of the National Academy of Sciences, 92**,** 9407-9411.

SASAKI, N., MITSUIYE, T. & NOMA, A. 1992. Effects of mechanical stretch on membrane currents of single ventricular myocytes of guinea-pig heart. Jpn J Physiol, 42**,** 957-70.

SASAKI, N., MITSUIYE, T., WANG, Z. & NOMA, A. 1994. Increase of the delayed rectifier K+ and Na(+)-K+ pump currents by hypotonic solutions in guinea pig cardiac myocytes. Circ Res, 75**,** 887-95.

SCHOBESBERGER, S., WRIGHT, P., TOKAR, S., BHARGAVA, A., MANSFIELD, C., GLUKHOV, A. V., POULET, C., BUZUK, A., MONSZPART, A., SIKKEL, M., HARDING, S. E., NIKOLAEV, V. O., LYON, A. R. & GORELIK, J. 2017. T-tubule remodelling disturbs localized β2-adrenergic signalling in rat ventricular myocytes during the progression of heart failure. Cardiovasc Res, 113**,** 770-782.

SCHOTT, M. B., GONOWOLO, F., MALISKE, B. & GROVE, B. 2016. FRET biosensors reveal AKAP-mediated shaping of subcellular PKA activity and a novel mode of Ca(2+)/PKA crosstalk. Cell Signal, 28**,** 294-306.

SCHOUTEN, V. J. & TER KEURS, H. E. 1985. The slow repolarization phase of the action potential in rat heart. J Physiol, 360**,** 13-25.

SCHULTHEISS, H.-P., FAIRWEATHER, D., CAFORIO, A. L. P., ESCHER, F., HERSHBERGER, R. E., LIPSHULTZ, S. E., LIU, P. P., MATSUMORI, A., MAZZANTI, A., MCMURRAY, J. & PRIORI, S. G. 2019. Dilated cardiomyopathy. Nature Reviews Disease Primers, 5**,** 32.

SEKAR, R. B. & PERIASAMY, A. 2003. Fluorescence resonance energy transfer (FRET) microscopy imaging of live cell protein localizations. J Cell Biol, 160**,** 629-33.

SENGUPTA, P. P., KHANDHERIA, B. K., KORINEK, J., WANG, J., JAHANGIR, A., SEWARD, J. B. & BELOHLAVEK, M. 2006a. Apex-to-Base Dispersion in Regional Timing of Left Ventricular

Shortening and Lengthening. Journal of the American College of Cardiology, 47**,** 163-172.

SENGUPTA, P. P., KORINEK, J., BELOHLAVEK, M., NARULA, J., VANNAN, M. A., JAHANGIR, A. & KHANDHERIA, B. K. 2006b. Left ventricular structure and function: basic science for cardiac imaging. J Am Coll Cardiol, 48**,** 1988-2001.

SHIMKUNAS, R., HEGYI, B., JIAN, Z., SHAW, J. A., KAZEMI-LARI, M. A., MITRA, D., LEACH, J. K., LI, X., JARADEH, M., BALARDI, N., CHEN, Y. J., ESCOBAR, A. L., BAKER, A. J., BOSSUYT, J., BANYASZ, T., CHIAMVIMONVAT, N., LAM, K. S., BERS, D. M., IZU, L. T. & CHEN-IZU, Y. 2021. Mechanical Load Regulates Excitation-Ca(2+) Signaling-Contraction in Cardiomyocyte. Circ Res, 128**,** 772-774.

SIMONS, K. & IKONEN, E. 1997. Functional rafts in cell membranes. Nature, 387**,** 569-72.

SINHA, B., KÖSTER, D., RUEZ, R., GONNORD, P., BASTIANI, M., ABANKWA, D., STAN, R. V., BUTLER-BROWNE, G., VEDIE, B., JOHANNES, L., MORONE, N., PARTON, R. G., RAPOSO, G., SENS, P., LAMAZE, C. & NASSOY, P. 2011. Cells respond to mechanical stress by rapid disassembly of caveolae. Cell, 144**,** 402-13.

SIRBU, A., BATHE-PETERS, M., INOUE, A., LOHSE, M. J. & ANNIBALE, P. 2023. Cell swelling enhances GPCR ternary complex formation, underpinning the potentiation of β2 adrenergic receptor-mediated cAMP response. bioRxiv**,** 2023.06.23.544496.

SKRZYPIEC-SPRING, M., GROTTHUS, B., SZELĄG, A. & SCHULZ, R. 2007. Isolated heart perfusion according to Langendorff—Still viable in the new millennium. Journal of Pharmacological and Toxicological Methods, 55**,** 113-126.

SMITH, K. J., BAILLIE, G. S., HYDE, E. I., LI, X., HOUSLAY, T. M., MCCAHILL, A., DUNLOP, A. J., BOLGER, G. B., KLUSSMANN, E., ADAMS, D. R. & HOUSLAY, M. D. 2007. 1H NMR structural and functional characterisation of a cAMP-specific phosphodiesterase-4D5 (PDE4D5) N-terminal region peptide that disrupts PDE4D5 interaction with the signalling scaffold proteins, βarrestin and RACK1. Cellular Signalling, 19**,** 2612-2624.

SMITH, S. O. 2021. Deconstructing the transmembrane core of class A G protein-coupled receptors. Trends Biochem Sci, 46**,** 1017-1029.

SOUDERS, C. A., BORG, T. K., BANERJEE, I. & BAUDINO, T. A. 2012. Pressure Overload Induces Early Morphological Changes in the Heart. The American Journal of Pathology, 181**,** 1226-1235.

SPEAR, J. F. & NEIL MOORE, E. 1972. Stretch-induced excitation and conduction disturbances in the isolated rat myocardium. Journal of Electrocardiology, 5**,** 15-24.

STEWART, L. & TURNER, N. A. 2021. Channelling the Force to Reprogram the Matrix: Mechanosensitive Ion Channels in Cardiac Fibroblasts. Cells, 10.

SUN, X. H., PROTASI, F., TAKAHASHI, M., TAKESHIMA, H., FERGUSON, D. G. & FRANZINI-ARMSTRONG, C. 1995. Molecular architecture of membranes involved in excitation-contraction coupling of cardiac muscle. J Cell Biol, 129**,** 659-71.

SUN, Z., LU, K., KAMLA, C., KAMERITSCH, P., SEIDEL, T. & DENDORFER, A. 2024. Synchronous force and Ca2+ measurements for repeated characterization of excitation-contraction coupling in human myocardium. Communications Biology, 7**,** 220.

SUNG, D., MILLS, R. W., SCHETTLER, J., NARAYAN, S. M., OMENS, J. H. & MCCULLOCH, A. D. 2003. Ventricular Filling Slows Epicardial Conduction and Increases Action Potential Duration in an Optical Mapping Study of the Isolated Rabbit Heart. Journal of Cardiovascular Electrophysiology, 14**,** 739-749.

SWAROOP, G. 2022. Post-myocardial Infarction Heart Failure: A Review on Management of Drug Therapies. Cureus, 14**,** e25745.

SZENTADRASSY, N., BANYASZ, T., BIRO, T., SZABO, G., TOTH, B. I., MAGYAR, J., LAZAR, J., VARRO, A., KOVACS, L. & NANASI, P. P. 2005. Apico–basal inhomogeneity in distribution of ion channels in canine and human ventricular myocardium. Cardiovascular Research, 65**,** 851-860.

SZENTANDRÁSSY, N., FARKAS, V., BÁRÁNDI, L., HEGYI, B., RUZSNAVSZKY, F., HORVÁTH, B., BÁNYÁSZ, T., MAGYAR, J., MÁRTON, I. & NÁNÁSI, P. P. 2012. Role of action potential configuration and the contribution of C^{2+}a and K^{+} currents to isoprenaline-induced changes in canine ventricular cells. Br J Pharmacol, 167**,** 599-611.

TAKESHIMA, H., KOMAZAKI, S., NISHI, M., IINO, M. & KANGAWA, K. 2000. Junctophilins: a novel family of junctional membrane complex proteins. Mol Cell, 6**,** 11-22.

TAYAL, U., PRASAD, S. & COOK, S. A. 2017. Genetics and genomics of dilated cardiomyopathy and systolic heart failure. Genome Med, 9**,** 20.

TERRACCIANO, C. M. & MACLEOD, K. T. 1997. Measurements of Ca2+ entry and sarcoplasmic reticulum Ca2+ content during the cardiac cycle in guinea pig and rat ventricular myocytes. Biophysical Journal, 72**,** 1319-1326.

THANGAVEL, M., LIU, X., SUN, S. Q., KAMINSKY, J. & OSTROM, R. S. 2009. The C1 and C2 domains target human type 6 adenylyl cyclase to lipid rafts and caveolae. Cell Signal, 21**,** 301-8.

THYGESEN, K., ALPERT, J. S., WHITE, H. D., JAFFE, A. S., APPLE, F. S., GALVANI, M., KATUS, H. A., NEWBY, L. K., RAVKILDE, J., CHAITMAN, B., CLEMMENSEN, P. M., DELLBORG, M., HOD, H., PORELA, P., UNDERWOOD, R., BAX, J. J., BELLER, G. A., BONOW, R., VAN DER WALL, E. E., BASSAND, J. P., WIJNS, W., FERGUSON, T. B., STEG, P. G., URETSKY, B. F., WILLIAMS, D. O., ARMSTRONG, P. W., ANTMAN, E. M., FOX, K. A., HAMM, C. W., OHMAN, E. M., SIMOONS, M. L., POOLE-WILSON, P. A., GURFINKEL, E. P., LOPEZ-SENDON, J. L., PAIS, P., MENDIS, S., ZHU, J. R., WALLENTIN, L. C., FERNÁNDEZ-AVILÉS, F., FOX, K. M., PARKHOMENKO, A. N., PRIORI, S. G., TENDERA, M., VOIPIO-PULKKI, L. M., VAHANIAN, A., CAMM, A. J., DE CATERINA, R., DEAN, V., DICKSTEIN, K., FILIPPATOS, G., FUNCK-BRENTANO, C., HELLEMANS, I., KRISTENSEN, S. D., MCGREGOR, K., SECHTEM, U., SILBER, S., TENDERA, M., WIDIMSKY, P., ZAMORANO, J. L., MORAIS, J., BRENER, S., HARRINGTON, R., MORROW, D., LIM, M., MARTINEZ-RIOS, M. A., STEINHUBL, S., LEVINE, G. N., GIBLER, W. B., GOFF, D., TUBARO, M., DUDEK, D. & AL-ATTAR, N. 2007. Universal definition of myocardial infarction. Circulation, 116**,** 2634-53.

TIMOFEYEV, V., MYERS, R. E., KIM, H. J., WOLTZ, R. L., SIRISH, P., HEISERMAN, J. P., LI, N., SINGAPURI, A., TANG, T., YAROV-YAROVOY, V., YAMOAH, E. N., HAMMOND, H. K. & CHIAMVIMONVAT, N. 2013. Adenylyl cyclase subtype-specific compartmentalization: differential regulation of L-type Ca2+ current in ventricular myocytes. Circ Res, 112**,** 1567-76.

TODAKA, K., OGINO, K., GU, A. & BURKHOFF, D. 1998. Effect of ventricular stretch on contractile strength, calcium transient, and cAMP in intact canine hearts. Am J Physiol, 274**,** H990-1000.

TRACY, R. E. & SANDER, G. E. 2011. Histologically measured cardiomyocyte hypertrophy correlates with body height as strongly as with body mass index. Cardiol Res Pract, 2011**,** 658958.

TSAI, C. T., CHIANG, F. T., TSENG, C. D., YU, C. C., WANG, Y. C., LAI, L. P., HWANG, J. J. & LIN, J. L. 2011. Mechanical stretch of atrial myocyte monolayer decreases sarcoplasmic reticulum calcium adenosine triphosphatase expression and increases susceptibility to repolarization alternans. J Am Coll Cardiol, 58**,** 2106-15.

TSUTSUMI, Y. M., HORIKAWA, Y. T., JENNINGS, M. M., KIDD, M. W., NIESMAN, I. R., YOKOYAMA, U., HEAD, B. P., HAGIWARA, Y., ISHIKAWA, Y., MIYANOHARA, A., PATEL, P. M., INSEL, P. A., PATEL, H. H. & ROTH, D. M. 2008. Cardiac-specific overexpression of caveolin-3 induces endogenous cardiac protection by mimicking ischemic preconditioning. Circulation, 118**,** 1979-88.

TUNG, L. & ZOU, S. 1995. Influence of stretch on excitation threshold of single frog ventricular cells. Exp Physiol, 80**,** 221-35.

UTO, A., ARAI, H. & OGAWA, Y. 1991. Reassessment of Fura-2 and the ratio method for determination of intracellular Ca2+ concentrations. Cell Calcium, 12**,** 29-37.

VAN DER VELDEN, J., DE JONG, J. W., OWEN, V. J., BURTON, P. B. J. & STIENEN, G. J. M. 2000. Effect of protein kinase A on calcium sensitivity of force and its sarcomere length dependence in human cardiomyocytes. Cardiovascular Research, 46**,** 487-495.

VANDENBERG, J. I., BETT, G. C. & POWELL, T. 1997. Contribution of a swelling-activated chloride current to changes in the cardiac action potential. American Journal of Physiology-Cell Physiology, 273**,** C541-C547.

VARRÓ, A., LATHROP, D. A., HESTER, S. B., NÁNÁSI, P. P. & PAPP, J. G. 1993. Ionic currents and action potentials in rabbit, rat, and guinea pig ventricular myocytes. Basic Res Cardiol, 88**,** 93-102.

VARRÓ, A., TOMEK, J., NAGY, N., VIRÁG, L., PASSINI, E., RODRIGUEZ, B. & BACZKÓ, I. 2021. Cardiac transmembrane ion channels and action potentials: cellular physiology and arrhythmogenic behavior. Physiological Reviews, 101**,** 1083-1176.

VELAZQUEZ, E. J., PFEFFER, M. A., MCMURRAY, J. V., MAGGIONI, A. P., ROULEAU, J. L., VAN DE WERF, F., KOBER, L., WHITE, H. D., SWEDBERG, K., LEIMBERGER, J. D., GALLO, P., SELLERS, M. A., EDWARDS, S., HENIS, M. & CALIFF, R. M. 2003. VALsartan In Acute myocardial iNfarcTion (VALIANT) trial: baseline characteristics in context. Eur J Heart Fail, 5**,** 537-44.

WACHTEN, S., MASADA, N., AYLING, L. J., CIRUELA, A., NIKOLAEV, V. O., LOHSE, M. J. & COOPER, D. M. 2010. Distinct pools of cAMP centre on different isoforms of adenylyl cyclase in pituitary-derived GH3B6 cells. J Cell Sci, 123**,** 95-106.

WAGNER, E., BRANDENBURG, S., KOHL, T. & LEHNART, S. E. 2014. Analysis of tubular membrane networks in cardiac myocytes from atria and ventricles. J Vis Exp**,** e51823.

WAGNER, E., LAUTERBACH, M. A., KOHL, T., WESTPHAL, V., WILLIAMS, G. S., STEINBRECHER, J. H., STREICH, J. H., KORFF, B., TUAN, H. T., HAGEN, B., LUTHER, S., HASENFUSS, G., PARLITZ, U., JAFRI, M. S., HELL, S. W., LEDERER, W. J. & LEHNART, S. E. 2012. Stimulated emission depletion live-cell super-resolution imaging shows proliferative remodeling of T-tubule membrane structures after myocardial infarction. Circ Res, 111**,** 402-14.

WAKAYAMA, Y., MIURA, M., SUGAI, Y., KAGAYA, Y., WATANABE, J., TER KEURS, H. E. D. J. & SHIRATO, K. 2001. Stretch and quick release of rat cardiac trabeculae accelerates Ca2+ waves and triggered propagated contractions. American Journal of Physiology-Heart and Circulatory Physiology, 281**,** H2133-H2142.

WALKER, C. A. & SPINALE, F. G. 1999. The structure and function of the cardiac myocyte: A review of fundamental concepts. The Journal of Thoracic and Cardiovascular Surgery, 118**,** 375-382.

WANG, H., PENG, M. S., CHEN, Y., GENG, J., ROBINSON, H., HOUSLAY, M. D., CAI, J. & KE, H. 2007. Structures of the four subfamilies of phosphodiesterase-4 provide insight into the selectivity of their inhibitors. Biochem J, 408**,** 193-201.

WANG, H. S. & COHEN, I. S. 2003. Calcium channel heterogeneity in canine left ventricular myocytes. J Physiol, 547**,** 825-33.

WANG, Y., JOYNER, R. W., WAGNER, M. B., CHENG, J., LAI, D. & CRAWFORD, B. H. 2009. Stretch-activated channel activation promotes early afterdepolarizations in rat ventricular myocytes under oxidative stress. Am J Physiol Heart Circ Physiol, 296**,** H1227-35.

WANG, Y., SHI, Q., LI, M., ZHAO, M., REDDY GOPIREDDY, R., TEOH, J. P., XU, B., ZHU, C., IRETON, K. E., SRINIVASAN, S., CHEN, S., GASSER, P. J., BOSSUYT, J., HELL, J. W., BERS, D. M. & XIANG, Y. K. 2021. Intracellular β(1)-Adrenergic Receptors and Organic Cation Transporter 3 Mediate Phospholamban Phosphorylation to Enhance Cardiac Contractility. Circ Res, 128**,** 246-261.

WARD, M. L., POPE, A. J., LOISELLE, D. S. & CANNELL, M. B. 2003. Reduced contraction strength with increased intracellular [Ca2+] in left ventricular trabeculae from failing rat hearts. J Physiol, 546**,** 537-50.

WARNE, T., SERRANO-VEGA, M. J., BAKER, J. G., MOUKHAMETZIANOV, R., EDWARDS, P. C., HENDERSON, R., LESLIE, A. G., TATE, C. G. & SCHERTLER, G. F. 2008. Structure of a beta1-adrenergic G-protein-coupled receptor. Nature, 454**,** 486-91.

WATANABE, T., DELBRIDGE, L. M., BUSTAMANTE, J. O. & MCDONALD, T. F. 1983. Heterogeneity of the action potential in isolated rat ventricular myocytes and tissue. Circ Res, 52**,** 280-90.

WEBER, S., MEYER-ROXLAU, S., WAGNER, M., DOBREV, D. & EL-ARMOUCHE, A. 2015. Counteracting Protein Kinase Activity in the Heart: The Multiple Roles of Protein Phosphatases. Front Pharmacol, 6**,** 270.

WETTWER, E., AMOS, G., GATH, J., ZERKOWSKI, H. R., REIDEMEISTER, J. C. & RAVENS, U. 1993. Transient outward current in human and rat ventricular myocytes. Cardiovasc Res, 27**,** 1662-9.

WHALLEY, D. W., HOOL, L. C., TEN EICK, R. E. & RASMUSSEN, H. H. 1993. Effect of osmotic swelling and shrinkage on Na(+)-K+ pump activity in mammalian cardiac myocytes. American Journal of Physiology-Cell Physiology, 265**,** C1201-C1210.

WHITE, E., LE GUENNEC, J., NIGRETTO, J., GANNIER, F., ARGIBAY, J. & GARNIER, D. 1993. The effects of increasing cell length on auxotonic contractions; membrane potential and

intracellular calcium transients in single guinea-pig ventricular myocytes. Experimental Physiology, 78**,** 65-78.

WHITE, E., WALTON, R., KAUR, S., POWER, A., HAÏSSAGUERRE, M., BERNUS, O. & WARD, M.-L. 2020. Mechanical stimulation of endocardial Purkinje fibres can trigger ventricular arrhythmias. bioRxiv**,** 2020.08.10.234195.

WILKINS, B. J. & MOLKENTIN, J. D. 2002. Calcineurin and cardiac hypertrophy: where have we been? Where are we going? J Physiol, 541**,** 1-8.

WOLFF, M. R., BUCK, S. H., STOKER, S. W., GREASER, M. L. & MENTZER, R. M. 1996. Myofibrillar calcium sensitivity of isometric tension is increased in human dilated cardiomyopathies: role of altered beta-adrenergically mediated protein phosphorylation. J Clin Invest, 98**,** 167-76.

WONG, S. M., DEBELL, M. C. & CHASE, H. S., JR. 1990. Cell swelling increases intracellular free [Ca] in cultured toad bladder cells. Am J Physiol, 258**,** F292-6.

WOODMAN, S. E., PARK, D. S., COHEN, A. W., CHEUNG, M. W., CHANDRA, M., SHIRANI, J., TANG, B., JELICKS, L. A., KITSIS, R. N., CHRIST, G. J., FACTOR, S. M., TANOWITZ, H. B. & LISANTI, M. P. 2002. Caveolin-3 knock-out mice develop a progressive cardiomyopathy and show hyperactivation of the p42/44 MAPK cascade. J Biol Chem, 277**,** 38988-97.

WRIGHT, A. R., REES, S. A., VANDENBERG, J. I., TWIST, V. W. & POWELL, T. 1995. Extracellular osmotic pressure modulates sodium-calcium exchange in isolated guinea-pig ventricular myocytes. J Physiol, 488 (Pt 2)**,** 293-301.

WRIGHT, P. T., BHOGAL, N. K., DIAKONOV, I., PANNELL, L. M. K., PERERA, R. K., BORK, N. I., SCHOBESBERGER, S., LUCARELLI, C., FAGGIAN, G., ALVAREZ-LAVIADA, A., ZACCOLO, M., KAMP, T. J., BALIJEPALLI, R. C., LYON, A. R., HARDING, S. E., NIKOLAEV, V. O. & GORELIK, J. 2018a. Cardiomyocyte Membrane Structure and cAMP Compartmentation Produce Anatomical Variation in β2AR-cAMP Responsiveness in Murine Hearts. Cell Reports, 23**,** 459-469.

WRIGHT, P. T., NIKOLAEV, V. O., O'HARA, T., DIAKONOV, I., BHARGAVA, A., TOKAR, S., SCHOBESBERGER, S., SHEVCHUK, A. I., SIKKEL, M. B., WILKINSON, R., TRAYANOVA, N. A., LYON, A. R., HARDING, S. E. & GORELIK, J. 2014. Caveolin-3 regulates

compartmentation of cardiomyocyte beta2-adrenergic receptor-mediated cAMP signaling. J Mol Cell Cardiol, 67**,** 38-48.

WRIGHT, P. T., SANCHEZ-ALONSO, J. L., LUCARELLI, C., ALVAREZ-LAVIADA, A., POULET, C. E., BELLO, S. O., FAGGIAN, G., TERRACCIANO, C. M. & GORELIK, J. 2018b. Partial Mechanical Unloading of the Heart Disrupts L-Type Calcium Channel and Beta-Adrenoceptor Signaling Microdomains. Frontiers in physiology, 9**,** 1302-1302.

WRIGHT, P. T., TSUI, S. F., FRANCIS, A. J., MACLEOD, K. T. & MARSTON, S. B. 2020. Approaches to High-Throughput Analysis of Cardiomyocyte Contractility. Frontiers in Physiology, 11.

XIANG, Y., NARO, F., ZOUDILOVA, M., JIN, S.-L. C., CONTI, M. & KOBILKA, B. 2005. Phosphodiesterase 4D is required for β2 adrenoceptor adrenoceptor subtype-specific signaling in cardiac myocytes. Proceedings of the National Academy of Sciences, 102**,** 909-914.

XIANG, Y. K. 2011. Compartmentalization of beta-adrenergic signals in cardiomyocytes. Circ Res, 109**,** 231-44.

XIAO, B., JIANG, M. T., ZHAO, M., YANG, D., SUTHERLAND, C., LAI, F. A., WALSH, M. P., WARLTIER, D. C., CHENG, H. & CHEN, S. R. 2005. Characterization of a novel PKA phosphorylation site, serine-2030, reveals no PKA hyperphosphorylation of the cardiac ryanodine receptor in canine heart failure. Circ Res, 96**,** 847-55.

XIAO, R.-P., AVDONIN, P., ZHOU, Y.-Y., CHENG, H., AKHTER, S. A., ESCHENHAGEN, T., LEFKOWITZ, R. J., KOCH, W. J. & LAKATTA, E. G. 1999a. Coupling of β2-Adrenoceptor to Gi Proteins and Its Physiological Relevance in Murine Cardiac Myocytes. Circulation Research, 84**,** 43-52.

XIAO, R.-P., CHENG, H., ZHOU, Y.-Y., KUSCHEL, M. & LAKATTA, E. G. 1999b. Recent Advances in Cardiac β2-Adrenergic Signal Transduction. Circulation Research, 85**,** 1092-1100.

XIAO, R. P., HOHL, C., ALTSCHULD, R., JONES, L., LIVINGSTON, B., ZIMAN, B., TANTINI, B. & LAKATTA, E. G. 1994. Beta 2-adrenergic receptor-stimulated increase in cAMP in rat heart cells is not coupled to changes in Ca2+ dynamics, contractility, or phospholamban phosphorylation. J Biol Chem, 269**,** 19151-6.

XIAO, R. P., JI, X. & LAKATTA, E. G. 1995. Functional coupling of the beta 2-adrenoceptor to a pertussis toxin-sensitive G protein in cardiac myocytes. Mol Pharmacol, 47**,** 322-9.

XIAO, R. P. & LAKATTA, E. G. 1993. Beta 1-adrenoceptor stimulation and beta 2-adrenoceptor stimulation differ in their effects on contraction, cytosolic Ca2+, and Ca2+ current in single rat ventricular cells. Circ Res, 73**,** 286-300.

XU, X., KAINDL, J., CLARK, M. J., HÜBNER, H., HIRATA, K., SUNAHARA, R. K., GMEINER, P., KOBILKA, B. K. & LIU, X. 2021. Binding pathway determines norepinephrine selectivity for the human β(1)AR over β(2)AR. Cell Res, 31**,** 569-579.

YANG, L. & SCARLATA, S. 2017. Super-resolution Visualization of Caveola Deformation in Response to Osmotic Stress*. Journal of Biological Chemistry, 292**,** 3779-3788.

YARBROUGH, T. L., LU, T., LEE, H.-C. & SHIBATA, E. F. 2002. Localization of Cardiac Sodium Channels in Caveolin-Rich Membrane Domains. Circulation Research, 90**,** 443-449.

YOUM, J. B., HAN, J., KIM, N., ZHANG, Y. H., KIM, E., LEEM, C. H., KIM, S. J. & EARM, Y. E. 2005. Role of Stretch-activated Channels in the Heart: Action Potential and Ca(2+) Transients. In: KAMKIN, A. & KISELEVA, I. (eds.) Mechanosensitivity in Cells and Tissues. Moscow: Academia

Copyright © 2005, Academia Publishing House Ltd.

ZABEL, M., KOLLER, B. S., SACHS, F. & FRANZ, M. R. 1996. Stretch-induced voltage changes in the isolated beating heart: importance of the timing of stretch and implications for stretch-activated ion channels. Cardiovascular research, 32 1**,** 120-30.

ZACCOLO, M. 2006. Phosphodiesterases and compartmentalized cAMP signalling in the heart. European Journal of Cell Biology, 85**,** 693-697.

ZACCOLO, M., ZERIO, A. & LOBO, M. J. 2021. Subcellular Organization of the cAMP Signaling Pathway. Pharmacol Rev, 73**,** 278-309.

ZACHARIAS, D. A., VIOLIN, J. D., NEWTON, A. C. & TSIEN, R. Y. 2002. Partitioning of Lipid-Modified Monomeric GFPs into Membrane Microdomains of Live Cells. Science, 296**,** 913-916.

ZENG, J., LAURITA, K. R., ROSENBAUM, D. S. & RUDY, Y. 1995. Two components of the delayed rectifier K+ current in ventricular myocytes of the guinea pig type. Theoretical formulation and their role in repolarization. Circ Res, 77**,** 140-52.

ZENG, T., BETT, G. C. L. & SACHS, F. 2000. Stretch-activated whole cell currents in adult rat cardiac myocytes. American Journal of Physiology-Heart and Circulatory Physiology, 278**,** H548-H557.

ZHANG, R., ZHAO, J. & POTTER, J. D. 1995. Phosphorylation of both serine residues in cardiac troponin I is required to decrease the Ca2+ affinity of cardiac troponin C. J Biol Chem, 270**,** 30773-80.

ZHANG, Y., QI, Y., LI, J.-J., HE, W.-J., GAO, X.-H., ZHANG, Y., SUN, X., TONG, J., ZHANG, J., DENG, X.-L., DU, X.-J. & XIE, W. 2020. Stretch-induced sarcoplasmic reticulum calcium leak is causatively associated with atrial fibrillation in pressure-overloaded hearts. Cardiovascular Research, 117**,** 1091-1102.

ZHANG, Y., WANG, W. E., ZHANG, X., LI, Y., CHEN, B., LIU, C., AI, X., ZHANG, X., TIAN, Y., ZHANG, C., TANG, M., SZETO, C., HUA, X., XIE, M., ZENG, C., WU, Y., ZHOU, L., ZHU, W., YU, D., HOUSER, S. R. & CHEN, X. 2019. Cardiomyocyte PKA Ablation Enhances Basal Contractility While Eliminates Cardiac β-Adrenergic Response Without Adverse Effects on the Heart. Circ Res, 124**,** 1760-1777.

ZHOU, P. & PU, W. T. 2016. Recounting Cardiac Cellular Composition. Circ Res, 118**,** 368-70.

ZHU, W. Z., ZHENG, M., KOCH, W. J., LEFKOWITZ, R. J., KOBILKA, B. K. & XIAO, R. P. 2001. Dual modulation of cell survival and cell death by beta(2)-adrenergic signaling in adult mouse cardiac myocytes. Proc Natl Acad Sci U S A, 98**,** 1607-12.